Phenomenology of models beyond LCDM

Rodrigo Calderon

THÈSE POUR OBTENIR LE GRADE DE DOCTEUR DE L'UNIVERSITE DE MONTPELLIER

En Physique Théorique

École doctorale : Information, Structures et Systèmes

Unité de recherche Laboratoire de Physique Charles Coulomb

Phénoménologie de modèles au-delà du modèle de concordance

Présentée par Rodrigo Calderón Bruni

Le 23/09/21

Sous la direction de Prof. David Polarski

Devant le jury composé de

PETER Patrick, Directeur de recherche, Institut d'Astrophysique de Paris	Président | Rapporteur
BRAX Philippe, Directeur de recherche, IPhT, CEA, Saclay	Rapporteur
BARRAU Aurélien, Professeur, LPSC, Université de Grenoble	Examinateur
KNEUR Jean-Loïc, Directeur de recherche, L2C, Université de Montpellier	Examinateur
POLARSKI David, Professeur, L2C, Université de Montpellier	Directeur de thèse

UNIVERSITÉ DE MONTPELLIER

Phenomenology of models beyond the standard ΛCDM paradigm

A DISSERTATION PRESENTED
BY
RODRIGO CALDERÓN BRUNI
TO
THE DOCTORAL SCHOOL: INFORMATION, STRUCTURES ET SYSTÈMES (I2S)

IN PARTIAL FULFILLMENT OF THE REQUIREMENTS
FOR THE DEGREE OF
DOCTOR OF PHILOSOPHY
IN THE SUBJECT OF
THEORETICAL PHYSICS

UNIVERSITÉ DE MONTPELLIER
MONTPELLIER, OCCITANIE
SEPTEMBER 2021

Contents

0 Overview/Introduction 1

I Foundations of Modern Cosmology 7

1 Cosmology in a Nutshell 8
- 1.1 An Isotropic and Homogeneous Universe . . . 9
- 1.2 The Concordance (ΛCDM) Model . . . 20
- 1.3 Observational Probes . . . 22
- 1.4 Tensions/Anomalies within the Concordance Model . . . 28

2 The Early Universe 30
- 2.1 Inflation: a solution to the *Big-Bang* puzzles . . . 32
- 2.2 Generating the primordial seeds . . . 34
- 2.3 Primordial Black Holes as a window to the very-early Universe . . . 36
- 2.4 Stochastic Gravitational Wave Background . . . 37

II Phenomenology of Dark Energy models: The Growth Index γ 40

3 Inhomogeneities around the FLRW background 41
- 3.1 Stages of Evolution . . . 44
- 3.2 Large Scale Structure Observables . . . 47

4 Modified Gravity 55
- 4.1 The Horndeski Action . . . 56
- 4.2 Phenomenology of Modified Gravity . . . 57
- 4.3 Some examples of Modified Gravity . . . 58

5 Global properties of the Growth Index γ 62
5.1 Characterizing the growth of perturbations with γ . . . 63
5.2 Global analysis in the (Ω_m, γ)-plane . . . 66
5.3 Global evolution of the slope $\Gamma(\Omega_m)$ . . . 70
5.4 Systems with a non-monotonic $\gamma(\Omega_m)$ . . . 72
5.5 Summary and conclusions . . . 79

6 The Growth Index γ: Mathematical Aspects and Physical Relevance 81
6.1 The growth index γ . . . 83
6.2 Dynamical System Analysis . . . 84
6.3 Presence of an Unclustered Dustlike Component . . . 89
6.4 Summary and Conclusions . . . 98

III A Negative Cosmological Constant in the Dark Sector? 100

7 Negative Cosmological Constant in the Dark Sector 101
7.1 Cosmic expansion with a negative cosmological constant . . . 103
7.2 Cosmic Relevance of λ and the H_0 tension . . . 109
7.3 Comparison with data: Model Selection and Parameter Estimation . . . 116
7.4 Summary and Conclusion . . . 122

8 Conclusions 124

List of Figures 132

References 169

Directeur de thèse: Prof. David Polarski Rodrigo Calderón Bruni

Phénomenologie de modèles au-delà du modèle de Concordance

Résumé en Français

Introduction

Les observations des dernières décennies ont fait émerger un modèle standard en cosmologie, appelé modèle de concordance. Le paradigme qui s'est imposé grâce aux observations aux échelles cosmologiques est celui d'un univers contenant deux phases d'expansion accelerée. La première permet d'expliquer l'origine des galaxies et amas de galaxies que l'on observe de nos jours, tandis que la deuxième rend compte de l'expansion accelérée actuelle, confirmée par de nombreuses observations. Le mécanisme physique à l'origine de cette expansion accelérée reste une des plus grandes questions ouvertes en physique. Néanmoins, des observations provenant du rayonnement fossile cosmologique (Cosmic microwave background - CMB), des oscillations acoustiques baryoniques (Baryon Acoustic Oscillations -BAO), des supernovae du type Ia (SNeIa) et de nombreuses autres observations, semblent en accord avec l'introduction d'une *constante cosmologique* Λ dans les équations du champ de la gravitation (les équations d'Einstein). Par ailleurs, une composante de matière "sombre" (noire) froide (non-relativiste) -appélée *Cold Dark Matter* ou CDM- est un ingrédient nécéssaire pour expliquer la croissance et la formation des grandes structures dans l'Univers. Ce modèle repose aussi sur des hypothèses concernant les fluctuations cosmologiques primordiales (supposées d'origine inflationaire). En fait, le modèle ΛCDM de base est entièrement caractérisé par 6 paramètres libres. On arrive ainsi au modèle ΛCDM - appelé aussi "modèle de concordance". Ce dernier est à ce jour, le modèle le plus simple pour décrire notre Univers. C'est pour cette raison, qu'il est devenu le modèle de référence. Malgré son énorme succès, le modèle de concordance reste un modèle phénomenologique, dans lequel 95% de son contenu est dans un secteur "*sombre*" - dont la nature nous échappe. De plus,

l'introduction d'une telle constante cosmologique pose un problème majeur du point de vue théorique. Son interprétation en tant qu'énergie du vide en théorie des champs est problématique du fait de sa petitesse, comparé aux valeurs planckiennes attendues dans une telle théorie. De plus, comme nous le rappelerons plus tard, les théories des hautes énergies supersymétriques préfèrent une constante cosmologique *négative*, plutôt que positive. Or pour être en accord avec les observations, il faut une constante cosmologique positive. Il est à noter que le modèle ΛCDM rencontre également des difficultés pour rendre compte de certaines observations aux petites échelles cosmologiques, en particulier aux échelles galactiques ("small-scale crisis"). C'est pour toutes ces raisons, aussi bien théoriques qu'observationelles, qu'il est nécessaire d'explorer d'autres mécanismes physiques qui pourraient également rendre compte de cette deuxième phase d'expansion accélérée, tout en étant en accord avec l'ensemble des observations.

Dans le cadre de cette thèse, nous allons étudier la phénoménologie de plusieurs modèles au-delà de ΛCDM . Nous nous concentrerons notamment sur une observable qui permet de distinguer les modèles d'énergie noire du modèle ΛCDM , en l'ocurrence l'indice de croissance (growth index) γ des perturbations. Cet indice de croissance γ est un outil efficace pour distinguer les modèles d'énergie noire en gravitation modifiée et ceux formulés dans le cadre de la relativité générale, dont le modèle ΛCDM . En effet, dans les théories de gravité modifiée, la croissance des perturbations est modifiée. Cela montre l'intêret essentiel d'inclure les observations relatives aux perturbations cosmologiques dans l'ensemble des observations lorsque l'on cherche à contraindre les modèles théoriques d'énergie noire. Remarquons que bien que pour des raisons historiques, on appelle cette quantité "indice" de croissance γ, il s'agit en realité d'une fonction du temps, et même des echelles cosmologiques quand il s'agit de modèles d'énergie noire en gravitation modifiée.

Dans la première partie de cette thèse, nous comencerons naturellement par une introduction à la cosmologie moderne, en mettant l'accent sur les différentes contraintes observationelles existantes (et à venir).

Phénomenologie des modèles d'énergie noire et croissance des perturbations.

Dans la deuxième partie de cette thèse, nous nous intéresserons à l'étude de la croissance des perturbations de matière dans le régime linéaire, en particulier à travers la dynamique de son indice de croissance (*growth index*) $\gamma \equiv \ln f / \ln \Omega_m$ - où $f = \frac{d \ln \delta_m}{d \ln a}$ est appelée *growth function* (fonction de croissance). Après avoir brièvement introduit les éléments nécéssaires à l'étude des perturbations et leur lien avec les quantités observables dans le Chapitre 3, nous allons ensuite introduire quelques extensions du modèle de concordance dans le Chapitre 4. Nous appliquerons par la suite le formalisme du *growth index* pour étudier leur phénomenologie et proprietés globales en termes de la variable Ω_m. Nous considérerons en particulier des modèles d'énergie noire où le comportement de γ est très different de celui de ΛCDM . En effet, dans le cadre de ΛCDM (et des modèles à l'interieur de la relativité générale avec un $w \neq -1$ constant), l'indice de croissance γ est une fonction monotone et décroissante. Ce comportement, peut être drastiquement modifié dans des théories de gravité modifiée et dans d'autres extensions du modèle ΛCDM - faisant de γ un outil extrêmement précieux pour détecter des déviations du modèle de concordance. La prochaine génération de relevés de galaxies, dont *Euclid*, permettra peut-être une mesure assez précise de l'indice de croissance $\gamma_0 \equiv \gamma(z = 0)$ et de sa derivée $\gamma_1 \equiv \frac{d\gamma}{dz}\big|_{z=0}$.

Nous poursuivons l'analyse par une extension de ΛCDM , *i.e.* une équation d'état variable parametrisée par $w_{\rm DE}(a) = w_0 + w_a(1 - a)$ (CPL). Pour les valeurs de parametres (w_0, w_a) que l'on considère, le comportement de γ reste essentiellement similaire à celui de ΛCDM (quasi-constant avec $\gamma \sim 0.55$), sauf dans le futur asymptotique ($\Omega_m \to 0$) où l'on trouve une valeur asymptotique $\gamma_\infty = \frac{1}{2}$ alors que $\gamma_\infty^{\Lambda\rm CDM} = \frac{2}{3}$. D'un point de vue observationel, cependant, ces modèles seront difficilement distinguables de ΛCDM à l'époque actuelle. La situation est différente lorsqu'on étudie des modèles du type $f(R)$ ou des modèles en dimensions supplementaires, comme le modèle Dvali-Gabadadze-Porrati (DGP). En effet,

dans le régime linéaire et pour les modes d'intérêt cosmologique, les modifications dans le secteur gravitationnel se traduisent par une modification de la constante "effective" de couplage $G_{\rm eff}(z,k)$ dans l'équation de Poisson $-\frac{k^2}{a^2}\Phi = 4\pi G_{\rm eff}(z,k)\rho_m\delta_m$ (*i.e.* dans le terme de source pour les perturbations). Par exemple, les modèles du type $f(R)$ prédisent une évolution de $G_{\rm eff}(z)$ dans le temps, et en particulier, $G_{\rm eff}(z) \geq G$, pouvant atteindre $G_{\rm eff} = \frac{4}{3}G$ - où G est la constante de Newton. Dans une approche phénoménologique, nous modélisons ces comportements à l'aide d'un "bump" ou d'un "dip" dans la quantité $g(z) \equiv G_{\rm eff}(z)/G$ et nous obtenons des solutions numériques pour γ. Le modèle DGP est un example parfait de la puissance de γ, et de l' avantage d'étudier son comportement (global) en fonction de Ω_m. Nous dérivons explicitement l'origine de sa valeur $\gamma^{\rm DGP}_{-\infty} = 11/16$ dans le passé asymptotique, differente de la valeur attendue $\gamma^{\rm DGP}_{-\infty} = 9/16$ puisque $g^{\rm DGP}(\Omega_m = 1) = 1$. Cela découle du fait que $g'(\Omega_m)\big|_{\Omega_m=1} \neq 0$. La dynamique de γ dans ces modèles est differente à celle de ΛCDM . Sa valeur aujourd'hui $\gamma^{\rm DGP}_0 \simeq 0.68$ est facilement distinguable de $\gamma^{\Lambda{\rm CDM}}_0 \simeq 0.55$.

Un autre système physique intéressant à considérer est celui incluant une composante de matière qui ne s'agglutine pas, comme par exemple les neutrinos massifs après leur transition dans le regime non-relativiste. On pourrait aussi penser à d'autres particules, comme les particules de type *axion*. Nous avons donc un système avec de la matière qui s'agglutine, une composante de matière (x) qui ne s'agglutine pas et de l'énergie noire, avec $\Omega_x + \Omega_m + \Omega_{\rm DE} = 1$. On introduit $\Omega^{\rm tot}_m = \Omega_m + \Omega_x$ et $\varepsilon \equiv \Omega_x/\Omega^{\rm tot}_m$. Nous étudions la dynamique de γ dans ce modèle, et on trouve en particulier la valeur asymptotique dans le passé $\gamma^{\varepsilon}_{-\infty} = \frac{3}{5} + \mathcal{O}(\varepsilon)$. On donne le développement de $\gamma^{\varepsilon}_{-\infty}$ jusqu'au troisième ordre en ε. On remarque que $\gamma^{\varepsilon}_{-\infty}$ ne dépend pas de la valeur $w_{-\infty}$ dans le passé asymptotique. Il n'est donc pas possible de retrouver la valeur $\gamma_{-\infty}$ quand la composante x est absente ($\varepsilon \to 0$). Ceci est possible, car comme on le montre, il existe une discontinuité dans les variables $(\varepsilon, \Omega^{\rm tot}_m)$, *i.e.* les limites $\Omega^{\rm tot}_m \to 1$ et $\varepsilon \to 0$ ne commutent pas.

Une constante cosmologique négative?

Finalement, motivés par des idées de la physique des hautes énergies, nous considérerons la possibilité d'avoir une *constante cosmologique négative*, que nous appelons λ, dans le secteur sombre de notre Univers. Clairement, une constante cosmologique négative ne peut être à l'origine de l'expansion accélérée suggérée par les observations des SNeIa. Pour assurer la viabilité de ces modèles (*i.e.* en accord avec une expansion accélérée actuelle) nous considérerons aussi la présence d'une composante "X". Cette composante serait responsable de l'expansion accélérée actuelle. Par conséquent, nous nous intéresserons à la phénoménologie d'un secteur sombre "composé" (*i.e.* $\Omega_{\rm DE} = \Omega_X + \Omega_\lambda$, avec $\Omega_\lambda < 0$) en considérant plusieurs comportements de la composante X. Une question immédiate, est de se demander si ces modèles pourraient éventuellement soulager ce que l'on appele "*la tension de Hubble*" [1]. Pour quantifier la viabilité de ces modèles, nous combinons des mesures provenant du CMB, des BAO et des Supernovae. Plus concrètement, nous nous intéressons à l'influence de λ, et supposons que l'univers primordial reste inchangé – l'horizon du son (*sound horizon*) r_s est fixé à sa valeur dans ΛCDM – et nous explorons la possiblité de changer la physique à bas redshifts z avec plusieurs comportements de $w_X(z)$.

Une façon élégante de comparer différents modèles avec différents degrés de liberté, est au moyen des méthodes (Bayesiennes) *Markov-Chain Monte-Carlo*, du type "*Nested-Sampling*". En prenant en compte les observations mentionées précédemment, nous comparons ainsi les différents modèles considérés à l'hypothèse nulle qui est ΛCDM. Parmi les differents modèles que l'on considère, nous trouvons plusieurs modèles avec $\Omega_\lambda \neq 0$ qui sont viables, certains scénarios étant favorisés par rapport à ΛCDM. C' est vrai en particulier pour ceux où les déviations de w_X par rapport $w_X = -1$ se passent à haut-redshift ($z \gtrsim 1$), là où les données sont moins contraignantes. Quant au rôle de H_0, nous étudions son impact dans une analyse sé-

[1] Une difference de $\sim 5\sigma$ dans la mesure du parametre de Hubble H_0 entre différentes sondes cosmologiques à hauts et bas redshifts.

parée, en incluant un "prior" Gaussien centré sur la valeur de $H_0 = 73.3 \pm 4.0$ km.s^{-1}.Mpc^{-1} mesurée par HST-Mira. Même si l'inclusion de λ permet d'obtenir des valeurs de H_0 plus élevées ($H_0 \sim 70$) que pour ΛCDM avec les données de Planck , ceci n'est pas suffissant pour retrouver les mesures locales ($H_0 \sim 73$). Nous concluons qu'une valeur substantiellement plus élevée que $H_0 \simeq 70$ serait un test crucial pour la viabilité de ces modèles.

Conclusion

L'un des plus grands mystères de la cosmologie moderne est celui de l'origine de l'expansion accélérée de l'Univers. Comme nous l'avons vu, le modèle de concordance offre une solution simple et élégante mais n'est pas sans problèmes. Dans le cadre de cette thèse, il a été question de caractériser la phénoménologie de modèles au-delà du modèle de concordance notamment en considérant l'évolution des perturbations de matière (dans le régime linéaire). Malgré sa simplicité, l'indice de croissance γ se révèle être un outil extrêmement puissant, et potentiellement capable de distinguer parmi les différents modèles d'énergie noire. Nous avons considéré par ailleurs, un modèle avec un secteur d'énergie noire "composite", contenant une constante cosmologique *négative* λ. Dans les années à venir les prochains relevés de galaxies, en complément avec les observations d'ondes gravitationelles, nous permettront de mieux cerner l'origine de cette expansion, et de placer de fortes contraintes sur les modèles viables au-delà du modèle de concordance.

Thesis advisor: Prof. David Polarski Rodrigo Calderón Bruni

Phenomenology of models beyond the standard ΛCDM paradigm

Abstract

The prevailing paradigm in Cosmology is that of General Relativity with a cosmological constant Λ - accounting for the late-time accelerated expansion of the Universe - and some form of non-relativistic (Cold) Dark Matter, responsible for seeding the potential wells at early times. Hence the ΛCDM - or *Concordance Model of Cosmology*. This (phenomenological) model is in remarkable agreement with a wide variety of observational probes - over many different scales and epochs in the cosmic history. Because of its simplicity, a positive cosmological constant Λ is quite appealing, but nevertheless poses the problem of its small value from a fundamental standpoint. In recent years, increasingly precise cosmological observations have reported a few statistically significant curiosities within the ΛCDM paradigm. The most interesting examples being the $(\sim 5\sigma)$ discrepancy in the value of H_0 and the $(\sim 2\sigma)$ discrepancy in the amplitude of matter fluctuations σ_8, as inferred by early and late-time probes. Due to this, many extensions to the simple Λ picture have been proposed over the years, these go by the name of *Dark Energy models*.

In this thesis, having high energy physics considerations in mind, we explore various extensions to the standard ΛCDM paradigm and asses the viability of such models in light of recent and future observations. Our approach is rather phenomenological, aimed at capturing various types of behaviors while focusing on tools that can efficiently discriminate between the wide variety of Dark Energy and Modified Gravity models. One *potential smoking gun* is the *growth index of density perturbations* γ. We study in detail the global behaviour of $\gamma(\Omega_m)$, focusing on models that could lead to *a change in its slope* - in sharp contrast with the monotonically decreasing ΛCDM case. These include, an $f(R)$-inspired bump in $G_{\text{eff}}(z)$, a varying $w_{\text{DE}}(z)$, or more intricate (higher-dimensional) models, such as the Dvali-Gabadadze-Porrati (DGP) model. We also study its behaviour in the presence of an *Axion-like* (unclustered) component during matter domina-

tion and derive interesting (mathematical) properties.

Finally, we explore the possibility of having a *negative cosmological constant*-dubbed λ- in the dark sector. For these models to be viable, and accelerate the Universe at late-times, the dark sector should also contain an additional (effective) degree of freedom -dubbed X- such that $\Omega_{\rm DE} = \Omega_X + \Omega_\lambda$. We consider various types of behaviours in the X-component, parametrized by a varying EoS $w_X(a)$. We further test the viability of these models through a nested-sampling of the parameter space, and use Bayesian techniques to compare them to ΛCDM for model selection. We also comment on the implications of introducing a high-H_0 prior in separate runs. Although we find no decisive evidence for $\Omega_{\lambda,0} \neq 0$, its presence remains viable as it hides behind an *effective* (positive) Λ with $w_X \sim -1$. Models with higher evidence are found to be those with new physics ($w_X \leq -1$) appearing at large-z. A value of H_0 substantially higher than $H_0 \sim 70$ km.s^{-1}.Mpc^{-1} would be a decisive test of their viability.

Publication List

This thesis is the result of my own research while being a PhD student at *Laboratoire de Physique Charles Coulomb, University of Montpellier* and under the supervision of Prof. David Polarski. It is mainly based on the following publications:

- Rodrigo Calderón, Radouane Gannouji, Benjamin L'Huillier and David Polarski
  A Negative Cosmological Constant in the Dark Sector?
  Appeared on *Physical Review D - 103, 023526 (2021)* [57]

- Rodrigo Calderón, Didier Felbacq, Radouane Gannouji, David Polarski and Alexei A. Starobinsky
  Global properties of the growth index: Mathematical aspects and physical relevance
  Appeared on *Physical Review D - 101, 103501 (2020)*[56]

- Rodrigo Calderón, Didier Felbacq, Radouane Gannouji, David Polarski and Alexei A. Starobinsky
  Global properties of the growth index of matter inhomogeneities in the Universe
  Appeared on *Physical Review D - 100, 083503 (2019)*[55]

This thesis is dedicated to my parents and grand-parents,
to whom I owe so much.

Acknowledgments

Ces dernières années d'études ont bouleversé ma vision du monde et changé profondément qui je suis à ce jour. La thèse a été pour moi une expérience inoubliable, pleine d'émotions et d'apprentissage. Loin d'être l'œuvre d'une seule personne, cette thèse est le résultat de nombreuses discussions et d'interactions avec mon directeur de thèse, mes collaborateurs, mes collègues et amis. Je me considère chanceux d'avoir eu l'opportunité de partager cette expérience avec des personnes que j'admire et que j'estime énormément.

Je tiens d'abord à remercier en particulier mes rapporteurs, Philippe Brax et Patrick Peter qui ont aimablement accepté de s'atteler à la lecture de ce manuscrit, ainsi que les autres membres du jury, Aurélien Barrau et Jean-Loïc Kneur d'assister à ma soutenance.

À David, mon directeur de thèse. Merci pour toutes ces années (7 ans déjà!) d'enseignements, de nombreuses discussions (de physique et autres) et de conseils précieux et chaleureux. Ta pédagogie, ta passion pour la physique et ton intelligence ont fortement contribué à ma formation en tant que scientifique et à la personne que je suis dorénavant. Tu es en effet l'une des principales raisons pour lesquelles je me suis intéressé à la Cosmologie. Merci de m'avoir donné cette opportunité, et de m'avoir transmis l'amour pour le métier de chercheur.

À mes collaborateurs, en particulier Radouane et Benjamin. Merci pour les nombreux échanges, pour votre soutien et vos conseils au cours de ces années, ce fut un réel plaisir d'apprendre et d'échanger avec vous.

Aux membres de mon laboratoire d'accueil (L2C) pour ce cadre enrichissant tant scientifiquement que personnellement. En particulier, à mes collègues et amis: Vivian, Riccardo, Mihael, Loïc, Michelle, Rupert, Guille, Maria, Gaëtan et tous les autres postdoctorants, doctorants et stagiaires avec qui j'ai échangé et que j'aurai pu oublier. Aux membres de l'équipe IFAC, de m'avoir accueilli dès le premier jour de thèse comme l'un des vôtres: Michele, Gilbert, Sacha, Jean-Loïc, ainsi que mes enseignants de licence et master:

Felix, Cyril et Julien. À mes amis de master: Jean-Baptiste, Khalil, Anne-Laure, Florian et autres. À mes encadrants de stage: Yohann et Sabine. À Lucyna, Andrea et l'ensemble des membres de l'école doctorale de Physique.

A mi familia, una de las familias más fuertes y unidas que jamás he visto. Tengo la suerte de haber crecido en un hogar pleno de amor y apoyo incondicional. A mis abuelos, con quienes tuve un vínculo muy estrecho desde pequeño. Quienes estuvieron siempre dispuestos a escucharme, aconsejarme y ayudarme cuando lo necesité. A mis papás, quienes a pesar de mi "rebeldía", no dejaron de creer en ningún momento en mis capacidades, y me dieron la libertad de perseguir mis sueños – por más surreales que parecieran. A la "Nina", más que una madrina, ha sido una segunda madre. Al resto de mis tíos y tías, hermanos, y numerosos primos y primas. Gracias totales.

A mi familia adoptiva: Enzo, Jorge, Louis, Clara, Amélie, Melara, Beto, Alvaro, Bobby, Toto, Chalo, Santiago, Drilo, China, Renske, Avilés, Rodrigo, Guillaume, Charles, Morgan, Laura... y toda la team Montpellieraine con la que pude compartir los mejores años de mi vida.

À ma Nol, Marie et Pascale. Merci pour ton soutien ces derniers mois, je n'aurais pas pu le faire sans toi. Je t'aime.

Enfin, un énorme merci à tous ceux qui ont croisé mon chemin.

"Physics is like sex: sure, it may give some practical results, but that's not why we do it."

Richard Feynman

0

Overview/Introduction

Over the last century, and due to tremendous efforts in both the experimental and theoretical physics communities, our understanding of the Universe we live in has been *dramatically revolutionized*. Astronomical observations have revealed the dynamical nature of space-time, while microscopic observations have unveiled the quantum nature of reality. Our current understanding of nature is mainly based on two well-accepted theories. Namely, *Quantum Mechanics* (QM) describing the microscopic world, and *General Relativity* (GR) describing interactions on the largest of scales. Theoretically, these are both heavily relying on *beautiful* and *well-established principles* in physics, such as *symmetry* and *conservation laws*, yielding extremely precise predictions that are now at the very core of all human technologies. Despite their great (experimental and technological) success, these are facing deep issues at the fundamental level, that have been puzzling physicist for more than 50 years.

The Standard Model of Particle Physics

On one hand, the Standard Model (SM) of particle physics provides a *remarkable* description of interactions up to the $\sim$ TeV scale[205], as probed by the current experiments such as the *Large Hadron Collider* (LHC) at CERN. It is undoubtedly the most successful theoretical accomplishment of Human kind. The SM is a gauge theory based on a $SU(3)_c \times SU(2)_L \times U(1)_Y$ symmetry group at high energies, which is spontaneously broken - via the *Brout-Englert-Higgs mechanism*[94, 112] - into a $SU(3)_c$ responsible for the strong nuclear force, $SU(2)_L$ responsible for weak interactions and $U(1)_{\text{e.m}}$ accounting for the well-known electromagnetic interactions at low-energies. Despite its *enormous* theoretical success, the SM - in its vanilla form - fails to include a viable Dark Matter candidate, capable of explaining observations- and *required* in the *cosmological structure formation* context. Furthermore, it does not tackle the hierarchy or neutrino masses problems, nor explains the origin of the clear *matter/anti-matter asymmetry* we observe in the Universe today; But more importantly for us, it does not provide an explanation for *dark energy*, nor includes a spin-2 field (massless particle) in its field content which would be responsible for long-range gravitational interactions - the so-called *graviton*. Thus, the SM provides an accurate enough (at low energies), but most definitely *effective* description of a more fundamental theory. The recent confirmation of a 20 year old ($\sim 4\sigma$) discrepancy between the SM prediction and observed values of the anomalous magnetic dipole moment of the muon (the so called g-2 anomaly) by the Fermilab collaboration is both proof of its enormous success and might as well be the very first failure of the SM [6]. At the same time, a *(statistically) less-significant* ($\sim 2\sigma$) deviation from the SM prediction has been observed at the LHCb experiment[68] . Thus supporting the evidence for new physics.

The Standard Model of Cosmology

On the other hand, *General Relativity* (GR) provides an equally good description of gravitational interactions. According to Einstein, gravity would be nothing more than the manifestation of the curvature of spacetime, in the presence of matter/energy. Moving bodies would then naturally follow geodesics (straight lines) in a curved space-time. Technically speaking, GR is said to be invariant under diffeomorphisms. In practice, this implies that the laws of physics should remain unchanged when changing the coordinate system. This has profound (sometimes counter-intuitive) implications[1], as we shall later discover

[1] Such phenomena include length contraction, time dilation or the bending of light near massive objects. The most famous one being the Perihelion precession of Mercury.

in this thesis. Since the time of Einstein, countless theoretical - general relativistic - predictions have been experimentally verified. Without GR ever failing a single one of these tests. When applied to the Universe as a whole, the field of Cosmology, Einstein quickly realized the Universe cannot be static, if described by the laws of GR[2]. In the late 1920's, E. Hubble discovered that distant galaxies where receding away from us, with a speed proportional to their distance - the so-called *Hubble's law* $v = H_\circ \ d$ - which ultimately implied that the universe was indeed expanding[120]. Another crucial implication of allowing for a dynamical spacetime, is the existence of *gravitational waves* (GW). These are ripples in the fabric of spacetime that can propagate freely throughout the universe. The existence of these waves was the last major prediction by Einstein's theory of GR. The discovery of the former over a century after the theory's prediction by the LIGO/VIRGO collaborations[3]was the ultimate test of General Relativity. Due to its *tremendous success*, GR remains the most widely accepted framework for describing gravitational interactions.

Nonetheless, in order to accommodate observations on the largest (cosmological) scales, GR requires a mysterious form of (what appears to be constant) energy density across space and time - with equal in magnitude, but opposite in sign, pressure $w_{\text{DE}} = \frac{P}{\rho} \simeq -1$. What is commonly referred to as *Dark Energy*. Indeed, by the end of the twentieth century, observations from two independent teams using 42 distant supernovae revealed that the expansion of the universe had been accelerated for the past 5 billion years. The urge to understand the reason for this acceleration has driven the field of precision cosmology for the last decades and remains today one of the *biggest open questions in fundamental physics*. Hence, the prevailing paradigm in cosmology is that of an expanding Universe; In which the late-time accelerated stage of expansion is driven by a *cosmological constant* Λ. However, the mismatch between observed and predicted values for Λ - from the otherwise *successful SM framework* - is 120 orders of magnitude away, when interpreted as *vacuum energy* in a *Quantum Field Theory* (QFT) context. Making it the *biggest failure* in theoretical physics. Moreover, ordinary matter, as described by the SM of particle physics, only accounts for $\sim$ 20% of the matter density needed for galaxies and clusters of galaxies to form. The remaining $\sim$ 80% would be in a form of non-relativisitic (cold) and non-interacting (dark) matter - the so-called *Cold Dark Matter* (CDM). This model is known as the *Concordance Model*, or ΛCDM and *it is the best and most widely accepted model describing the universe today*.

[2] Upon which, he introduced a constant Λ in his field equations, to ensure the Universe remains unchanging.

Fundamental and Observational Issues

At the fundamental level, there are many reasons to go beyond Einstein's theory of gravity. It is well known that GR suffers from a singularity at early times (where QM plays a crucial role). Within the standard QFT prescription, Classical Physics emerges as constructive interference of probability amplitudes given in terms of Feynman Diagrams (in the path integral approach). GR however is a purely classical (geometrical) theory. At high-energies, the theory breaks down. A quantum description of gravitational interactions is needed to describe such high-energies - what is commonly referred to as *Quantum Gravity*. It has proven to be an incredibly difficult challenge to reconcile these two theoretical giants into a unified framework. Similarly, even if we decided to postpone or ignore the problem of the initial singularity (at the Big Bang), there is now irrefutable evidence for the existence of Black Holes (BH), objects where we know GR fails [3][180].

Moreover, aside from theoretical issues, as experimental and theoretical precision have rapidly increased, the concordance Model of cosmology might be starting to show some of its very first cracks. Suggesting that perhaps the simple Λ is just an effective description, and that we might need to go beyond this simple and elegant -although phenomenological- framework. The most interesting example being the discrepancy in the value of H_0 as inferred from early universe observables such as the *Cosmic Microwave Background* (CMB), assuming ΛCDM and local (late-time) measurements using calibrated *Type Ia Supernovae* (SNeIa), and as reported by various other (low-z) observational probes. A milder, but longstanding tension also exists in the amplitude of matter fluctuations σ_8 (or more recently $S_8 \equiv \sigma_8\sqrt{\Omega_m/0.3}$) - as measured by *weak lensing* (WL) surveys[67, 111] and the one inferred using CMB observations[69] - characterizing the *smoothness or clumpiness* in the (matter) density field in the late-universe. In the last couple of years, a lot of effort has gone in trying to address and come up with solutions to these tensions [83, 84, 184].

While the physical mechanism for the late-time accelerated expansion of the universe remains an open question, its phenomenology is known with ever increasing accuracy. Cosmology is said to be living in its Golden Era, where precise measurements allows us to rule-out or at least tightly constrain many alternative cosmological scenarios. Any viable beyond-ΛCDM candidate must therefore be able to, in some sense, reproduce the ΛCDM phenomenology (at the background level at least). The urge to try and solve these "discrepancies" has launched a huge theoretical (model-building) program, and many extensions to the simple ΛCDM picture have been proposed over the years. Because of its simplicity - and in view of *Occam's*

[3] Sir. Roger Penrose showed that singularities are unavoidable in GR, which got him the 2020 Nobel Prize in Physics.

razor - the ΛCDM remains the preferred model by observations, and has proven to be extremely robust to any changes in its content.

Possible Extensions and The Road Ahead

It is therefore quite natural (and very much needed) to explore modifications of the gravitational sector beyond General Relativity. Although this idea has attracted a lot of interest in the last decades, GR turns out to be the unique theory [155] one can write in 4 dimensions, yielding second order equations of motion - the *Einstein Field Equations*. In practice, this implies that if one is to modify the gravitational sector, one has to give up or relax some of its assumptions.

While the particle physics of Inflation is still unknown, observations of the CMB and LSS seems to favor a Gaussian *nearly adiabatic, nearly scale-invariant* primordial spectrum of fluctuations. This is typically achieved by invoking a *slowly-rolling* scalar field - the *inflaton* φ. While interestingly, the Starobinsky inflationary model is a modified gravity of the form $f(R) = R + aR^2$ which provides a very good fit to current CMB data. Such theories are also interesting as they can naturally lead to an accelerated expansion of the Universe because of the presence of the aR^2-term (with $a > 0$). Furthermore, $f(R)$ models are well-known to be conformally equivalent to Scalar-Tensor theories of gravity - which can be thought-of as low-energy descriptions of more fundamental (high-energy) theories. Another "expected" -and highly motivated- DM candidate are *axions*, or *axion-like particles* (ALP). These were first considered by Peccei and Quinn to solve the CP problem in the theory of strong interactions (QCD) [174, 175]. The last missing piece in the SM of particle physics - *the Higgs boson* - predicted in the sixties by P. Higgs, F. Englert and R. Brout was indeed observed more than 5 decades later at the LHC[2]. It is the first experimental evidence for a fundamental scalar (*spin-0*)-field in nature[61, 112]. Many extensions to the SM of particle physics, and to the SM of cosmology involve a scalar field. Scalar fields are also quite natural and expected from a high-energy perspective.

Recent technological progress has made possible to study theories beyond Einstein's GR with gravitational waves. These place stringent constraints on alternative theories of gravity. More specifically, the fact that electromagnetic and gravitational radiation travel at the same speed [4, 5] ruled-out a gigantic class of MG theories (see *e.g.* [75, 95, 125]). Furthermore, next generation of LSS surveys such as Euclid, Nancy Grace Roman Space Telescope (former WFIRST), Vera Rubin Observatory (former LSST) are going to collect enormous amounts of data and are expected to constrain cosmological parameters at the same level

of accuracy as CMB experiments currently do. In the next decades, in combination with space and ground-based 3G Gravitational Waves observatories such as the *Laser Interferometer Space Antenna (LISA)*, *Einstein Telescope (ET)* or *Cosmic Explorer (CE)* and many more, we will probing the dark side of the Universe to unprecedented precision.

Outline

In this thesis, following high-energy physics considerations, we will explore various extensions to the standard ΛCDM paradigm and asses the viability of such models in light of recent observations. Our approach is rather phenomenological, aimed at capturing various types of behaviors while focusing on tools that can efficiently discriminate between the wide variety of Dark Energy and Modified Gravity models, as for the growth index of density perturbations γ. We shall naturally start by reviewing the standard cosmological picture (that of an expanding, homogeneous and isotropic universe) in Chapter 1 and explore its deep connection to an accelerated stage of expansion during the very-early Universe in Chapter 2. In Chapter 3, we briefly review the linear formalism of perturbation theory and derive the basic observables needed throughout this thesis. Chapter 4 is devoted to modified theories of gravity and other extensions to the ΛCDM paradigm. In particular, we discuss a large family of models belonging to the *Horndeski class* and briefly review current observational constraints - specifically, those coming from recent gravitational wave observations- and further motivate higher-dimensional theories of gravity. We will then apply the formalism developed in Chapter 3 to the (linear) growth of matter perturbations in Chapters 5 and 6. In particular, we shall focus on the dynamics of the growth index γ using dynamical system techniques, considering simple extensions to the standard paradigm (Λ) *e.g.* a varying EoS $w_{\rm DE}(a)$, a phenomenological $f(R)$-like bump/dip in $G_{\rm eff}(z)$, in the presence of an unclustered *(axion/neutrino-like)* component during matter domination and in braneworld models, such as the Dvali-Gabadadze-Porrati model[89]. Finally, in Chapter 7, following the aforementioned (high-energy physics) considerations, we investigate the possibility that the dark sector of our Universe contains a negative cosmological constant, dubbed λ. We explore the impact of introducing λ and further asses the viability of such models when incluiding *Baryon Acoustic Oscillations*(BAO), SNeIa and (geometrical) CMB data. We performed a *Nested sampling* of the parameter space, thus obtaining the *(Bayesian) evidence* needed for model selection.

Part I

Foundations of Modern Cosmology

"It seems that scientists are often attracted to beautiful theories in the way that insects are attracted to flowers — not by logical deduction, but by something like a sense of smell."

Steven Weinberg

1

Cosmology in a Nutshell

The Homogeneous Universe: A Review. The aim of this chapter, is to provide the reader with a pedagogical, self-contained introduction to the material needed throughout this thesis. We will review the very basics of what is now well-established, textbook material in Cosmology -*i.e.* an isotropic and homogeneous spacetime- focusing on the derivation of the observables we will be needing in this work. The reader familiar with these concepts is invited to proceed to the next chapters.

1.1 An Isotropic and Homogeneous Universe

1.1.1 The Cosmological Principle and the RW metric

The night sky may not look the same to us, depending on the direction we observe, but when averaging the matter distribution over large distances[1], the Universe seems to be isotropic, meaning that there is no *preferred* direction. Most of our cosmological models today rely on the assumption that the universe at large scales is homogeneous and isotropic - commonly known as *The Cosmological Principle*. Observations of the Universe on the largest of scales (Large Scale Structure - **LSS**) as shown on the left in Figure 1.1.1, among others, seems to be supporting this assumption. Moreover, fluctuations in the temperature of the *Cosmic Microwave Background* (**CMB**) have been measured to be of the order of $\frac{\delta T}{T} \sim 10^{-5}$[69] around the average temperature of 2.7251 K[100], just a few degrees above absolute zero (right panel in Figure 1.1.1).

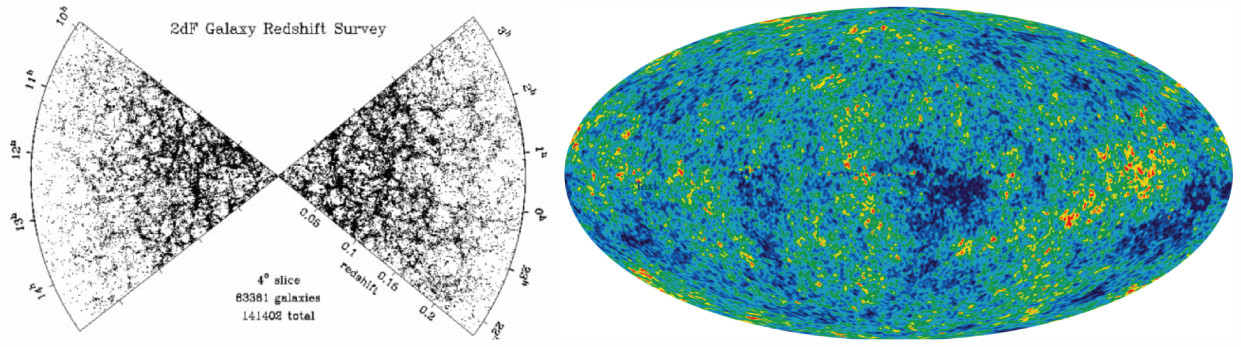

Figure 1.1.1: Left Panel: Distribution of galaxies as a function of distance, taken by 2dFGRS / Sloan Digital Sky Survey (SDSS III)[70]. Each point represents a galaxy, containing about 100 billion stars each. Right Panel: Cosmic Microwave Background Radiation,the heat remnants of the big bang taken by Planck satellite.

The Cosmological Principle, in a way, is just a humble restatement of saying that *we* -conscious observers- are in no *privileged* part of the Universe. After all, the laws of physics governing the evolution of the universe, from its earlier stages up until now, should hold -independently of the location we consider.

[1] This assumption is valid at cosmological scales (a few Mpc), or for wavenumbers $k \lesssim 0.1$ Mpc^{-1}

The Friedmann-Lemaître-Robertson-Walker Universe

Modern Cosmology relies on the homogeneity and isotropy assumptions discussed earlier. These assumptions can be encoded into a single mathematical object, called *The Robertson-Walker Metric* (**RW**). The line element in a FLRW spacetime is most commonly expressed in polar comoving coordinates and physical time t by :

$$ds^2 = g_{\mu\nu}dx^\mu dx^\nu = -dt^2 + a^2(t)\left[\frac{dr^2}{1-kr^2} + r^2 d\Omega^2\right], \qquad d\Omega^2 \equiv d\theta^2 + \sin^2\theta d\varphi^2 \ . \tag{1.1}$$

Where we characterize its geometry by the means of a constant k, taking the discrete values $k \in \{-1, 0, 1\}$ corresponding to *open*, *flat* and *closed* geometries respectively. Notice the scale factor $a(t)$ multiplying the spatial components of the metric, reflecting the dynamical property of spacetime (expansion).

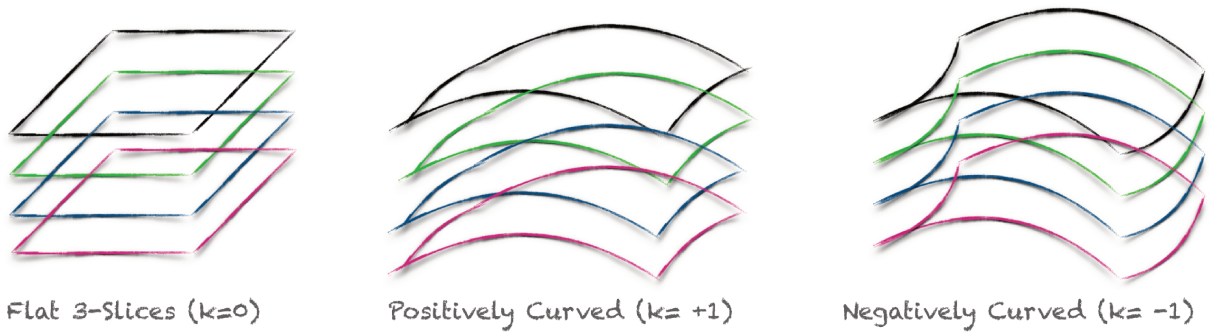

Figure 1.1.2: 3-dimensional hypersurfaces Σ_t at different times t, representing the different possible geometries of the universe. Each slice corresponds to a moment in time. Space-time can be thought of as a collection of time-ordered 3-dim hypersurfaces, characterized by the induced metric γ_{ij} defined on such (curved) hypersurfaces (the so-called 3+1 decomposition).

The *metric* fully describes a space and its geometrical properties. As we will discover, more complicated objects can be obtained from the metric. Two crucial objects in GR and differential geometry in general are the Riemann and Ricci tensors, which will be defined in due time.

The Robertson-Walker (RW) metric takes the following matrix form:

$$g_{\alpha\beta} = \begin{pmatrix} -1 & 0 & 0 & 0 \\ 0 & \frac{a^2(t)}{1-kr^2} & 0 & 0 \\ 0 & 0 & a^2(t)r^2 & 0 \\ 0 & 0 & 0 & a^2(t)r^2 \sin^2\theta \end{pmatrix} \tag{1.2}$$

Notice the off-diagonal elements of the metric (1.2) all vanish. Having any non-zero element off the diagonal would imply a preferred spatial direction. The same argument will considerably simplify our calculations throughout this work.

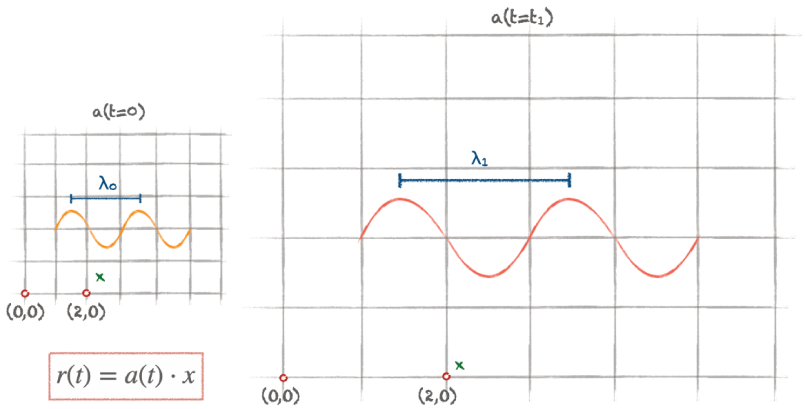

Figure 1.1.3: Illustration of a comoving coordinate system. The lefthand side shows a grid-like coordinate system at $t = 0$, $a(t)$ is the scale factor accouting for the expansion of spacetime. The righthand side shows the same coordinate system some later moment in time $t = t_1$. Notice the *comoving coordinates* x^i are the same for the two red points, but the physical distance separating them has grown by a factor of $a(t)$. The scale factor $a(t)$ inherits the physical interpretation of distance and becomes the important variable that we need to keep track of. In orange, we represent a photon, whose initial wavelength λ_1 gets *strechted* as the universe expands with time.

In a comoving coordinate system, we have the relation $r = a(t)x$, from which we obtain :

$$u = \frac{dr}{dt} = \dot{a}(t)x + a(t)\dot{x} \equiv H(t)r + v_{\text{pec}}, \tag{1.3}$$

where r is called the *proper*, or *physical coordinate*, and x are *comoving coordinates*. The first term in (1.3) is dubbed *the Hubble flow* coming from the expansion of the universe, and the second term comes from the

peculiar motions $v_{\rm pec} \equiv a\dot{x}$. Notice we have explicitly introduced the Hubble parameter $H \equiv \frac{\dot{a}}{a}$. This is an extremely important quantity in cosmology, as it encodes the rate at which the universe expands with time. Its value today is called the Hubble constant H_0, it has units of inverse time and allows to determine the age and size of the Universe, as it sets a fundamental time and thus length scale $d \sim H_0^{-1}$ in spacetime. Measuring this quantity is crucial in cosmology. Notice also how by ignoring the contribution from the peculiar motion $v_{\rm pec}$, we recover the famous Hubble law $v = H_0 d$ [120]. Nonetheless, the study of peculiar velocities turns out to be extremely useful for constraining the growth of structure in the largest of scales, and therefore to probe the underlying laws of gravity, as we shall discuss in Chapters 3, 4 and 5.

1.1.2 From Einstein to Friedmann

In GR, the fundamental (spin-2) field is the metric $g_{\mu\nu}$. The **Einstein Field Equations** (EFE) can (somewhat elegantly) be obtained by varying the Einstein-Hilbert action $S_{EH} \equiv \int d^4x\sqrt{-g}R$ w.r.t the inverse metric $g^{\mu\nu}$.

$$\delta S_{\rm EH} = \delta \int_\Omega d^4x\sqrt{-g}R = \int d^4x\{(\delta\sqrt{-g})R + \sqrt{-g}\delta R\} \ , \tag{1.4}$$

where g is the determinant of the metric $g_{\mu\nu}$, which stems from the fact that the volume element d^4x is not invariant under diffeomorphisms but transforms as $d^4x \to |J|d^4x'$, where $|J|$ is the determinant of the Jacobian Matrix $|J| = \frac{\sqrt{-g'}}{\sqrt{-g}}$. Thus the combination $\sqrt{-g}d^4x$ becomes the relevant *invariant* quantity. The first term in Eq (1.4) gives a famous result worth remembering from GR, we will extensively use this result on the following chapters. Namely

$$\delta\sqrt{-g} = -\frac{1}{2}\sqrt{-g}g_{\mu\nu}\delta g^{\mu\nu} \tag{1.5}$$

The second term in the integral (1.4) can easily be evaluated using the definition of the Ricci scalar

$$\delta R = \delta(R_{\mu\nu}g^{\mu\nu}) = \underbrace{\delta(R_{\mu\nu})g^{\mu\nu}}_{=0} + R_{\mu\nu}\,\delta g^{\mu\nu} \ . \tag{1.6}$$

The first term in Eq.(1.6) vanishes in account for Gauss theorem, it corresponds to a boundary term and can be written as a total derivative and integrated out by impossing that the variations of the metric vashishes

at the boundary, *i.e.* $\delta g^{\mu\nu}|_{\partial\Omega} = 0$. Then, by imposing Eq (1.4) = 0, we finally get

$$\int d^4x(\sqrt{-g})\{R_{\mu\nu} - \frac{1}{2}g_{\mu\nu}R\} = 0 \ . \tag{1.7}$$

The terms in the brackets are the Field Equations *in vacuum*, or the so-called *Einstein tensor* $G_{\mu\nu}$. In order to include any form of energy (matter) we need to modify Eq. (1.4) to include an action S_m describing the matter fields. This is done by writting $\delta S = \delta S_{\text{EH}} + \delta S_m$ and defining the *Energy-Momentum tensor* for matter $T_{\mu\nu}$ as

$$T_{\mu\nu} = -\frac{2}{\sqrt{-g}}\frac{\delta(\sqrt{-g}\mathcal{L}_m)}{\delta g^{\mu\nu}} \ . \tag{1.8}$$

In which case, the full Einstein Field Equations in the presence of any form of matter simply reads

$$G_{\mu\nu} \equiv R_{\mu\nu} - \frac{1}{2}g_{\mu\nu}R = \kappa T_{\mu\nu} \tag{1.9}$$

where $\kappa \equiv 8\pi G/c^4$ is the coupling of matter to the geometry[2] and is chosen such that in the weak-field limit, the equations reduce to that of Newtonian gravity.

Uniqueness of GR

It turns out that the only possible modification we can do[3] to Eq. (1.4) is to include a constant Λ in the action such that

$$S = \frac{M_{\text{pl}}^2}{2}\int_\Omega d^4x\sqrt{-g}\,(R - 2\Lambda) \ , \tag{1.10}$$

leading to the modern version of the Einstein equations

$$\boxed{R_{\mu\nu} - \frac{1}{2}g_{\mu\nu}R + \Lambda g_{\mu\nu} = \frac{8\pi G}{c^4}T_{\mu\nu}} \tag{1.11}$$

We shall come back to the different ways one can extend the gravitational sector - beyond the simple Λ - in Chapter 4.

[2] We have explicitly reintroduced the speed of light $c \simeq 3 \cdot 10^8$ m.s^{-1}, showing how we need gigantic amounts of energy densities, such as two merging Black Holes, to generate disturbances in the geometry of the Universe (gravitational waves)- Because of the factor c^4 in the denominator.

[3] This has been proven in [155] and goes by the name of *Lovelock's Theorem.*

1.1.3 The geometry of FLRW universes

As discussed earlier, the Einstein field equations relate the energy content of the universe encoded in the Stress-Energy tensor $T_{\mu\nu}$ to its geometrical properties encoded in the Einstein tensor $G_{\mu\nu}$ through the relation $G_{\mu\nu} = \kappa T_{\mu\nu}$. We have to calculate the geometrical properties that characterizes the FLRW universe. In other words, we have to calculate the Christoffel connections associated with (1.1), from which we will derive all the rest. For this, it is convenient to rewrite Eq. (1.1) as:

$$ds^2 = -dt^2 + a^2(t)\gamma_{ij}dx^i dx^j \ , \tag{1.12}$$

where we have isolated the spatial components γ_{ij} of the metric $g_{\mu\nu}$, the so-called *induced metric* (*c.f.* Fig. 1.1.2). The Christoffel connections associated with $g_{\mu\nu}$ are as usual given by

$$\Gamma^{\rho}_{\mu\nu} = \frac{1}{2}g^{\rho\sigma}(\partial_\mu g_{\nu\sigma} + \partial_\nu g_{\mu\sigma} - \partial_\sigma g_{\mu\nu}) \ . \tag{1.13}$$

In a FLRW universe, all the off-diagonal elements of $g_{\mu\nu}$ are zero. From this, we immediately see that $\Gamma^0_{00} = 0$ since the only contribution would be coming from the $\sigma = \rho = 0$, where $g_{00} = constant$. The sum of derivatives of the metric in parenthesis vanishes. Similarly, because we assumed space to be isotropic, we can conclude that $\Gamma^i_{00} = \Gamma^0_{i0} = \Gamma^0_{0i} = 0$ since having any single one of these connections different from zero would imply a *preferred direction*, therefore violating the *isotropy assumption*. The remaining (non-vanishing) Christoffel symbols are given by[4]:

$$\Gamma^i_{j0} = \Gamma^i_{0j} = \frac{\dot{a}}{a}\delta^i_j \quad , \qquad \Gamma^0_{ij} = \Gamma^0_{ji} = a\dot{a}\gamma_{ij} \equiv a^2 H\gamma_{ij} \ , \tag{1.14}$$

$$\Gamma^i_{jk} = \frac{1}{2}\gamma^{il}(\partial_j\gamma_{kl} + \partial_k\gamma_{jl} - \partial_l\gamma_{jk}) \ , \tag{1.15}$$

Where γ_{ij} is the spatial part of the RW metric and we have introduced the Hubble parameter $H \equiv \frac{\dot{a}}{a}$. For the sake of simplicity, we will derive the Friedmann equations in a Flat Universe where $k = 0$ and so $\gamma_{ij} = \delta_{ij}$ and thus $\Gamma^i_{jk} = 0$, but keep in mind that in general, these connections do not vanish. We now have the

[4] We have used the fact that for a Torsion-free metric, which is assumed throughout this work, the connection is symmetric in their lower components $\Gamma^a_{\nu\mu} = \Gamma^a_{\mu\nu}$.

ingredients to calculate the Riemmann Curvature Tensor :

$$R^{a}{}_{\beta\mu\nu} \equiv 2\partial_{[\mu}\Gamma^{a}_{\nu]\beta} + 2\Gamma^{a}_{\sigma[\mu}\Gamma^{\sigma}_{\nu]\beta} \ , \tag{1.16}$$

From which we obtain the Ricci tensor

$$R_{\mu\nu} \equiv R^{\sigma}_{\mu\sigma\nu} = \partial_{\sigma}\Gamma^{\sigma}_{\mu\nu} - \partial_{\nu}\Gamma^{\sigma}_{\sigma\mu} + \Gamma^{\sigma}_{\sigma\rho}\Gamma^{\rho}_{\mu\nu} - \Gamma^{\sigma}_{\nu\rho}\Gamma^{\rho}_{\sigma\mu} \ , \tag{1.17}$$

and Ricci scalar (also called Scalar Curvature) defined as $R = R_{\mu\nu}g^{\mu\nu} = R^{\mu}_{\mu}$. Again, using the symmetries of the metric we can easily conclude that $R_{0i} = 0$. We are left with the (00)-component of the Riemman Tensor

$$R_{00} = -\partial_t(3H) - 3H^2 = -3(\dot{H} + H^2) \ , \tag{1.18}$$

and the spatial components R_{ij} of the Riemann tensor yield

$$R_{ij} = \partial_t(a^2\delta_{ij}H) + 3a^2\delta_{ij}H^2 - 2a^2\delta_{ij}H^2 = a^2\delta_{ij}(\dot{H} + 3H^2) \ . \tag{1.19}$$

Ultimately leading to the Ricci scalar $R = 6(H^2 + \ddot{a}/a)$. The geometrical picture being complete, *i.e.* the LHS of (1.9) defined, we need to further specify the matter (or energy) content of our Universe. Once again, and from simple symmetry arguments we can already deduce that the stress-energy tensor $T_{\mu\nu}$ must be a diagonal tensor, since any non-zero component outside the diagonal would again imply a preferred direction. Thus, we can stipulate:

$$T_{00} = \rho(t), \qquad T_{0i} = 0 \qquad \text{and} \qquad T_{ij} = g_{ij}P(t) \ . \tag{1.20}$$

In FLRW universes, we will use (comoving) perfect fluids, whose energy-momentum tensor $T_{\mu\nu}$ is given by[5]

$$T_{\mu\nu} = (\rho + P)u_{\mu}u_{\nu} + g_{\mu\nu}P, \tag{1.21}$$

where $u^{\mu} = (1, 0, 0, 0)$ is the four-velocity of a comoving fluid and $g_{\mu\nu}u^{\mu}u^{\nu} = -1$. Taking (1.21) together

[5] In general, for a real fluid, the stress-energy takes the same form $T_{\mu\nu} = (\rho + P)u_{\mu}u_{\nu} + g_{\mu\nu}P + \Pi_{\mu\nu}$ - Where $\Pi_{\mu\nu}$ is the anisotropic-stress, encoding the deviations from a perfect fluid. It is well known that neutrinos, because of their free-streaming, induce a small but non-vanishing anisotropic stress. In the remaining of this thesis, we shall neglect this effects and set $\Pi_{\mu\nu} = 0$.

with (1.18) and (1.19) (with $k = 0$) leads to

$$H^2 \equiv \left(\frac{\dot{a}}{a}\right)^2 = \frac{8\pi G}{3}\rho(t) \qquad \text{and} \qquad \frac{\ddot{a}}{a} = -\frac{4\pi G}{3}(\rho + 3P) \ . \tag{1.22}$$

We have derived the Einstein Equations for a flat FRLW metric, if we allow for an arbitrary curvature term k, one finds that the Friedmann Equations can be written as :

$$\boxed{H^2 \equiv \left(\frac{\dot{a}}{a}\right)^2 = \frac{\rho}{3M_{\rm pl}^2} - \frac{k}{a^2}} \tag{1.23}$$

Where $M_{\rm pl}^{-2} \equiv 8\pi G$ and G is the usual newtonian gravitational coupling constant

$$\boxed{\frac{\ddot{a}}{a} = H^2 + \dot{H} = -\frac{1}{6M_{\rm pl}^2}(\rho + 3P)} \tag{1.24}$$

By defining a critical density $\rho_{\rm cr} \equiv 3H^2M_{\rm pl}^2$, we can rewrite equation (1.23) in terms of the fractional energy density $\Omega \equiv \frac{\rho}{\rho_{\rm cr}}$ to give

$$\Omega - 1 = \frac{\rho}{3H^2M_{\rm pl}^2} - 1 = \frac{k}{a^2H^2} \equiv \Omega_k \ . \tag{1.25}$$

The critical energy density today $\rho_{\rm cr,0}$ has been measured to be[224]

$$\rho_{cr,0} = 3M_{\rm pl}^2\, H_0^2 = 1.878\,340(4) \times 10^{-29}\, h^2\, {\rm g\,cm^{-2}} \ . \tag{1.26}$$

Where we have introduced the reduced Hubble parameter h, which characterizes our ignorance on the measure of the Hubble constant H_0 through the relation

$$\boxed{H_0 = 100\,h \ \ {\rm km/s/Mpc}} \qquad \text{and} \qquad \boxed{h \simeq 0.67} \ . \tag{1.27}$$

The *"true"* value of h is a highly debated topic in the literature, but quite likely lies within the range $0.67 < h < 0.76$. We shall later see in Chapter 7, how this discrepancy in the measurement of H_0 might be interpreted as a sign of new physics, beyond the standard ΛCDM picture. Already at this stage, we see once again the direct relation stated by Eq. (1.1) between k and the geometry of the universe. It turns out

that Eq.(1.25) is an unstable fixed point for the dynamical system, as we will later discuss in chapter 2. For now, let us just state that the universe had to have the exact amount of energy density ρ_{cr} in order to stay flat. Which requires a *gigantic* amount of fine-tunning (see 2). From now on, we shall consider $k = 0$, as geometrical probes (BAO+CMB) suggest the universe is extremely close to being flat[6]. One important quantity in observational cosmology is the Hubble Radius

$$R_H = \frac{1}{H(t)} \,, \tag{1.28}$$

which has units of length. The co-moving Hubble Radius is thus given by $(aH)^{-1}$. We will see in Chapter 2 the crucial role played by the comoving Hubble radius during the inflationary epoch. It is closely related to the curvature Ω_k, as can be seen from (1.25).

Stress-Energy and Conservation laws

In order to relate the physical quantities accessible today, and compare them to the theoretical predictions at a certain epoch in the cosmic history, we need to determine how these quantities evolve with time. As a consequence of the Bianchi Identities ($\nabla_\mu G^{\mu\nu} = 0$) we get:

$$\nabla_\mu T^{\mu\nu} = 0 \tag{1.29}$$

The $\nu = 0$ component yields the conservation of energy

$$\dot{\rho} + 3\frac{\dot{a}}{a}(\rho + P) = 0 \tag{1.30}$$

It is of common practice at this stage to introduce the equation of state parameter $w \equiv P/\rho$. Rewriting in

[6] Planck's satellite found $\Omega_{k,0} \simeq 0.0007$[69]. See also recent discussions on spatial curvature in [229]

terms of w and using the fact that $H = \partial_t \ln a$, Eq. (1.30) becomes[7]:

$$\dot{\rho} = -3H(1+w)\rho \Leftrightarrow d\ln\rho = -3(1+w)d\ln a \ . \tag{1.32}$$

Considering a constant equation of state w, the solution to Eq. (1.32) is given by

$$\boxed{\rho_i \propto a^{-3(1+w_i)}} \tag{1.33}$$

We have the following picture:

$$\rho = \rho_{\rm tot} = \{\rho_r \equiv \rho_\gamma + \rho_\nu\} + \{\rho_m \equiv \rho_b + \rho_{\rm cdm}\} + \rho_\Lambda \tag{1.34}$$

Thus, for presureless matter ($w = 0$) we obtain $\rho_m \propto a^{-3}$ and for radiation, with $w_r = 1/3$ we get $\rho_r \propto a^{-4}$. The vanilla ΛCDM assumes $w_{DE} = w_\Lambda = -1$. In this work, we will not restrict ourselves to a constant w. By allowing for a time variation in $w(a)$ we get

$$\boxed{\rho(a) \propto e^{-3\int_1^a (1+w(a'))d\ln a'}} \tag{1.35}$$

From this, it follows that the relation $\Omega = \rho/\rho_{\rm cr}$ can be generalized to any of the above mentioned components so that $\Omega_i = \rho_i/\rho_{i,\rm cr}$ and

$$\Omega_{\rm tot} = \sum_i \Omega_i = \Omega_r + \Omega_m + \Omega_\Lambda = 1 - \Omega_k \tag{1.36}$$

The Friedmann equations can be cast into the more compact form

$$H^2(a) = H_0^2\left[\Omega_{r,0}\left(\frac{a_0}{a}\right)^4 + \Omega_{m,0}\left(\frac{a_0}{a}\right)^3 + \Omega_{k,0}\left(\frac{a_0}{a}\right)^2 + \Omega_{\Lambda,0}\right] \tag{1.37}$$

[7] As an analogy, one might see Eq. (1.30) as the *first law of thermodynamics*, namely $TdS = dU + PdV$. The internal energy U can be written as $U = \rho a^3$, and volume V as $V = a^3$, therefore obtaining

$$d(\rho a^3) + Pd(a^3) = 0 \Leftrightarrow \dot{\rho} + 3\frac{\dot{a}}{a}(\rho + P) = 0 \tag{1.31}$$

and so we see that the expansion is adiabatic (*i.e.* to a good approximation we have $dS = 0$). This means the energy density ρ and pressure P are intrinsically related to one another and justifies our previous assumption of writting $P = w \cdot \rho$ in terms of an equation of state parameter w.

1.1.4 Distances and Redshift in Cosmology

As a result of the expansion of the universe, the distance between two events in spacetime is always changing. For a really longtime, until very recently with the detection of gravitational waves[8] [3], the only messenger carrying information about the universe's past were photons. It is of extreme importance to understand what happens to light as it travels through an expanding universe if we want to conclude something about the former, just from cosmological observations. As the universe expands (see Fig. 1.1.3) the wavelength λ of light is stretched by a linear factor such that $\lambda(t) \propto a(t)$, which also implies that photons travelling through an expanding universe loose energy as $E(t) \propto a^{-1}$. If we observe light from distant stars, the observed wavelength is larger than the emmited one, is convenient to introduce the redshift factor z defined as

$$z = \frac{\lambda_{\text{obs}} - \lambda_{\text{em}}}{\lambda_{\text{em}}} = \frac{\lambda_{\text{obs}}}{\lambda_{\text{em}}} - 1 \,, \tag{1.38}$$

which implies

$$\boxed{\frac{a(t = t_{\text{today}})}{a(t)} = 1 + z(t) \,.} \tag{1.39}$$

In this thesis, and as usually done in the literature, we set the value of the scale factor today $a_0 \equiv a(z = 0) = 1$. Measuring distances in an expanding universe can be tricky, but fortunately all physical quantities can be obtained from the *Metric* or *Comoving Distance*. Photons follow null geodesics ($ds^2 = 0$) from (1.1) and for $k = 0$, we get the expression for the comoving distance :

$$r(a) = \int \frac{dt'}{a(t')} = \int_a^1 \frac{da'}{a'^2 H(a')} \tag{1.40}$$

Luminosity Distance

In the same way we intuitively estimate the distance to *e.g.* a moving car at night, by looking at its headlights, we can use the light from distant objects with known luminosity, to infer their distance to us. These are the so called *standard candles*. *Type Ia Supernovae* are such candles[9], which ultimately led to the astonishing

[8] On September 14, 2015 at 09:50:45 UTC, shortly after turning on the two detector located at .. opening a new window to study the universe - *The dawn of multi-messenger astronomy*

[9] These are binary systems involving a white-dwarf accreting matter from some other companion star, until the former exceeds the Chandrasekar limit of about 1.44 $M_\odot$ and explodes. Releasing a "standardizable" amount of photons (Luminosity). Another

discovery of our Universe's acceleration[12, 199]. Starting from the flux of light we observe from distant sources, the (bolometric) flux F received is given by $F = \frac{L}{4\pi d^2}$, this then defines the luminosity distance in a cosmological context[113]

$$d_L = \sqrt{\frac{L}{4\pi F}} \,. \tag{1.41}$$

We finally arrive at the expression for the luminosity distance in a spatially flat FLRW universe:

$$d_L(z) = (1+z)\frac{c}{H_0}\int_0^z \frac{dz'}{h(z')}. \tag{1.42}$$

Where we have introduced the dimensionless Hubble parameter $h(z) \equiv H(z)/H_0$.

Angular Diameter Distance

Another useful way of determining distances in astronomy is by measuring the angle of an object (of known physical size) in the sky. As its name suggests, it is defined as the ratio between physical size of an object and its angle subtended in the sky $d_A = \frac{x}{\theta}$. In metric theories of gravity, the following relation holds $d_L(z) = (1+z)\, r(z) = (1+z)^2 d_A(z)$ where d_A is the angular diameter distance. Yielding

$$d_A(z) = \frac{c}{(1+z)}\int_0^z \frac{dz'}{H(z')}. \tag{1.43}$$

In the same way objects with known luminosity distance can be used as standard candles to infer distances, objects with known physical size, can also be used through (1.43) to infer distances. Such objects are called *standard rulers*. One of the most powerful probes in modern cosmology is the BAO scale (*cf.* 1.3.3), which serves as a *standard ruler*.

1.2 The Concordance (ΛCDM) Model

In the standard ΛCDM picture, we assume GR to be the correct theory describing gravitational interactions on the largest of scales. Furthermore, as we previously discussed in Section 1.1.1, it also relies on the assumption that on those scales, the Universe is accurately described by the (flat) FLRW metric (*i.e.* an isotropic & homogeneous spacetime). The late-time accelerated expansion of the universe is driven by a

important example of such standard candles are *Cepheids* - stars whose lumonisity is periodic.

cosmological Λ, whose small value remains a mystery today. This mysterious form of *dark energy* constitutes $\sim 70\%$ of the energy budget of the Universe. Furthermore, a pressure-less fluid ($w = 0$) accounting for $\sim 25\%$ of the energy density is needed for structures to efficiently form at early times. Yet in order to accommodate observations, this particle needs not to (or weakly) interact -other than gravitationally- with the rest of the SM. While ordinary (baryonic) matter constitutes the remaining 5% of the energy density in the universe, the rest is still unknown. This is known as the concordance, or ΛCDM model. It can describe, to some accuracy, a wide variety of observation in the cosmic history. This model is completely specified by 6 parameters, from which we can derive all the rest. The values of these parameters are given in Table 1.2.1.

Notation	Value	Definition	Physical Origin
ω_b	0.02237 ± 0.0015	Fraction of baryons	Baryogenesis
ω_c	0.1200 ± 0.0012	Fraction of Cold Dark Matter	TeV-Scale Physics (?)
$100\theta_s$	1.04092 ± 0.00031	Angular Sound Horizon	Geometrical
$\ln(10^{10}A_s)$	3.044 ± 0.014	Scalar Amplitude	Inflation
n_s	(0.9649 ± 0.0042)	Spectral (Scalar) Index	Inflation
τ	0.0544 ± 0.0073	Optical Depth	First Stars

Table 1.2.1: `PlanckTT+TE+EE+lowE+lens` constraints on the 6 ΛCDM parameters[69]

where the fractional energy densities are typically expressed in terms of physical energy densities

$$\omega_i = \Omega_i h^2, \tag{1.44}$$

and where $h = H_0/100$ eludes to the Hubble constant defined in (1.27). This turns out to be an inferred parameter using θ_s, as we shall discuss in Chapter 7. The parameters A_s and n_s in table 1.2.1 are the amplitude and tilt of (primordial) scalar fluctuations, respectively. τ is dubbed *the optical depth* and is related to reionization epoch and the birth of the first stars. These are free-parameters to be inferred by observations within a given model, namely ΛCDM . Because of its simplicity and its remarkable success to cope with observations, this model provides a benchmark for assessing the viability of more intricate dark energy models. Nonetheless the ΛCDM remains a phenomenological (toy) model, where most of the energy budget in the universe remains in a *dark sector* ($\Omega_{\rm CDM}$, Ω_Λ) - whose fundamental nature is yet unknown. In the next section, we shall go over the most important observational probes, and see how we can constrain

the 6 cosmological parameters of the ΛCDM model.

1.3 Observational Probes

1.3.1 Big Bang Nucleosynthesis

The light elements abundance, as predicted by a hot and dense state in the early universe is a major success of the standard cosmological picture. Observational evidence put stringent bounds on *Big Bang Nucleosynthesis* (BBN) - that is the formation of nuclei (other than a single proton) - to take place during the Radiation Dominated epoch. This is believed to have happen around $z \sim 3 \cdot 10^8$. The quantity ρ_b is very well constrained by BBN studies and is in perfect agreement with CMB observations [69, 226, 242].

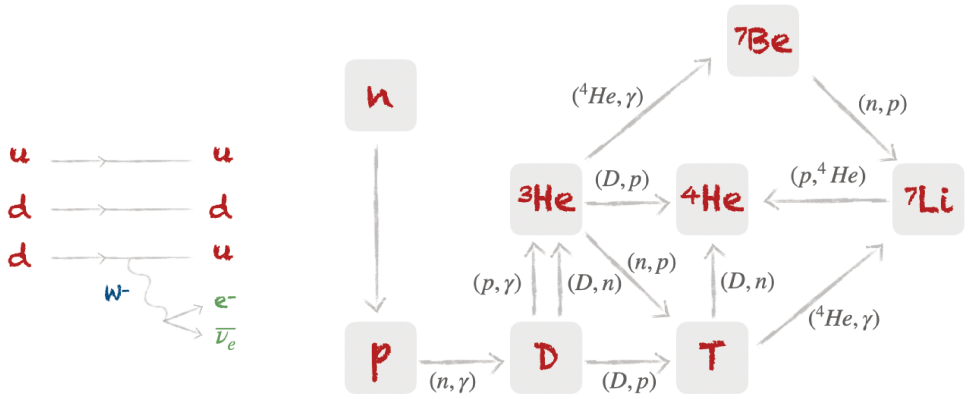

Figure 1.3.1: Schematic view of the relevant processes happening during *Big Bang Nucleosynthesis* (BBN) - The formation of light elements. Essentially all of the elements that are heavier than lithium were cooked and produced much later in the history of our Universe, by *Stellar Nucleosynthesis* in evolving and eventually exploding stars.

Indeed, one intuitively sees from Fig.1.3.1 that the production of light elements in the Universe is highly sensitive to the initial amount of photons and baryons that were present. One of the key quantities in the early Universe, relevant for BBN, BAO and CMB analyses is the *photon-to-baryon ratio*, denoted R and defined in 1.3.3.

Despite the well known ^{7}Li problem, both the deuterium (D) and Helium (^{4}He) predictions from BBN are in excellent agreement with observations[186]. The theory of BBN is thought to be a robust theory, changes to the standard BBN scenario leads to very different predictions for the abundance of light elements, or creates tensions with other cosmological observables. For a recent discussion, see *e.g.* [224, 242] and references therein. Primordial nucleosynthesis is extremely sensitive to the expansion history $H(z)$ at early times, and as such, can been used to constrain deviations from Newton's constant G, thereby placing stringent constraints on deviations from GR at early times- (see *e.g.* [17, 73, 170]). For a thourough review of BBN cosmology see Refs. [76, 163, 186]

1.3.2 Cosmic Microwave Background Radiation

The other pillar of "big-bang" cosmology is the cosmic microwave background (CMB). The reader is referred to *e.g.* Refs. [35, 85, 115, 116] for a more detailed treatment of the CMB anisotropies. During the early universe, photons were tightly coupled to baryons[10] primarily through Thomson scattering.

Recombination

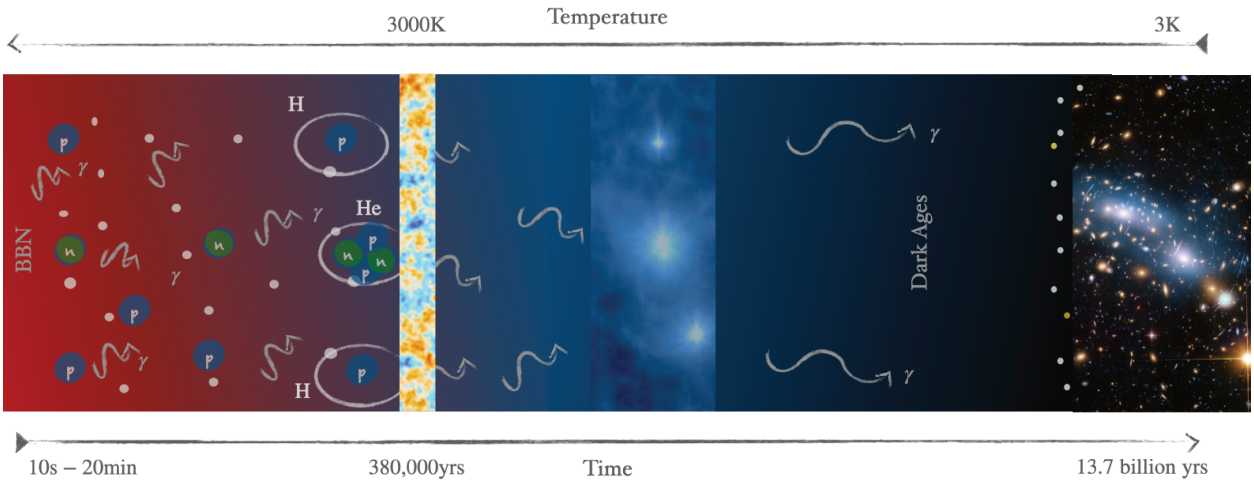

Figure 1.3.2: Schematic picture of recombination.

[10] In the cosmological jargon, by baryons we mean electrons, protons, neutrons, He^{++}, and every ordinary (SM) particles.

At around $z \sim 1089$, or $\sim 380\,000$ years after the "*Big Bang*", the universe became cool enough for the first atoms to form - what is historically referred to as *Recombination*, despite it being the first time atoms form. Prior to that, temperatures and energy densities were extremely high, so that all the matter was in a form of a primordial (ionised) plasma. The Universe was opaque, meaning that no light could escape from the primordial soup of particles (see Fig.1.3.2). At recombination, the first atoms formed and the universe became transparent for the first time, photons could propagate freely throughout the expanding universe. This is the very first light we observe, corresponding to photons scattering for the very last time (surface of last scattering), known as the *Cosmic Microwave Background* (CMB).

This process of recombination is not instantaneous and a lot of progress has been made in this direction since the first model of recombination proposed by J. Peebles in the sixties [176]. Nowadays, many (precise) numerical codes for accurately computing the recombination history of the Universe are freely available. Such codes include (but are not limited to) `HyREC`[16, 139] or `CosmoREC` [212].

Black Body Spectrum

A perfect blackbody with temperature T will emit a spectrum of electromagnetic radiation according to the famous *Planck's law*

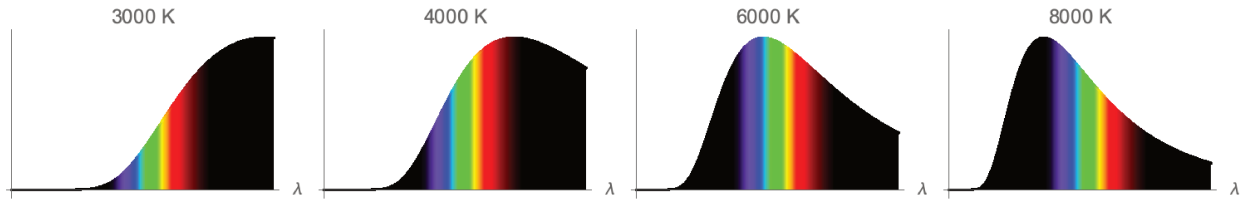

Figure 1.3.3: Blackbody spectrum in the range $10 - 10^3$nm for different temperatures (in K) of the black body. From this, we can estimate with great precision the temperature of the *cosmic microwave background*. The sun's temperature is $T_\odot \sim 5777\,\mathrm{K}$ and thus emits visible light.

$$B(\lambda, T) = \frac{2hc^2}{\lambda^5 \left(e^{\frac{hc}{\lambda k_B T}} - 1 \right)} , \tag{1.45}$$

where k_B is the Boltzmann constant, c is the speed of light and h is Planck's constant. The peak of this radiation is shifted toward higher energies (smaller wavelengths) as the temperature increases, as can be seen

from Fig. 1.3.3. The light we receive from the surface of last scattering, *i.e. the Cosmic Microwave Background* (CMB) is a perfect black body *by definition*. Furthermore, due to expansion of the universe, $T_\gamma \propto a^{-1}$. The initial temperature of $T \simeq 3000$ K decreases with time, and we observe it as a radiation with temperature $T \sim 3$ K, which explains why Penzias and Wilson[181], detected this very first light in the form of (static noise) radio waves (at 4080 Hz) in the sixties. The theoretical understanding of the blackbody radiation by Planck, Einstein and others, ultimately led to the development of Quantum Mechanics. Its application to the physics of the early Universe - prediciting the spectrum of the CMB - is a major success of modern Cosmology. The COBE-FIRAS measurement yielded $T_\circ = 2.7255(6)$ K [100] - perfectly consistent with an idealized blackbody. Indeed, deviations from the perfect blackbody law allows us to constrain any type of exotic energy injection in the early Universe[195, 210]. It is always possible to write

$$T(\nu, n) = T_\circ + \underbrace{\Delta T(n)}_{\text{Anisotropies}} + \underbrace{\Delta T(\nu)}_{\text{Spectral Distortions}} + \underbrace{\delta T(\nu, n)}_{\text{Spectral}-\text{Spatial Distortions}} \tag{1.46}$$

where $T_\circ$ is the average (blackbody) temperature, and n is the direction we observe in the sky. Deviations from Planck's law can depend on: *(i)* on the direction we observe (the well-known CMB anisotropies), *(ii)* the frequency (the so-called y/μ - spectral distortions) and *(iii)* on both (SZ effect)[126] (see *e.g.* [14, 15] and references therein). Because of this, and due to the high level of precision of current CMB experiments, it has proven to be an extremely difficult task to introduce new physics at early times, without spoiling BBN or CMB constraints. Thus, if something funny happens in the early universe that changes the size of the sound horizon, it has to happen just prior to recombination, in order to avoid (as much as possible) current BBN+CMB constraints. This is the motivation behind early-time solutions to the Hubble tension [24, 132, 194]- to change the size of the sound horizon, by injecting energy just prior to recombination - effectively changing the distance at which we observe the CMB[11]. There has been a lot of debate recently in the literature [24, 123, 132, 193] on whether such (early-time) solutions are actually viable.

1.3.3 Baryon Acoustic Oscillations

Because of the large pressure provided by photons, the initial overdensities set up acoustic (sound) waves in the photon-baryon fluid that propagate as long as these two are coupled and behave as a perfect fluid. In

[11] the CMB would appear closer, and therefore we would infer a larger value of $H_\circ$. Another possibility is to play with the value of $z_{\rm rec}$, as discussed in *e.g.* [122, 209].

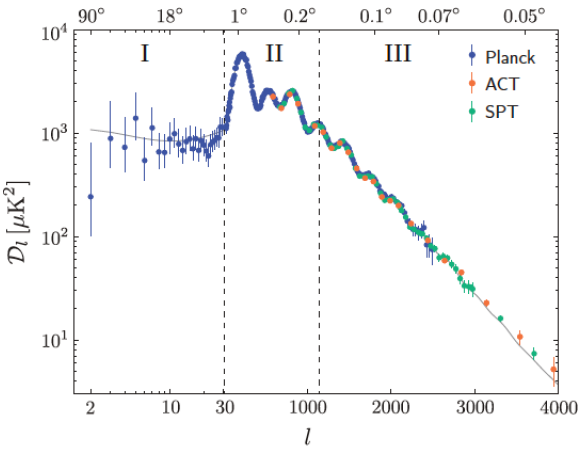

Figure 1.3.4: Angular (Temperature) Power Spectrum of the Cosmic Microwave Background Radiation, as measured by various experiments. Namely, Planck[69], Atacama Cosmology Telescope (ACT)[64] and South-Pole Telescope (SPT)[87]. Solid line represents the ΛCDM prediction. Credit: D.Baumman

Chapter 3, we will further comment on the origin of these propagating acoustic waves.

The sound speed

The sound speed c_s in the photon-baryon fluid determines the speed at which the waves propagate through the plasma, it can be expressed as

$$c_s^2 = \frac{1}{3\left(1+\frac{3}{4}\frac{\rho_b}{\rho_\gamma}\right)} \equiv \frac{1}{3(1+R)} \tag{1.47}$$

where adiabatic primordial fluctuations are assumed. Notice in the last equality, we introduced the photon-to-baryon ratio R. In the limit $\rho_\gamma \gg \rho_b$, we simply get $c_s \simeq \frac{1}{\sqrt{3}}$ which is valid for most of the early (relevant) times. As photons dilute $\rho_\gamma \propto a^{-4}$ and by the time matter comes to dominate, the sound speed $c_s \to 0$. This has important consequences as we shall discuss below.

The sound horizon

An extremely important quantity following from these propogating (acoustic) waves, is the so-called *sound horizon*. This corresponds to the maximum distance the sound wave could have traveled from the big bang,

until recombination. The size of this *sound horizon* can be calculated easily as[91]

$$r_s(z) = c_s \tau_{\rm rec} = \int_0^{t_{\rm rec}} c_s(t) \frac{dt}{a(t)} = \frac{1}{a_0} \int_z^{\infty} c_s(z') \frac{dz'}{H(z')} \,, \tag{1.48}$$

At the time of recombination, photons can propagate freely and hence the acoustic (sound) wave "freezes" and a *characteristic scale* r_s is imprinted in the density field, thereby providing us with a *standard ruler* to measure the Universe's expansion history. Eqs. (1.48) together with (1.47) show the dependence of this quantity on the cosmological parameters, encoded in $H(z)$ and $c_s(z)$- specially on ω_b and ω_γ.

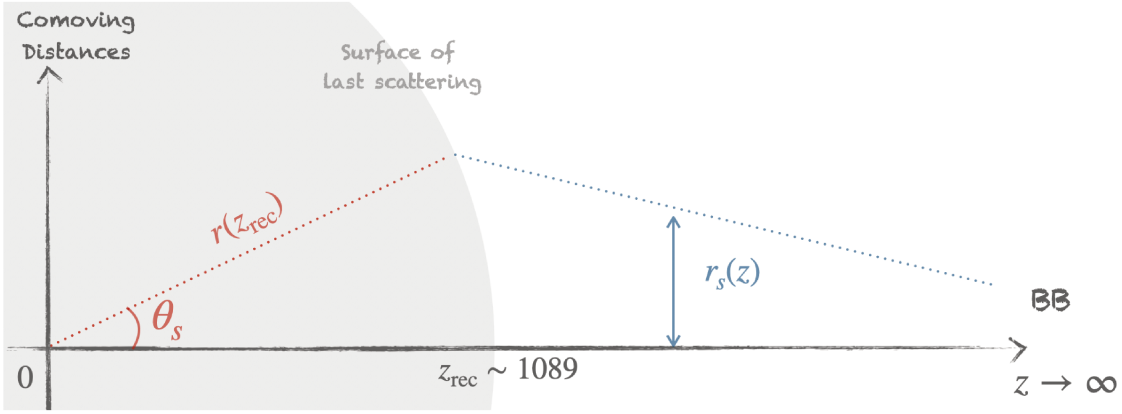

Figure 1.3.5: Schematic view of the sound horizon. From right to left, the sound horizon r_s propagates through the primordial plasma and grows with time, baryons are carried along this propagating sound wave until recombination happens, when the photons decouple from baryons and can propagate freely. The sound horizon "freezes" and a characteristic wavelength is imprinted in the *surface of last scattering* (CMB). We observers, seat at the origin, and should find a correlation between points separated by the comoving length $r_s(z_{\rm rec})$. This has indeed been measured in various observational probes, such as the correlation function (or matter power spectrum) and in the acoustic peaks of the CMB.

Remembering that it is the physical distance $r^{\rm phys} = a \cdot r^{\rm com}$ entering in (1.43), the corresponding angle θ_s subtended in the sky is given by - See Fig. 1.3.5

$$\theta_s = \frac{a_1 \, r_s(z_1)}{d_A(z_1)} \,, \tag{1.49}$$

the comoving acoustic scale is measured to be $r_s \sim 147$ Mpc, and has been detected both in the CMB and LSS observables [67, 79, 93]. The angle θ_s is exquisitely measured by the Planck collaboration [69]. As we

shall later discuss in Chapter 7, the size of the sound horizon plays a crucial role at inferring cosmological parameters, and is tightly related to the so-called *Hubble tension* [24, 132]. The BAO scale r_s constitutes one of the most important observational probes of the (late-time) cosmic acceleration. We refer the reader to Refs. [23, 93, 115, 239] for a more thorough discussion of the physics of BAO.

1.4 Tensions/Anomalies within the Concordance Model

In recent years, several analyses coming from different cosmological probes have reported curiosities between cosmological parameters, as measured in the local (low-z) universe, and high-z, assuming ΛCDM . Two notable examples are H_0 and σ_8 "tensions". Note however, other shortcomings of the ΛCDM at small (galactic) scales paradigm have been pointed out [54]. The reader is referred to [84, 184, 235] for a recent and full account of the challenges the ΛCDM paradigm is facing.

Figure 1.4.1 ***(following page)*:** Compilation of early vs. late-time (local) measurements H_0. Figure taken from [83].

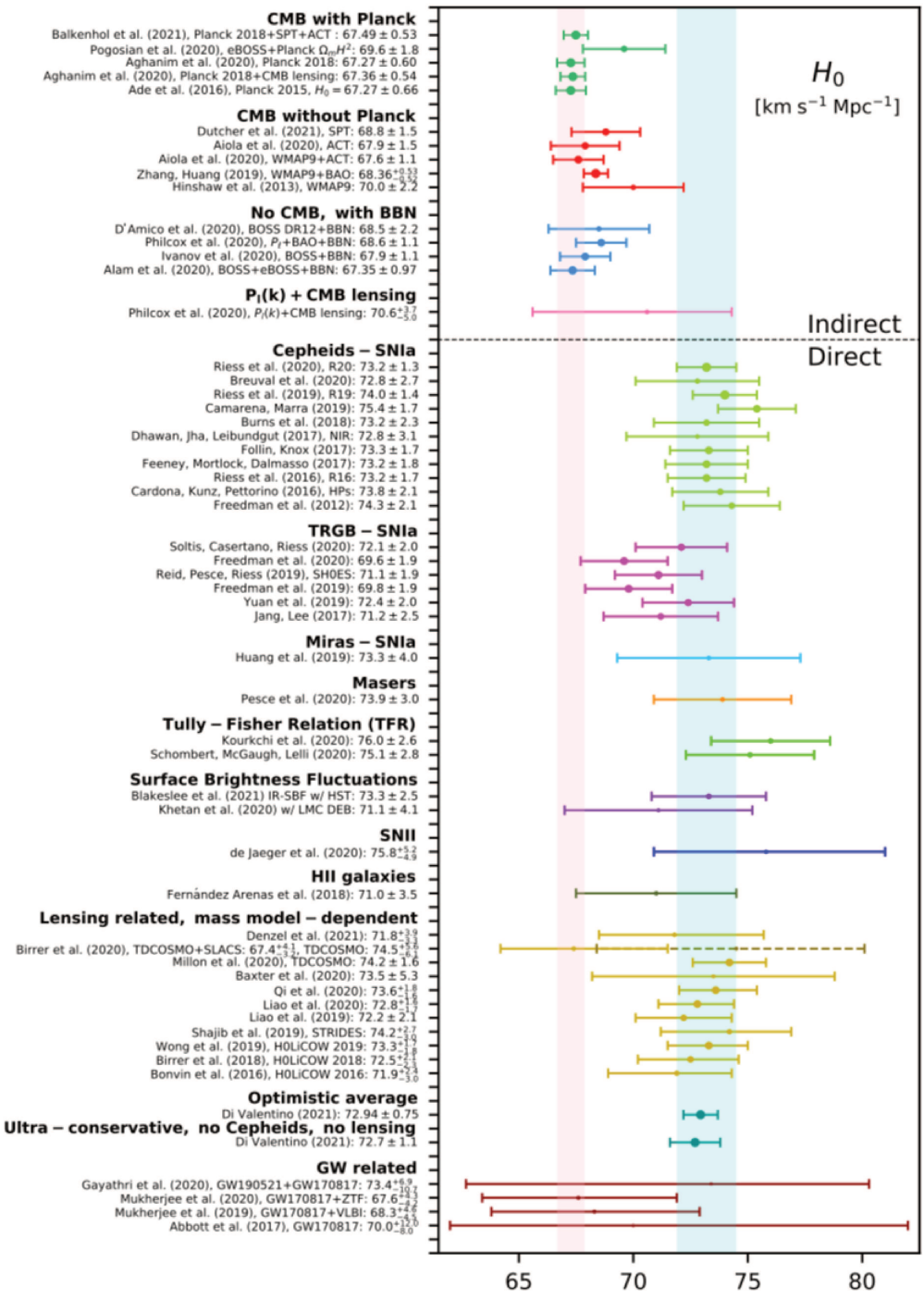
CMB with Planck
Balkenhol et al. (2021), Planck 2018+SPT+ACT : 67.49 ± 0.53
Pogosian et al. (2020), eBOSS+Planck $\Omega_m h^2$: 69.6 ± 1.8
Aghanim et al. (2020), Planck 2018: 67.27 ± 0.60
Aghanim et al. (2020), Planck 2018+CMB lensing: 67.36 ± 0.54
Ade et al. (2016), Planck 2015, H_0 = 67.27 ± 0.66
CMB without Planck
Dutcher et al. (2021), SPT: 68.8 ± 1.5
Aiola et al. (2020), ACT: 67.9 ± 1.5
Aiola et al. (2020), WMAP9+ACT: 67.6 ± 1.1
Zhang, Huang (2019), WMAP9+BAO: 68.36$^{+0.53}_{-0.52}$
Hinshaw et al. (2013), WMAP9: 70.0 ± 2.2
No CMB, with BBN
D'Amico et al. (2020), BOSS DR12+BBN: 68.5 ± 2.2
Philcox et al. (2020), P_l+BAO+BBN: 68.6 ± 1.1
Ivanov et al. (2020), BOSS+BBN: 67.9 ± 1.1
Alam et al. (2020), BOSS+eBOSS+BBN: 67.35 ± 0.97
P_l(k) + CMB lensing
Philcox et al. (2020), $P_l(k)$+CMB lensing: 70.6$^{+3.7}_{-5.0}$
Cepheids − SNIa
Riess et al. (2020), R20: 73.2 ± 1.3
Breuval et al. (2020): 72.8 ± 2.7
Riess et al. (2019), R19: 74.0 ± 1.4
Camarena, Marra (2019): 75.4 ± 1.7
Burns et al. (2018): 73.2 ± 2.3
Dhawan, Jha, Leibundgut (2017), NIR: 72.8 ± 3.1
Follin, Knox (2017): 73.3 ± 1.7
Feeney, Mortlock, Dalmasso (2017): 73.2 ± 1.8
Riess et al. (2016), R16: 73.2 ± 1.7
Cardona, Kunz, Pettorino (2016), HPs: 73.8 ± 2.1
Freedman et al. (2012): 74.3 ± 2.1
TRGB − SNIa
Soltis, Casertano, Riess (2020): 72.1 ± 2.0
Freedman et al. (2020): 69.6 ± 1.9
Reid, Pesce, Riess (2019), SH0ES: 71.1 ± 1.9
Freedman et al. (2019): 69.8 ± 1.9
Yuan et al. (2019): 72.4 ± 2.0
Jang, Lee (2017): 71.2 ± 2.5
Miras − SNIa
Huang et al. (2019): 73.3 ± 4.0
Masers
Pesce et al. (2020): 73.9 ± 3.0
Tully − Fisher Relation (TFR)
Kourkchi et al. (2020): 76.0 ± 2.6
Schombert, McGaugh, Lelli (2020): 75.1 ± 2.8
Surface Brightness Fluctuations
Blakeslee et al. (2021) IR-SBF w/ HST: 73.3 ± 2.5
Khetan et al. (2020) w/ LMC DEB: 71.1 ± 4.1
SNII
de Jaeger et al. (2020): 75.8$^{+5.2}_{-4.9}$
HII galaxies
Fernández Arenas et al. (2018): 71.0 ± 3.5
Lensing related, mass model − dependent
Denzel et al. (2021): 71.8$^{+3.9}_{-3.3}$
Birrer et al. (2020), TDCOSMO+SLACS: 67.4$^{+4.1}_{-3.2}$, TDCOSMO: 74.5$^{+5.6}_{-6.1}$
Millon et al. (2020), TDCOSMO: 74.2 ± 1.6
Baxter et al. (2020): 73.5 ± 5.3
Qi et al. (2020): 73.6$^{+1.8}_{-1.7}$
Liao et al. (2020): 72.8$^{+1.7}_{-1.7}$
Liao et al. (2019): 72.2 ± 2.1
Shajib et al. (2019), STRIDES: 74.2$^{+2.7}_{-3.0}$
Wong et al. (2019), H0LiCOW 2019: 73.3$^{+1.7}_{-1.8}$
Birrer et al. (2018), H0LiCOW 2018: 72.5$^{+2.1}_{-2.3}$
Bonvin et al. (2016), H0LiCOW 2016: 71.9$^{+2.4}_{-3.0}$
Optimistic average
Di Valentino (2021): 72.94 ± 0.75
Ultra − conservative, no Cepheids, no lensing
Di Valentino (2021): 72.7 ± 1.1
GW related
Gayathri et al. (2020), GW190521+GW170817: 73.4$^{+6.9}_{-10.7}$
Mukherjee et al. (2020), GW170817+ZTF: 67.6$^{+4.3}_{-4.2}$
Mukherjee et al. (2019), GW170817+VLBI: 68.3$^{+4.6}_{-4.5}$
Abbott et al. (2017), GW170817: 70.0$^{+12.0}_{-8.0}$
H_0
[km s^{-1} Mpc^{-1}]
Indirect
Direct
65
70
75
80

"... And if inflation is wrong, then God missed a good trick. But, of course, we've come across a lot of other good tricks that nature has decided not to use."

Jim Peebles, interview at Princeton (1994)

2

The Early Universe

Quantum mechanical seeds during the early Universe. The ΛCDM paradigm relies on the assumption of a nearly *adiabatic*, and nearly *scale-invariant* spectrum of primordial fluctuations - as encoded in the amplitude and tilt parameters A_s and n_s, respectively. In this Chapter, we shall briefly introduce one of the most commonly investigated mechanisms responsible for generating these primordial seeds[1] - namely Inflation. In Chapter 3 we will see how through gravitational instability, these tiny (quantum) fluctuations grow to form the LSS we observe in the late-universe. Let us also mention that other alternatives to inflation have been explored in the literature, such as bouncing cosmologies (see *e.g.* Ref. [47]).

[1] And solving the horizon and flatness puzzles.

The Horizon Problem

The (comoving) particle horizon is the maximum distance light could have traveled from time $t = 0$ and time t. It is expressed as

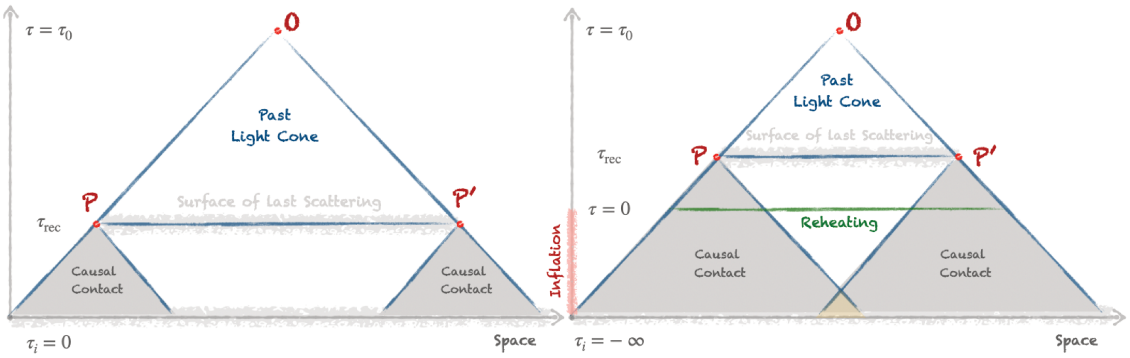

Figure 2.0.1: Schematic representation of the "Horizon problem". *Left Panel:* Points P and P' at the surface of last-scattering never talked to each other, *i.e.* their past light-cones do not overlap in the spacetime diagram. A straightforward calculations leads to $\sim 10^5$ casually disconnected regions in the CMB. Yet, regardless of the direction we observe in the sky, the temperature appears to be homogeneous, with small fluctuations $\mathcal{O}(10^{-5})$ around the mean.*Right Panel:* Solution by the inflationary paradigm. The big bang singularity is pushed to the infinite past $\tau_i \to -\infty$.

$$\tau = \int_0^t \frac{dt'}{a(t')} = \int_0^{t(a)} \frac{da'}{a'^2 H(a')} = \int_z^\infty \frac{dz'}{H(z')} \,, \tag{2.1}$$

This defines regions in spacetime that are causally connected - as depicted in Fig. 2.0.1. It is seen from (2.1) that the comoving horizon can be expressed as a logarithmic integral of the comoving Hubble Radius $(aH)^{-1}$, *i.e.* $\tau = \int d\ln a \frac{1}{aH}$, which in is a monotonically increasing function of time. In the standard "Big Bang" picture (without inflation), we would expect regions separated by a maximum angular separation $\theta \sim$ deg to have been in causal contact. Any larger scales in the sky could not communicate with each other- these are said to be *causally disconnected*. However, the CMB appears homogeneous on (angular) scales much larger than 2 deg. How can two regions that have never communicated with each other have the same temperature? This is known as the horizon problem.

The Flatness Problem

Another interesting observation, is to realize the universe is extremely close to flat [69], as we previously discussed in Chapter 1. If we allow for $k \neq 0$, in a universe dominated by a fluid with equation of state w, it is easy to show from (1.23) and (1.25) that the fractional energy density evolves as

$$\frac{d\Omega}{d\ln a} = (1+3w)\Omega(\Omega-1)\ . \tag{2.2}$$

The case $\Omega = 1$ is an unstable critical point of the dynamical system- *i.e.* any deviation from exactly $\Omega = 1$ will grow with time - in particular during the standard radiation and matter dominated epochs where the expansion is decelerated ($w = 1/3$ and $w = 0$, respectively). To explain the small value of $|\Omega_{k,0}|$ we observe today, one finds that the universe had to start with $\Omega(a_{\rm pl}) \sim 1 \pm 10^{-60}$ at the planck epoch. Which represents an unacceptable amount of fine-tunning. Unless of course, $w < -1/3$ - which implies through (1.24) $\ddot{a} > 0$. If the expansion of the universe is accelerated, the solution $\Omega_k = 0$ becomes an attractor of the system. Inflation is precisely an epoch of accelerated expansion during the early Universe, and as such, provides a solution to the flatness and homogeneity problems. We should emphasize however, that Inflation does not affect the overall geometry of the universe. It only does so that locally, the universe seems to be flat.

2.1 Inflation: a solution to the *Big-Bang* puzzles

During inflation, the comoving Hubble radius $(aH)^{-1}$ shrinks, as H is nearly constant and $a(t) \propto \exp(Ht)$. Figure 2.1.1 shows the behaviour of the (comoving) Hubble radius during inflation, large scales fluctuations leave the horizon earlier than small scale fluctuations, and they are frozen for $k < aH$. After inflation stops, the comoving Hubble radius starts to grow again during the usual radiation and matter dominated epochs, and scales re-enter the progressively - See Fig. 2.2.1.

2.1.1 Single Field Inflation

The easiest and simplest way to produce a period of accelerated expansion is by supposing that during the very early universe, the energy density was governed by a scalar field φ. The simplest Lagrangian for a Scalar

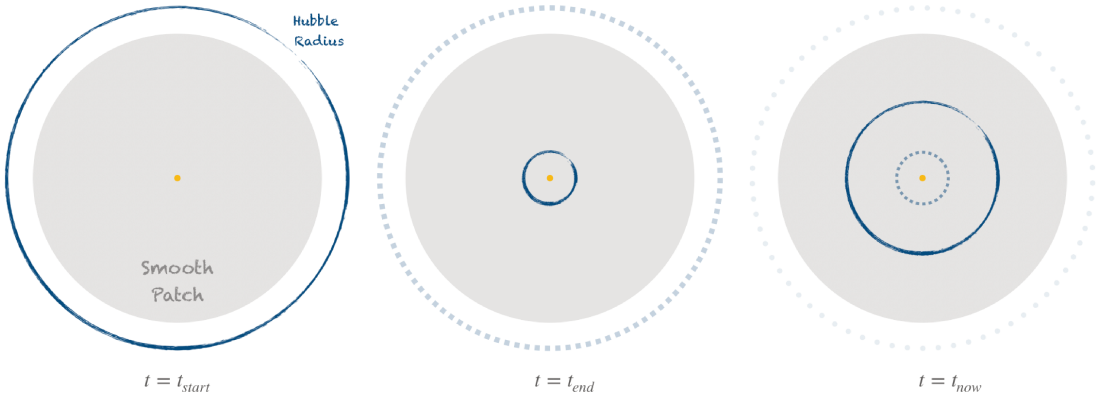

Figure 2.1.1: Solution to the Homogeneity Problem in the standard inflationary picture. From left to right, the evolution of the Hubble Radius (in comoving coordinates) at the beginning and end of Inflation, and nowadays, respectively. The comoving Hubble radius shrinks exponentially during inflation, as can be seen from Eq. (1.28), since $a(t) \propto \exp(Ht)$. Those regions that were causally connected before inflation, exit the horizon during inflation and re-enter progressively after it stops; when the Hubble radius starts to grow again.

Field φ with a kinetic term and an arbitrary potential $V(\varphi)$ is given by:

$$\mathcal{L}_\varphi = \frac{1}{2} g^{\mu\nu} \partial_\mu \varphi \partial_\nu \varphi + V(\varphi) \ . \tag{2.3}$$

The dynamics of this field is governed by the well-known *Klein-Gordon Equation* (KGE):

$$\Box\varphi \equiv \frac{1}{\sqrt{-g}} \partial_\mu (\sqrt{-g} g^{\mu\nu} \partial_\nu \varphi) = -\frac{\partial V}{\partial \varphi} \ , \tag{2.4}$$

Assuming an FLRW background and a spatially homogeneous fluid $\varphi(x,t) = \varphi(t)$, Eq.(2.4) reduces to:

$$\ddot{\varphi} + 3H\dot{\varphi} + \partial_\varphi V = 0 \tag{2.5}$$

2.1.2 Slow-Roll Approximation

The energy-momentum tensor for the scalar field is as usual given by

$$T^{(\varphi)}_{\mu\nu} = -\frac{2}{\sqrt{-g}} \frac{\delta(\sqrt{-g}\mathcal{L}_\varphi)}{\delta g^{\mu\nu}} = \partial_\mu \varphi \partial_\nu \varphi - g_{\mu\nu} \mathcal{L}_\varphi \ , \tag{2.6}$$

We can then identify from (1.21) the expressions for the energy density and pressure as

$$p_\varphi = \frac{1}{2}\dot{\varphi}^2 - V(\varphi) \ , \quad \rho_\varphi = \frac{1}{2}\dot{\varphi}^2 + V(\varphi) \ . \tag{2.7}$$

From Eqs. (2.7), and in the limit $V(\varphi) \gg \dot{\varphi}^2$, we immediately see that a scalar field minimally coupled to gravity behaves like a DE-like fluid with equation of state $w_\varphi = p_\varphi/\rho_\varphi \simeq -1$. We get accelerated expansion ($\ddot{a} > 0$) in slow-roll inflationary models if $\varepsilon, \eta \ll 1$, where these are dubbed the "slow-roll" parameters defined as [148]

$$\varepsilon = -\frac{d\ln H}{dN} = -\frac{\dot{H}}{H^2} \Longrightarrow \varepsilon_V = \frac{2}{M_{\rm pl}^2}\left(\frac{V'}{V}\right)^2 \ , \tag{2.8}$$

$$\eta = -\frac{\ddot{\varphi}}{H\dot{\varphi}} = \varepsilon - \frac{1}{2\varepsilon}\frac{d\varepsilon}{dN} \Longrightarrow \eta_V = \frac{1}{M_{\rm pl}^2}\frac{V''}{V} = \frac{V''}{3H^2} \ . \tag{2.9}$$

where in the last equality, we assume slow roll and write ε and η in terms of the potential $V(\varphi)$ and its derivatives (wrt φ). A plethora of inflationary models have been proposed over the years, we refer the reader to Refs. [65, 162]

2.2 Generating the primordial seeds

Inflation seems to be driven by the vacuum energy of the Inflation field (in the SR approximation). Due to its quantum nature, the inflaton φ fluctuates with $\delta\varphi \equiv \varphi(x,t) - \bar{\varphi}(t)$ and these fluctuations - through the Einstein equations- lead to fluctuations in the metric and ultimately to fluctuations in the temperature we observe in the CMB. The perturbed Einstein equations schematically read

$$\delta G_{\mu\nu} = 8\pi G \delta T_{\mu\nu} \ , \tag{2.10}$$

if the perturbations are small, the full non-linear solution is well approximated by the linear treatment. The statistical properties of those fluctuations is encoded in the so called *correlation function*

$$\langle \delta(k)\delta^*(k')\rangle = (2\pi)^3 \delta_D^{(3)}(k-k')P(k) \tag{2.11}$$

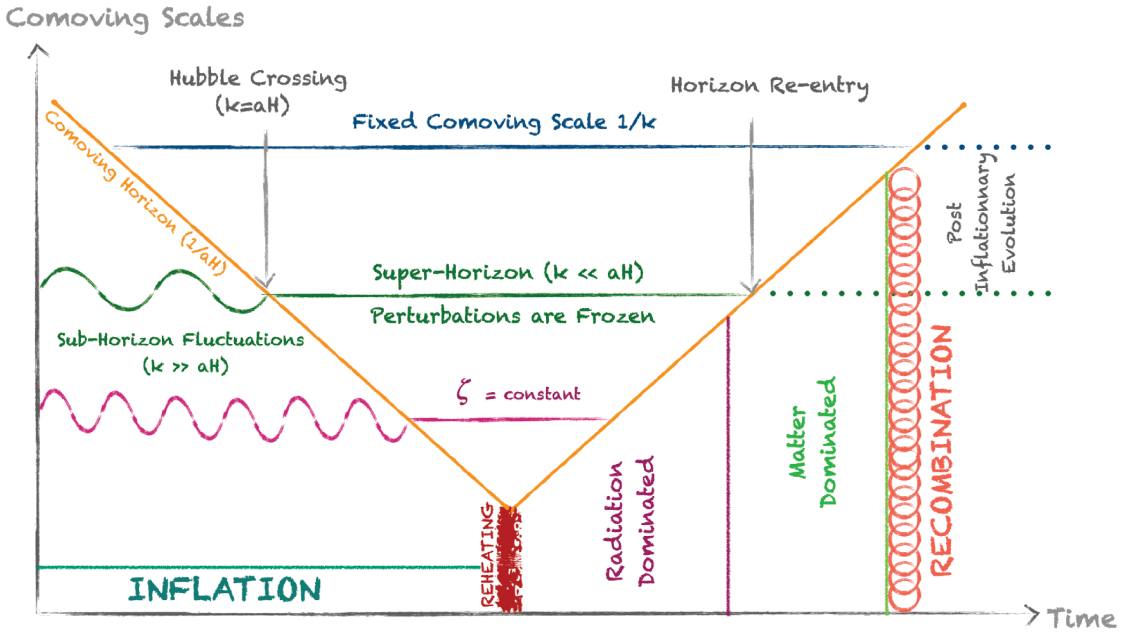

Figure 2.2.1: Schematic picture of the evolution of perturbations generated during inflation, as a function of time. The Hubble crossing corresponds to the time t_k, when the mode $k = aH$ crosses the Hubble radius. The quantity ζ is an extremely important conserved quantity outside the horizon. The power spectrum P_ζ encodes the statistical properties of the fluctuations at horizon crossing.

where $\delta_D^{(3)}(\vec{r})$ is the three dimensional Dirac delta function, and $P(k)$ is called the *Power Spectrum*. It is also convenient to introduce the *dimensionless power spectrum* $\mathcal{P}(k)$, typically taken to be a power law

$$\mathcal{P}_\zeta(k) \equiv \frac{k^3}{2\pi^2} P_\zeta(k) = A_s \left(\frac{k}{k_o}\right)^{n_s - 1} \tag{2.12}$$

where k_o is a normalization scale - typically chosen to be $k_o = 0.05$ Mpc^{-1} in the context of CMB analyses - and ζ is the primordial curvature perturbation - a conserved and important (gauge-invariant) quantity. The particular case $n_s = 1$ is called the Harrison-Zel'dovich or "scale-invariant" spectrum. However, the deviations from the exact scale-invariant case stem from the fact the H is not exactly constant during inflation, as quantified by slow-roll parameters. Observations constrain $n_s = 0.965 \pm 0.004$ [69], in excellent agreement with inflationary predictions. Fig. 2.3.1 shows an example of SR inflationary potential (at scales probed by CMB experiments). In the case of Gaussian statistics - as predicted by most single-field inflationary models- all the information is encoded in the two-point correlation function (or its Fourier-space

analog - the power spectrum). The power spectrum thus encodes almost all of the information about the primordial curvature fluctuations $\mathcal{R}_k$ (or equivalently ζ_k). The origin of these fluctuations is purely quantum mechanical. As discussed in the literature, these fluctuations evolve into random classical perturbations [127, 141, 190].

Due to the exponential expansion of the universe, fourier modes k are stretched by the expansion and leave the horizon, as depicted in Fig.2.2.1. Once these leave the horizon, they remain frozen [157] until horizon re-entry and provide the seeds needed for the formation of galaxies.

2.3 Primordial Black Holes as a window to the very-early Universe

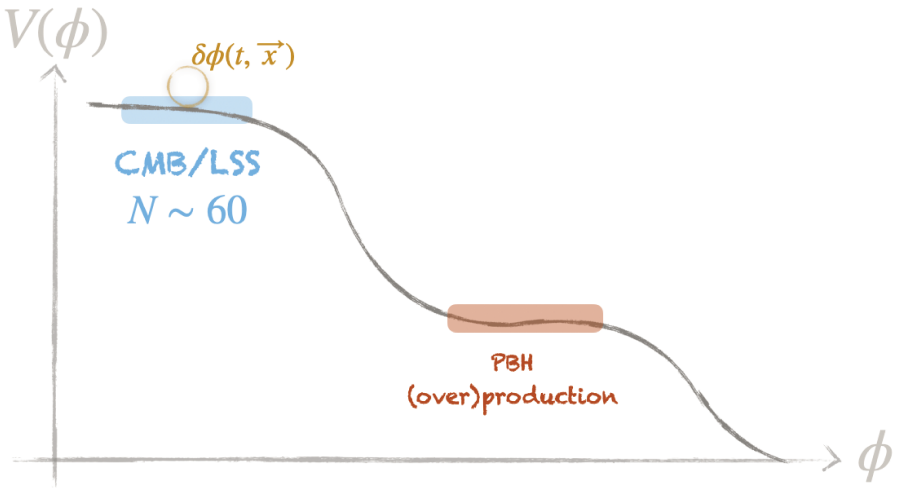

Figure 2.3.1: Schematic illustration of an inflationary potential. Cosmic Microwave Background (CMB) and Large Scale Structure (LSS) surveys are consistent with the predictions from slow-roll (single) field inflation. These probe the shape of the inflationary potential around $\sim$ 60 e-folds before the end of inflation. Scales of interest for PBH formation will leave the horizon much later on, only a few e-folds before the end of inflation. The non-observation of PBH in certain mass ranges, could in principle, constrain the shape of the inflationary potential near the reheating epoch.

A quite natural, and in recent years, very popular dark matter candidate are *Primordial Black Holes* (PBH's). It was soon realized that primordial fluctuations in the energy density above some critical threshold ($\delta_{\rm th} \sim 0.3 - 0.7$) re-entering the horizon during *e.g.* the Radiation Dominated epoch could lead to the collapse

of the former into a Black Hole - Primordial Black Holes. So far, the LIGO-VIRGO collaboration has detected $\mathcal{O}(50)$ gravitational wave events from BH binary mergers, most of them in the $\sim 30\, M_\odot$ mass range. PBH were first proposed by Hawking [109] in the early seventies. Inflationary models can naturally lead to the formation of PBH. Nonetheless, CMB constraints makes it hard to produce large enough $\mathcal{O}(1)$ fluctuations on small scales. Note however that recent studies using the stochastic inflation (or δN) formalism [221, 222] suggest that PBH production is a generic feature of inflationary models coming from quantum diffusion of the inflaton along its potential [97, 233]. The tantalizing possibility that a fraction of the BH binary mergers events detected by LIGO/Virgo are from primordial origin is not excluded [101]. Excitingly, even the non observation of PBH in those mass ranges could in principle exclude or at least constrain a wide class of inflationary potentials near the reheating epoch. By gathering more data from current and next generation of GW observatories, we will be probing the last numbers of e-folds before the end of inflation.

2.4 Stochastic Gravitational Wave Background

The unexpected gift we get from the inflationary paradigm, is the generation of a *primordial (stochastic) gravitational wave background* (SGWB) permeating spacetime. In analogy with its scalar counterpart, we parametrize the spectrum of tensor modes as

$$\mathcal{P}_t = A_t \left(\frac{k}{k_*}\right)^{n_T} \tag{2.13}$$

Due to historical reasons, the scale-invariant case is n_T=0. One interesting quantity in inflationary cosmology is the tensor-to-scalar ratio r

$$r = \frac{A_t}{A_s} \tag{2.14}$$

The simplest inflationary models predict a relation between the tilt of tensor modes and the tensor-to-scalar ratio $r = 16\varepsilon = -8n_T$ - known as *consistency relation*. In the next decade, we might be able to probe physics up to extremely high-energies with GW observatories. Many (BSM) early-universe scenarios predict a first-order phase transition (among other mechanisms) that can lead to a detectable SGWB with future space-based GW observatories, such as LISA [50, 58, 244].

Figure 2.4.1 ***(following page)*****:** Top-left panels: Observations of clusters of galaxies in redshift space by the 2dFGRS and SGW surveys. Bottom right: Comparison with numerical N-body simulations from the *Millennium Simulation*[216] - This assumes a $\Lambda\mathrm{CDM}$ cosmology - Structure formation will happen differently in a non-cold DM filled-universe. Simulations in a $\Lambda\mathrm{CDM}$ universe qualitatively reproduces the structure of the cosmic web. In fact, since observations are done in redshift space, galaxies appear *strechted* or *squished* from their "original" positions. This due to effect of peculiar velocities (typically of the order $\sim 1000\,\mathrm{km\,s^{-1}}$), an effect known as the *fingers of god*. Figure taken from [216].

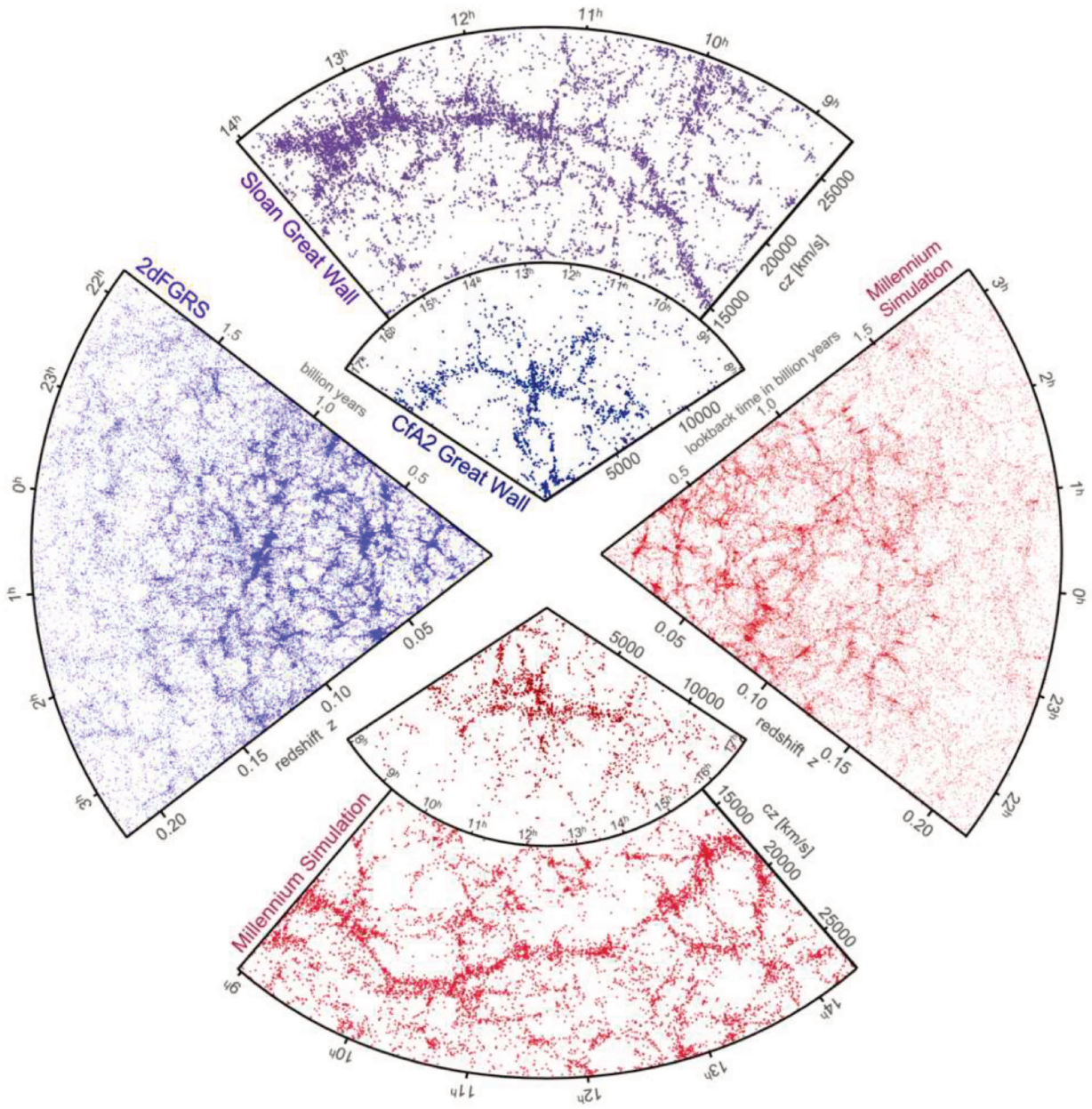
Sloan Great Wall
2dFGRS
CfA2 Great Wall
Millennium Simulation
Millennium Simulation
billion years
lookback time in billion years
redshift z
cz [km/s]

Part II

Phenomenology of Dark Energy models: The Growth Index γ

3

Inhomogeneities around the FLRW background

Evolution of cosmic inhomogeneities as a probe of gravity. So far, we have treated the universe as being perfectly homogeneous and isotropic. This is just a first approximation, which is extremely accurate at large scales, but far from reality at small-scales - where we evidently see large deviations from homogeneity. If the universe was perfectly homogeneous and isotropic there wouldn't be any stars or galaxies to harvest life. And *we* humans would not be here to study the cosmos. This part of the thesis is dedicated to the study of small fluctuations, or perturbations, and their evolution around the FLRW universe we studied in Part I. In Chapter 2, we explored how an epoch of (rapid) accelerated expansion naturally sets the initial conditions for our Universe to evolve into the inhomogeneous Universe we observe today. In this chapter, we review the basics of (linear) perturbation theory needed to relate the former with the Large Scale Structures (LSS) we observe in the late-universe. Throughout this section, we will limit our discussion to the linear (quasi-static) regime. This is justified by the fact that at scales of cosmological interest, and in particular for CMB and LSS studies, the universe can accurately be described by (small) perturbations around

the FLRW universe.

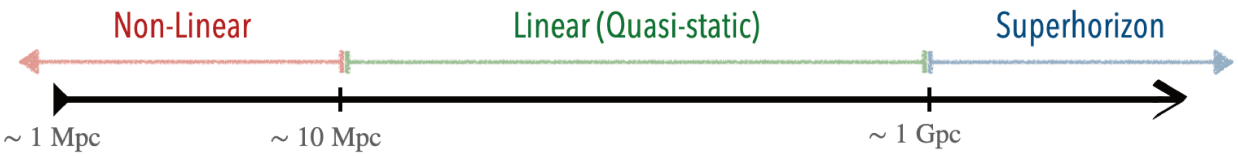

Figure 3.0.1: Schematic view of the differents regimes as function of scale. The study of fluctuations in the superhorizon regime requires treating cosmological perturbations relativistically. For reference, a typical cluster of galaxies with total mass $M \sim 10^{10} M_{\odot}$ has a virial radius $R_{\rm vir} \sim 1$ Mpc below which non-linear gravitational interactions can no longer be neglected. In such cases, one typically relies on numerical N-body simulations.

Review of Perturbation Theory

The understanding of CMB anisotropies has widely contributed to establishing what we now call the concordance model of cosmology. Perturbation theory is an extremely useful tool in all areas of physics. It has indeed played a significant role in our understanding of the cosmos, and as we shall discover in this chapter, it will most likely play a crucial role in determining the true nature of Dark Energy. In this thesis, we only consider perturbations at the linear level (1st order in perturbation theory), but a huge amount of information is disguised in higher-order contributions that we will not discuss. Throughout this section, we will decompose a generic quantity Q into an homogeneous (averaged) background quantity plus some smallfluctuation (spacial and time-dependent) around the FLRW background

$$Q(\mathbf{r}, t) = \overline{Q}(t) + \delta Q(\mathbf{r}, t) \tag{3.1}$$

The treatment of perturbations in cosmology is more easily done in the language of fluid dynamics. As usual, we will consider matter, radiation and almost everything to be well approximated by a perfect fluid. There are 3 equations worth remembering from fluid dynamics. Namely, *Euler's Equation*

$$D_t \mathbf{u} \equiv (\partial_t + \mathbf{u} \cdot \boldsymbol{\nabla}_{\mathbf{r}})\mathbf{u} = -\frac{\boldsymbol{\nabla}_{\mathbf{r}} P}{\rho} - \boldsymbol{\nabla}_{\mathbf{r}} \Phi \tag{3.2}$$

which comes from momentum conservation and where $\mathbf{u}$ is the velocity field, and Φ is the gravitational

potential. Similarly, mass conservation yields the famous *Continuity Equation*

$$\partial_t \rho = -\boldsymbol{\nabla}_{\mathbf{r}} \cdot (\rho \mathbf{u}) \ . \tag{3.3}$$

The peculiar velocity is tightly related to the density field, as seen from (3.3). The last equation, which will be of crucial importance when discussing modified theories of gravity is *Poisson's Equation*

$$\boldsymbol{\nabla}_{\mathbf{r}}^2 \Phi = 4\pi G \rho \tag{3.4}$$

Relating the gravitational potential Φ to the energy density ρ. Notice the gradient $\boldsymbol{\nabla}_{\mathbf{r}}$ with respect to the physical coordinate r. In an expanding universe, r is related to the comoving coordinates x by the relation $r = a(t)x$ with $a(t)$ being the scale factor (see Fig.1.1.3). It will be useful to reformulate the problem in the comoving coordinates [42], remembering

$$\boldsymbol{\nabla}_{\mathbf{r}} = a^{-1}\boldsymbol{\nabla}_x, \qquad \left.\frac{\partial}{\partial t}\right|_r = \partial_t\big|_x - \frac{1}{a} v \cdot \boldsymbol{\nabla}_x = \partial_t\big|_x - Hx \cdot \boldsymbol{\nabla}_x \ . \tag{3.5}$$

We apply the procedure (3.1) for all quantities of interest, namely the pressure P, bulk velocity $\mathbf{u}$, density ρ, and gravitational potential Φ. Assuming that the fluctuations are small, we can linearize Eqs. (3.2),(3.3) and (3.4) and drop the product of fluctuations (which are negligible if they are small) to obtain

$$\boxed{\ddot{\delta} + 2H\dot{\delta} - \frac{c_s^2}{a^2}\boldsymbol{\nabla}^2\delta = 4\pi G\bar{\rho}\delta} \tag{3.6}$$

Where we have introduced the fractional density perturbation, or sometimes called *density contrast* δ as well as the speed of sound c_s^2.

$$\delta \equiv \frac{\delta\rho}{\bar{\rho}} \ , \quad c_s^2 \equiv \frac{\partial P}{\partial \rho} \tag{3.7}$$

We explicitly assume here that the perturbations are adiabatic (as predicted by most single-field inflationary models), which allows us to relate the pressure to energy density via its sound speed c_s, effectively removing the pressure dependence from our equations. Furthermore, it is convenient to work in Fourier space. We decompose $\delta\rho$ as

$$\delta\rho(\mathbf{r}, t) = \int \frac{d^3k}{(2\pi)^3} e^{-i\mathbf{k}\cdot\mathbf{r}} \delta\rho_k(t) \tag{3.8}$$

This is particularly useful since at the linear level in perturbation theory, Fourier modes decouple and evolve independently. For each wavenumber k, from (3.6) their evolution is dictated by:

$$\ddot{\delta}_k + \underbrace{2H\dot{\delta}_k}_{\textit{expansion}} = \underbrace{4\pi G\rho\delta_k}_{\textit{gravity}} - \underbrace{c_s^2\frac{k^2}{a^2}\delta_k}_{\textit{pressure}} \tag{3.9}$$

From the above equation, we distinguish 2 different regimes, for small scales λ (large $k > k_J$) below the Jeans scale $\lambda_J(t) = 2\pi/k_J = c_s(t)\sqrt{\pi/G\bar{\rho}(t)}$ modes oscillate in time with decreasing amplitude. On the other hand, for scales larger than the Jeans scale ($k < k_J$), pressure forces cannot longer compensate for gravitational attraction, and thus the perturbations grows as a power law, as opposed to exponentially in a static universe ($\dot{a} = 0$). The factor $2H\dot{\delta}$ - often called *Hubble drag* - is related to the expansion of the universe and plays the role of a friction term in the EOM for δ, slowing down the growth of perturbations.

A few words on scales:

A given scale λ is said to cross the horizon when

$$\lambda = R_H \Leftrightarrow \frac{2\pi}{k}a = \frac{1}{H}\,. \tag{3.10}$$

where $R_H = 1/H$ is the Hubble radius defined in (1.28) and the numerical factor (2π) is often left out so we talk about a scale crossing the Hubble Radius R_H when $k = aH$. Modes with $k \gg aH$ and $k \ll aH$ are said to be *sub-horizon* and *super-horizon modes*, respectively. For a more detailed (and pedagogical) treatment of structure formation and perturbation theory, the reader is referred to *e.g.* [131].

3.1 Stages of Evolution

Remarkably, the Newtonian approach to cosmological perturbation theory already gives us a huge amount of information about the evolution of the inhomogeneities in the universe and the underlying theory of gravity. In this thesis, we will mainly be interested in large-scale perturbations entering the horizon during Matter domination. From (3.6), considering matter to be accurately described by a pressure-less fluid($c_s^2 =$

0) the gradient term vanishes and we get the master equation for DM perturbations.

$$\ddot{\delta}_m + 2H\dot{\delta}_m - 4\pi G\rho_m\delta_m = 0 \tag{3.11}$$

3.1.1 Matter Dominated stage

During matter domination we have $H \simeq 2/3t$, and thus Eq. (5.1) simply reads

$$\ddot{\delta}_m + \frac{4}{3t}\dot{\delta}_m - \frac{2}{3t^2}\delta_m = 0 \tag{3.12}$$

By simple substitution of a power law solution of the form $\delta_m \propto t^p$, we get the following two solutions:

$$\delta_m \propto \begin{cases} t^{-1} \propto a^{-\frac{3}{2}}, & \text{“decaying mode”} \\ t^{\frac{2}{3}} \propto a, & \text{“growing mode”} \end{cases} \tag{3.13}$$

This is an important result worth remembering. *i.e.* matter (density) perturbations grow like the scale factor $a(t)$ during matter domination (Einstein-DeSitter with $\Omega_m = 1$). By the time matter dominates, the decaying mode is no longer present. Therefore we will only consider the growing mode in (3.13), but we shall later on comment on the decaying mode in Chapters 5 and 6.

3.1.2 Radiation Dominated stage

During the *Radiation-Dominated* (RD) stage, on scales smaller than the Hubble radius, the growth of perturbations was inhibited by the large pressure provided by photons in the photon-baryon plasma. The competition between the gravitational and pressure forces led to the formation of acoustic waves that propagated through the plasma, and leaved an imprint on the surface of last scattering. We observe this oscillations in the acoustic peaks of the CMB and in the matter power spectrum $P_m(k)$.

We can consider the growth of non-relativistic matter perturbations in a model where the expansion is driven by a mixture of radiation and matter (*i.e.* just before decoupling). Using $H^2 = (\rho_m + \rho_r)/3M_{\rm pl}^2$ and introducing $y \equiv \frac{\rho_m}{\rho_r}$ as integration variable, (5.1) is recast into

$$\delta'' + \frac{2+3y}{2y(1+y)}\delta' - \frac{3}{2y(1+y)}\delta = 0 \tag{3.14}$$

where prime denotes differentiation with respect to $y \equiv \rho_m/\rho_r = a/a_{\rm eq}$. The solutions to this equation are given by: *(i)* $\delta \propto y + 2/3$ - implying $\delta \propto a$ at late-times, while being constant during the RD stage. *(ii)* The other solution being $\delta \propto \ln y$ in the regime $y \ll 1$ ($a \ll a_{\rm eq}$). These results are confirmed by the relativistic treatment, and we can conclude that non-relativistic perturbations grow only logarithmically until the universe becomes matter-dominated.

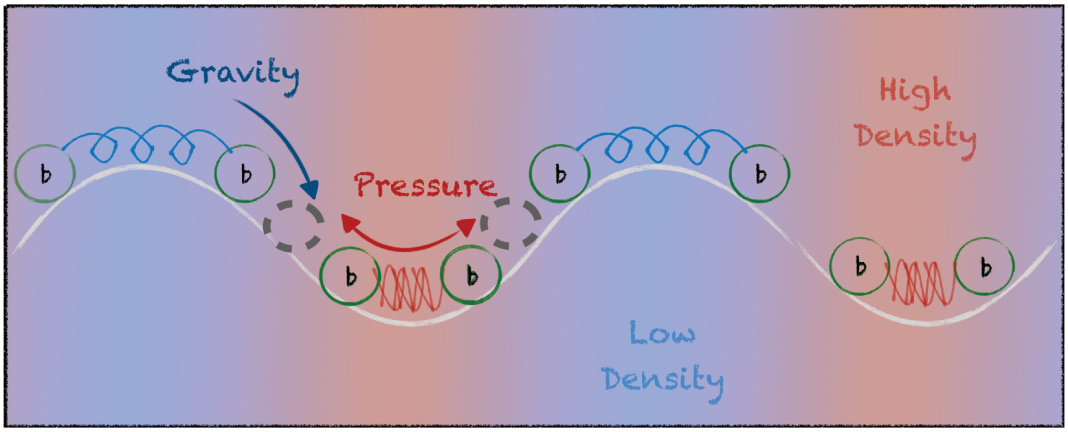

Figure 3.1.1: Schematic Illustration of the physics of *Baryonic Acoustic Oscillations* (BAO). A constant battle between gravitational attraction and electromagnetic repulsion. Baryons are constantly shifted out of equilibrium due to a dynamical gravitational potential arena. This in turn translate into areas with higher baryonic density (Hot spots in the temperature of the CMB) and areas with lower density (blue spots). This is just a first approximation, in reality, the non-interacting (cold) Dark Matter sits at the bottom of those wells and enhance the gravitational potential. The fractional abundance of DM compared to baryonic matter determines the shape of the acoustic peaks in the CMB, and allows us to precisely measure the quantities $\omega_{\rm b}$ and $\omega_{\rm CDM}$.

Baryons being tightly coupled to photons, primarily though *Thomson scattering*, feel a non-vanishing pressure force. Which then translate into a slow-down of the growth of perturbations. It is indeed possible

to show (see *e.g.*[85]) that the time-averaged density contrast of radiation fluctuations vanishes, whereas DM perturbations grow logarithmically $\delta_m \propto \ln a$ during the RD stage. A presure-less (dark) fluid is therefore needed for the perturbations to grow efficiently during the RD stage. This is reflected in the dependence of the acoustic peaks in the CMB on the fractional energy density of DM $\omega_{\rm CDM} \equiv \Omega_{\rm CDM} h^2$.

Dark matter out weights ordinary matter by a factor of 5, and unlike baryons, it does not interact with photons, and thus feels no pressure. As DM flowed inwards towards over dense regions, baryons feel an enormous pressure exerted by the imprisoned photons. After decoupling, baryons fall into the (enhanced) potential wells and track DM perturbations.

3.1.3 Λ-Dominated stage

By the time matter has been diluted away, the main contribution in the energy density is that of DE. It seems that DE is described (to a good approximation) by a cosmological constant Λ, which by definition remains constant across spacetime and therefore does not cluster ($\delta_\Lambda = 0$). In a Λ-dominated universe, it is straightforward to show that the solutions to $\ddot{\delta} + 2H\dot{\delta} \simeq 0$ are

$$\delta_m \propto \begin{cases} \text{const.} \\ e^{-2Ht} \propto a^{-2} \end{cases} \tag{3.15}$$

implying that the growth of perturbations is frozen once DE starts to dominate over matter.

3.2 Large Scale Structure Observables

So far, we have explored how the initial seeds evolve during the history of our Universe. Here we will relate the fluctuations in matter density to actual cosmological observables that we can measure with galaxy surveys. In the nineties, Peebles, Efstathiou and others used LSS observations to predict the presence of a Λ-term [90, 178] - before the discovery of the accelerated expansion by SNeIa[185, 199]. LSS has proven to be extremely useful in constraining the properties of Dark Energy, as it probes the late-time growth of structures when DE starts to dominate over DM. Recent results from large-scale structure surveys, such as eBOSS[11] and DES(Y3) [67] show the potential of these to infer cosmological parameters, by cleverly using and combining different Late-time observables, such as Galaxy Clustering, Weak Lensing, Redshift

Space Distortions among others.

Ongoing and future LSS surveys have been (or will soon be) measuring the distribution of matter across a wide variety of scales and redshifts, thus allowing us to contrain the expansion history of the Universe during DE domination to unprecedented precision, allowing for the inference of cosmological parameters at the same level of accuracy as CMB analyses currently do. We will soon be able to further test the concordance model of cosmology and probe the nature of Dark Energy. As we already stated previously, the linear formalism of perturbation theory is thus valid at large (early) enough scales (times), such that the requirement $\delta_m \ll 1$ is satisfied.

The reader is referred to [41, 131] for a more detailed treatment of LSS and Perturbation Theory. Let us also mention that higher-order statistics beyond the simple power spectrum, (or two-point correlation function) could potentially yield valuable information about the laws of gravity on the largest of scales, driving the late-time accelerated expansion as discussed in [146].

Matter Power Spectrum

One crucial quantity mentioned before, is the matter power spectrum. We cannot predict the precise value of δ_m in any point in space-time, but rather we can predict the statistical properties of these overdensities. One can define the correlation function as

$$\langle \delta_m(k)\delta_m^*(k')\rangle = (2\pi)^3\delta_D(k-k')P_m(k) \tag{3.16}$$

where $\delta_D(x)$ is the Dirac delta function, and $P_m(k)$ is called the matter *Power Spectrum*. It is then possible to write [85]

$$\delta(\vec{k},a) = \delta_p(\vec{k}) \times \left\{\text{Transfer Function } T(\vec{k})\right\} \times \{\text{Growth } \delta(a)\} \ , \tag{3.17}$$

where δ_p indicates the initial primordial amplitude for a given mode k and $\delta(a)$ accounts for its evolution as a function of a. The exact computation of the transfer function $T(k)$ is complicated, and is typically done numerically, as one needs to solve the hierarchy of Boltzmann equations and take into account interactions between different species, free-streeming effects, etc. Nowadays, many (fast) numerical Boltzmann solvers for computing the matter power spectrum are readily avaible, such as `CLASS` [43, 142] or `CAMB`[143]. The

basic (qualitative) features of the Power spectrum are nontheless easy to understand. First, it is easy to see that $P(k) \propto \langle |\delta_m(k)|^2 \rangle$ is always a positive quantity. At larges scales (small k) we must recover the homogeneity assumption, thus $P(k) \to 0$ for $k \to 0$. We further saw in the previous section that during matter domination, perturbations grow efficiently ($\delta_m \propto a$), whereas during radiation domination, the e.m. pressure inhibited the growth, so that their growth is logarithmic only $\delta_m \propto \ln a$. There is a difference between the growth of perturbations in RD and MD epochs, thus we should expect a preferred scale $k_{\rm eq} = a_{\rm eq} H_{\rm eq}$ distinguishing the two "regimes" of growth (before and after matter-radiation equality $a_{\rm eq}$) - see Fig.3.2.1. The transfer function $T(k)$ has the following limits:

$$T(k) \propto \begin{cases} 1, & \text{for } k \lesssim k_{\rm eq} = a_{\rm eq} H_{\rm eq} \\ (\frac{k}{k_{\rm eq}})^{-2}, & \text{for } k \gtrsim k_{\rm eq} \end{cases} \tag{3.18}$$

The key idea, is that at late-time when matter dominates all fourier modes evolve identically. Before that, their evolution is essentially determined on whether these modes re-enter the horizon before or after $a_{\rm eq}$. Modes satisfying $k > k_{\rm eq}$ are suppressed relative to $k < k_{\rm eq}$. The small wavelength modes that enter the horizon during RD feel their growth suppressed by a factor $(k/k_{\rm eq})^{-2}$ at late-times[1]. For larger-wavelengths that re-enter at the time matter dominates, the transfer function is close to unity, and thus evolve as $\delta \propto a$. Numerical calculations can be reasonably well-approximated by the BBKS formula [2][31]

$$T(k) = \frac{\ln(1 + 2.34\, q)}{2.34\, q} \left[1 + 3.89\, q + (16.2\, q)^2 + (5.47\, q)^3 + (6.71\, q)^4\right]^{-1/4} , \tag{3.19}$$

with $q \equiv \frac{k}{\Omega_m h^2 \mathrm{Mpc}}$. This approximation assumes a vanishing anisotropic stress ($\Phi = -\Psi$) and ignores baryonic effects, which definitely change the small scale behaviour of the power spectrum. However, throughout this thesis, we will focus on large-scales, so we can safely neglect these effects.

[1] Up to a logarithmic correction accounting for the logarithmic growth at early times.

[2] A simpler, and more accurate approximation for the transfer function was also derived in [92]

Figure 3.2.1 ***(following page)*****:** *Top :* The *Matter Power Spectrum* at $z = 0$. *Bottom :* Residuals wrt Planck's ΛCDM best-fit. We see the remarkable agreement with the wide variety of observational probes . Notice how at large scales (small k), as probed by Planck, we are limited by cosmic variance. Figure taken from [60] to which we refer for the details on the data sets under consideration.

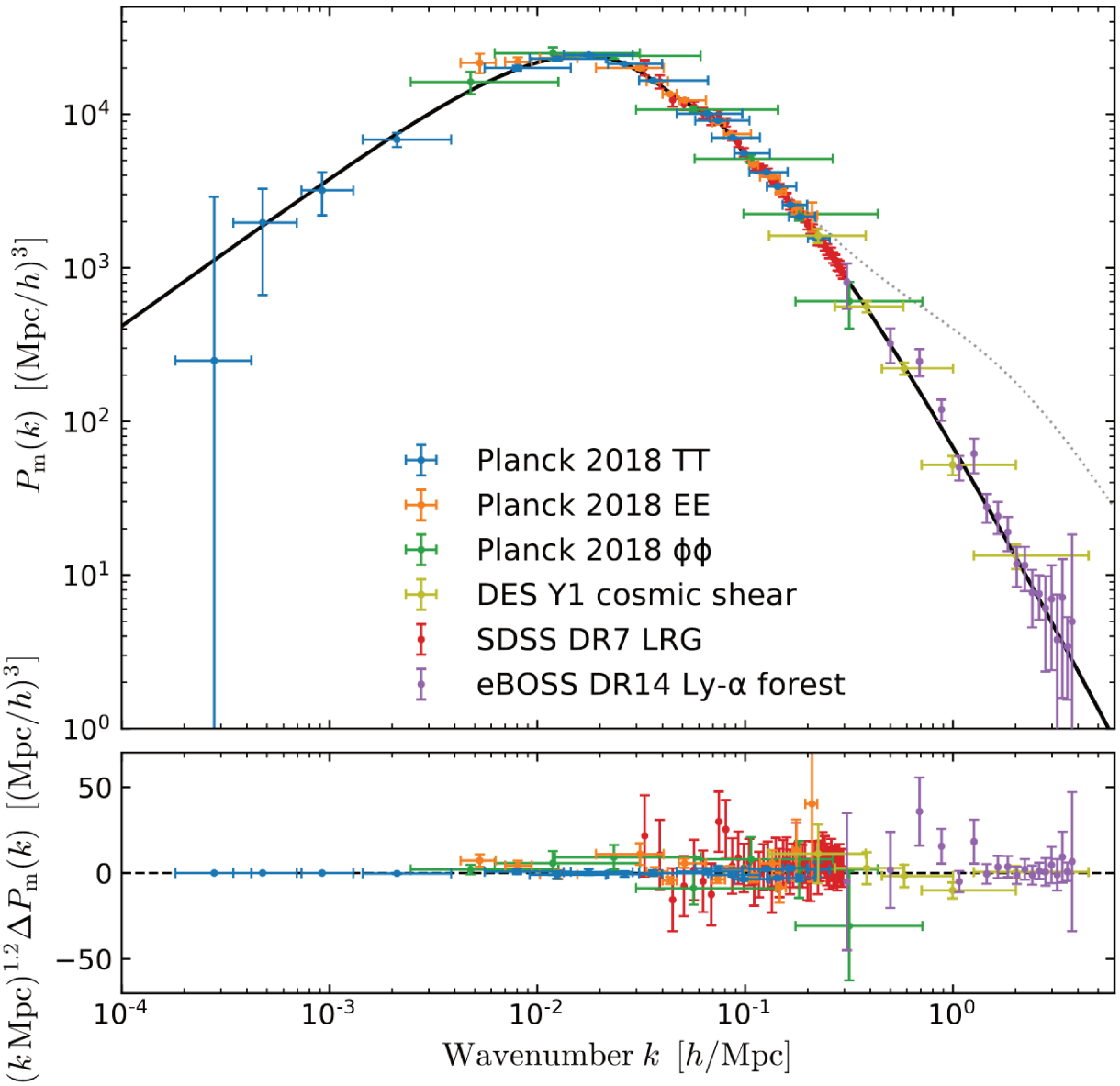
$P_{\rm m}(k)$ $[({\rm Mpc}/h)^3]$
10^4
10^3
10^2
10^1
10^0
Planck 2018 TT
Planck 2018 EE
Planck 2018 ϕϕ
DES Y1 cosmic shear
SDSS DR7 LRG
eBOSS DR14 Ly-α forest
$(k\,{\rm Mpc})^{1.2}\,\Delta P_{\rm m}(k)$ $[({\rm Mpc}/h)^3]$
50
0
−50
10^{-4}
10^{-3}
10^{-2}
10^{-1}
10^0
Wavenumber k $[h/{\rm Mpc}]$

From the Poisson equation(3.4), we see $k^2\Phi(k) \propto \delta_m(k)$ which implies the matter power spectrum is a power law of the form

$$P(k) \propto k^{n_s} \tag{3.20}$$

where n_s is the spectral tilt, measured to be $n_s = 0.965 \pm 0.004$ by CMB experiments [69], which is in perfect agreement with inflationary predictions. The exact case $n_s = 1$ is known as the Harrison-Zel'dovich power spectrum.

Weak Lensing & Galaxy Clustering

Observationally speaking, galaxy surveys measure the statistical properties of the distribution of galaxies (and/or *voids*[3]). The galaxy overdensity is related to the usual (dark) matter overdensity via the simple linear relation

$$\delta_g = b \cdot \delta_m \ , \tag{3.21}$$

where b is the galaxy bias. There is yet another subtlety, we do not observe the galaxy density constrast δ_g directly, but rather its density constrast in redshift space δ_z, which leads to *Redshift Space Distortions* (RSD) which we will briefly discuss in the next section. On large scales, where the linear treatment is accurate, one can safely assume

$$P_g(k,z) = b^2 P_m(k,z) \ . \tag{3.22}$$

A common way of characterizing the amplitude of the over densities at a given scale is by means of the *root mean squared* (RMS) in a sphere of radius R, defined as

$$\sigma_R^2 \equiv \langle \delta_R^2(x) \rangle \ , \tag{3.23}$$

where $\delta_R(x) \equiv \int d^3x' \delta(x') W_R(x - x')$ is the *smoothed density contrast* and $W(x)$ is some window function. Because of historical reasons, we typically express this in a sphere of radius $R = 8$ Mpc$/h$[4]. For more details

[3] In the same way that galaxy provides a biased tracer of the underlying dark matter overdensities, cosmic voids (underdense regions) can yield valuable information about the growth of structure in the universe. A particular interesting application is the cross-correlation of these two datasets, allowing us to test *e.g.* the isotropic and homogeneous assumptions.

[4] Although it has been pointed out recently that the use of h^{-1}.Mpc units in cosmology might be responsible for misconceptions regarding the normalization of $P(k)$ encoded in σ_8, and is therefore at the heart of the discrepancy in the measure of σ_8 [223]

on galaxy clustering see *e.g.* [74]

Figure 3.2.2: Weak gravitational lensing in the Abell 2218 galaxy cluster. The shapes of galaxies appear to be distorted, or elongated in some direction. Advanced Statistical methods can be used to quantify this effect, and estimate the mass distribution along the line of sight[130, 217]. Figure taken by the Hubble Space Telescope. Credit: NASA/ESA https://esahubble.org/images/heic0814a/

Morevover, galaxy surveys not only give us information about the positions of galaxies, but also their shape (cosmic shear measurements [128]- See Fig. 3.2.2) and their cross-correlation. These are the so callled 3x2pt analyses - because of the three types of 2pt correlation functions: position-position, shear-shear, shear-position. Such surveys are extremely sensitive to the combination

$$S_8 \equiv \sigma_{8,0}\sqrt{\Omega_m/0.3} \tag{3.24}$$

which effectively removes the degeneracy between Ω_m and σ_8 and characterizes the smoothness or *clumpiness* of the DM density field in our Universe. In Fig. 3.2.3 we report the new measurements from the 3-Year Dark Energy Survey.

Redshift space distortions

The observed redshift receives contributions from the *real redshift*, and an additional contribution coming from the *peculiar motion* of *e.g.* galaxies, so that

$$z_{\rm obs} = z_{\rm real} + \frac{1}{a}\frac{v_{\parallel}}{c} \tag{3.25}$$

where $v_{\parallel}$ refers to the line-of-sight component of the peculiar velocity. This ultimately leads to[5].

$$\delta_z = (1 + \frac{f}{b}\mu_k^2)\delta_g \tag{3.26}$$

where $\mu_k = \frac{\mathbf{k}\cdot\hat{z}}{k}$ is the cosine of the angle between the line-of-sight and the wave-vector $\mathbf{k}$, $f \equiv \frac{d\ln\delta_m}{d\ln a}$ is the growth function and b is the bias factor encountered before (3.21). This is the so-called Kaiser effect[6] [124]. RSD surveys are sensitive to the combination $\beta \equiv f(z)/b$ - often called the distortion parameter (see more in [41, 81]). Eq. (3.26) is telling us that the observed matter power spectrum is modulated by a factor $f(z) \simeq \Omega_m(z)^{\gamma(z)}$, encoding the logarithmic growth of matter perturbations and - as we will see in Chapters 5 and 6 - is sensitive to the nature of DE. In practice, one prefers to work with the (unbiased) combination $f(z)\cdot\sigma_8(z)$. By definition we have

$$f(z) = -\frac{d\ln\delta_m}{d\ln(1+z)} \qquad \text{and} \qquad \sigma_8(z) = \sigma_{8,0}\cdot\frac{\delta_m(z)}{\delta_m(z=0)} \tag{3.27}$$

From there, it is straightforward to find

$$\boxed{f\sigma_8(a) \equiv \sigma_{8,0}\cdot a\cdot\frac{\delta_m'(a)}{\delta_{m,0}}}\,. \tag{3.28}$$

This is the actual observable in RSD surveys. We again refer the reader to Ref.[182] for a clear account of observations done in redshift space.

[5] See *e.g.* [41, 81, 124] for a more detailed derivation.
[6] Although it seems these ideas were first discussed in [206].

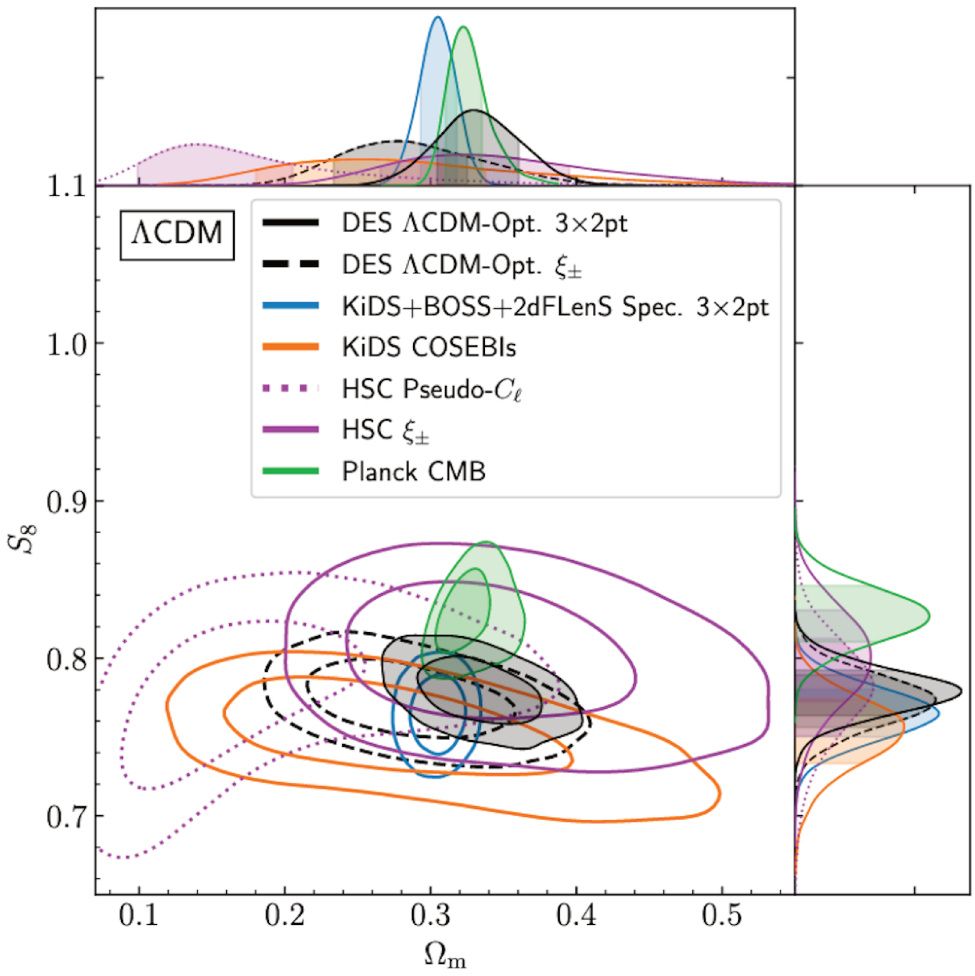

Figure 3.2.3: Most recent constraints on the (S_8, Ω_m) plane in the ΛCDM model from the 3-year Dark Energy Survey (DES) results. It is seen that both (Kids & DES) weak-lensing surveys prefer a lower value for S_8 than early-universe (CMB) measurements from Planck - although it is not statistically significant yet to call it a "tension". Figure taken from [67] (Fig. 19)

"In Physics we have Heroes, not prophets."

Steven Weinberg

4

Modified Gravity

Scalar fields are ubiquitous in High Energy Physics and Cosmology. The "recent" discovery of the Higgs boson is the very first experimental evidence of a fundamental scalar (spin-0) field in nature. We further saw in Chapter 2 how the standard ΛCDM paradigm relies on an early stage of *quasi-De Sitter expansion* - with nearly constant H- for generating the primordial seeds. While the exact particle physics of Inflation is still unknown, observations of the CMB and LSS seem to favor a Gaussian - *nearly adiabatic, nearly scale-invariant* - primordial spectrum of fluctuations. This is typically achieved by invoking a *slowly-rolling* scalar field - the *Inflaton* φ. Interestingly, one of the most widely accepted (and first) inflationary models is a modified gravity of the form $f(R) = R + aR^2$ which provides a very good fit to current CMB data[220]. The discovery of DE in the late 90's provides further motivations to consider modifications to Einstein's GR. Moreover, it is known that scalar degrees of freedom arise quite naturally- as an effective description- in the context of UV-complete theories of gravity (*e.g.* the Dilaton in String Theory) . More generally, many interesting extensions to the SM of particle physics predict new (light) species which are

very-weakly coupled to ordinary matter, making them very hard to detect on terrestrial experiments. One such example, are *Axion-like Particles* (ALP). More specifically, the original QCD axion is the emerging Nambu-Goldstone boson of a spontaneously broken $U(1)_{\rm PQ}$ (*Peccei-Quinn*) symmetry[174]. It is one of the most highly-motivated BSM candidates in particle physics as it solves two of the most important shortcomings in the SM[1]. More recently, ALP have received a lot of attention in the cosmological community because of their potential to ease the Hubble tension [166, 194], by effectively reducing the size of sound horizon at recombination[2]. A lot of effort has also gone in constructing such models in the context of modified gravity (see *e.g.* [27, 28, 245] and references therein for recent works in this direction). It is therefore quite natural (and insightful!) to study the dynamics of scalar fields in a gravitational context. In this chapter, we shall briefly review recent advances in modified gravity theories, and provide further motivations for the kind of (phenomenological) features considered in this thesis. The interested reader is referred to Refs. [1, 66, 96, 125] for a more thorough discussion of modified gravity.

4.1 The Horndeski Action

The most general action involving a scalar field φ plus the metric $g_{\mu\nu}$ leading to second order field equations[3] has already been written[114]. It takes the following, rather cumbersome form:

$$S[g_{\mu\nu},\varphi] = \int \mathrm{d}^4x\,\sqrt{-g}\left[\sum_{i=2}^{5}\frac{1}{8\pi G}\mathcal{L}_i[g_{\mu\nu},\varphi] + \mathcal{L}_{\rm m}[g_{\mu\nu},\psi_M]\right] . \tag{4.1}$$

The above action includes a wide variety of dark energy (and inflationary) models with a single degree of freedom added to the Einstein-Hilbert Action. These include the good-old Quintessence/K-essence models, Scalar-Tensor (Brans-Dicke) theories, Kinetic Gravity Braiding ,Generalized Galileons and many more (see *e.g.* [125]). The Lagrangian densities $\mathcal{L}_i$ are given by

$$\mathcal{L}_2 = G_2(\varphi,\, X)\ , \qquad \mathcal{L}_3 = G_3(\varphi,\, X)\Box\varphi\ , \tag{4.2}$$

[1] Namely, the strong CP (θ-term) problem in *Quantum Chromo-Dynamics* (QCD) and it was soon realized it is also a perfect Dark Matter candidate. See *e.g.* Ref.[161] for more details on axions and their relation to cosmology

[2] Although it has been debated whether LSS observables exclude such models [121, 214]. Indeed, these models suffer from higher (inferred) values of σ_8, in tension with recent WL measurements.

[3] Theories having higher-order equations of motion as thought to be plagued by the *Ortogradsky instability*, yielding ghost degrees of freedom - *i.e.* particles with $M < 0$. Recently, a class of theories known as Degenerate Higher-Order Scalar-Tensor Theories (DHOST)have been found to evade the Ortogradsky instability[138]. See [137, 207] for a review

$$\mathcal{L}_4 = G_4(\varphi,\, X)R + G_{4,X}(\varphi,\, X)\left[(\Box\varphi)^2 - \varphi_{;\mu\nu}\varphi^{;\mu\nu}\right] \,, \tag{4.3}$$

$$\mathcal{L}_5 = G_5(\varphi,\, X)G_{\mu\nu}\varphi^{;\mu\nu} - \frac{1}{6}G_{5,X}(\varphi,\, X)\left[(\Box\varphi)^3 + 2\varphi_{;\mu}{}^{\nu}\varphi_{;\nu}{}^{\alpha}\varphi_{;\alpha}{}^{\mu} - 3\varphi_{;\mu\nu}\varphi^{;\mu\nu}\Box\varphi\right] \,, \tag{4.4}$$

where $\Box\varphi \equiv g^{\mu\nu}\varphi_{;\mu\nu}$, $X \equiv -\frac{1}{2}\partial_\mu\varphi\partial^\mu\varphi$ and $G_{\mu\nu}$ is the Einstein Tensor in (1.9). It is seen from the above Lagrangians the gigantic class of theories that could lead to second order equations of motion (EOM). However, many of the terms $G_i(\varphi, X)$ in (4.1) have now been ruled out -or have stringent constraints- by recent gravitational wave observations. Namely, GW170817 and its electromagnetic counterpart GRB170817A [4, 5] (see *e.g.* [72, 75, 95, 125] and references therein). It seems appropriate at this stage to try and classify the wide variety of DE models contained in (4.1) according to the phenomenological implications for cosmological observables. This is indeed along the lines of the *Effective Field Theory* formalism of DE [37, 106] (see *e.g.* [103] for a pedagogical introduction). In recent years, the correspondence between Horndeski's models[4] and the EFT description of DE became transparent [37].

4.2 Phenomenology of Modified Gravity

When expanding Horndeski's action up to second order in perturbations and imposing the symmetries of the background, there are 4 remaining functions of time $\alpha_i(t)$ parametrizing the deviations from GR. These are: α_M denoting the running of the Planck Mass, α_K related to the kinetic part of the scalar lagrangian, α_B characterizing the mixing between metric and scalar perturbations and α_T which parametrizes the deviations in the tensor speed w.r.t. unity ($c = 1$). These α-functions can be expressed as combinations of the functions $G_i(\varphi, X)$, but their closed-form expressions are irrelevant for our purposes. The reader is referred to [37, 103, 106]. The key point being that the α_i's encapture the phenomenology of deviations from General Relativity. As an example, one can show that tensor modes (gravitational waves) in modified gravity theories evolve as

$$\ddot{h}_{ij} + (3 + \alpha_M)\, H\, \dot{h}_{ij} + (1 + \alpha_T)k^2 h_{ij} = 0 \tag{4.5}$$

with $\alpha_T = 1 - c_T^2$ encoding the deviations in the tensor speed from unity and $\alpha_M = \frac{d\ln M_*^2}{d\ln a}$ being the running of the Planck mass. As mentioned before, the tensor speed excess has been measured to be vanishingly

[4] Beyond-Horndeski theories can also be encaptured by the EFT functions α_i, by incluiding an additional function α_H.

small $a_T \leq \mathcal{O}(10^{-15})$[5]. This severely constrained the landscape of possible DE models in (4.1), as many predicted $c_T \neq c$ [26, 95] . The parameter a_M also enters as a friction term in the equations of motion for GW, modulating the way in which GW feel the expansion of the Universe and as such, could play a crucial role in determining the nature of DE - through the next generation of GW observations. Another key (generic) feature of MG models is that their (scalar) density perturbations evolve differently than in GR, since $G \to G_{\rm eff}(a,k)$ which *effectively* encodes the additional degree of freedom and sources the perturbations through Poisson's equation. For modes well-within the horizon, their evolution is dictated by

$$\ddot{\delta}_m + 2H\dot{\delta}_m = 4\pi G_{\rm eff}(a,k)\rho_m\delta_m \tag{4.6}$$

where $G_{\rm eff}(a,k)$ is a time and scale dependent effective gravitational coupling. Therefore, from a phenomenological point of view, an interesting place to look for departures from GR is the evolution of cosmic inhomogeneities. Such a phenomenological tool is the *growth index* γ of matter perturbations. We shall come back to this in great depth in Chapters 5 and 6.

4.3 Some examples of Modified Gravity

One of the most natural, and simplest possibilities is to extend the Einstein-Hilbert action (1.4) to include higher-order contribution in terms of geometrical (covariant) objects, such as the Ricci scalar R, $R_{\mu\nu}R^{\mu\nu}$ and so on. In the following, we will consider $f(R)$ theories, as it is one of the few subclass of models in (4.1) surviving current constraints. These have been classified in *e.g.* [26, 95, 125].

$f(R)$ Gravity

Throughout this section, we follow the notations of Ref. [1]. One of the minimal extensions to GR is to promote R to $f(R)$, such that

$$S_{\rm EH} = \frac{1}{2\kappa^2}\int d^4x\sqrt{-g}R \longrightarrow S = \frac{1}{2\kappa^2}\int d^4x\sqrt{-g}f(R) \tag{4.7}$$

where $f(R)$ is a generic function of the Ricci scalar R. By taking the variational derivative with respect to $g^{\mu\nu}$, we can define the equivalent of the Einstein tensor:

$$\Sigma_{\mu\nu} \equiv F(R)R_{\mu\nu}(g) - \frac{1}{2}f(R)g_{\mu\nu} - \nabla_\mu\nabla_\nu F(R) + \Box F(R)g_{\mu\nu} = \kappa^2 T_{\mu\nu} \tag{4.8}$$

where we have introduced $F \equiv \partial_R f(R)$ and $T_{\mu\nu}$ is the usual energy-momentum tensor (1.8). Taking the trace of the above equation (*i.e.* $g^{\mu\nu}\Sigma_{\mu\nu}$) gives

$$3\Box F(R) + F(R)R - 2f(R) = \kappa^2 T \tag{4.9}$$

where $T \equiv T^{\mu}_{\ \mu} = g^{\mu\nu}T_{\mu\nu}$ is the trace of the energy-momentum tensor. One immediately sees from (4.9), that there is a propagating (dynamical) degree of freedom- the so-called *Scalaron* $\varphi \equiv F(R) = \partial f/\partial R$. These theories are well-known to be *conformally equivalent* to the good-old *Scalar-Tensor (ST) Theories*[5] in the Einstein and Jordan Frames. $f(R)$ theories have also been studied in the context of Dark Energy models[6]. There are nonetheless general stability conditions this function must satisfy for our theory to be viable (and ghost-free). These can be summarized as[219]

$$F \equiv \partial_R f > 0 \qquad \text{and} \qquad \partial_R F > 0. \tag{4.10}$$

The viability conditions for $f(R)$ DE models were derived in [18] and many interesting observational constraints have been studied throughout the years in the literature [34, 49, 98, 165, 198, 230]. In particular, an important thing to mention is that such theories require screening-mechanisms (due to the coupling of the scalar to matter) in order to evade solar-system and laboratory constraints[48]. One functional (viable) form for $f(R)$ has been proposed in [117, 219]

$$f(R) = R + \lambda R_s \left[\left(1 + \frac{R^2}{R_s^2} \right)^{-n} - 1 \right] \tag{4.11}$$

The growth of perturbations in such models is modified because of the *effective gravitational constant* $G_{\rm eff}$ appearing in (4.6) (see *e.g.* [104, 227]). It is well-known that in the quasi-static approximation (QSA)[44], *i.e.* on subhorizon scales, the modification to effective gravitational constant can be written as

$$G_{\rm eff}(z,k) = \frac{G_N}{F}\left(\frac{1 + 4\frac{k^2}{a^2}m}{1 + 3\frac{k^2}{a^2}m} \right) , \qquad m \equiv \frac{\partial_R F}{F} . \tag{4.12}$$

[5] both at the classical and (one-loop) quantum level [172]

[6] although it is hard to construct viable theories with the usual decelerated stages of expansion during the radiation and matter dominated epochs.

Braneworld (DGP) Gravity

We have seen before how GR is the unique theory describing a spin-2 field in 4D. If one is to modify the gravitational action, one needs to give up on some of its assumptions. One possibility, is to add an additional degree of freedom. Like the scalar φ in (4.1). Another possibility, is to add extra-dimensions to the theory. Since the work of Kaluza and Klein, many higher-dimensional theories of gravity have been proposed over the years (*e.g.* Kaluza-Klein[129], Randall-Sundrum [196], ADD model [22] etc).

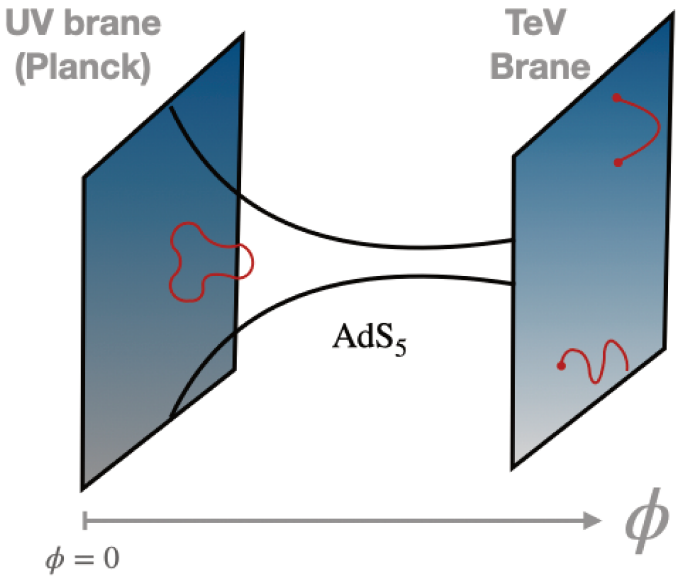

Figure 4.3.1: Schematic representation of brane world theories.

Braneworld models naturally emerge in the context of high energy theories, such as *string theory* or *M-theory*. In the UV, the fundamental objects turn out to be membranes or *branes* for short, (*e.g. D-brane*). In such theories, the SM content - made up of open strings - is said to be bound to the D-brane, where as gravity, consisting of closed strings is able to propagate in the 5D spacetime - *The Bulk*. From a particle physics standpoint, brane-world models are well motivated, as they help easing the hierarchy problem bringing $M_5 \ll M_{\rm pl}$. Understanding its effect on cosmological observables is crucial, and could yield valuable information of such high-energies behaviors (and possibly small/large (warped) extra-dimensions). In this work, let us focus on the Dvali-Gabadadze-Porrati (DGP) model, as it serves as a simple 5D (toy)

model, to explore the implications of higher dimensions in cosmological observables. The DGP model is an IR modification to GR, the effective Friedmann equation can be cast in the form

$$H^2 - \frac{H}{r_c} = \frac{8\pi G}{3} \sum_i \rho_i(t) \ , \tag{4.13}$$

where r_c is a critical scale, above which GR is modified to include the effects of the extra dimension. This model had attracted a lot of interest in the cosmological community, since the (modified) Friedmann equation above has a (late-time) accelerating solution $a(t) \propto e^{t/r_c}$ without the need for a *dark energy* component.

$$H(t) = \frac{1}{2}\left(\frac{1}{r_c} \pm \sqrt{\frac{1}{r_c^2} + \frac{32\pi G}{3}\rho_m(t)} \right) \tag{4.14}$$

This can be seen by taking the limit $\rho_m \to 0$ of (4.14), the so-called *self-accelerating branch* in the DGP model. However, it has been pointed out that this branch suffers from a ghost at the linear level [135] The most interesting aspect of the DGP is that its *effective* gravitational coupling constant decreases with the expansion (5.37), and therefore perturbations feel a weaker gravity than in GR. Thus, the growth of structures in such models is drastically modified, as we will show in Chapter 5. In particular, the *growth index* $\gamma(z = 0)$ in such models has very different values and appears to be excluded by - or is in tension with - current data. Showing the potential of such *phenomenological tool* in studying the high-energy world.

The dawn of multi-messenger astronomy has opened up a new window to study the fundamental nature of DE, and possibly its connection to the high-energy/particle physics content of the models. Although the tensor speed excess has been measured to be vanishingly small $\mathcal{O}(10^{-15})$, there are many surviving models satisfying the constraint $a_T \simeq 0$, with viable but *potentially detectable cosmological signatures* (*e.g.* [152, 164]). One particularly interesting observable is the modified luminosity distance of tensor perturbations $d_L^{\rm GW}(z)$, which could help further constrain e.g. *non-minimally coupled theories* [125].

5

Global properties of the Growth Index γ

Adapted from

R. Calderón, D. Felbacq, R. Gannouji, D. Polarski and A. A. Starobinsky

Global properties of the growth index of matter inhomogeneities in the Universe

Physical Review D - 100, 083503 (2019)[55]

Despite intensive activity in recent years, the late-time accelerated expansion rate of the Universe remains a theoretical challenge. A wealth of theoretical models and mechanisms were put forward for its solution; see reviews [71, 145, 173, 179, 202, 203]. Remarkably, the simplest model – GR with a non-relativistic matter component (mainly a non-baryonic one) and a cosmological constant Λ – is in fair agreement with observational data, especially on large cosmic scales. Notwithstanding the theoretical problems it raises, this model provides a benchmark for the assessment of other dark energy (DE) models phenomenology. One can make progress by exploring carefully the phenomenology of the proposed models and comparing it with observations [239]. Tools which can efficiently discriminate between models, or between classes of

models (e.g. [201]) are then needed. The growth index γ which provides a representation of the growth of density perturbations in dust-like matter, is an example of such phenomenological tool. Its use was pioneered long time ago in order to discriminate spatially open from spatially flat universes [177] and then generalized to other cases [136]. It was later revived in the context of dark energy [153], with the additional incentive to single out DE models beyond GR. The growth index has a clear and important signature in the presence of Λ: it approaches $6/11$ for $z \gg 1$ and it changes little from this value even up to $z = 0$. This behaviour still holds for smooth non-interacting DE models inside GR with a constant equation of state w_{DE}, as depicted in Fig5.3.1. A strictly constant γ is very peculiar [189, 191]. On the other hand, this behaviour is strongly violated for some models beyond GR, see e.g. [104, 165]. Surprisingly, important properties of the growth index behaviour can be understood by making a connection with a strictly constant γ. Further, while present observations probe low redshifts $z \lesssim 2$, still as we will see, more insight is gained looking at the global evolution of γ. Before starting this analysis, we first review the basic formalism for the study of the growth index γ.

5.1 Characterizing the growth of perturbations with γ

A particularly useful way of characterizing the evolution and growth of scalar (density) perturbations for non-relativistic matter is by the means of the growth index γ introduced a while ago [149].In this section, we will briefly derive the important equations for γ. Our starting point will be Eq. (3.6). For modes well inside the Hubble radius, their evolution is dictated by

$$\ddot{\delta}_m + 2H\dot{\delta}_m - 4\pi G\rho_m\delta_m = 0 \tag{5.1}$$

To do so, we will consider a non-interacting mixture of dust-like matter and DE components, since we happen to live close to the transition era between a matter dominated and a DE dominated universe. The dimensionless Hubble function $h(z) \equiv H(z)/H_0$ at $z \ll z_{eq}$ (long after the radiation dominated epoch) reads

$$h^2(z) = \Omega_{m,0}(1+z)^3 + (1-\Omega_{m,0})\exp\left[3\int_0^z dz'\,\frac{1+w_{DE}(z')}{1+z'}\right] \tag{5.2}$$

with $w_{\rm DE}(z) = P_{\rm DE}(z)/\rho_{\rm DE}(z)$. From this, we can calculate the entire evolution of $\Omega_m(a)$ through the

useful relation

$$\Omega_m(a) = \Omega_{m,o}\, a^{-3}\, h^{-2}(a)\ . \tag{5.3}$$

Moreover, it is easy to show the following relation holds

$$w_{DE} = \frac{1}{3\,\Omega_{DE}} \frac{d\ln\Omega_m}{dN} \tag{5.4}$$

For later convenience, we may want to work with the scale factor $a(t)$ as the main variable. Remembering that $d/dt = aH(d/da) = H(d/d\ln a)$, Eq (5.1) can be written as a non-linear first-order differential equation in terms of the growth function f (see e.g. [189] and references therein)

$$\frac{df}{d\ln a} + f^2 + \left(2 + \frac{\dot{H}}{H^2}\right) f = \frac{3}{2}\,\Omega_m(a) \tag{5.5}$$

Where we have introduced the usual definition for $f \equiv \frac{d\ln\delta_m}{d\ln a}$, and used $4\pi G\rho_m = \frac{3}{2}H^2\,\Omega_m$. Notice however the definition of Ω_m in terms of Newton's coupling constant $G = G_N$. In general, modified theories of gravity can (and generically do) have a time-dependent (and even scale-dependent) effective coupling's constant $G_{\rm eff}(a,k)$ (see.e.g. [227]).
In many DE models outside GR the modified evolution of matter perturbations is recast into

$$\ddot{\delta}_m + 2H\dot{\delta}_m - 4\pi G_{\rm eff}\rho_m\delta_m = 0\ , \tag{5.6}$$

where $G_{\rm eff}$ is some effective gravitational coupling appearing in the model. For example, for effectively massless scalar-tensor models [44], $G_{\rm eff}$ is varying with time but it has no scale dependence while its value today is equal to the usual Newton's constant G. Introducing for convenience the quantity

$$g \equiv \frac{G_{\rm eff}}{G}\ , \tag{5.7}$$

equation (5.6) is easily recast into the modified version of Eq. (5.5), viz[1].

$$\frac{df}{dN} + f^2 + \frac{1}{2}\left[1 - \frac{d\ln\Omega_m}{dN}\right] f = \frac{3}{2}\,g\,\Omega_m\ ; \qquad g \equiv \frac{G_{\rm eff}}{G} \tag{5.8}$$

[1] See E. Linder's paper[151] on the different ways we can write this equation and it use in cosmology.

With $N \equiv \ln a$ is the number of e-folds. Clearly $f = p$ if $\delta_m \propto a^p$ (with p constant). In particular, when the growing mode dominates, $f \to 1$ in ΛCDM for large z and $f = 1$ in the Einstein-de Sitter universe (we recover the solutions in (3.13)). In the peculiar situation where the decaying mode dominates, $f \to -\frac{3}{2}$ in ΛCDM for large z and $f = -\frac{3}{2}$ in the Einstein-de Sitter universe. We will return to the consequences of a non-negligible decaying mode later. Also, if the dependence $f(N)$ is known from observations, the Hubble function $H(z)$ and finally the scale factor $a(t)$ dependence can be determined unambiguously in an analytical form [218] (see [158] for implementation of this to recent observational data). Note that we can easily reconstruct the familiar quantity $\delta_m(a)$ using

$$\delta_m(a) = \delta_{m,i} \exp\left[\int_{N_i}^{N} f(N')dN'\right] \tag{5.9}$$

It is well known now that a useful parametrization for the growth function f is given by

$$f(z) \equiv \frac{d\ln\delta_m}{d\ln a} = -\frac{d\ln\delta_m}{d\ln(1+z)} = \Omega_m(z)^{\gamma(z)} \tag{5.10}$$

where γ is dubbed growth index, though in general $\gamma(z)$ is a genuine function of redshift. It can even depend on scales for models where the growth of matter perturbations has a scale dependence. The representation (5.10) has attracted a lot of interest with the aim to discriminate between DE models based on modified gravity theories and the ΛCDM paradigm. It turns out that the growth index is quasi-constant for the standard ΛCDM from the past untill today. Such a behaviour holds for smooth non-interacting DE models when w_{DE} is constant, too [189] - See Figs. (5.1.1)and (5.3.1).

When the growth index γ is strictly constant, it is straightforward to deduce from (5.8) that $w_{DE} = \overline{w}$ with

$$\overline{w} = -\frac{1}{3(2\gamma-1)}\,\frac{1+2\Omega_m^{\gamma}-3g\Omega_m^{1-\gamma}}{1-\Omega_m} \tag{5.11}$$

$$\equiv -\frac{1}{3(2\gamma-1)}\,F(\Omega_m;g,\gamma). \tag{5.12}$$

The quantity $\overline{w}(\Omega_m,\gamma)$ defines a function in the (Ω_m,γ) plane which will be useful even when γ is not constant. The case $g = 1$ reduces to GR and we will simply write

$$F(\Omega_m; g=1,\gamma) \equiv F(\Omega_m;\gamma)\ . \tag{5.13}$$

Below, for any quantity v, v_∞, resp. $v_{-\infty}$, will denote its (limiting) value for $N \to \infty$ in the DE dominated era ($\Omega_m \to 0$), resp. $N \to -\infty$ (generically $\Omega_m \to 1$). We have in particular from (5.11) for $g = 1$ (GR)

$$\gamma = \frac{3\overline{w}_\infty - 1}{6\overline{w}_\infty} \tag{5.14}$$

$$\gamma = \frac{3(1 - \overline{w}_{-\infty})}{5 - 6\overline{w}_{-\infty}} \, . \tag{5.15}$$

Here we assume that $\overline{w} < 0$ to ensure a matter dominated stage in the past and dark energy dominated stage in the future. In addition, Eq. (13) requires that $\overline{w}_\infty < -\frac{1}{3}$ to have $0 < \gamma < 1$, otherwise $\overline{w}_\infty$ becomes infinite. As it was found in [191], these relations between a *constant* γ and the corresponding asymptotic values $\overline{w}_\infty$ and $\overline{w}_{-\infty}$ apply also for the *dynamical* γ obtained for an arbitrary but given w_{DE}. In the latter case, we obtain for $g = 1$

$$\gamma_\infty = \frac{3w_\infty - 1}{6w_\infty} \tag{5.16}$$

$$\gamma_{-\infty} = \frac{3(1 - w_{-\infty})}{5 - 6w_{-\infty}} \, , \tag{5.17}$$

with w_∞, respectively $w_{-\infty}$, the asymptotic value of w_{DE} in the future, respectively past. We will return later to this important property.

5.2 Global analysis in the (Ω_m, γ)-plane

It is natural to consider Ω_m as the fundamental integration variable. In this case the evolution equation for γ obtained from (5.8) using (5.10) yields

$$2a\Omega_m \ln(\Omega_m) \frac{d\gamma}{d\Omega_m} + a(2\gamma - 1) + F(\Omega_m; g, \gamma) = 0 \, , \tag{5.18}$$

where we have defined

$$a \equiv 3w_{DE} \, . \tag{5.19}$$

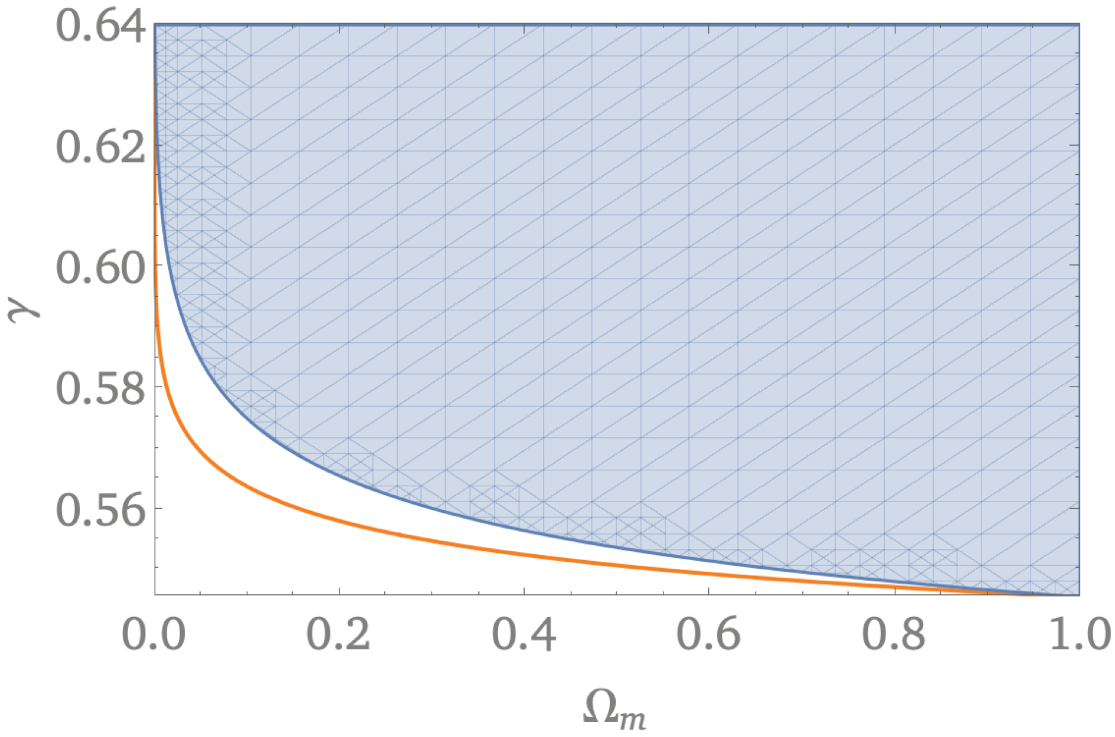

Figure 5.1.1: The growth index with $w = -1$, blue shaded region corresponds to regions satisfying $\frac{d\gamma}{d\Omega_m} > 0$.

We restrict ourselves in this section to GR i.e. $g = 1$. This equation is well defined provided w_{DE} is a given function of Ω_m only. In particular (6.1) can be readily used for constant w_{DE}. For arbitrary $w_{DE}(a)$ we can either express a as a function of Ω_m or write (6.1) using the integration variable a. Note that the function $a(\Omega_m)$ is one-to-one for $w_{DE} < 0$. We consider here all the solutions to equation (6.1) on the entire Ω_m interval. Each integral curve of equation (6.1) is the envelope of its tangent vectors

$$\begin{pmatrix} 1 \\ \frac{d\gamma}{d\Omega_m} \end{pmatrix} \tag{5.20}$$

The collection of all these tangent vectors defines a vector field that can be written

$$\begin{pmatrix} 2a\Omega_m(1-\Omega_m)\ln(\Omega_m) \\ -a(2\gamma-1)(1-\Omega_m) - \tilde{F}(\Omega_m;\gamma) \end{pmatrix} \tag{5.21}$$

where we have defined

$$\tilde{F}(\Omega_m;\gamma) \equiv (1-\Omega_m)F(\Omega_m;\gamma) = 1 + 2\Omega_m^{\gamma} - 3\Omega_m^{1-\gamma} \ . \tag{5.22}$$

For convenience, we have written the vector field in this way in order to have explicitly regular functions, so this vector field is well-defined everywhere for $(\Omega_m, \gamma) \in [0,1] \times \mathbb{R}$. The associated unit vector field is represented in fig.(5.2.1) for $w_{DE} = -1$.
The integral curves of this vector field (i.e. the phase portrait), are obtained by solving the autonomous differential system

$$\begin{aligned} \frac{d\Omega_m}{ds} &= 2a\Omega_m(1-\Omega_m)\ln(\Omega_m) \\ \frac{d\gamma}{ds} &= -a(2\gamma-1)(1-\Omega_m) - \tilde{F}(\Omega_m;\gamma) \end{aligned} \tag{5.23}$$

where $s \in \mathbb{R}^+$ is a dummy variable parametrizing the curves.

The vector field corresponding to $w_{DE} = -1$ is displayed on Fig.5.2.1 and will be considered now for concreteness. The growth index $\gamma(\Omega_m)$ which starts at $\gamma(1) \equiv \gamma_{-\infty} = 6/11$ is the only curve $\gamma(\Omega_m)$ which is finite everywhere. This curve corresponds to the presence solely of the growing mode of eq.(5.1) or equivalently to the limit of a vanishing decaying mode. Let us consider this point in more details. Generally, in the presence of two modes $\delta \equiv \delta_1 + \delta_2$, we have

$$f = \frac{\delta_1}{\delta} f_1 + \frac{\delta_2}{\delta} f_2 \ , \tag{5.24}$$

where $f_1 > 0$, resp. $f_2 < 0$, corresponds to the growing mode δ_1, resp. decaying mode δ_2. Inspection of (5.24) shows that $f < f_1$ if $\delta_1\delta_2 > 0$ while $f < f_1$ or $f > f_1$ when $\delta_1\delta_2 < 0$. For concreteness we consider the situation around today. If both modes are positive we have $f < f_1$ and hence $\gamma > \gamma_1$. As we go back in time ($\Omega_m \to 1$), $f \to f_2$ and so $\gamma \to \infty$ when $f \approx 0$. Let us consider now the situation $\delta_1 \times \delta_2 < 0$ with $|\delta_1| > |\delta_2|$ today. Now we have today $f > f_1$ and therefore $\gamma < \gamma_1$. When we go backwards, $f \to \infty$ at some point where the absolute value of both modes become equal, hence in that case $\gamma \to -\infty$. These different situations are shown on figures (5.2.1) and (6.2.1).

Another interesting point concerns the asymptotic future ($\Omega_m \to 0$). Inside GR, the solution to eq.

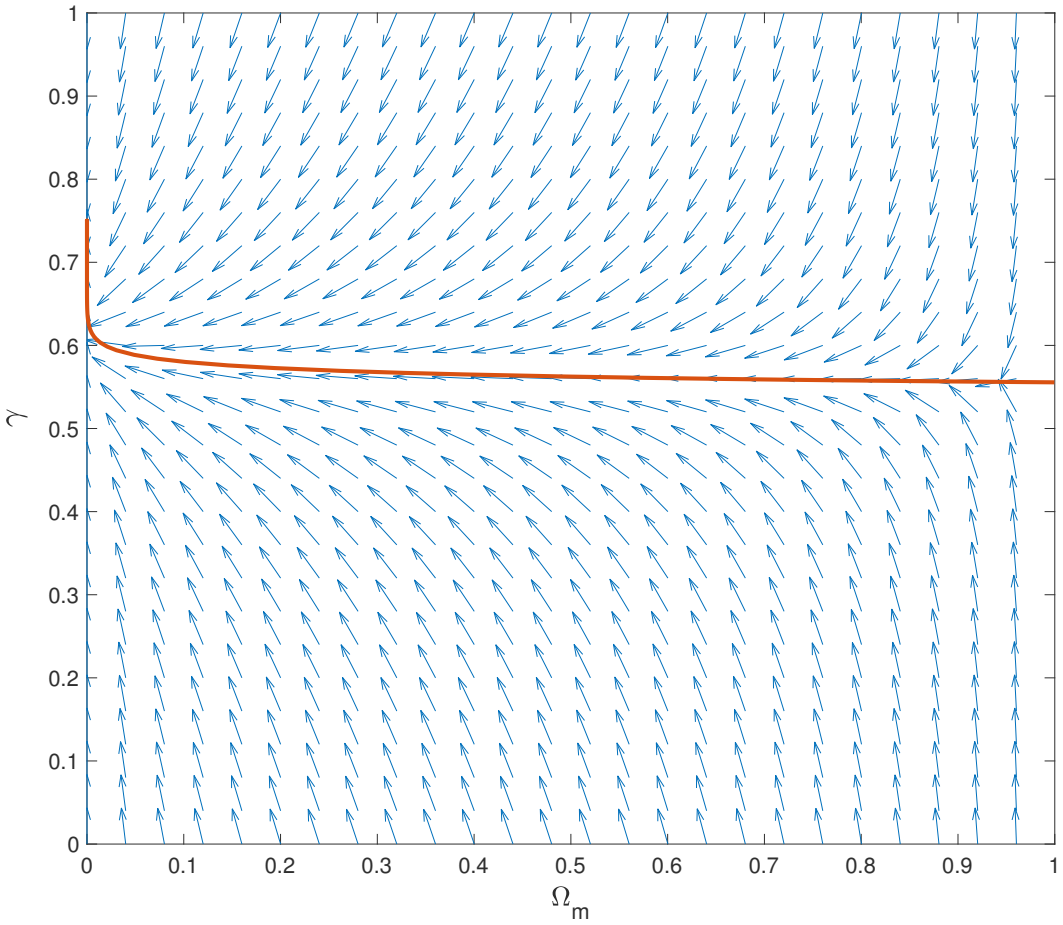

Figure 5.2.1: The (unit time-oriented) vector field tangent to the solutions γ of Eq.(6.1) is displayed for $w_{DE} = -1$. The red curve corresponds to the solution for γ, with boundary condition $\gamma(1) \equiv \gamma_{-\infty} = 6/11$. It is the only solution which is finite on the entire Ω_m interval, physically it corresponds to the presence of the growing mode of (5.6) only. The difference can be important in the far past only. All the other solutions correspond to solutions containing also the decaying mode solution. As explained in the text, these solutions (if physical) tend to the same value of γ, namely $\gamma_\infty = \frac{2}{3}$, for $\Omega_m \to 0$, and they diverge for $\Omega_m \to 1$.

(6.1) gives $\gamma \to \gamma_\infty$, eq. (5.16), with

$$f \propto \frac{1}{a^2 H} \propto a^{-\frac{1}{2}(1-3w_\infty)} \to 0 \,. \tag{5.25}$$

The crucial point is that the same asymptotic behaviour is obtained for all cases where the decaying mode is present, up to a change of the prefactor in (6.5) which depends on the initial conditions and on the amplitude of the decaying mode with respect to the growing mode. This immediately follows from the fact that one can neglect the last term in Eq.(5.1) in this regime, so that

$$\delta_m = \delta_\infty + \text{const} \int \frac{dt}{a^2} = \delta_\infty + \text{const} \int \frac{dN}{a^2 H} \,. \tag{5.26}$$

The same occurs for the more general modified gravity eq.(5.6), apart from the case of an anomalously large growth of G_{eff} in the future. On the other hand we have in the future $(w_\infty < -\frac{1}{3})$

$$\Omega_m \sim a^{3w_\infty} \,. \tag{5.27}$$

Using the definition of γ, eq. (5.10), it is straightforward to obtain

$$\gamma = \frac{\ln f}{\ln \Omega_m} \to \gamma_\infty \,, \tag{5.28}$$

for *all* curves with γ today smaller or larger than the value obtained when we integrate eq.(6.1) with $\gamma(1) = \gamma_{-\infty} (= \frac{6}{11}$ for $w_{DE} = -1)$. This is somehow complementary to the results obtained in [154] where the limit of a vanishing decaying mode was considered, however allowing for models beyond GR. Of course, in standard cosmological scenarios, the decaying mode is negligible already deep in the matter era so this result is essentially of mathematical interest. This is nicely illustrated with figure (6.2.1) for $w_{DE} = -1$, all curves tend to the same limit $\gamma_\infty = \frac{2}{3}$ but only one curve, corresponding to the limit of a purely growing mode, tends to the finite value $\gamma_{-\infty} = \frac{6}{11}$ in the past.

5.3 Global evolution of the slope $\Gamma(\Omega_m)$

In this section we want to consider more closely the slope of $\gamma(\Omega_m)$ when γ evolves with time and this will allow us to find an interesting connection with the constant γ case. It is seen from (6.1) that a solution can satisfy $\frac{d\gamma}{d\Omega_m} = 0$ in the (γ, Ω_m) plane only on the curve $\Gamma(\Omega_m)$ defined as

$$\overline{w} = w_{DE} \,, \tag{5.29}$$

where w_{DE} is the true equation of state (EoS) of the DE component of the system under consideration, while $\overline{w}$ is given in (5.11). We can view $\overline{w}(\Omega_m, \gamma)$ as a given function of both variables Ω_m and γ, while w_{DE} is the EoS of DE given in function of Ω_m. Hence in each value of Ω_m, the curve $\Gamma(\Omega_m)$ takes that value of γ such that $\overline{w} = w_{DE}$, namely

$$\overline{w}\left(\Omega_m, \Gamma(\Omega_m)\right) = w_{DE}(\Omega_m) \ . \tag{5.30}$$

The fact that $\Gamma(\Omega_m)$ is not constant just means that the solution $\gamma(\Omega_m)$ of (6.1) is not constant. The curve $\Gamma(\Omega_m)$ defined by (5.29) satisfies by construction in the asymptotic future

$$\overline{w}\left(0, \Gamma(0)\right) = w_\infty \ . \tag{5.31}$$

Hence we have in view of equalities (5.16) and (5.14)

$$\Gamma(0) = \frac{3w_\infty - 1}{6w_\infty} = \gamma_\infty \ . \tag{5.32}$$

Analogously, we get in the asymptotic past

$$\overline{w}\left(1, \Gamma(1)\right) = w_{-\infty} \ , \tag{5.33}$$

with, using (5.17) and (5.15)

$$\Gamma(1) = \frac{3(1 - w_{-\infty})}{5 - 6w_{-\infty}} = \gamma_{-\infty} \ . \tag{5.34}$$

It is exactly here that we can use the crucial property reminded at the end of Section 5.1. Indeed, as it was shown in [191], the solution $\gamma(\Omega_m)$ of (6.1) starts at $\gamma_{-\infty}$ in the past and tends to γ_∞ in the future (whence our choice of notation). In other words the curves $\Gamma(\Omega_m)$ and $\gamma(\Omega_m)$ meet at their endpoints (see figure (5.1.1)). It is also seen from (6.1) that all points (γ, Ω_m) above the curve $\Gamma(\Omega_m)$ satisfy $\frac{d\gamma}{d\Omega_m} > 0$; on the other hand in the region below $\Gamma(\Omega_m)$ we have $\frac{d\gamma}{d\Omega_m} < 0$.

Let us assume that (5.29) represents a monotonically decreasing function of Ω_m, hence $\gamma_\infty > \gamma_{-\infty}$. This holds for example for all constant EoS of DE inside GR. Then it is clear that $\gamma(\Omega_m)$ cannot cross the curve $\Gamma(\Omega_m)$ at some value γ_1 with $\gamma_{-\infty} < \gamma_1 < \gamma_\infty$. If it did, $\gamma(\Omega_m)$ would cross with a zero derivative and have its minimum at γ_1. This is in contradiction with $\gamma_{-\infty} < \gamma_1$.

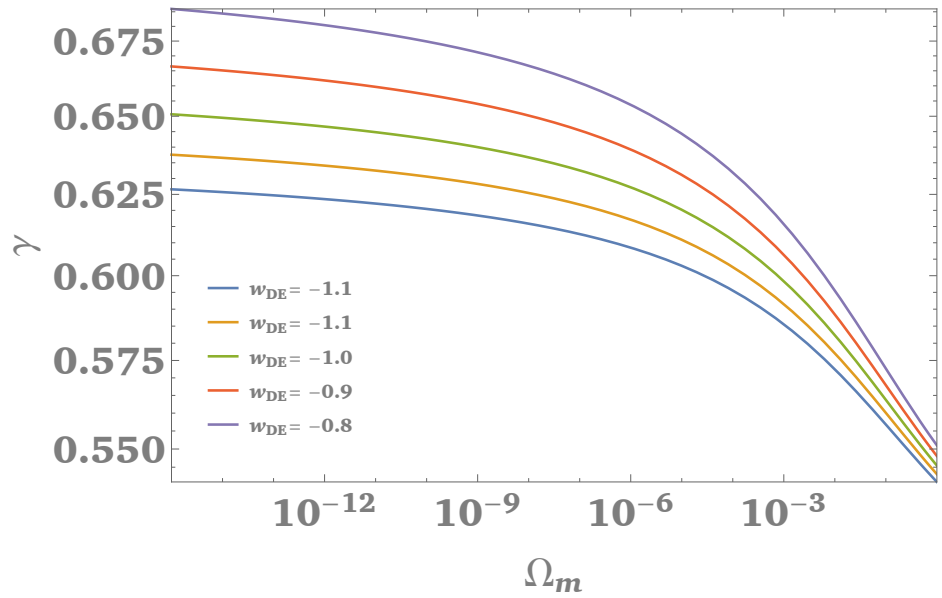

Figure 5.3.1: The growth index with various constant equations of state w_{DE}. As explained before, the monotonically decreasing behaviour of $\gamma(\Omega_m)$ holds in these models. We have used a logarithmic-scale in Ω_m.

This also shows that a change in the sign of the slope of $\gamma(\Omega_m)$ is possible only if $\Gamma(\Omega_m)$ is not a monotonically decreasing function of Ω_m. Note that the slope of $\gamma(\Omega_m)$ does not vanish at $\Omega_m = 1$ and $\Omega_m = 0$ even though $\gamma(\Omega_m)$ and $\Gamma(\Omega_m)$ meet there. Actually it even diverges in $\Omega_m = 0$ [191]. Indeed, we have that the prefactor of the first term of (6.1) vanish there leaving the slope a priori unspecified.

For a given growth function f, a lower Ω_m implies a lower γ. For a given Ω_m on the other hand, a decrease in f induces an increase in γ. All this is clearly understood from the equality $\gamma = \frac{\ln f}{\ln \Omega_m}$. When $\gamma(\Omega_m)$ is monotonically descreasing, and this is the case for generic w_{DE} inside GR, it is the second effect which prevails.

5.4 Systems with a non-monotonic $\gamma(\Omega_m)$

We can consider now several cases where the growth index is not a monotonically decreasing function of Ω_m - in sharp contrast with ΛCDM.

5.4.1 Varying equation of state $w_{\rm DE}(z)$

The first case that comes to one's mind is an oscillating equation of state w_{DE}. Indeed, it is easy to show that $\Gamma(\Omega_m)$ is no longer monotonically decreasing in this case and that γ may oscillate provided the oscillations in w_{DE}, and hence in $\Gamma(\Omega_m)$, are sufficiently pronounced. Observations however do not seem to favour such oscillations. We rather want to investigate whether a smoothly varying EoS can lead to a change in slope of γ. For this purpose we use the parametrization in terms of $x \equiv \frac{a}{a_0}$ [62]

$$w_{DE} = w_0 + w_a(1-x) \ . \tag{5.35}$$

We consider the cases with

$$w_{-\infty} = w_0 + w_a < 0 \ , \qquad w_a > 0 \ . \tag{5.36}$$

The first inequality is to enforce the domination of matter (and the disappearance of DE) in the past. We also restrict our attention to $w_a > 0$ in order to have a varying EoS leading to the opposite case in the future, namely DE domination and disappearance of matter. Also we will not impose the restriction $w_{DE} \geq -1$ valid for quintessence (a self-interacting scalar field minimally coupled to gravity) and admit arbitrarily negative values of w_{DE}.

We consider conservative values $0 < w_a \leq 0.5$ and $w_0 \approx -1$. We obtain that $\gamma(x)$ is quasi-constant deep in the matter dominated stage and starts decreasing (with the expansion) in the past typically at $z \simeq 10$, this decrease being stronger as w_a is larger. In the future, a bump is obtained typically at $z \simeq -0.9$, which is higher for lower w_a, this bump would essentially disappear for $w_a = 0.8$. Finally in the asymptotic future $\gamma \to \frac{1}{2}$ as we expect for $w_\infty \to -\infty$.

As a function of Ω_m, γ will be increasing deep in the DE domination typically until $\Omega_m \simeq 10^{-5}$, then decreasing until $\Omega_m \simeq 0.7$, and finally increasing again for $w_a \gtrsim 0.2$. To summarize, $\gamma(\Omega_m)$ is essentially slowly varying and decreasing from the past to the future in this case covering in particular the range probed by observations. The significant changes in slope are pushed around $\Omega_m \approx 0$. While this is interesting in itself, from an observational point of view models with $w_a \lesssim 0.2$ follow essentially the ΛCDM phenomenology regarding their growth index. Strong departure from ΛCDM takes place in the remote future only. These features are shown on figure 5.4.1.

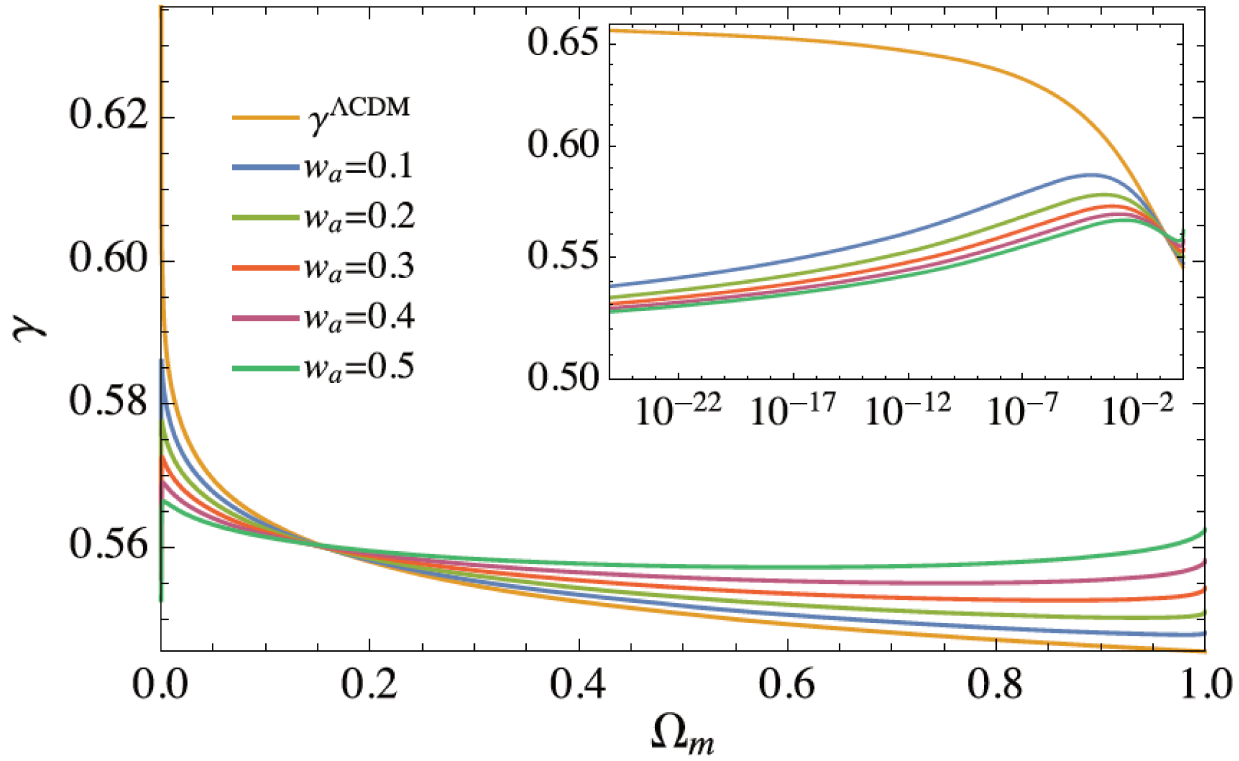

Figure 5.4.1: The evolution of γ is shown for CPL varying w_{DE}. We see that $\gamma(\Omega_m)$ is essentially decreasing except in the remote future and, for $w_a \gtrsim 0.2$, in the far past. Note the value $\gamma_\infty = \frac{1}{2}$ as expected for $w_\infty = -\infty$.

5.4.2 Beyond GR: A Bump/Dip in $g(\Omega_m)$

There is however another way to have a change of slope of γ, and possibly in the range probed by observations. This is in the framework of modified gravity (see e.g. [77]) when g is substantially varying and this can take place even when w_{DE} is almost constant and close to -1. We have to use the modified version of (6.1) with $F(\Omega_m;\gamma)$ replaced by $F(\Omega_m; g, \gamma)$ where g can be some arbitrary function, no longer equal to one as in GR. As we have already said earlier, a decreasing Ω_m tends to decrease γ while a decreasing f tends to increase it, see Eq.(5.28). A substantially varying $g(\Omega_m)$ can work in both ways depending on how it boosts or dampens the growth and on the time this process takes place. In other words it can strongly affect f even if the background evolution remains "standard".

A boost in g was already found some time ago for $f(R)$ modified gravity. Let us consider more closely this

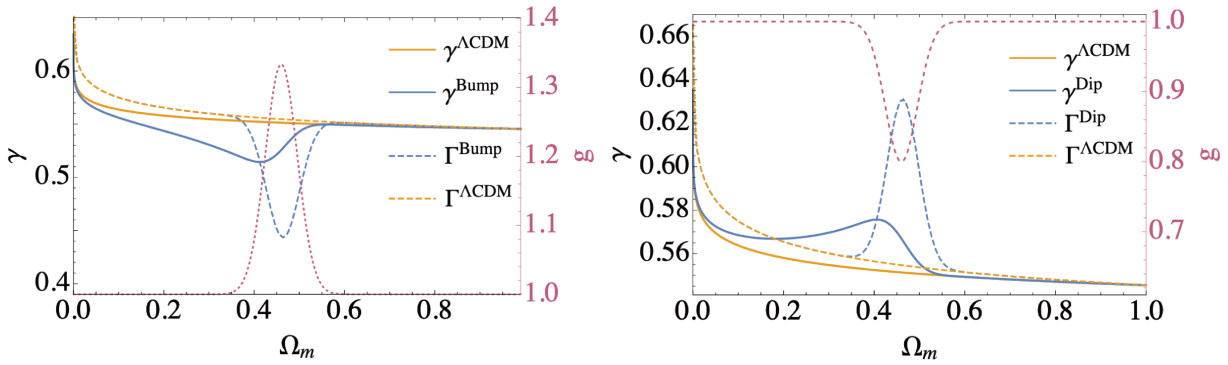

Figure 5.4.2: (a) *Left-hand panel:* A schematic representation is given when there is a bump in g, chosen here to be slightly in the past (with $\Omega_{m,0} = 0.3$) while the background expansion is fixed ($w_{\rm DE} = -1$). We see that γ decreases first (with the expansion) when g goes up before increasing when g decreases back to one. It is this last behaviour that was found today in many $f(R)$ models. Hence, the sign of the derivative tells us that we (just) passed the maximum of the bump. Note that $\gamma^{\rm Bump}$ and $\gamma^{\Lambda\rm CDM}$ shown here have the same asymptotic values both in the past and future because $g \to 1$ in a smooth way and they have identical $w_{\rm DE}$. The behaviour on small redshifts and in the future captures essentially the $f(R)$ phenomenology. (b)*Right-hand panel:* the same as on the left panel but now with a dip in g starting today. At the present time, $\gamma > \gamma^{\Lambda\rm CDM}$ and γ are decreasing with the expansion, reflecting that g is increasing and we just have passed the minimum of the dip.

case. When the bump in g has reached its maximum ($\approx \frac{4}{3}$) in the past, g is already starting on low redshifts its decrease towards its asymptotic value 1 while still being higher today than 1. This explains the low value $\gamma_0 \approx 0.42$ obtained in [104, 165] but also the large *negative* slope $\frac{d\gamma}{dz} \approx -0.25$. It would also be possible in principle in $f(R)$ models to have a bump whose maximum is reached in the future with g today already substantially larger than one. In that case γ_0 could be again substantially lower than 0.55 however now the slope on low redshifts would be positive, increasing with z. While in $f(R)$ models we have $g \geq 1$, one can have modified gravity models with gravity weaker than GR. Then a decrease of g on low redshifts yields an increasing γ on these redshifts. This is in agreement with results found in [105]. These provide good examples for which a global analysis gives more insight: on a background with $w_{DE} = -1$, γ today higher than $\gamma^{\Lambda CDM}$ with $\frac{d\gamma}{dz} > 0$ tells us that that we have presently passed a dip in g. On the other hand γ today lower than $\gamma^{\Lambda CDM}$ with $\frac{d\gamma}{dz} < 0$ occurs if we have presently passed a bump in g. Roughly speaking, we have γ increasing, resp. decreasing when g is decreasing, resp. increasing, so they have opposite behaviours. We note finally a shift in the location of the extrema of g and of γ and as expected a dependence on the location and on the width of the bump in g. These properties are shown on Fig. 5.4.2. The presence of a bump in

g will manisfest itself as a bump in the growth function $f(z)$. This behavior is schematically represented in Fig.5.4.3 for different widths and locations of the bump.

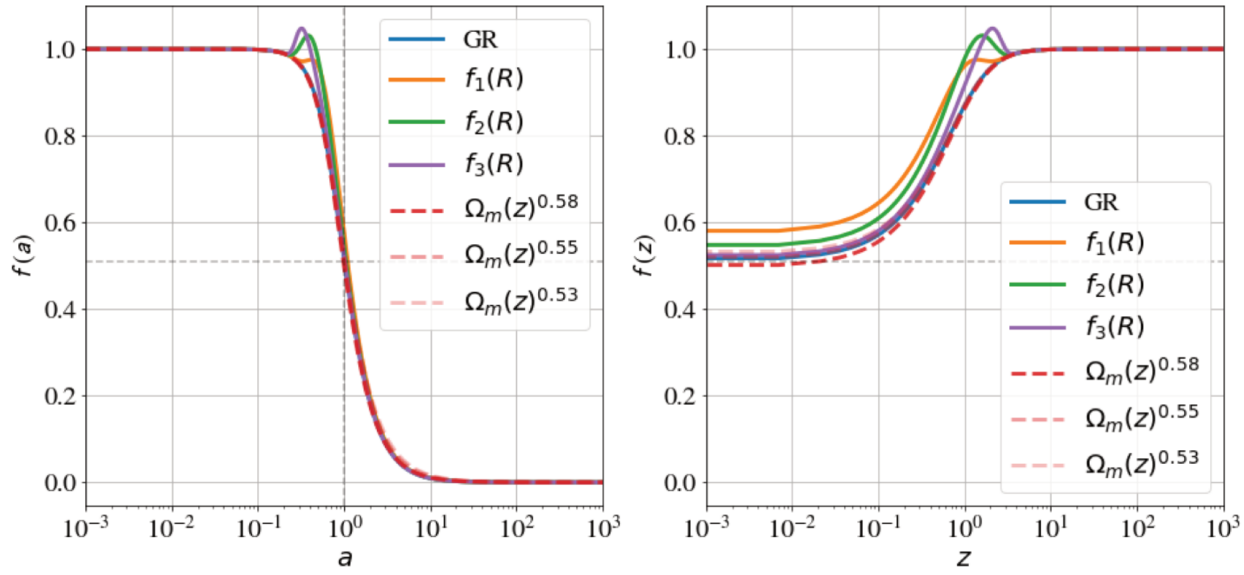

Figure 5.4.3: Left panel: The growth function $f \equiv \frac{d\ln\delta_m}{d\ln a}$ in the presence of a bump in $g = \frac{G_{\rm eff}}{G}$. Right panel: Evolution of f as a function of redshift. The approximation $f = \Omega_m^\gamma$ is shown for comparison, for different values of γ. It is seen that the growth of perturbations in GR is well approximated by $\gamma \simeq 0.55$. In the past, already at $z \sim 10$ where matter dominates their evolution is nearly identical with $f = 1$, and thus $\delta_m \propto a$ as expected. Small departures from the "*true*" numerical solution (GR) can be seen at low-z, where γ starts to depart from its "nearly constant" regime.

5.4.3 Beyond GR: DGP (Braneworld) Gravity

Another interesting example is provided by DGP brane models [89]. Let us note first that in this model both g and w_{DE} are given explicitly in terms of Ω_m as follows [156]

$$w^{\rm DGP} = -[1+\Omega_m]^{-1} \quad , \qquad g^{DGP} = 1 - \frac{1}{3}\frac{1-\Omega_m^2}{1+\Omega_m^2} \ . \tag{5.37}$$

Hence it is straightforward to integrate $\gamma(\Omega_m)$ using the integration variable Ω_m as in (6.1). It is seen from (5.37) that w^{DGP} tends to $w^{DGP}_\infty = -1$ in the future while g^{DGP} tends to $g^{DGP}_\infty = \frac{2}{3}$ in the future. So in the future the expansion looks like ΛCDM, however cosmic perturbations feel a weaker gravity. In the

past w^{DGP} tends to $w^{DGP}_{-\infty} = -\frac{1}{2}$ while g^{DGP} tends to $g^{DGP}_{-\infty} = 1$, so the gravitational driving force for the perturbations growth tends to its GR value. There are many interesting features when we solve for $\gamma(\Omega_m)$. Let us start with the behaviour in the future. As gravity becomes *weaker* than GR in the future, γ^{DGP} tends to γ^{GR}_{∞} corresponding to $w^{GR}_{\infty} = w^{DGP}_{\infty} = -1$. Note that this can still be so even if g grows but not too quickly, see the discussion in [154]. This can also be understood by looking at the asymptotic form of equation (6.1) for $\Omega_m \to 0$. Indeed, the same equation is obtained in GR when $g \to$ constant, also for $g \neq 1$, and even more generally if $g\Omega_m^{1-\gamma} \to 0$. Hence we obtain

$$\gamma^{DGP}_{\infty} = \frac{2}{3}\,. \tag{5.38}$$

In other words the same future asymptotic value is obtained as for ΛCDM.

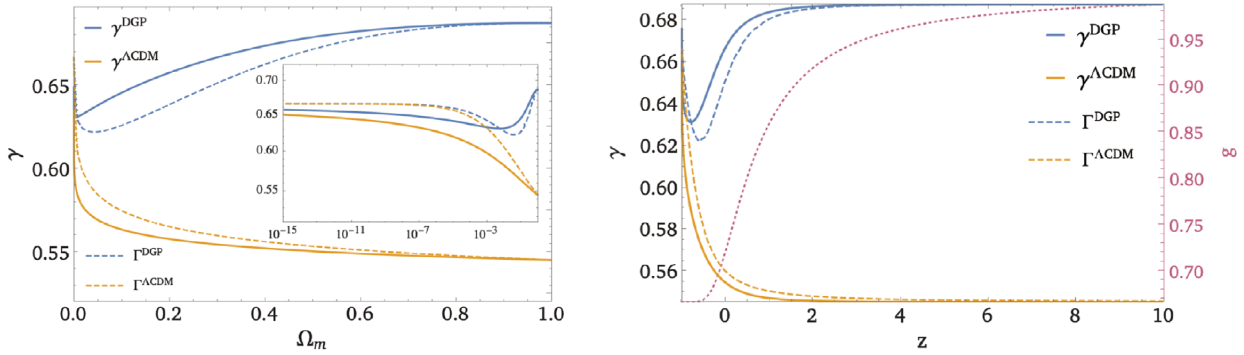

Figure 5.4.4: The behaviour of γ in DGP models is shown and compared to that in ΛCDM. We see that $\gamma^{DGP} > \Gamma^{DGP}$ and hence $\gamma^{DGP}(\Omega_m)$ is an increasing function, except for the tiny interval $\Omega_m \lesssim 10^{-3}$. While $w^{DGP}_{-\infty} = -\frac{1}{2}$, $\gamma^{DGP}_{-\infty} = \frac{11}{16}$ and not $\frac{9}{16}$ as one would have in GR. This is because the DGP model does not tend to GR in a smooth enough way, namely $\left(\frac{dg^{DGP}}{d\Omega_m}\right)_{-\infty} = \frac{1}{3} \neq 0$. In the future however, while DGP does not tend to GR with $g^{DGP}_{\infty} = \frac{2}{3}$ and $w^{DGP}_{\infty} = -1$, the same asymptotic value $\gamma^{DGP}_{\infty} = \frac{2}{3}$ is obtained as in GR for $w_{\infty} = -1$ because gravity in DGP is weaker than in GR in the far future. Note that all four curves tend to $\frac{2}{3}$ in the future.

We turn now our attention to the behaviour in the past. Curiously, while $g^{DGP}_{-\infty} = 1$ we would naively expect to have the same relation between $\gamma^{DGP}_{-\infty}$ and $w^{DGP}_{-\infty} = -\frac{1}{2}$ as between $\gamma^{GR}_{-\infty}$ and $w^{GR}_{-\infty} = -\frac{1}{2}$. However

this is not so due to the non-vanishing derivative

$$\left(\frac{dg^{DGP}}{d\Omega_m}\right)_{-\infty} = \frac{1}{3} \,. \tag{5.39}$$

In order to find $\gamma(\Omega_m)$, we can use the same method as in [191] and write Eq.(6.1) for $\Omega_m \to 1$. After some calculation, solving for $\gamma(\Omega_m)$ we obtain in the asymptotic past for the finite constant solution $\gamma_{-\infty}$ for arbitrary modified gravity models

$$\boxed{\gamma_{-\infty} = \frac{3\left(w_{-\infty} - 1 - d\right)}{6w_{-\infty} - 5}} \,, \tag{5.40}$$

where we have set

$$d \equiv \left(\frac{dg}{d\Omega_m}\right)_{-\infty} \,. \tag{5.41}$$

The GR result is recovered setting $d = 0$. Note that a similar relation was found between a constant γ corresponding to $\overline{w}_{-\infty} = w_{-\infty}$ in an arbitrary modified gravity model [191]. We finally obtain for the DGP model

$$\gamma_{-\infty}^{DGP} = \frac{11}{16} \,. \tag{5.42}$$

So the (finite) $\gamma_{-\infty}$ corresponding to $w_{-\infty} = -\frac{1}{2}$ has the value $\gamma_{-\infty}^{DGP} = \frac{11}{16}$ for a DGP model instead of $\frac{9}{16}$ for GR. The derivation given here relies *solely* on the properties of the DGP model, eq. (5.37), and exhibits the origin of this anomalous value in an explicit way (see [153],[119] for other approaches).

This value for $\gamma_{-\infty}^{DGP}$ corresponds to the constant γ^{DGP} (and $g = g^{DGP}$) yielding identical equations of state, $\overline{w}_{-\infty} = w_{-\infty}^{DGP}$, in the past. We can summarize this in the following way

$$\gamma_{-\infty}^{DGP}\left(w_{-\infty}^{DGP}\right) = \gamma\left(\overline{w}_{-\infty} = w_{-\infty}^{DGP}\right) \,. \tag{5.43}$$

The left hand side corresponds to a varying γ – the true γ obtained for w^{DGP} and g^{DGP} – while the right hand side corresponds to a constant γ in a modified gravity model with $g = g^{DGP}$. A similar equality holds in the future and we have shown it here with the DGP model

$$\gamma_{\infty}^{DGP}\left(w_{\infty}^{DGP}\right) = \gamma\left(\overline{w}_{\infty} = w_{\infty}^{DGP}\right) \,. \tag{5.44}$$

Analogous equalities were found in [191] for GR and imply that the curves $\Gamma(\Omega_m)$ and $\gamma(\Omega_m)$ meet at $\Omega_m = 0$ and $\Omega_m = 1$, a property that we have used in the previous section. We have generalized this result to a class of modified gravity models including DGP models. As a corollary, we have the following important result: any modified gravity model with $g(1) = 1$, i.e. tending to GR in the past, however in a smooth way satisfying $d = 0$, will have the same limit $\gamma^{GR}_{-\infty}(w_{-\infty})$ as in GR. As can be seen from Fig. (5.4.4), the curve $\Gamma^{DGP}(\Omega_m)$ and $\gamma^{DGP}(\Omega_m)$ intersect indeed at $\Omega_m = 0$ and $\Omega_m = 1$. In contrast to generic models inside GR, here we have $\gamma^{DGP}_{\infty} = \frac{2}{3} < \gamma^{DGP}_{-\infty} = \frac{11}{16}$. Hence $\Gamma(\Omega_m)$ cannot be monotonically decreasing, at best it would be monotonically increasing. If that were the case, $\gamma^{DGP}(\Omega_m)$ would be monotonically increasing as well, always lying above Γ^{DGP}. Actually this is what happens between $\Omega_m \simeq 10^{-3}$ and $\Omega_m = 1$. It is only in the far future, $\Omega_m \lesssim 10^{-3}$, that the slope of $\gamma^{DGP}(\Omega_m)$ is negative (i.e. γ^{DGP} increases with expansion) and that the behaviour is similar to ΛCDM.

5.5 Summary and conclusions

The growth index γ allows to distinguish efficiently the phenomenology of dark energy (DE) models and has been used extensively for this purpose (see e.g. [7, 25, 29, 33, 36, 52, 78, 86, 107, 140, 159, 160, 167–169, 237, 238, 240]). In this work we have performed an analysis of the growth index evolution from deep in the matter era till the asymptotic future. In this way global properties are exhibited. While from an observational point of view the main focus lies in the low-redshift behaviour of the growth index γ still, a global analysis yields some interesting insight and results. Some of the properties found here become transparent when we perform a global analysis of the growth index evolution. We have shown that when the growth index had a bump, resp. dip, in the recent past while the background evolution is similar to ΛCDM, today it is substantially lower, resp. larger, than 0.55 with a negative, resp. positive, slope $\frac{d\gamma}{d\Omega_m}$ reflecting that the gravitational coupling G_{eff} of the underlying modified gravity model is already decreasing, resp. increasing, with the expansion. The behaviour with a bump is a schematic representation of many $f(R)$ models [104, 165], the second case was considered in e.g. [105].

Using results valid for a constant growth index, we suggest a condition giving the global sign of the slope $\frac{d\gamma}{d\Omega_m}$: when the curve $\Gamma(\Omega_m)$ introduced in Section 5.3 is monotonically decreasing then we have *globally* $\frac{d\gamma}{d\Omega_m} < 0$. This is the case in particular for models inside GR with a constant equation of state $w_{DE} =$ constant. Another interesting point concerns the value of the growth index for a given cosmological model at a given time. Actually the growth index γ can take a range of values. What is really meant by the value of

$\gamma(\Omega_m)$ which corresponds to a given model is its value when the decaying mode of the perturbations mode tends to zero. We show that while the presence of a substantial decaying mode does not change the value of γ in the asymptotic future, this leads (as expected) to a divergence in the asymptotic past. It is only in the limit of a vanishing decaying mode that γ takes a finite value from $\gamma_{-\infty}$ in the asymptotic past ($\Omega_m \to 1$) – $\frac{6}{11}$ for ΛCDM – up to γ_{∞} in the asymptotic future ($\Omega_m \to 0$) – $\frac{2}{3}$ for ΛCDM.

We have studied further the global behaviour of γ for the DGP model. In contrast to generic models in GR, we have $\gamma^{DGP}_{-\infty} = \frac{11}{16} > \gamma^{DGP}_{\infty} = \frac{2}{3}$ with $w^{DGP}_{-\infty} = -\frac{1}{2}$ and $w^{DGP}_{\infty} = -1$. While $g^{DGP} \to \frac{2}{3}$ in the future, we have $\gamma^{DGP}_{\infty} = \gamma^{\Lambda CDM}_{\infty}$, so we get the same relation as in GR between γ^{DGP}_{∞} and $w^{DGP}_{\infty} = -1$. Interestingly, while $g^{DGP} \to 1$ in the past so this model tends to GR in the past, $\gamma^{DGP}_{-\infty} \neq \frac{9}{16}$, the value expected in GR for $w_{-\infty} = -\frac{1}{2}$. This is because the DGP model does not tend to GR in a way which is "smooth enough". Indeed, it satisfies $\frac{dg^{DGP}}{d\Omega_m}_{-\infty} = \frac{1}{3} \neq 0$. As a corrolary we find that any modified gravity model which tends to GR in the past yields a $\gamma_{-\infty}$ which is the same function of $w_{-\infty}$ as in GR provided $\frac{dg^{DGP}}{d\Omega_m}_{-\infty} = 0$. Finally we find that $\gamma^{DGP}(\Omega_m)$ is monotonically *increasing* from the past until the far future ($\Omega_m \approx 10^{-3}$) where it crosses the curve $\Gamma(\Omega_m)$ in accordance with the condition mentioned above. The results presented in this work indicate that a measurement of γ on a significant part of the expansion could give interesting constraints and a deeper insight into the physics governing the Universe dynamics.

6

The Growth Index γ: Mathematical Aspects and Physical Relevance

Adapted from

R. Calderón, D. Felbacq, R. Gannouji, D. Polarski and A. A. Starobinsky

Global properties of the growth index: Mathematical aspects and physical relevance

Physical Review D - 101, 103501 (2020)[56]

The present accelerated expansion rate of the Universe remains an outstanding challenge for theoretical cosmology. Despite intensive ongoing activity, the nature of dark energy (DE) driving the present accelerated expansion stage (physical, geometrical, or both) and its relation to known particles and fields remain unsettled [71, 145, 173, 179, 203, 204]. Many DE models inside, as well as outside, general relativity (GR)

were suggested for this purpose. While the increasing accuracy of observations allow to rule out many of them, a large number still remains viable. Among the successful DE models, ΛCDM has a very particular place due to its remarkable simplicity: it is based on GR with cold non-relativistic matter as a source, and requires only the addition of a (cosmological) constant Λ into the Einstein field equations. However, the attempt to interpret Λ in terms of 'vacuum energy' of quantum fields requires understanding why its effective energy density is so small compared to all other known substances. On the other hand, from the classical point of view, the ΛCDM is intrinsically consistent and its phenomenology serves as a benchmark for the interpretation of observational data and comparison to other DE models. Future observations will strongly constrain surviving models [19, 53, 239]. It is therefore important to have tools characterizing their phenomenology (see e.g. [201]). One such tool is the growth index γ.

The growth index has a nice property valid for ΛCDM and more generally for non-interacting smooth DE models inside GR [189]: up to a small correction depending on $\Omega_{m,0}$, its value today γ_0 is well constrained, $\gamma_0 \approx 0.55$. In addition, at higher redshifts it is quasi-constant, as depi5.3.1 (see also [191]). For example, in the presence of a cosmological constant Λ, γ tends to $\frac{6}{11}$ for $z \gg 1$ and it departs little from that value even up to the present time. Its discriminative power is therefore limited for these models. However modified gravity DE models can exhibit a strong departure from this behaviour [153],[104], [165]. The growth index offers therefore the possibility to discriminate between DE models inside and outside GR, motivating its study in the context of DE models. Hence, while the growth index was initially introduced in order to characterize the growth of matter perturbations for open Universes [177], and later generalized to other models inside GR [136], interest in the growth index was revived recently [153] for the assessment of DE models.

The study of the growth index is also of mathematical interest in its own. A global analysis of its dynamics, from deep in the matter era till the future DE dominated stage, often offers a better insight on its evolution including low redshift behavior probed by observations [55]. We will study in details a system with partially unclustered dust-like matter (or, DE tracking dust-like matter), showing interesting connections with results obtained earlier for a strictly constant growth index. We will also study the evolution of γ using the dynamical system analysis. We first review the basic formalism in the next section, as well as results and methods from our earlier work [55].

6.1 The growth index γ

Taking Ω_m as the integration variable, the evolution equation for γ obtained from (5.8) using (5.10) yields

$$2a\Omega_m \ln(\Omega_m)\frac{d\gamma}{d\Omega_m} + a(2\gamma - 1) + F(\Omega_m; g, \gamma) = 0 \ , \tag{6.1}$$

where we introduce for simplicity

$$a \equiv 3w_{DE} \ , \qquad F(\Omega_m; g, \gamma) \equiv \frac{1 + 2\Omega_m^{\gamma} - 3\,g\,\Omega_m^{1-\gamma}}{1 - \Omega_m} \ . \tag{6.2}$$

The solutions to equation (6.1) on the entire Ω_m interval is the envelope of its tangent vectors

$$\begin{pmatrix} 1 \\ \frac{d\gamma}{d\Omega_m} \end{pmatrix} .$$

All these tangent vectors define a vector field that can be written

$$\begin{pmatrix} 2a\Omega_m(1 - \Omega_m)\ln(\Omega_m) \\ -a(2\gamma - 1)(1 - \Omega_m) - \tilde{F}(\Omega_m; \gamma) \end{pmatrix} .$$

where we have defined

$$\tilde{F}(\Omega_m; g, \gamma) \equiv (1 - \Omega_m)F(\Omega_m; g, \gamma) = 1 + 2\Omega_m^{\gamma} - 3\,g\,\Omega_m^{1-\gamma} \ . \tag{6.3}$$

We write the vector field in this way in order to have explicitly regular functions everywhere for $(\Omega_m, \gamma) \in [0, 1] \times \mathbb{R}$. One obtains the integral curves of this vector field (i.e. the phase portrait) by solving the autonomous differential system

$$\begin{aligned} \frac{d\Omega_m}{ds} &= 2a\Omega_m(1 - \Omega_m)\ln(\Omega_m) \\ \frac{d\gamma}{ds} &= -a(2\gamma - 1)(1 - \Omega_m) - \tilde{F}(\Omega_m; \gamma) \end{aligned} \tag{6.4}$$

where $s \in \mathbb{R}^+$ is a dummy variable parametrizing the curves. Clearly, the trajectories $\gamma(\Omega_m)$ are not

unique. Only one integral curve however is finite everywhere: for ΛCDM, it is the curve $\gamma(\Omega_m)$ which starts (in the past) at $\gamma(1) \equiv \gamma_{-\infty} = 6/11$ and ends (in the future) at $\gamma(0) \equiv \gamma_\infty = 2/3$. It corresponds to the presence solely of the growing mode of Eq.(3.13), or equivalently to the limit of a vanishing decaying mode. For cosmological constraints on DE models, one is essentially interested in that unique trajectory corresponding to a vanishing decaying mode. It is the only trajectory which has a finite initial condition $\gamma_{-\infty}$ at $\Omega_m = 1$, for all other trajectories γ will diverge in the past. However, concerning the asymptotic future ($\Omega_m \to 0$), inside GR the solution to Eq. (6.1) gives $\gamma \to \gamma_\infty$, Eq. (5.16), with ($w_\infty < -\frac{1}{3}$)

$$f \propto C\, a^{-\frac{1}{2}(1-3w_\infty)} \to 0\ . \tag{6.5}$$

The crucial point is that this asymptotic behaviour is identical for *all* cases where the decaying mode is present, up to a change of the prefactor in (6.5) which depends on initial conditions and on the amplitude of the decaying mode with respect to the growing mode. Taking into account that $\Omega_m \sim a^{3w_\infty}$, it is straightforward to obtain from Eq. (5.10) that

$$\gamma = \frac{\ln f}{\ln \Omega_m} \to \gamma_\infty \tag{6.6}$$

for *all* curves. This is complementary to the results obtained in [154], where the growing mode for models beyond GR was considered.

6.2 Dynamical System Analysis

In this section, we will study our equations using the dynamical system approach. While the introduction of the variable Ω_m is natural for a global analysis of the evolution of the growth index γ, we use the integration variable $N \equiv \ln a$ for the dynamical system approach, and we obtain for $g = 1$ (GR)

$$2\ln(\Omega_m)\frac{d\gamma}{dN} + a(2\gamma - 1)(1 - \Omega_m) + \tilde{F}(\Omega_m; \gamma) = 0\ . \tag{6.7}$$

This is equivalent to the following differential system

$$\frac{d\Omega_m}{dN} = a(1-\Omega_m)\Omega_m \ . \tag{6.8}$$

$$\frac{d\gamma}{dN} = -\frac{a(2\gamma-1)(1-\Omega_m)+\tilde{F}(\Omega_m;\gamma)}{2\ln(\Omega_m)} \ . \tag{6.9}$$

We will use these equations in order to find the critical (or stationary) points of our system satisfying $\frac{d\Omega_m}{dN} = 0$, $\frac{d\gamma}{dN} = 0$. Note that Eq.(6.8) is independent of γ and can therefore be integrated independently. When the function $a(a) \equiv 3w_{DE}(a)$ is known, we can obtain $a(\Omega_m)$ using (5.4). We find readily from (6.8) that $\frac{d\Omega_m}{dN} = 0$ in the following three cases: $\Omega_m = 0$, $\Omega_m = 1$, $a(\Omega_m) = 0$. The stability of a dynamical system is given by the Hartman-Grobman theorem which asserts that there is a certain 2×2 matrix whose eigenvalues characterize the behavior of the system around the critical points.
For the critical point corresponding to $\Omega_m = 1$

$$S = \left(\Omega_m = 1, \gamma = \gamma_{-\infty}\right) \ , \tag{6.10}$$

we find that the eigenvalues of our system are $(-2a_{-\infty}, 2a_{-\infty} - 5)$ and therefore the critical point is a saddle point for $a_{-\infty} \leq 0$. For the critical point corresponding to $\Omega_m = 0$

$$A = \left(\Omega_m = 0, \gamma = \gamma_{\infty}\right) \ , \tag{6.11}$$

the eigenvalues of the linearized system are $(a_\infty, 0)$ and therefore we conclude that it is an attractor for $a_\infty \leq 0$. Notice that the zero eigenvalue does not point to any stability or instability, but a simple centre manifold analysis allows us to conclude about the stability of the critical point. To study the structure of the phase space at infinity, we define $u = 1/\gamma$. We obtain that $u = 0$ ($\gamma = \pm\infty$) is also a critical point and it is easy to show that $u = 0$ is a repeller. These results of the dynamical system analysis confirm the asymptotic properties found analytically and numerically in [55] and summarized in Section 5.1.

The remaining critical points correspond to $a(\Omega_m) = 0$ and $\tilde{F} = 0$. Indeed, various critical points can exist if $a(\Omega_m)$ has different zeroes. These critical points can have a richer structure. The eigenvalues associated to this system are $(-2\Omega_m^\gamma - 1/2, \Omega_m(1-\Omega_m)a'(\Omega_m))$. If $\frac{da}{d\Omega_m} \equiv a'(\Omega_m) < 0$, the critical point is an attractor, if $a'(\Omega_m) > 0$, the critical point is a saddle point. In particular for constant γ, these

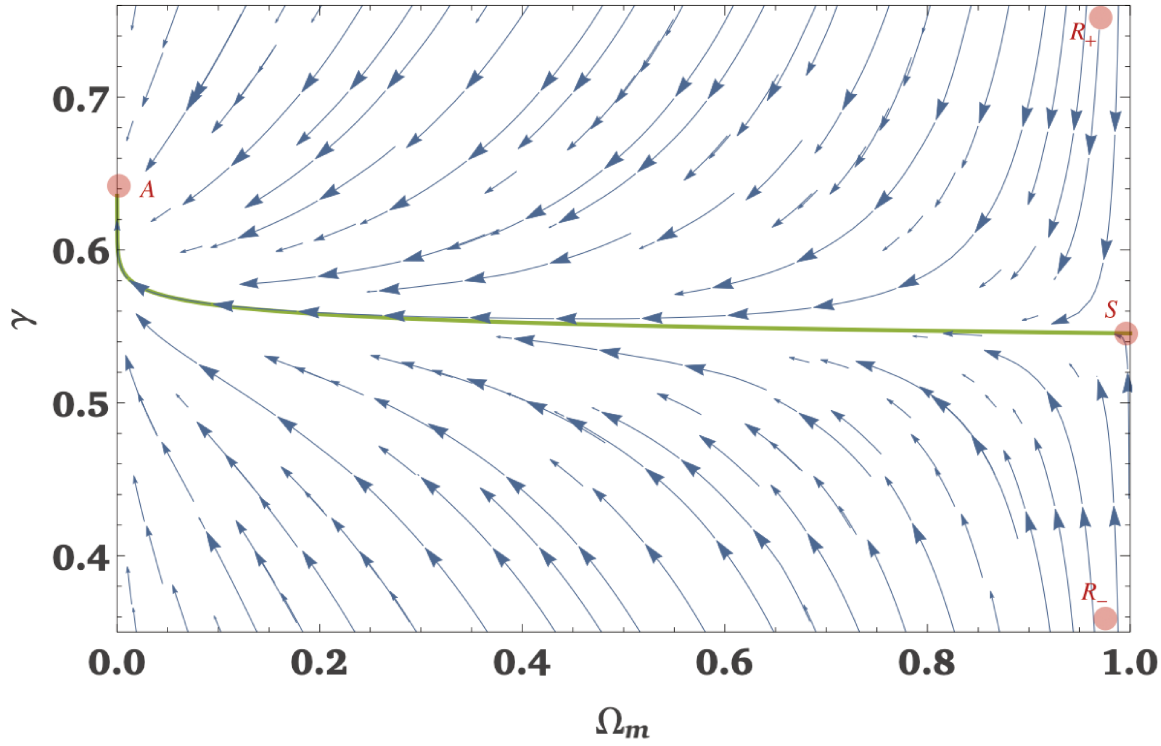

Figure 6.2.1: Streamlines (Phase Portrait) for the dynamical system {(6.8),(6.9)}. Point $A = (\Omega_m = 0, \gamma_\infty)$ corresponds to an attractor of the system, $S = (\Omega_m = 1, \gamma_{-\infty})$ is a saddle point and $R_\pm$ refers to the two critical points at infinity, which are both repellers of the system. The green line denotes the so-called *heteroclinic orbit* (connecting the two critical points S & A.), which corresponds to the solely presence of the growing mode for $\delta(a)$[55].

critical points correspond to the family of tracking DE solutions for $\Omega_m < 1$ and $\tilde{F} = 0$ found in [191]. As $\frac{d\bar{w}}{d\Omega_m} > 0$ in this case, our calculations confirm that these critical points correspond to saddle points. In the simpler (and generic) case where a has no zeroes ($a < 0$), we can sketch the evolution of the system in the phase space (Ω_m, γ) (see Fig. 6.2.1).

We see from Fig.(6.2.1), the existence of a special orbit, known as an heteroclinic orbit which connects the 2 critical points. Because it follows the repelling direction of the saddle point, it is easy to find from the eigenvector of the linearized system the behavior of this orbit around the critical point at $\Omega_m = 1$ and one

obtains

$$\gamma = \gamma_{-\infty} + \frac{(a_{-\infty}-2)(a_{-\infty}-3)+2a'_{-\infty}(2a_{-\infty}-5)}{2(5-4a_{-\infty})(5-2a_{-\infty})^2}(1-\Omega_m) + \mathcal{O}\Big((1-\Omega_m)^2\Big)\,. \tag{6.12}$$

This line is the asymptote of the heteroclinic orbit. Note that (6.12) generalizes the result given in [191] for constant a. One checks easily that ΛCDM satisfies indeed (6.12). Because we consider a dynamical system (system of first order differential equations), the trajectories (orbits) in phase space cannot intersect. But of course other curves which are not orbits of the system can intersect these orbits, e.g. we can consider the curve for which $\frac{d\gamma}{dN} = 0$ everywhere. For $a < 0$, it satisfies $\frac{d\gamma}{d\Omega_m} = 0$ for $0 < \Omega_m < 1$ and goes through the endpoints $\gamma_{-\infty}$, resp. γ_{∞}, at $\Omega_m = 1$, resp. $\Omega_m = 0$. from eqs.(6.10),(6.11).So it corresponds to the curve dubbed $\Gamma(\Omega_m)$ in [55]. It satisfies $\overline{w}(\Omega_m,\ \Gamma(\Omega_m) = w_{DE}(\Omega_m))$ and we have indeed $\Gamma(1) = \gamma_{-\infty}$ and $\Gamma(0) = \gamma_{\infty}$. For arbitrary w_{DE}, γ is not constant and hence $\Gamma(\Omega_m)$ is not constant either. As Γ satisfies by construction $\frac{d\gamma}{dN} = 0$ and critical points are defined by $(\frac{d\gamma}{dN} = 0, \frac{d\Omega_m}{dN} = 0)$, Γ must intersect the critical points, but of course it can also intersect orbits at points which are not critical points. We can ask if it is above or under the heteroclinic orbit that we previously defined because they start and end at the same points. A global analysis is impossible, but we can at least analyze the behavior around $\Omega_m = 1$. We have already found the tangent to the heteroclinic orbit (see Eq.6.12). We can also calculate the tangent to Γ and we find around $\Omega_m = 1$

$$\Gamma = \gamma_{-\infty} + \frac{(a_{-\infty}-2)(a_{-\infty}-3)+2a'_{-\infty}(2a_{-\infty}-5)}{2(5-2a_{-\infty})^3}(1-\Omega_m) + \mathcal{O}\Big((1-\Omega_m)^2\Big)\,. \tag{6.13}$$

Therefore Γ lies above the heteroclinic orbit iff

$$a'_{-\infty} < \frac{(a_{-\infty}-2)(a_{-\infty}-3)}{10-4a_{-\infty}}\,. \tag{6.14}$$

One checks easily that ΛCDM satisfies (6.14). These results can be easily generalized to modified gravity for which the system becomes

$$\frac{d\Omega_m}{dN} = a(1-\Omega_m)\Omega_m \tag{6.15}$$

$$\frac{d\gamma}{dN} = -\frac{a(2\gamma-1)(1-\Omega_m)+\tilde{F}(\Omega_m;g,\gamma)}{2\ln(\Omega_m)} \tag{6.16}$$

We recover the same critical points as in GR if $g = 1$. Note that $g_{-\infty} = 1$ and $\left(\frac{dg}{dN}\right)_{-\infty} = 0$ in order to avoid that $w_{-\infty}$ becomes singular [191]. The coordinate of the critical point at $\Omega_m = 1$ changes into

$$\left(\Omega_m = 1, \gamma = \frac{a_{-\infty} - 3 - 3g'_{-\infty}}{2a_{-\infty} - 5}\right) . \tag{6.17}$$

As expected, the expression for γ in Eq.(6.17) corresponds to the only finite value in the asymptotic past found earlier [55]. Finally, we can also find the condition for which the curve Γ starts at $\Omega_m = 1$ with an inclination larger than that of the heteroclinic orbit, viz.

$$\begin{aligned} a'_{-\infty} &< \frac{(a_{-\infty}-2)(a_{-\infty}-3)}{10-4a_{-\infty}} + \frac{3}{2}g''_{-\infty}(2a_{-\infty}-5) \\ &+ 3g'_{-\infty}\frac{33-28a_{-\infty}+6a_{-\infty}^2-27g'_{-\infty}+12a_{-\infty}g'_{-\infty}-6(5-2a_{-\infty})^2 g''_{-\infty}}{2(2a_{-\infty}-5)(6g'_{-\infty}+1)} . \end{aligned} \tag{6.18}$$

When we apply this equation to the Dvali-Gabadadze-Porrati (DGP) model [89] ($g'_{-\infty} = \frac{1}{3}$), it is found that the inequality (6.19) is satisfied. Hence the heteroclinic orbit in the DGP model is a decreasing function of Ω_m in the neighbourhood of $\Omega_m = 1$. This contrasts with the general shape of the heteroclinic orbit in the DGP model: it is an increasing function of Ω_m except for $\Omega_m \lesssim 10^{-3}$ and $\Omega_m \gtrsim 0.9$, the latter decrease (in the asymptotic past) is very tiny as compared to the sharp decrease in the asymptotic future [55].

6.3 Presence of an Unclustered Dustlike Component

We consider yet another case inside GR where the growth index $\gamma(\Omega_m)$ is not monotonically decreasing in contrast to ΛCDM. Let us note first that in the particular case where Ω_m is constant, we readily get from (5.8)

$$f' + f^2 + \frac{1}{2}f - \frac{3}{2}C = 0 \,, \tag{6.19}$$

and we set $\Omega_m = C$ to emphasize the constancy of Ω_m. Equation (6.19) has two constant solutions

$$p_1 = -\frac{1}{4} + \frac{1}{4}\sqrt{1+24C} \,, \qquad p_2 = -\frac{1}{4} - \frac{1}{4}\sqrt{1+24C} \,. \tag{6.20}$$

For $C > 0$, we have necessarily $p_1 > 0$ and $p_2 < 0$. In other words, there are two genuinely growing and decaying modes for δ_m. When $C = 1$ we recover the standard results in an Einstein-de Sitter universe.

An interesting situation arises when dust-like matter has some (small) relative fraction Ω_x which does not cluster and only usual matter denoted by Ω_m does, with

$$\Omega_m^{\rm tot} \equiv \Omega_m + \Omega_x = 1 \,. \tag{6.21}$$

Phenomenologically, this unclustered component could be ultra-light dark matter, or DE tracking matter[1] *exactly*, thought later we will consider the presence of a DE component different from the unclustered (dustlike) matter component. It can also represent a light relativistic species like massive neutrinos once they become non-relativistic. Then Eq.(6.19) is obtained with $C = \Omega_m < 1$. Let us consider for concreteness the situation with $\Omega_x \ll 1$. From (6.20) the growing mode scales $\propto a^{p_1}$ with

$$p_1 \approx 1 - \frac{3}{5}\Omega_x \approx \Omega_m^{\frac{3}{5}} \,. \tag{6.22}$$

The last term in (6.22) makes contact with the growth index γ. In the case under consideration, both Ω_m and $f = p_1 > 0$ are constant, hence γ is constant, too, and from (6.22) it is close to $\frac{3}{5}$ (see the nice discussion in [225]). In [191], a family of solutions with constant $\gamma > \frac{3}{5}$ was found corresponding to the roots of $F(\Omega_m;\gamma)$ for $\Omega_m < 1$ with $\overline{w} = 0$ so that Ω_m remains constant. This corresponds to our system with

[1] *i.e.* having the effective equation of state $w_{DE} = 0$ at this stage

$\overline{w} = w_x$. For $\Omega_x \ll 1$ it was found [191]

$$p_1 = \Omega_m^{\frac{3}{5}\left(1+\frac{\Omega_x}{25}\right)} , \tag{6.23}$$

when we expand γ up to first order in Ω_x. We see that (6.23) refines the result (6.22) (see also [153], [149]). We now extend these results to a universe where the expansion is driven also by an additional non-tracking (genuine) dark energy component so that Ω_m is no longer constant. The equation for γ in the presence of a dust-like matter component Ω_x that does not cluster simply becomes

$$\left[2\ \Omega_m^{\rm tot} \ln\left((1-\varepsilon)\Omega_m^{\rm tot}\right) \frac{d\gamma^\varepsilon}{d\Omega_m^{\rm tot}} + (2\gamma^\varepsilon - 1)\right]\ a(1-\Omega_m^{\rm tot}) + \tilde{F}((1-\varepsilon)\Omega_m^{\rm tot}; \gamma^\varepsilon) = 0 , \tag{6.24}$$

with

$$\Omega_{DE} = 1 - \Omega_m^{\rm tot}, \qquad \Omega_m = (1-\varepsilon)\Omega_m^{\rm tot} , \qquad \Omega_x = \varepsilon\ \Omega_m^{\rm tot} , \tag{6.25}$$

obviously satisfying

$$\Omega_m^{\rm tot} + \Omega_{\rm DE} = \Omega_m + \Omega_x + \Omega_{\rm DE} = 1 . \tag{6.26}$$

We have noted $\gamma^\varepsilon(\Omega_m^{\rm tot})$ the solution of Eq.(6.24) for $\varepsilon > 0$. In the asymptotic past, $\Omega_{DE} \to 0$, this reduces to

$$-6\ w_{-\infty} \ln(1-\varepsilon) \frac{d\gamma^\varepsilon}{d\ln(1-\Omega_m^{\rm tot})} + \tilde{F}(1-\varepsilon; \gamma^\varepsilon) = 0 . \tag{6.27}$$

It is seen from (6.27) that any finite solution γ^ε of (6.24) must tend in the past to the root of $\tilde{F}(1-\varepsilon;\gamma)$, viz.

$$\tilde{F}(1-\varepsilon; \gamma^\varepsilon_{-\infty}) = 0 , \tag{6.28}$$

with $\gamma^\varepsilon_{-\infty} \equiv \gamma^\varepsilon(\Omega_m^{\rm tot} \to 1)$. Considering the change of variable, $X = (1-\varepsilon)^{\gamma^\varepsilon_{-\infty}}$, the Eq.(6.28) transforms into

$$2X^2 + X - 3(1-\varepsilon) = 0 \tag{6.29}$$

A simple characteristic (polynomial) equation, whose solutions are

$$X_{\pm} = \frac{-1 \pm \sqrt{25 - 24\varepsilon}}{4} \tag{6.30}$$

Considering only the positive root, we get

$$\gamma^{\varepsilon}_{-\infty} = \frac{\ln\left(\frac{-1+\sqrt{25-24\varepsilon}}{4}\right)}{\ln(1-\varepsilon)} \tag{6.31}$$

Expanding this expression in series near $\varepsilon = 0$ leads to

$$\boxed{\gamma^{\varepsilon}_{-\infty} \equiv \gamma^{\varepsilon}(\Omega_m^{\text{tot}} \to 1) = \frac{3}{5} + \frac{3}{125}\varepsilon + \frac{97}{6250}\varepsilon^2 + \frac{737}{62500}\varepsilon^3 + \mathcal{O}(\varepsilon^4)} \tag{6.32}$$

We recover the first two terms, the root of $\tilde{F}(1-\varepsilon;\gamma)$ to first order in ε[191] mentioned above, (6.23). Expression (6.32) extends these earlier calculations to third order in ε. We note the intriguing property that $\gamma^{\varepsilon}_{-\infty}$ does not depend on any nonzero $w_{-\infty}$. In order to understand this, we consider the corresponding vector field $\mathcal{F}[\Omega_m^{\text{tot}}, \gamma^{\varepsilon}; \varepsilon]$ tangent to the solutions γ^{ε}

$$\mathcal{F}[\Omega_m^{\text{tot}}, \gamma^{\varepsilon}; \varepsilon] = \begin{pmatrix} 2a\Omega_m^{\text{tot}}(1-\Omega_m^{\text{tot}})\ln((1-\varepsilon)\Omega_m^{\text{tot}}) \\ -a(2\gamma^{\varepsilon}-1)(1-\Omega_m^{\text{tot}}) - \tilde{F}((1-\varepsilon)\Omega_m^{\text{tot}};\gamma^{\varepsilon}) \end{pmatrix} \tag{6.33}$$

and to look for its streamlines as we have done in Section 3. For $\Omega_m^{\text{tot}} \simeq 1$ and $\varepsilon \simeq 0$, we can write the vector field (6.33) to leading order

$$\mathcal{F}[\Omega_m^{\text{tot}}, \gamma^{\varepsilon}; \varepsilon] \simeq \begin{pmatrix} (\Omega_m^{\text{tot}}-1)\ \varepsilon\ 6w_{-\infty} \\ (\Omega_m^{\text{tot}}-1)\left[(6w_{-\infty}-5)\gamma^{\varepsilon} - 3w_{-\infty} + 3\right] + \varepsilon(3 - 5\gamma^{\varepsilon}) \end{pmatrix} \tag{6.34}$$

It is seen that the leading order of the upper component $\left(\frac{d\Omega_m^{\text{tot}}}{ds}\right)$ is of order $(\Omega_m^{\text{tot}}-1)\times\varepsilon$ in the small parameters $(\Omega_m^{\text{tot}}-1)$ and ε. In the lower component $\left(\frac{d\gamma}{ds}\right)$, we have neglected all higher order terms. For

$\varepsilon = 0$ ($\Omega_x = 0$), in the neighbourhood of $\Omega_m^{\rm tot} = 1$, we obtain to leading order in $\Omega_m^{\rm tot} (= \Omega_m)$

$$\mathcal{F}[\Omega_m^{\rm tot}, \gamma; 0] \simeq \begin{pmatrix} 0 \\ (\Omega_m^{\rm tot} - 1)\left[(6w_{-\infty} - 5)\gamma_{-\infty} - 3w_{-\infty} + 3\right] \end{pmatrix} , \tag{6.35}$$

with

$$\gamma_{-\infty} \equiv \gamma(\Omega_m^{\rm tot} \to 1,\ \varepsilon = 0) . \tag{6.36}$$

To avoid that $\left.\frac{d\gamma}{d\Omega_m^{\rm tot}}\right|_{\varepsilon=0}$ diverges in the neighborhood of $\Omega_m^{\rm tot} = 1$, the lower component of $\mathcal{F}[\Omega_m^{\rm tot} \simeq 1, \gamma; \varepsilon = 0]$ must vanish too and hence we get

$$\gamma_{-\infty} = \frac{3w_{-\infty} - 3}{6w_{-\infty} - 5} , \tag{6.37}$$

so we recover the (expected) result, Eq.(5.17). On the other hand, for $\varepsilon > 0$ fixed and however small, from (6.34) the limit $\Omega_m^{\rm tot} \to 1$ gives to leading order in the small parameter ε

$$\mathcal{F}[\Omega_m^{\rm tot} \to 1, \gamma^\varepsilon; \varepsilon] \simeq \begin{pmatrix} 0 \\ \varepsilon\ \left(-5\gamma_{-\infty}^\varepsilon + 3\right) \end{pmatrix} . \tag{6.38}$$

We obtain now $\frac{3}{5}$ to lowest order in ε, viz.

$$\gamma_{-\infty}^\varepsilon = 3/5 + \mathcal{O}(\varepsilon) , \tag{6.39}$$

in agreement with (6.22), (6.23). Actually, if we take the limit $\Omega_m^{\rm tot} \to 1$ in (6.33), without expanding in ε, we obtain

$$\mathcal{F}[\Omega_m^{\rm tot} \to 1, \gamma_{-\infty}^\varepsilon; \varepsilon] = \begin{pmatrix} 0 \\ -\tilde{F}\left(1 - \varepsilon; \gamma_{-\infty}^\varepsilon\right) \end{pmatrix} , \tag{6.40}$$

showing again that $\gamma_{-\infty}^\varepsilon$ must be a root of $\tilde{F}(1-\varepsilon; \gamma)$, and the value $\frac{3}{5}$ obtained from (6.38) is just the lowest order of the expansion of $\gamma_{-\infty}^\varepsilon$ in powers of ε.

Interestingly, there is another situation where an identical result appears [191]. Let us assume that we have a two-component system ($\varepsilon = 0$) with $\Omega_m^{\rm tot} = \Omega_m \to 1 - \delta,\ \Omega_{DE} \to \delta$. This is possible only if DE

behaves asymptotically like dust, $w_{-\infty} = 0$. If we take $\delta > 0$, we have from (6.33) in analogy with (6.40)

$$\mathcal{F}\left[1-\delta, \gamma^{\delta}_{-\infty}; \delta\right] \simeq \begin{pmatrix} 0 \\ -\tilde{F}\left(1-\delta; \gamma^{\delta}_{-\infty}\right) \end{pmatrix} , \tag{6.41}$$

which is just (6.40) with ε replaced by δ. So in this case, the small parameter that goes to zero is w instead of $1 - \Omega_m^{\rm tot}$ previously.

To summarize, the system with a small amount of unclustered dustlike component is not continuous in the variables $(\Omega_m^{\rm tot}, \varepsilon)$ at $\Omega_m^{\rm tot} = 1,\ \varepsilon = 0$ and taking the limit is affected by the order in which it is taken, viz

$$\lim_{\varepsilon\to 0} \gamma^{\varepsilon}_{-\infty} \equiv \lim_{\varepsilon\to 0} \gamma^{\varepsilon}(\Omega_m^{\rm tot} \to 1) \neq \lim_{\Omega_m\to 1} \gamma(\Omega_m) \equiv \gamma_{-\infty} \ . \tag{6.42}$$

This explains why it is possible that $\gamma^{\varepsilon}_{-\infty}$ does not depend on $w_{-\infty}$. We recover consistently from (6.33) that for $\varepsilon = 0,\ \Omega_m^{\rm tot} = \Omega_m \to 1 - \delta \neq 1,\ w_{-\infty} = 0$ (tracking DE), roots of $\tilde{F}\left(1-\delta; \gamma\right)$ yield the tracking DE solutions with a constant growth index γ found in [191].

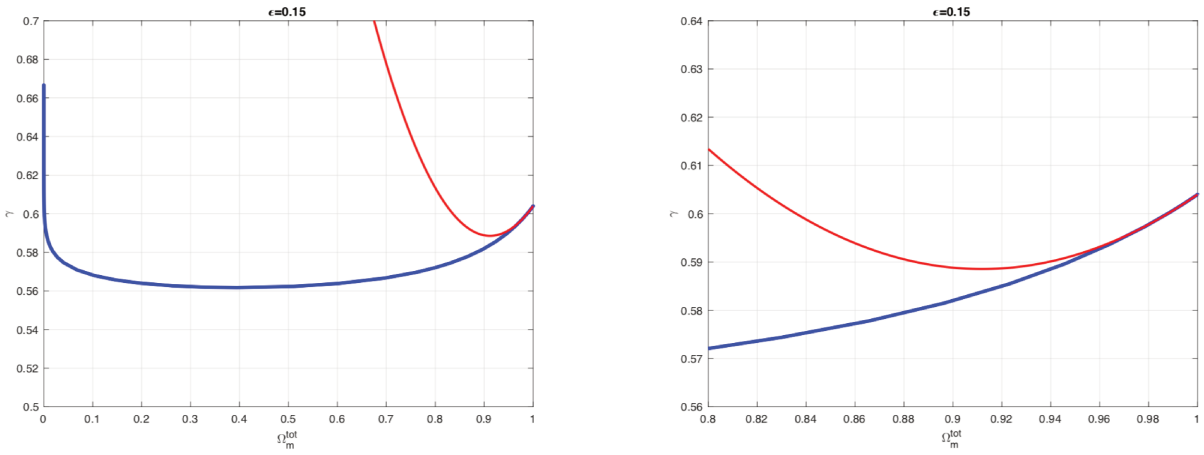

Figure 6.3.1: Left panel: The blue curve shows the reconstruction of $\gamma(\Omega_m^{\rm tot}, \varepsilon)$ for $\varepsilon = 0.15$. The red curve is the second order approximation given by Eq. (6.52). We see that they match nicely for $\Omega_m^{\rm tot} \simeq 1$. Right panel shows a zoom for $\Omega_m^{\rm tot} \simeq 1$.

After some calculations, detailed in the next subsection 6.3, for $a = -3$ ($w_{DE} = -1$) we obtain

$$\gamma_\Omega = \frac{3}{55\varepsilon} - \frac{399}{30250} - \frac{10161\varepsilon}{16637500} \tag{6.43}$$

$$\gamma_{\Omega\Omega} = \frac{6}{55\varepsilon^2} - \frac{31083}{257125\varepsilon} + \frac{12960073}{1202059375}. \tag{6.44}$$

These results are illustrated with Figure (6.3.1) where we can see that the approximation (6.52) gives an excellent match to the solution $\gamma^\varepsilon(\Omega_m^{\text{tot}})$ for $\varepsilon = 0.15$, $\Omega_m^{\text{tot}} \simeq 1$. Note that we have obtained a double expansion with respect to both Ω_m^{tot} and ε (neglecting all terms $\mathcal{O}(\varepsilon)$)

$$\begin{aligned}\gamma^\varepsilon(\Omega_m^{\text{tot}}) \simeq\ & \frac{3}{5} + \left[\frac{3}{55\varepsilon} - \frac{399}{30250}\right](\Omega_m^{\text{tot}} - 1) \\ & + \frac{1}{2}\left[\frac{6}{55\varepsilon^2} - \frac{31083}{257125\varepsilon} + \frac{12960073}{1202059375}\right](\Omega_m^{\text{tot}} - 1)^2 + \dots\end{aligned} \tag{6.45}$$

This suggests that, as a function of ε, γ^ε has an essential singularity (i.e. a pole of infinite order) at $\varepsilon = 0$. These expressions given above show explicitely the discontinuity expressed by (6.42). For $\varepsilon > 0$, γ tends in the asymptotic past to $\gamma^\varepsilon_{-\infty}$, which has been calculated here up to terms $\mathcal{O}(\varepsilon^4)$, (6.32). For $\varepsilon = 0$ on the other hand, γ tends to $\gamma_{-\infty}$ (5.17). While $\gamma_{-\infty}$ depends on $w_{-\infty}$, $\gamma^\varepsilon_{-\infty}$ doest not and is in this sense universal. Clearly it would not be possible to recover $\gamma_{-\infty}$ by taking the limit $\varepsilon \to 0$. This is what the equations above show: while $\gamma^\varepsilon_{-\infty}$ is consistently obtained from (6.45) at $\Omega_m^{\text{tot}} = 1$, the limit $\varepsilon \to 0$ does not even exist in the neighborhood $\Omega_m^{\text{tot}} \simeq 1$. Note that at $\Omega_m^{\text{tot}} = 1$, the limit $\varepsilon \to 0$ gives $\frac{3}{5}$.
We will see now other situations were the value $\frac{3}{5}$ appears. Until now we were interested in an unclustered component which behaves like dust, hence $\varepsilon =$ constant. For such a system we see from (6.45) that $\gamma^\varepsilon(\Omega_m^{\text{tot}} \to 1) \to \frac{3}{5}$. The same limit is obtained if the unclustered component instead of behaving like dust tends to such a behaviour in the past, in other words if it is a tracking component in the past with ε tending to some constant value. Finally we note that our results hold for $\varepsilon < 0$, see e.g. [46].

It is also interesting to consider an unclustered component with $w_{DE} < w_{\text{uncl}} < 0$. Specializing to

$w_{DE} = -1$, taking only the leading order term in ε at each order of the expansion (6.45), we obtain

$$\begin{aligned}
\gamma^{\varepsilon}(\Omega_{DE}) &= \frac{3}{5} + \frac{3}{55}\frac{\Omega_{DE}}{\varepsilon} + \frac{3}{55}\left(\frac{\Omega_{DE}}{\varepsilon}\right)^2 + \frac{3}{55}\left(\frac{\Omega_{DE}}{\varepsilon}\right)^3 + \cdots && (6.46)\\
&= \frac{3}{5}\left[1 + \frac{1}{11}\sum_{k=1}^{\infty}\left(\frac{\Omega_{DE}}{\varepsilon}\right)^k\right] + \cdots && (6.47)\\
&= \frac{3}{5}\left[1 + \frac{1}{11}\left(-1 + \sum_{k=0}^{\infty}\left(\frac{\Omega_{DE}}{\varepsilon}\right)^k\right)\right] + \cdots && (6.48)\\
&= \frac{6}{11} + \frac{3}{55}\sum_{k=0}^{\infty}\left(\frac{\Omega_{DE}}{\varepsilon}\right)^k + \cdots && (6.49)
\end{aligned}$$

For our system, $\frac{\Omega_{DE}}{\varepsilon} \to 0$ so the sum is well-defined and yields

$$\gamma^{\varepsilon}(\Omega_{DE}) = \frac{6}{11} + \frac{3}{55}\frac{1}{1 - \frac{\Omega_{DE}}{\varepsilon}} + \cdots \tag{6.50}$$

For $\frac{\Omega_{DE}}{\varepsilon} \to 0$ we obtain again

$$\gamma^{\varepsilon}(\Omega_{DE} \to 0) \to \frac{6}{11} + \frac{3}{55} = \frac{3}{5}\,. \tag{6.51}$$

Computing the derivative of $\gamma^{\varepsilon}(\Omega_m^{\mathrm{tot}})$

In order to evaluate the derivative of $\gamma^{\varepsilon}(\Omega_m^{\mathrm{tot}})$ with respect to Ω_m^{tot} at $\Omega_m^{\mathrm{tot}} = 1$, let us assume $\gamma^{\varepsilon}(\Omega_m^{\mathrm{tot}})$ is analytic with respect to Ω_m^{tot} and use an expansion at second order in $(\Omega_m^{\mathrm{tot}} - 1)$, viz.

$$\gamma^{\varepsilon}(\Omega_m^{\mathrm{tot}}) = \gamma^{\varepsilon}_{-\infty} + \left.\frac{d\gamma^{\varepsilon}}{d\Omega_m^{\mathrm{tot}}}\right|_{-\infty}(\Omega_m^{\mathrm{tot}} - 1) + \frac{1}{2}\left.\frac{d^2\gamma^{\varepsilon}}{d(\Omega_m^{\mathrm{tot}})^2}\right|_{-\infty}(\Omega_m^{\mathrm{tot}} - 1)^2 + \mathcal{O}\left((\Omega_m^{\mathrm{tot}} - 1)^3\right)\,. \tag{6.52}$$

For simplicity, we denote

$$\gamma_{\Omega} \equiv \left.\frac{d\gamma^{\varepsilon}}{d\Omega_m^{\mathrm{tot}}}\right|_{-\infty}, \quad \gamma_{\Omega\Omega} \equiv \left.\frac{d^2\gamma^{\varepsilon}}{d(\Omega_m^{\mathrm{tot}})^2}\right|_{-\infty}\,. \tag{6.53}$$

The derivative $\frac{d\gamma^{\varepsilon}}{d\Omega_m^{\rm tot}}$ has therefore the following expansion up to first order

$$\frac{d\gamma^{\varepsilon}}{d\Omega_m^{\rm tot}} = \gamma_{\Omega} + \gamma_{\Omega\Omega}(\Omega_m^{\rm tot} - 1)$$

Let us use this expansion in $\mathcal{F}[\Omega_m^{\rm tot}, \gamma; \varepsilon]$ given in (6.34) and compute the ratio of the components, which then gives the derivative $\left.\frac{d\gamma^{\varepsilon}}{d\Omega_m^{\rm tot}}\right|_{-\infty}$. We will assume here that a is constant. The first component is

$$2a\Omega_m^{\rm tot}(1-\Omega_m^{\rm tot})\ln\left((1-\varepsilon)\Omega_m^{\rm tot}\right) \simeq -2a\left[\ln(1-\varepsilon)(\Omega_m^{\rm tot}-1) + (\ln(1-\varepsilon)+1)(\Omega_m^{\rm tot}-1)^2\right] \ , \quad (6.54)$$

while the second component is

$$\begin{aligned} -a(2\gamma^{\varepsilon}-1)(1-\Omega_m^{\rm tot}) \quad &- \quad \tilde{F}\left((1-\varepsilon)\Omega_m^{\rm tot}; \gamma^{\varepsilon}_{-\infty} + \gamma_{\Omega}\,(\Omega_m^{\rm tot}-1) + \frac{1}{2}\gamma_{\Omega\Omega}\,(\Omega_m^{\rm tot}-1)^2\right) \\ &\equiv \quad f_0(\varepsilon) + f_1(\varepsilon)(\Omega_m^{\rm tot}-1) + f_2(\varepsilon)(\Omega_m^{\rm tot}-1)^2 + \ldots \end{aligned} \quad (6.55)$$

Considering $\Omega_m = 1$, it is trivial to find

$$f_0(\varepsilon) = -\tilde{F}\left((1-\varepsilon); \gamma^{\varepsilon}_{-\infty}\right) = 0, \quad (6.56)$$

The derivative $\frac{d\gamma}{d\Omega_m^{\rm tot}}$ is therefore given by

$$\frac{f_0(\varepsilon) + f_1(\varepsilon)(\Omega_m^{\rm tot}-1) + f_2(\varepsilon)(\Omega_m^{\rm tot}-1)^2}{-2a\ln(1-\varepsilon)(\Omega_m^{\rm tot}-1) - 2a(\log(1-\varepsilon)+1)(\Omega_m^{\rm tot}-1)^2} \ , \quad (6.57)$$

and using Eq.(6.28), we obtain $f_0(\varepsilon) = 0$. We have further

$$\begin{aligned} f_1(\varepsilon) =& a(2\gamma^{\varepsilon}_{-\infty} - 1) - 2(1-\varepsilon)^{\gamma^{\varepsilon}_{-\infty}}(\gamma^{\varepsilon}_{-\infty} + \gamma_{\Omega}\ln(1-\varepsilon)) - \\ & 3(1-\varepsilon)^{1-\gamma^{\varepsilon}_{-\infty}}(\gamma^{\varepsilon}_{-\infty} + \gamma_{\Omega}\ln(1-\varepsilon) - 1) \end{aligned} \quad (6.58)$$

$$
\begin{aligned}
f_2(\varepsilon) =& 2a\gamma_\Omega - 3(1-\varepsilon)^{1-\gamma^\varepsilon_{-\infty}} \times \\
& \left(\gamma_\Omega + \frac{1 + (-\gamma^\varepsilon_{-\infty} + \gamma_{\Omega\Omega}\log(1-\varepsilon)) - (-1 + \gamma^\varepsilon_{-\infty} + \gamma_\Omega \log(1-\varepsilon))^2}{2}\right) \\
& - 2(1-\varepsilon)^{\gamma^\varepsilon_{-\infty}} \left(\gamma_\Omega + \frac{-\gamma^\varepsilon_{-\infty} + \gamma_{\Omega\Omega}\log(1-\varepsilon) + (\gamma^\varepsilon_{-\infty} + \gamma_\Omega \log(1-\varepsilon))^2}{2}\right)
\end{aligned} \tag{6.59}
$$

If $\varepsilon > 0$, this expression is not singular at $\Omega_m^{\text{tot}} = 1$ provided that $f_0(\varepsilon) = 0$. That is to say

$$
\gamma^\varepsilon_{-\infty} = \frac{\ln\left(\frac{\sqrt{25-24\varepsilon}-1}{4}\right)}{\ln(1-\varepsilon)}. \tag{6.60}
$$

Expanding this expression in series near $\varepsilon = 0$ leads to

$$
\gamma^\varepsilon_{-\infty} \equiv \gamma^\varepsilon(\Omega_m^{\text{tot}} \to 1) = \frac{3}{5} + \frac{3}{125}\varepsilon + \frac{97}{6250}\varepsilon^2 + \frac{737}{62500}\varepsilon^3 + \mathcal{O}(\varepsilon^4) \tag{6.61}
$$

We recover the first two terms, the root of $\tilde{F}(1-\varepsilon;\gamma)$ up to first order in ε [189] mentioned above, Eq.(6.23). We can proceed to the identification

$$
\gamma_\Omega = \frac{f_1(\varepsilon)}{-2a\ln(1-\varepsilon)} \tag{6.62}
$$

$$
\gamma_{\Omega\Omega} = \frac{f_2(\varepsilon)}{-2a\ln(1-\varepsilon)} - \frac{f_1(\varepsilon)(-2a(\ln(1-\varepsilon)+1))}{(-2a\ln(1-\varepsilon))^2}\,. \tag{6.63}
$$

We first solve for γ_Ω, using (7.38)

$$
\gamma_\Omega = \frac{(1-\varepsilon)^{\gamma^\varepsilon_{-\infty}}(2\gamma^\varepsilon_{-\infty}(1-\varepsilon)^{\gamma^\varepsilon_{-\infty}} + 3(\gamma^\varepsilon_{-\infty}-1)(1-\varepsilon)^{1-\gamma^\varepsilon_{-\infty}} - a(2\gamma^\varepsilon_{-\infty}-1))}{\ln(1-\varepsilon)(3\varepsilon - 2(1-\varepsilon)^{2\gamma^\varepsilon_{-\infty}} + 2a(1-\varepsilon)^{\gamma^\varepsilon_{-\infty}} - 3)} \tag{6.64}
$$

expanding in series of ε gives

$$
\gamma_\Omega = \frac{a}{5(2a-5)\varepsilon} - \frac{26a^2 - 5a + 150}{250(2a-5)^2}\,. \tag{6.65}
$$

Finally, we use this expression in f_2 (see Eq. (7.40)) in order to solve for $\gamma_{\Omega\Omega}$ and we obtain the following

expansion (the close form expression is too complicated to be of interest)

$$\gamma_{\Omega\Omega} = \frac{2a}{5(2a-5)\varepsilon^2} - \frac{a(504a^2-1525a+1250)}{125(2a-5)^2(4a-5)\varepsilon} + \frac{61696a^5-141960a^4+658150a^3-2382375a^2+3413125a-1818750}{18750(2a-5)^3(4a-5)^2} . \tag{6.66}$$

Let us remark that near $\Omega_m^{\rm tot} = 1$, the derivative is given, up to terms of order $\mathcal{O}(\varepsilon)\mathcal{O}(\gamma_{-\infty}^{\varepsilon})$ by

$$\frac{d\gamma}{d\Omega_m^{\rm tot}} \simeq \frac{(5\gamma_{-\infty}^{\varepsilon}-3)\varepsilon}{2a(1-\Omega_m^{\rm tot})\ln((1-\varepsilon)\Omega_m^{\rm tot})} - \frac{a(2\gamma_{-\infty}^{\varepsilon}-1)+3-5\gamma_{-\infty}^{\varepsilon}}{2a\ln((1-\varepsilon)\Omega_m^{\rm tot})} \tag{6.67}$$

For $\varepsilon > 0$, this expression is not singular at $\Omega_m^{\rm tot} = 1$ provided that the first term is null, i.e. $\gamma_{-\infty}^{\varepsilon} = \frac{3}{5} + \mathcal{O}(\varepsilon)$, whereas for $\varepsilon = 0$, the first term is identically zero and the condition for the derivative to be non singular at $\Omega_m^{\rm tot} = 1$ is $\gamma_{-\infty} = (a-3)/(2a-5)$ as obtained in (6.37).

6.4 Summary and Conclusions

The growth index γ is an interesting tool for the study of the evolution of matter perturbations on cosmic scales in various cosmological models (see e.g. [7, 25, 29, 33, 36, 52, 78, 86, 107, 140, 159, 160, 167–169, 237, 238, 240] for its use in different contexts). Though it was introduced in order to characterize the influence of a non-vanishing spatial curvature on the growth of matter perturbations, interest for its study was revived in the context of DE models. Indeed, the growth index is a particularly efficient tool for the assessment of DE models in modified gravity. We are interested in the global dynamics of γ from the asymptotic past to the asymptotic future. Though only a restricted interval of redshifts is relevant for observations, a global analysis yields a deeper insight [55]. Using the dynamical system approach we have found all critical points of the system. That unique trajectory for which the growth index remains finite from the asymptotic future to the asymptotic past is identified as the heteroclinic orbit connecting the critical points $(\Omega_m = 0,\ \gamma_\infty)$ in the asymptotic future and $\left(\Omega_m = 1,\ \gamma_{-\infty}\right)$ in the asymptotic past. The critical point $(\Omega_m = 0,\ \gamma_\infty)$ is an attractor while the critical point $\left(\Omega_m = 1,\ \gamma_{-\infty}\right)$ is a saddle point. These results confirm our earlier findings [55]. We recall that this unique trajectory corresponds to a vanishing decaying mode. As an additional result, we have refined our earlier results regarding the behaviour of $\gamma(\Omega_m)$ in the DGP model and we find its very tiny decrease in the past, while it is essentially an increasing function

except in the asymptotic future ($\Omega_m \lesssim 10^{-3}$).

Finally, we have also considered a system consisting of DE with an effective equation of state having arbitrary dependence on redshift and partially clustered dust-like matter with some (small) component of the latter remaining smooth at all scales, and investigated the growth of perturbations in it at scales exceeding the Jeans (or *free-streaming*) length of gravitationally clustering matter (but much less than the Hubble scale). We have shown both analytically and numerically that $\gamma^{\varepsilon}_{-\infty}$ is the root of $\tilde{F}(1-\varepsilon;\gamma)$ for $\Omega_m \to 1-\varepsilon < 1$. Interestingly $\gamma^{\varepsilon}_{-\infty}$ does not depend on w_{DE} which is possible because, as we have shown $\lim_{\varepsilon\to 0}\gamma^{\varepsilon}_{-\infty} \neq \gamma_{-\infty}$ where the last quantity corresponds to (usual) clustered dust and depends of course on w_{DE}. The quantity $\gamma^{\varepsilon}_{-\infty}$ was found earlier to correspond to the constant growth index corresponding to tracking DE in the matter era with $\Omega_{DE} \to \varepsilon$. We find further that $\frac{d\gamma^{\varepsilon}_{-\infty}}{d\Omega_m} \sim \frac{1}{\varepsilon^2}$ for $\varepsilon \simeq 0$ suggesting that $\gamma^{\varepsilon}_{-\infty}$ has an essential singularity at $\varepsilon = 0$. The results presented in this work show that besides its use for the assessment of DE models, the growth index γ has also interesting mathematical properties reflecting physical properties of the underlying cosmological model, as in the case of an unclustered axion-like component.

Part III

A Negative Cosmological Constant in the Dark Sector?

7

Negative Cosmological Constant in the Dark Sector

Adapted from Rodrigo Calderón, R. Gannouji, B. L'Huillier and D. Polarski

Negative Cosmological Constant in the Dark Sector?

Physical Review D - 103, 023526 (2021) [57]

While the physical mechanism behind the late-time accelerated expansion rate of the Universe still remains an open question [71, 173, 179, 202], its phenomenology is known with ever increasing accuracy [20, 239]. It is interesting that perhaps the simplest model, the Λ Cold Dark Matter (ΛCDM) model, where gravity is described by general relativity whereas dark energy (DE) is simply a positive constant Λ, can account for the data to some accuracy. Hence the concordance model in which the present accelerated expansion rate is driven by a cosmological constant Λ has become the reference cosmological model. Aside from the theoretical problems, the smallness of Λ compared to expected Planckian values, it is not clearly established whether this model can successfully cope with all observations especially on small cosmic scales (see e.g. [54]). Hence one is still investigating other DE models, both inside and outside gen-

eral relativity, which are able to roughly reproduce the ΛCDM phenomenology and are therefore viable with the hope that some specific signature will single them out. Recently the so-called tensions with the concordance model, and more generally possible discrepancies [197] between early and late time measurements of cosmic quantities, have attracted a lot of interest with a special emphasis on the H_0 tension [40, 144, 211, 234, 235]. This latter tension–a substantial difference at the $\sim 4\sigma$ level between the value of the present Hubble constant H_0 derived from the cosmic microwave background (CMB) Planck data [187] on one hand and from local data on the other hand, when the concordance model is assumed–could imply that the DE sector is more complicated than in the concordance model. This is one more incentive to consider models which are more sophisticated than ΛCDM. It is well known on the other hand that the presence of a positive cosmological constant Λ in superstring models is problematic. These theories prefer a negative cosmological constant, dubbed here λ, reflecting the embedding of the anti de Sitter rather than the de Sitter symmetry group. It is therefore interesting to investigate the possibility that our homogeneous expanding Universe contains a λ term and it may come as a surprise that this is indeed viable. In some sense this is so as long as the presence of the λ term does not change radically the main properties of the expansion history of our Universe compared to the concordance model. This requires first of all that the (smooth) dark sector (which we call here for simplicity the DE sector) contains an additional component, dubbed here X component, responsible for the late-time accelerated expansion rate (see e.g. [59, 236]). Note that a transient effective λ switching around recombination to a positive Λ was considered in [241] while [9] considers the intriguing possibility of such a spontaneous switch at $z \sim 2$. Let us mention that a negative, not necessarily constant, energy component can also appear as a result of the equations of motion like the negative dark radiation component found in [45]. Among other interesting examples of components that can have negative energy is the "missing matter" of [232], the dynamical $\Lambda(t)$ term in [108], or the reconstructed total dark energy component (see e.g. [88, 192]).

We address in this work the observational viability of models in the presence of a negative λ term for several behaviors of the dark sector, investigating more specifically the constraint coming from a high H_0. Independently of observations, we study also the future evolution of such universes with constant w_X, in which case a λ term can crucially change the dynamics of our Universe. We address as well the nontrivial appearance of transient accelerated stages in the past.

7.1 Cosmic expansion with a negative cosmological constant

We recall first the basic equations and concepts. We intend to study here a universe containing a *negative* cosmological constant λ. Obviously, such a model cannot accelerate the late-time expansion rate of the Universe in the absence of some additional component in the dark sector. To comply with observations we add an X component with $w_X < -\frac{1}{3}$ on very low redshifts. For a spatially flat Friedmann-Lemaître-Robertson-Walker (FLRW) universe, the evolution of the Hubble parameter as a function of the redshift $z = \frac{a_0}{a} - 1$ at $z \ll z_{eq}$ reads

$$H^2(z) = H_0^2 \left[\Omega_{m,0}\ (1+z)^3 + \Omega_{\lambda,0} + \Omega_{X,0}\, f_X(z)\right] \ , \tag{7.1}$$

where $H(t) \equiv \dot{a}(t)/a(t)$ is the Hubble parameter, a is the scale factor and a dot stands for the derivative with respect to cosmic time t, $\Omega_i \equiv \frac{\rho_i}{\rho_{cr}}$ with $3H^2 \equiv 8\pi G \rho_{cr}$, finally $f_X(z) = \frac{\rho_X(z)}{\rho_{X,0}}$ is given by

$$f_X(z) = \exp\left[3\int_0^z dz'\ \frac{1+w_X(z')}{1+z'}\right] \ , \tag{7.2}$$

with $w_X \equiv p_X/\rho_X$. When we consider later constraints involving much larger redshifts, we will add radiation and neutrinos. It is crucial that in (7.1) we have

$$\Omega_{\lambda,0} < 0 \ , \tag{7.3}$$

as we assume the presence of a negative cosmological constant $\lambda < 0$. For such a model it is natural to make the following identification

$$\Omega_{DE,0} \equiv \Omega_{\lambda,0} + \Omega_{X,0} \simeq 1 - \Omega_{m,0} \ . \tag{7.4}$$

The combined dark energy (DE) sector must of course be able to produce the late-time accelerated expansion of the universe. Its evolution is shown in Fig.7.1.1 as a function of z and w_X. While a negative cosmological constant can hide in the dark sector during the past evolution of our Universe, it can significantly modify its future evolution. Before considering the asymptotic future it is also very interesting to study the appearance of accelerated stages in such models.

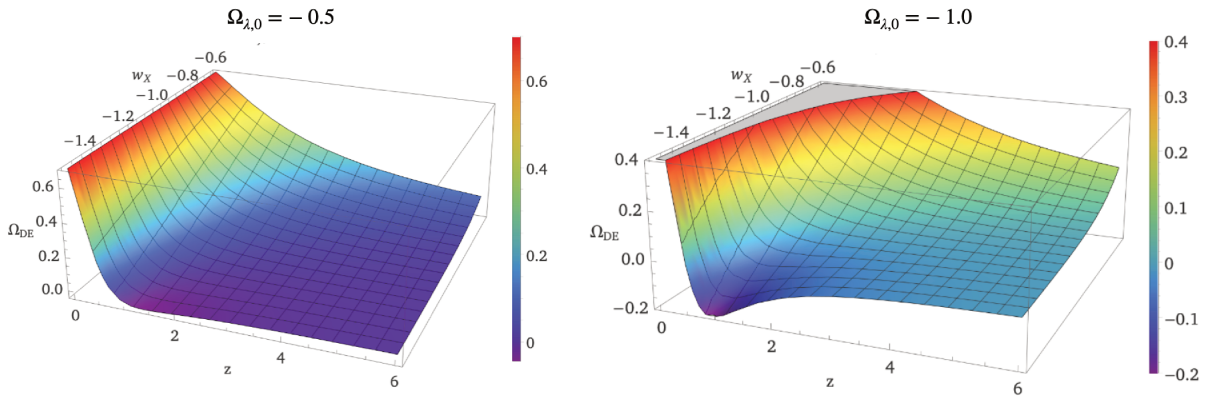

Figure 7.1.1: 3D-Plot showing regions in parameter space (z, w_X) where $\Omega_{DE} < 0$. By construction, $\Omega_{\mathrm{DE},0} = 1 - \Omega_{m,0}$ - we choose $\Omega_{m,0} = 0.3$ here. The color bar on the right, shows the different values for the effective DE density $\Omega_{\mathrm{DE}}(z, w_X)$ and for a fixed value of $\Omega_{\lambda,0} = -0.5$ (on the left) and $\Omega_{\lambda,0} = -1.0$ (on the right). The function Ω_{DE} can become negative as we will later see.

7.1.1 Transient accelerated stages

The inclusion of a negative cosmological constant has various interesting features. Let us first remember that for a model of universe with matter and dark energy with a constant equation of state parameter w, the universe accelerates today if $w < -1/(3\,\Omega_{DE,0})$ which for $\Omega_{DE,0} = 0.7$ gives $w < -0.48$. In the presence of two fluids, the problem becomes more complicated. In our case, we consider a negative cosmological constant and a constant equation of state, w_X, for the X-component. The condition of an acceleration of the universe today reduces to

$$w_X < \frac{\Omega_{\lambda,0} - 1/3}{1 - \Omega_{m,0} - \Omega_{\lambda,0}} \,. \tag{7.5}$$

We have an additional degree of freedom, $\Omega_{\lambda,0}$. In fact even if $\Omega_{\lambda,0} + \Omega_{X,0} = 0.7$, $\Omega_{\lambda,0}$ is free to take any value. Considering $\Omega_{\lambda,0} < 0$, we find that the universe accelerates today for some value of w_X in the range $-1 < w_X < -0.48$ depending on the value of $\Omega_{\lambda,0}$. For a large negative value of $\Omega_{\lambda,0}$, we need a more negative w_X, with $w_X \to -1$, in order to produce an acceleration today. Considering now the more complicated situation of an acceleration of the universe not only today but which could occur at any time, we find some peculiar results when $\Omega_{\lambda,0} < 0$. First, it is trivial to see that during the matter era, the two fluids are negligible (assuming $w_X < 0$) and therefore the universe decelerates. In the future, if the X component is not phantom, the negative cosmological constant eventually dominates and we have

recollapse and therefore a non-accelerating universe. Only if the X component is phantom, we will have acceleration in the asymptotic future. Considering the situation where the X component is not phantom, we have deceleration in the past and in the future. Therefore, we conclude that for non-phantom dark energy with a negative cosmological constant, if the universe accelerates, it will always be transient. To have an acceleration, we need the situation where dark energy starts to dominate over matter, which always happens at some cosmic time, but it should be sufficiently large at that time in comparison to the negative cosmological constant, otherwise the expansion of the universe would always be decelerated.

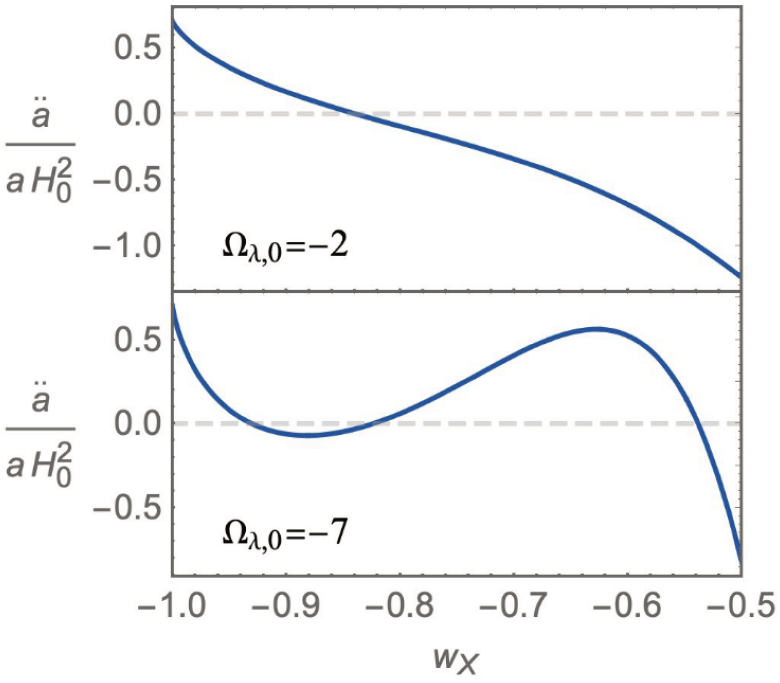

Figure 7.1.2: Evolution of the maximum value of $\ddot{a}/a$ reached from matter era until today, as a function of w_X for two different values of $\Omega_{\lambda,0}$ and $\Omega_{m,0} = 0.3$.

We see in Fig. 7.1.2 the maximum of the acceleration reached by the universe from matter era until today. For $\Omega_{\lambda,0} = -2$, we observe that for $-1 < w_X < -0.84$, there is an epoch during which we have acceleration while for $-0.84 < w_X < -0.5$, the universe always decelerates until today. This follows our standard intuition: we need w_X sufficiently negative to produce an acceleration. On the other hand, for $\Omega_{\lambda,0} = -7$, we observe a more complicated evolution. For $-1 < w_X < -0.93$ and $-0.82 < w_X < -0.54$ the universe reached in the past or today a phase of acceleration, while for $-0.93 < w_X < -0.82$ and $-0.54 < w_X$, the

universe never accelerated in the past. The maximum value for $\ddot{a}/a$ is given by

$$\left.\frac{\ddot{a}}{aH_0^2}\right|_{\max} = \Omega_{\lambda,0} - \frac{w_X \Omega_{m,0}}{2(1+w_X)} \left[\frac{\Omega_{X,0}(1+3w_X)(1+w_X)}{-\Omega_{m,0}}\right]^{-\frac{1}{w_X}} , \tag{7.6}$$

which shows the nontrivial dependence of the acceleration parameter on w_X and $\Omega_{\lambda,0}$. In Fig. 7.1.3, we extended this analysis to a large range of $\Omega_{\lambda,0}$ and w_X. In white, the universe accelerates today while in gray the universe decelerates today. The latter is divided in areas (light gray) where the universe never accelerated until today and situations (darker gray) where the universe had an acceleration in the past but does not accelerate today.

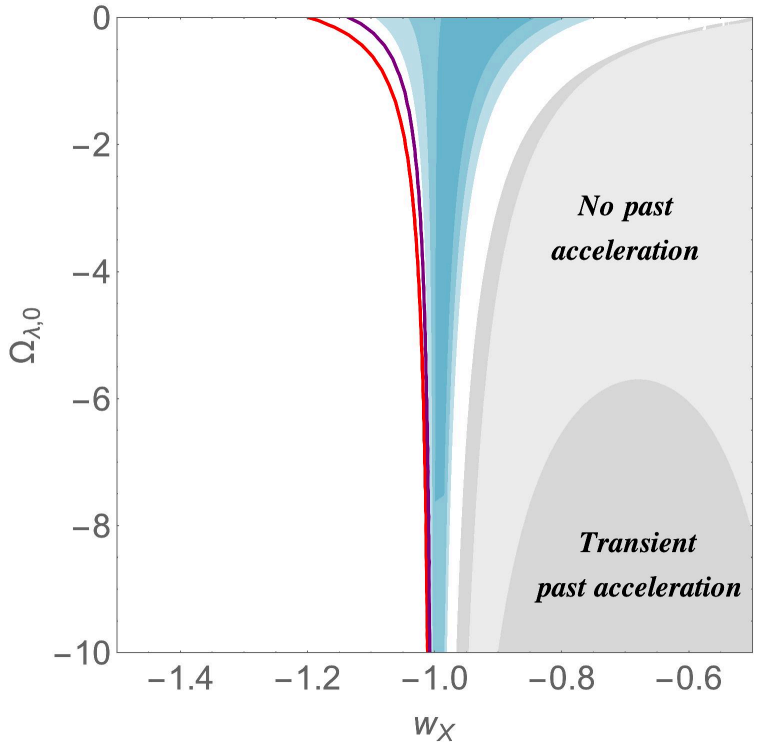

Figure 7.1.3: Evolution of the universe in the space $(w_X, \Omega_{\lambda,0})$. In white, the universe accelerates today, in light gray, the universe never accelerated until today while in darker gray, we have a transient situation where the universe accelerated in the past but does not accelerate today. In blue, we have represented the SNe Ia data constraints at $(1\sigma, 2\sigma, 3\sigma)$. Finally the red and purple lines represent the $(\Omega_{\lambda,0}, w_X)$ values which satisfy Eq. (7.27) for $h = 0.74$ and $h = 0.72$ respectively.

Having in mind the observational constraints which will be addressed more thoroughly later, we have also represented in the same figure the set of parameters satisfying Eq. (7.27) in red for $h = 0.74$, and SNe Ia data constraints in blue. Notice that for SNe Ia, we have marginalized over H_0 and assumed for ω_m the CMB best fit value. This is somehow naive and a more rigorous analysis will be performed in the next section. We see that SNe Ia data exclude any decelerated universe today if w_X is constant. Notice also that if $\Omega_{\lambda,0} = 0$, we need $w_X = -1.2$ to obtain $h = 0.74$ as it was already noticed in [13]. For negative values of the cosmological constant the required phantomness is milder as we will see in Section III, but we see that SNe Ia constraints are also tighter and no intersection is possible. The SNe Ia data are marginally consistent with $h = 0.72$ at 3σ for any value of $\Omega_{\lambda,0}$. We conclude therefore that even though a negative cosmological constant is appealing and easily motivated from string theory, its impact on the Hubble tension is rather marginal for constant w_X, which will be confirmed by our numerical results.

7.1.2 Future asymptotic solutions

Let us consider now the limit in the future where dust-like matter density becomes negligible compared to the dark sector density. As we have our Universe in mind, we consider the regime in the future for which $\Omega_{m,0}\left(\frac{a_0}{a}\right)^3 \ll |\Omega_{\lambda,0}| < \Omega_{X,0}$. Then, we have to solve the effective Friedmann equation

$$H^2 = -|\alpha| + \frac{\beta}{a^p} \ , \tag{7.7}$$

where we have set for brevity

$$\begin{aligned} \alpha &\equiv \Omega_{\lambda,0}\, H_0^2 < 0 \\ \beta &\equiv \Omega_{X,0}\, H_0^2\, a_0^p \\ p &\equiv 3(1+w_X) \ . \end{aligned} \tag{7.8}$$

The exact solution of Eq. (7.7) is

$$a = \left(\frac{\beta}{|\alpha|}\right)^{\frac{1}{p}} \sin^{\frac{2}{p}}\left(\frac{p}{2}\sqrt{|\alpha|}\, t + C\right) \ , \tag{7.9}$$

or more explicitly in function of the cosmological parameters

$$\frac{a}{a_o} = \left(\frac{\Omega_{X,o}}{|\Omega_{\lambda,o}|}\right)^{\frac{1}{p}} \sin^{\frac{2}{p}}\left(\frac{p}{2}\sqrt{|\Omega_{\lambda,o}|}\, H_o t + C\right) \ , \tag{7.10}$$

where C is an integration constant. We obtain further

$$\frac{H}{H_o} = \sqrt{|\Omega_{\lambda,o}|}\, \cot\left(\frac{p}{2}\sqrt{|\Omega_{\lambda,o}|}\, H_o t + C\right) \tag{7.11}$$

$$\frac{\dot{H}}{H_o^2} = \frac{p}{2}|\Omega_{\lambda,o}|\left[-1 - \cot^2\left(\frac{p}{2}\sqrt{|\Omega_{\lambda,o}|}\, H_o t + C\right)\right] \tag{7.12}$$

If $p = 0$ ($w_X = -1$), the two terms on the r.h.s. of Eq. (7.7) combine to give an effective positive cosmological constant. The resulting future evolution is that of ΛCDM. Note that it is possible in this case to give the exact analytic expression even when dustlike matter is taken into account.

We consider next $p > 0$, in other words the X-component is not of the phantom type. As its density is decreasing with expansion, the universe will eventually recollapse. Note that the density of dustlike matter decreases even more rapidly ($\propto a^{-3}$) so Eq. (7.7) applies if $|\Omega_{\lambda,o}| \ll \Omega_{DE,o} \approx 0.7$ and $w_X \approx -1$. Indeed, we can read off from Eq. (7.10) the condition for the existence of a time interval before the contraction during which dustlike matter can be neglected, viz.

$$\left(\frac{|\Omega_{\lambda,o}|}{|\Omega_{\lambda,o}| + \Omega_{DE,o}}\right)^{\frac{3}{p}} \ll \frac{|\Omega_{\lambda,o}|}{\Omega_{m,o}} \tag{7.13}$$

As expected, we verify further with Eqs. (7.11), (7.12), that the expansion is decelerating, $\ddot{a} < 0$, (at least) in the neighbourhood of a_M, the maximal value of the scale factor. As expected this is only so for $0 < p < 2$ ($-1 < w_X < -\frac{1}{3}$) otherwise there is no acceleration at all. So even if the universe is accelerating today, it passes again through $\ddot{a} = 0$, from an accelerating to a decelerating expansion rate. When (7.13) is satisfied, this takes place at

$$\frac{a_M}{a} \simeq \left(1 + \frac{p}{2}\right)^{\frac{1}{p}} \ , \tag{7.14}$$

which is close to a_M and lies in the regime described by (7.7).

We now turn to $p < 0$, the phantom case. It is clear that the universe will eventually reach the Big Rip singularity in a finite time t_∞. In some range before t_∞, the dust-like component will be negligible

compared to the negative cosmological constant. In that case, $a(t)$ is given to high accuracy by the solution (7.9) or (7.10). To ensure the presence of a Big Rip at t_∞, we write the integration constant C in a way to have a Big Rip at $t = t_\infty$ and the solution for $a(t)$ then reads

$$a(t) = \left(\frac{|\Omega_{\lambda,0}|}{\Omega_{X,0}}\right)^{\frac{1}{|p|}} a_0 \sin^{-\frac{2}{|p|}}\left(\frac{|p|}{2}\sqrt{|\Omega_{\lambda,0}|}\, H_0(t_\infty - t)\right) . \tag{7.15}$$

We verify easily that in the limit $t \to t_\infty$, this solution tends asymptotically to

$$a(t) \sim \frac{A}{(t_\infty - t)^{\frac{2}{|p|}}} , \tag{7.16}$$

with A given by

$$A = \left(\frac{|p|}{2}\sqrt{\Omega_{X,0}}\, H_0\right)^{-\frac{2}{|p|}} a_0 . \tag{7.17}$$

This is the well-known singular behaviour in the vicinity of t_∞, depending solely on the phantom component, here the X component. The solution (7.15) gives a nearly exact fit in the regime $\Omega_{m,0} \ll |\Omega_{\lambda,0}|$ and improves on (7.17) when t is sufficiently far from t_∞.

7.2 Cosmic Relevance of λ and the H_0 tension

We now turn to the cosmic relevance of models admitting a negative cosmological constant λ. As for any cosmological model differing from ΛCDM , an important question to address is how viable the model is if the measured value of h is substantially higher than 0.67. It is well known that there is a tension between the value of H_0 obtained by Planck and the value obtained with many local (low redshifts) measurements. This is a very interesting problem which has been widely investigated recently in various ways (see e.g. [8, 21, 27, 30, 32, 38, 39, 80, 82, 110, 122, 147, 194, 209, 215, 228, 231, 246] for a non exhaustive list). This tension can be traced back to the measurement of the standard ruler r_s, the comoving sound horizon at recombination time (very close to the drag epoch) relevant for the corresponding angle θ_s sustended on the CMB. Refer reader to schematic picture in 1.3.5

$$r_s(z_1) = \int_0^{t_1} c_s \frac{dt}{a(t)} = \frac{1}{a_0}\int_{z_1}^{\infty} c_s \frac{dz}{H(z)} , \tag{7.18}$$

where adiabatic primordial fluctuations are assumed. The angle θ_s is given by

$$\theta_s = \frac{a_1\, r_s(z_1)}{d_A(z_1)} \ , \tag{7.19}$$

where $d_A(z)$ is the angular-diameter distance out to a redshift z. We finally obtain

$$\theta_s = \frac{r_s(z_1)}{r(z_1)} \ , \tag{7.20}$$

with

$$r(z_1) = \frac{c}{a_0} \int_0^{z_1} \frac{dz}{H(z)} \ . \tag{7.21}$$

We have reintroduced explicitly the speed of light c and a_0 in (7.18), (7.21) ($c = 1$ and $a_0 = 1$ in this work but will sometimes be written explicitly). We choose the Planck 2018 TT,TE,EE+LowE+Lensing constraints (no BAO), with one massive neutrino species [188]. We take the following values

$$z_1 = z_{\rm rec} = 1089.92, \quad \theta_s^{\rm Planck} = 1.04110 \times 10^{-2}, \quad r_s^{\rm Planck}(z_{\rm rec}) = 144.43 {\rm Mpc} \tag{7.22}$$

see Table 7.2.1. The relative energy density $\Omega_{i,0} \equiv \frac{\rho_{i,0}}{\rho_{cr,0}}$, defined as

$$\Omega_{i,0} = \frac{8\pi G \rho_{i,0}}{3H_0^2} \ , \tag{7.23}$$

suffers from the uncertainty of the value of H_0 even if ρ_i is otherwise known. However, it is often possible to find observationally the numerical value of the combined quantities

$$\omega_i \equiv \Omega_{i,0}\, h^2 \ , \tag{7.24}$$

with $h \equiv \frac{H_0}{100\,{\rm km\,s^{-1}\,Mpc^{-1}}}$. For our models, we have obviously on low redshifts

$$H(z) = \left[\omega_m\, (1+z)^3 + \omega_\lambda + \omega_X\, f_X(z)\right]^{\frac{1}{2}} \times 100\,{\rm km\,s^{-1}\,Mpc^{-1}}. \tag{7.25}$$

In the standard ΛCDM model, the value of $r_s(z_1)$ is controled by the quantities ω_i contained in the model with the notable exception of ω_Λ. Measuring these quantities yields in turn $r_s^{\rm Planck}(z_1)$. As the angle $\theta_s^{\rm Planck}$

is accurately measured by the Planck collaboration, the numerical value of $r(z_1)$ becomes fixed in turn (for given θ_s measured by Planck) to its value $r^{\rm Planck}(z_1)$,

$$r^{\rm Planck}(z_1) = 13\,872.8\,{\rm Mpc}\ . \tag{7.26}$$

Hence, once a cosmological model is adopted which does not change the early-time physics of ΛCDM, such a model is compelled to give the same $r(z_1)$. For ΛCDM this boils down to fix the value $\omega_\Lambda^{\rm Planck}$ and therefore the value of H_0. The Planck collaboration finds $H_0 = 67.36\,{\rm km\,s^{-1}\,Mpc^{-1}}$ a value substantially lower than the value measured locally. We refer the interested reader to the excellent account given in [132]. In this work we are interested in models which depart from ΛCDM regarding the universe expansion for $z < z_1$, however in a way that they satisfy

$$r(z_1) = r^{\rm Planck}(z_1) \tag{7.27}$$

for a *larger* H_0 value. Used in our theoretical investigations, the constraint (7.27) assumes that both r_s *and* θ_s are fixed to their Planck values (see Table 7.2.1). It is obvious from (7.25), (7.20) that a larger H_0 requires

$$\omega_{DE} = \omega_\lambda + \omega_X > \omega_\Lambda^{\rm Planck}\ , \tag{7.28}$$

and a phantom behaviour of the X component, hence also an effective phantom behaviour of the DE sector. This amounts to explore models with $w_X < -1$ at least during part of the late-time expansion. It is straightforward to obtain the exact equality

$$\omega_{DE} - \omega_\Lambda^{\rm Planck} = h^2 - (h^{\rm Planck})^2\ , \tag{7.29}$$

It is further clear that our models satisfy (by construction)

$$\Omega_{m,0} = \left(\frac{h^{\rm Planck}}{h}\right)^2 \Omega_{m,0}^{\rm Planck} < \Omega_{m,0}^{\rm Planck}\ , \qquad \Omega_{DE,0} \simeq 1 - \Omega_{m,0} > \Omega_{\Lambda,0}^{\rm Planck}\ . \tag{7.30}$$

Since we have to calculate distances up to $z = z_{\rm rec}$, where radiation is subdominant but not negligible, we have to properly take into account the effect of photons and neutrinos. At high redshifts ($z \gtrsim 50$),

Eq. (7.25) becomes [133]

$$\frac{H(z)}{100\,\mathrm{km\,s^{-1}\,Mpc^{-1}}} = \left[\omega_m\,(1+z)^3 + \omega_\lambda + \omega_X\,f_X(z)\;+\omega_\gamma\,(1+z)^4\left(1+0.2271\,\frac{N_{\rm eff}}{3}\sum_i f_\nu\left(\frac{m_{\nu_i}}{T_\nu}\right)\right)\right]^{\frac{1}{2}}, \tag{7.31}$$

with $\omega_\gamma = 2.47\times10^{-5}$ while f_ν is well fitted with $f_\nu(y)\simeq(1+(Ay)^p)^{1/p}$ with $A=\frac{180\zeta(3)}{7\pi^4}$ and $p=1.83$ [134]. The function f_ν interpolates between the relativistic behaviour, $m_\nu \ll T_\nu$ ($T_\nu\sim a^{-1}$), and the non-relativistic regime, $m_\nu \gg T_\nu$. Even for m_ν as light as 0.06eV, the transition occurs rather early around $z\simeq 110$. Given these considerations, we fix the early Universe cosmology as in table 7.2.1.

$100\omega_b$	$100\omega_c$	$N_{\rm eff}$	m_ν (eV)	r_s (Mpc)	r_d (Mpc)	$100\theta_s$
2.237	12.00	3.046	(0,0,0.06)	144.43	147.09	1.04110

Table 7.2.1: Parameter values as given by the Planck 2018 TT,TE,EE+LowE+lensing results (Table 2). r_s is the comoving sound horizon at recombination ($z_1 = 1089.92$), and rd at the drag epoch $z_d = 1059.94$

7.2.1 The Models

When assessing the viability of our models with respect to the low-redshift data and the constraint on their free parameters coming from a high H_0, we will consider various types of equation of state (EoS) parameters w_X and various values of ω_λ.

Scenario w: We consider first models with constant equation of state w_X = constant. In this case we obviously have

$$f_X(z) = (1+z)^{3(1+w_X)}\ . \tag{7.32}$$

As we have seen earlier, to ease the H_0 tension necessarily requires a phantom behaviour and for a constant

w_X the only possible choice is to take $w_X < -1$. We take an EoS of the form

$$w_X = -1 + \Delta_1 = w_0 \ , \qquad \Delta_1 < 0 \ , \tag{7.33}$$

and we obtain immediately

$$f_X(z) = (1+z)^{3\Delta_1} \ . \tag{7.34}$$

While a constant w_X gives us some insight, it is clearly advisable to explore also models with varying equations of state.

CPL scenarios: here we adopt the CPL parametrization of w_X corresponding to a smoothly (differentiable) varying EoS with

$$w_X = w_0 + w_a(1-a) \equiv -1 + \Delta + w_a(1-a) \tag{7.35}$$

which gives [63],[150]

$$f_X(z) = (1+z)^{3(\Delta + w_a)} \ \exp^{-3w_a \frac{z}{1+z}} \ . \tag{7.36}$$

We consider also two constrained versions: CPLw_a, with $w_0 = -1$ while w_a is free; and CPLw_0, where w_0 is free and $w_a = -1 - w_0$ so that $w_X \to -1 \equiv w_\infty$.

Scenario I: In this scenario, we take a piece-wise constant w_X where dark energy is of a phantom type below some transition redshift z_c and a cosmological constant Λ above, with

$$w_X(z) = \begin{cases} -1 + \Delta_1 = w_0, & \text{for } z \leq z_c \qquad \Delta_1 < 0 \\ -1 = w_\infty, & \text{for } z > z_c \end{cases} \tag{7.37}$$

Here we take $\Delta_1 < 0$ in order to ensure a phantom behaviour and we fix $z_c = 1$. As z_c increases, it is easier to meet the data on small redshifts but it requires stronger phantomness on large redshifts in order to comply with the observed θ_s and a higher H_0. We note that most of the SN Ia data are in the range $z_c \leq 1$. In this scenario, the evolution of the X-component is given by

$$f_X(z) = \begin{cases} (1+z)^{3\Delta_1}, & \text{for } z \leq z_c \\ (1+z_c)^{3\Delta_1}, & \text{for } z > z_c \end{cases} \tag{7.38}$$

Scenario II: This scenario has also a piece-wise constant w_X, but it is now opposite to the previous scenario, i.e.

$$w_X(z) = \begin{cases} -1 = w_0, & \text{for } z \leq z_c \\ -1 + \Delta_2 = w_\infty, & \text{for } z > z_c, \quad \Delta_2 < 0 \end{cases} \tag{7.39}$$

We have now

$$f_X(z) = \begin{cases} 1, & \text{for } z \leq z_c \\ \left(\frac{1+z}{1+z_c}\right)^{3\Delta_2}, & \text{for } z > z_c \end{cases} \tag{7.40}$$

In this case too, we take $z_c = 1$.

Scenario III:

$$w_X(z) = \begin{cases} -1 + \Delta_1 = w_0, & \text{for } z \leq z_{c1}, \quad \Delta_1 < 0 \\ -1, & \text{for } z_{c1} < z \leq z_{c2} \\ -1 + \Delta_2 = w_\infty, & \text{for } z > z_{c2}, \quad \Delta_2 < 0 \end{cases} \tag{7.41}$$

We have in this case

$$f_X(z) = \begin{cases} (1+z)^{3\Delta_1}, & \text{for } z \leq z_{c1} \\ (1+z_{c1})^{3\Delta_1}, & \text{for } z_{c1} < z \leq z_{c2} \\ \frac{(1+z_{c1})^{3\Delta_1}}{(1+z_{c2})^{3\Delta_2}}(1+z)^{3\Delta_2}, & \text{for } z > z_{c2} \end{cases} \tag{7.42}$$

For this scenario we take $z_{c1} = 0.1$ and $z_{c2} = 1$. A significant change in w_X on very small redshifts is viable and we exploit also this possibility here.

Once a specific model is adopted we can find the dependence of h on the model parameters for a model satisfying (7.27). This gives insight into the phenomenology of these models irrespective of the observational constraints. For constant w_X, we can study its behaviour in terms of the following three free parameters: ω_λ, w_X and h. Indeed the parameter ω_X is fixed once ω_λ and h are given. From the constraint (7.27) however, only two free parameters are left. In Figure 7.2.1, we show the value of h in terms of w_X, when ω_λ is fixed and as a function of w_X and ω_λ in a 3-dim plot. In the first case, we confirm the linear relation

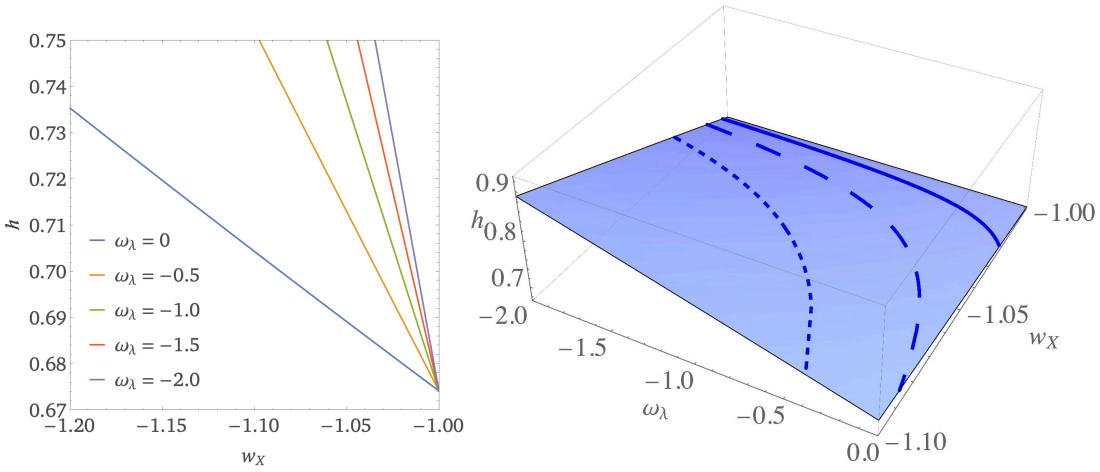

Figure 7.2.1: Parameters (h, ω_λ, w_X) which satisfy the relation (7.27) for models with constant w_X. a) In the upper panel, ω_λ is fixed and we see that an increasing $|\omega_\lambda|$ (from left to right) gives the same h with less phantomness. We note the quasilinear relation, which follows from (7.43) for constant ω_λ. b) In the lower panel all parameters are free. For the latter, we show the lines corresponding to a constant h when (7.27) is satisfied: continuous line ($h = 0.68$), long dashed line ($h = 0.7$) and dashed line ($h = 0.74$). They satisfy to good accuracy (7.43).

obtained in [13] (for $\omega_\lambda = 0$), which we have generalized here to

$$h = 0.673 + (w_X + 1)(0.93\omega_\lambda - 0.33). \tag{7.43}$$

At this point we emphasize another interesting aspect of our models which we discuss here for a constant w_X. As we will see later, observations favour models of the phantom type, $w_X < -1$. This implies that $\rho_{DE} = \rho_\lambda + \rho_X$ will necessarily become negative in the past at some redshift z_λ and it is straightforward to find

$$1 + z_\lambda = \left[1 + \frac{h^2 - \omega_m}{|\omega_\lambda|}\right]^{-\frac{1}{3(1+w_X)}} . \tag{7.44}$$

We have used $\omega_{DE} \approx h^2 - \omega_m$ which is valid to high accuracy. On the other hand, $H^2(z)$ is necessarily positive $\forall z > z_m$ with

$$1 + z_m = \left[\frac{|\omega_\lambda|}{\omega_m}\right]^{\frac{1}{3}} . \tag{7.45}$$

It is seen from (7.44) that $z_\lambda \to 0$ as $|\omega_\lambda|$ is increasing and w_X is more phantom. When this is the case

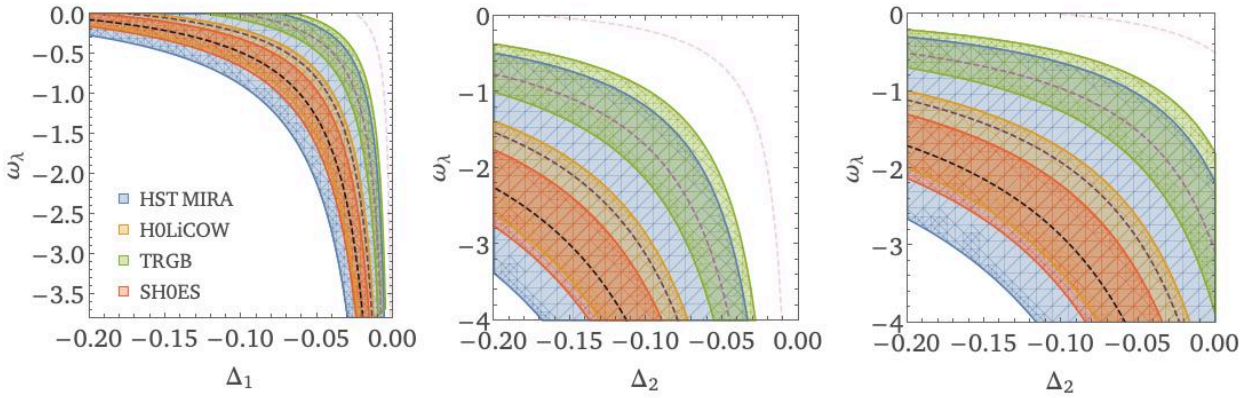

Figure 7.2.2: We show iso-h curves for scenarios I (left), II (middle), and III with $\Delta_1 = -0.04$ (right-hand panel) in the $(\Delta_{1,2}, \omega_\lambda)$ parameter plane. The shaded areas correspond to the following H_0 values (in km.s^{-1}.Mpc^{-1} units): 73.30 ± 4 (HST-Mira) [118]), 74.03 ± 1.42 (SH0ES) [200] and 69.8 ± 1.9 (TRGB) [102].

there might be some parameter values for which $H^2(z)$ itself becomes negative for some redshifts in the range $z_\lambda < z < z_m$, such models are not viable and must be rejected. The condition $H^2(z) > 0$ is easily translated into

$$\omega_m \left[(1+z)^3 - f_X(z)\right] + h^2 f_X(z) > |\omega_\lambda| \left(1 - f_X(z)\right) \ . \tag{7.46}$$

This inequality depends on the free parameters $w_X,\ \omega_\lambda,\ h$. However, we should remember that in our theoretical analysis once w_X and ω_λ are given, because of the constraint (7.27) h is no longer free as we illustrate with Figures 7.2.1 and 7.2.2. We see that a priori, for given w_X, large$|\omega_\lambda|$ and low h^2 values can lead to a violation of (7.46). Once a two-dimensional surface $h(w_X,\ \omega_\lambda)$ is found satisfying (7.46) (see the lower panel of Figure 7.2.1), the projection in the $(w_X,\ \omega_\lambda)$ plane satisfies it automatically too.

7.3 Comparison with data: Model Selection and Parameter Estimation

In this section, we are interested in the question of model selection: namely, comparing the different models to the reference ΛCDM model. Let M be the model, D the data, and Θ the parameters of the model. Bayes

Models	Parameter	Prior range
All	h	$[0.5, 1]$
λ all	ω_λ	$[-4, 0]$
$(\lambda)w$/I/III/CPLw_0	w_0	$[-1.2, -0.8]$
(λ)II/III	w_∞	$[-1.2, -0.8]$
(λ)CPLw_a	w_a	$[-0.2, 0.2]$

Table 7.3.1: Flat prior range used in the nested sampling. For each model, (λ) denotes both cases with and without λ

theorem can be written as

$$\Pr(\Theta|M, D) = \frac{\Pr(D|\Theta, M)\Pr(\Theta|M)}{\Pr(D|M)}, \tag{7.47}$$

where $\mathcal{P}(\Theta) = \Pr(\Theta|M, D)$ is the posterior distribution, $\mathcal{L}(\Theta) = \Pr(D|\Theta, M)$ is the likelihood, $\pi(\Theta) = \Pr(\Theta|M)$ is the prior, and $\mathcal{Z} = \Pr(D|M)$ is the evidence.

For parameter evaluation within a given model, the evidence can be seen as a normalization constant, and thus ignored. However, in order to perform model selection, the Bayesian evidences of the models have to be evaluated and compared. Calculating the evidence can be computationally challenging, in particular when using Monte Carlo Markov Chains. Therefore, in order to calculate the posterior distributions and the evidence, we use the nested-sampling algorithm [213] as implemented in `pymultinest` [51, 99]. We follow the authors' recommendations and use different sampling efficiencies for evidence evaluation and parameter estimation (0.3 and 0.8, respectively). We used 1000 live points and a tolerance factor of 1. We checked that the tolerance factor does not affect too much the results. The priors are shown in Table 7.3.1. As for h, because of its crucial role in this work, we choose rather wide, uninformative priors. For the other parameters associated to dark energy, we base our priors on physical properties of existing dark energy models, for example the difficulty to obtain realistic phantom models with $w \ll -1$. Finally, we take the priors $\omega_\lambda \in [-4, 0]$; see Figs. 7.2.1 and 7.2.2 of Sec. 7.2.

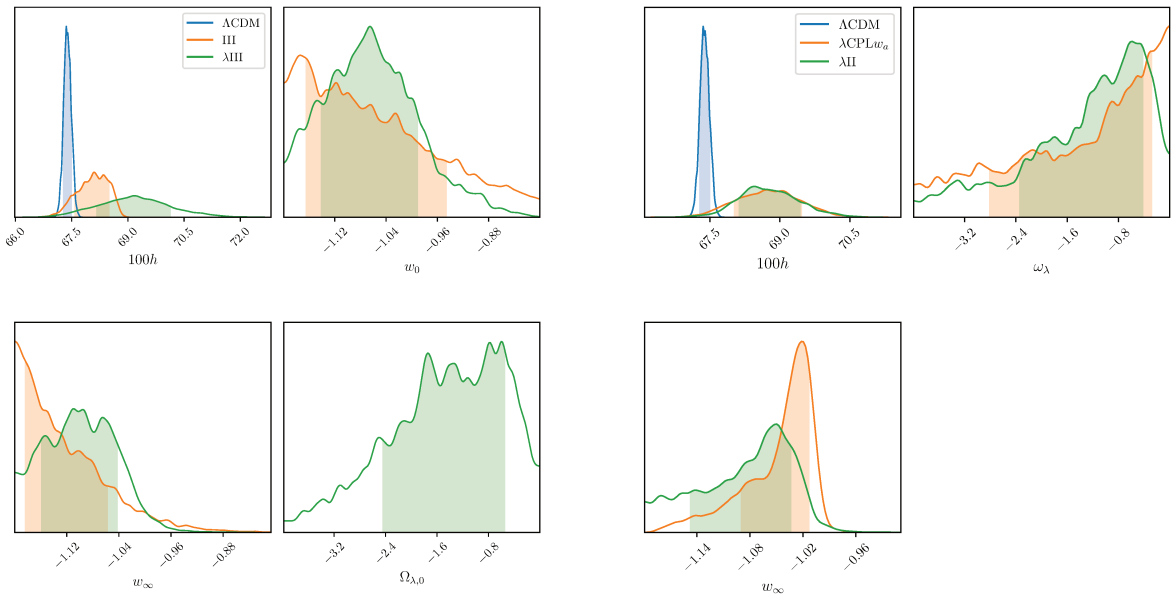

Figure 7.3.1: Marginalized posteriors for different models using SNIa, BAO, θ_s, and H_0 from HST Mira. The central value is the median, and the shared areas show the 68% credible intervals around it. Left: ΛCDM (blue), III (orange), and λIII (green). Right: ΛCDM (blue), λCPLw_a (orange), λII (green).

Bayesian Evidence and Bayes Factor

An elegant way to compare two models (say model M_1 and the null hypothesis M_0) with different degrees of freedom is to compute the posterior ratio

$$\frac{\Pr(M_1|D)}{\Pr(M_0|D)} = \frac{\Pr(D|M_1)\Pr(M_1)}{\Pr(D|M_0)\Pr(M_0)} \tag{7.48}$$

$$= \frac{\mathcal{Z}_1}{\mathcal{Z}_0} \equiv K. \tag{7.49}$$

In (7.49), we assume $\Pr(M_1) = \Pr(M_0)$. Therefore, $K > 1$ shows a preference for model 1 over model 0. The value of K gives the degree of preference for one model over the other. Several scales have been used, such as the Jeffreys scale, although the latter should be taken as an indication and interpreted with caution.

The data

The quantities ω_m and ω_r are kept to their fiducial Planck value, and thus so are r_s and r_d. We vary h and the parameters ω_λ, w_X associated with dark energy and obtain $\theta_{s,\text{model}}$ for each set of free parameters which is then compared to $\theta_{s,\text{Planck}}$ and gives us a likelihood for θ_s.

In addition, we used the 1048 distance modulus measurements from the Pantheon type Ia supernovae (SNIa) compilation [208], and the BAO from the Baryon Oscillation Spectroscopic Survey (BOSS) and extended-BOSS (eBOSS) surveys [10, 243]. Since the measurements from the SHoES project are in tension with ΛCDM , we instead use a measurement with larger error bars which is not inconsistent [118]. In general, supernovae show a degeneracy between the absolute magnitude and the Hubble constant. Therefore, SNIa alone cannot measure H_0. However, in this particular study, since we fixed ω_m, choosing a certain value for $\Omega_{m,0}$ uniquely fixes h; therefore we can use SNIa data to obtain h. The BAO provide us with $H(z)r_d$ and $d_A(z)/r_d$, where d_A is the angular diameter distance and the sound horizon at the drag epoch $r_d$is fixed to its Planck value (Table 7.2.1). The three pairs of data points (d_A/r_d and $H\,r_d$) from BOSS are correlated, and so are the four eBOSS pairs, and the BAO covariance matrix is thus

$$\mathbf{C}_{\text{BAO}} = \begin{pmatrix} \mathbf{C}_{\text{BOSS}} & 0 \\ 0 & \mathbf{C}_{\text{eBOSS}} \end{pmatrix}. \tag{7.50}$$

θ_s and H_0 are one data point each, and their associated likelihood is thus trivial. We used flat priors as shown in Table 7.3.1.

Table 7.3.2 summarizes our results for SN+BAO+θ_s while in Table 7.3.3 the H_0 data point from HST-Mira is added. The quoted central values and error bars correspond to the median and 68% credible intervals around it. We remind the reader that in this analysis, ω_m , ω_b, N_{eff}, and $\sum m_\nu$ are fixed to their Planck value, and thus so are r_s and r_d (see Table 7.2.1).

Figure 7.3.1 shows the posterior distributions of the parameters for models ΛCDM , III, and λIII (left-hand panel), and ΛCDM , λCPLw_a, and λII (right-hand panel). Model III shows preference for a higher value of h, and adding a negative λ pushes h even higher, although this is not sufficient to reconcile it with the SHoES value. An interesting property of the negative cosmological constant is that it allows to satisfy the observational constraints with an equation of state which is less phantom. This is clearly seen in partic-

Table 7.3.2: 68% credible intervals for SN+BAO+θ_s.

Model	$100h$	w_o	w_∞ or w_a	ω_λ	$\ln \mathcal{Z}$	K
Λ	$67.382^{+0.107}_{-0.096}$				-532.4	1
w	$68.62^{+0.85}_{-0.83}$	$-1.042^{+0.028}_{-0.029}$		$[0]$	-533.1	0.54
λw	$68.66^{+0.79}_{-0.75}$	$-1.0102^{+0.0076}_{-0.0203}$		$-0.91^{+0.73}_{-1.88}$	-534.7	0.11
CPL	$68.60^{+0.78}_{-0.84}$	$-1.038^{+0.032}_{-0.029}$	$-0.020^{+0.074}_{-0.055}$	$[0]$	-532.6	0.83
λCPL	$68.72^{+0.77}_{-0.87}$	$-1.007^{+0.016}_{-0.028}$	$-0.58^{+0.43}_{-1.11}$	$-0.032^{+0.058}_{-0.044}$	-534.1	0.18
CPLw_o	$68.52^{+0.83}_{-0.85}$	$-1.052^{+0.039}_{-0.038}$	$[-(1+w_o)]$	$[0]$	-533.0	0.60
λCPLw_o	$68.51^{+0.72}_{-0.74}$	$-1.014^{+0.011}_{-0.021}$	$[-(1+w_o)]$	$-0.84^{+0.65}_{-1.57}$	-534.6	0.12
CPLw_a	$68.34^{+0.39}_{-0.63}$	$[-1]$	$-0.124^{+0.083}_{-0.050}$	$[0]$	-532.1	1.48
λCPLw_a	$68.63^{+0.78}_{-0.75}$	$[-1]$	$-0.034^{+0.024}_{-0.057}$	$-1.03^{+0.78}_{-1.81}$	-533.1	0.52
I	$68.46^{+0.82}_{-0.83}$	$-1.042^{+0.033}_{-0.032}$	$[-1]$	$[0]$	-533.2	0.48
λI	$68.41^{+0.82}_{-0.75}$	$-1.0092^{+0.0081}_{-0.0242}$	$[-1]$	$-0.92^{+0.76}_{-1.92}$	-534.8	0.093
II	$67.86^{+0.21}_{-0.34}$	$[-1]$	$-1.127^{+0.090}_{-0.053}$	$[0]$	-532.2	1.33
λII	$68.58^{+0.66}_{-0.59}$	$[-1]$	$-1.059^{+0.035}_{-0.070}$	$-1.15^{+0.75}_{-1.76}$	-532.1	1.36
III	$67.93^{+0.47}_{-0.50}$	$-1.04^{+0.14}_{-0.11}$	$-1.128^{+0.092}_{-0.049}$	$[0]$	-532.3	1.20
λIII	$68.93^{+1.03}_{-0.89}$	$-1.046^{+0.070}_{-0.083}$	$-1.090^{+0.054}_{-0.068}$	$-0.65^{+0.43}_{-0.95}$	-531.4	2.96

Table 7.3.3: 68% credible intervals for SN+BAO+θ_s+H_o (HST Mira).

Model	$100h$	w_o	w_∞ or w_a	ω_λ	$\ln Z$	K
Λ	$67.386^{+0.105}_{-0.099}$				-533.5	1
w	$68.83^{+0.82}_{-0.83}$	$-1.049^{+0.028}_{-0.027}$		$[0]$	-533.7	0.82
λw	$68.81^{+0.86}_{-0.77}$	$-1.0122^{+0.0086}_{-0.0251}$		$-0.81^{+0.66}_{-1.75}$	-535.4	0.16
CPL	$68.77^{+0.75}_{-0.80}$	$-1.044^{+0.031}_{-0.028}$	$-0.020^{+0.072}_{-0.057}$	$[0]$	-533.3	1.26
λCPL	$68.75^{+0.84}_{-0.78}$	$-1.005^{+0.015}_{-0.022}$	$-0.035^{+0.053}_{-0.042}$	$-0.71^{+0.52}_{-1.26}$	-534.8	0.30
CPLw_o	$68.71^{+0.82}_{-0.83}$	$-1.061^{+0.038}_{-0.037}$	$[-(1+w_o)]$	$[0]$	-533.7	0.87
λCPLw_o	$68.72^{+0.83}_{-0.93}$	$-1.016^{+0.012}_{-0.033}$	$[-(1+w_o)]$	$-0.72^{+0.58}_{-1.64}$	-535.3	0.18
CPLw_a	$68.42^{+0.35}_{-0.48}$	$[-1]$	$-0.134^{+0.063}_{-0.044}$	$[0]$	-532.8	1.99
λCPLw_a	$68.76^{+0.70}_{-0.73}$	$[-1]$	$-0.035^{+0.022}_{-0.054}$	$-1.12^{+0.83}_{-1.69}$	-533.7	0.81
I	$68.67^{+0.80}_{-0.82}$	$-1.050^{+0.032}_{-0.031}$	$[-1]$	$[0]$	-533.9	0.69
λI	$68.51^{+1.09}_{-0.77}$	$-1.0096^{+0.0076}_{-0.0272}$	$[-1]$	$-0.96^{+0.80}_{-1.92}$	-535.6	0.13
II	$67.89^{+0.18}_{-0.30}$	$[-1]$	$-1.137^{+0.083}_{-0.044}$	$[0]$	-533.1	1.53
λII	$68.73^{+0.70}_{-0.60}$	$[-1]$	$-1.074^{+0.040}_{-0.073}$	$-1.09^{+0.67}_{-1.24}$	-532.6	2.54
III	$68.09^{+0.41}_{-0.50}$	$-1.077^{+0.131}_{-0.087}$	$-1.137^{+0.080}_{-0.045}$	$[0]$	-533.1	1.52
λIII	$69.28^{+0.99}_{-1.00}$	$-1.063^{+0.062}_{-0.080}$	$-1.083^{+0.054}_{-0.071}$	$-0.74^{+0.45}_{-1.18}$	-533.3	1.31

ular for scenario w, where the addition of λ shifts the central value of w_0 from -1.049 to -1.0122. We note that given our priors on w_0 and w_∞, the equation of state is not always constrained, as seen, for instance, for model III. It is also interesting that the best models λII are those where the phantom behavior, and hence the departure from ΛCDM, takes place at $z \gtrsim 1$. This suggests new physics appearing at these redshifts rather than at redshifts $z \lesssim 1$ can yield viable models. Models (λ)III fare reasonably well while having an additional departure from ΛCDM at very low redshifts $z \leq 0.1$ but it is clear when we compare them with models (λ)I that their main advantage comes from their phantomness at $z \gtrsim 1$. This seems further supported by the better evidence for (λ)CPLw_a, where $w_0 = -1$ with a phantom behavior at higher redshifts ($w_a < 0$), compared to (λ)CPLw_0 with w tending asymptotically to -1 and departure from -1 takes place essentially at low redshifts. Note that CPLw_a models have the best evidence for $\lambda = 0$, while models II have the highest evidence for $\lambda \neq 0$ (λII). Interestingly, λCPLw_a lowers the evidence compared to CPLw_a. As we have said earlier, perhaps with the exception of the models λII, the higher evidence compared to ΛCDM is not decisive and should be interpreted with caution.

7.4 Summary and Conclusion

In this work, we have considered the possibility that the dark energy sector contains a negative cosmological constant λ. Indeed, theoretical considerations from high energy physics suggest the possible presence of a negative cosmological constant rather than a positive one. This constitutes a radical change as in that case, and contrary to a positive cosmological constant Λ, this constant cannot produce the late-time accelerated expansion rate and a more sophisticated dark sector is required. The Universe acceleration is produced here by the X component. Clearly the presence of λ can affect the expansion history and we have studied the viability of these models, also when a high H_0 is considered.

While as we have shown some models can achieve a higher H_0 when the equation of state of the X component w_X is of the phantom type–this is of course a generic property not restricted to $\lambda \neq 0$ – we have investigated whether these models are viable when SNIa and BAO data are taken into account. We find indeed that most of our models are viable with a fair evidence for the models λII. Taking into account the H_0 value of the HST-Mira experiment reinforces the evidence of the models λII, reaching a value $h \approx 0.7$ but not higher. Hence, while these models do alleviate the H_0 tension, a value for H_0 substantially higher would rule them out. We note also that the CPLw_a models are the best models for $\lambda = 0$ while the presence of a nonvanishing λ lowers the evidence for λCPLw_a versus CPLw_a. It is further interesting that the best

models λII are equal to ΛCDM on $z \leq 1$ and of the phantom type only at higher redshifts.

The constant λ will manifest itself in a very explicit way in another context, namely, the future evolution of our Universe. Considering for concreteness a constant w_X, it is clear that an equation of state $-1 < w_X$, sufficiently negative in order to produce an accelerated expansion rate today, will necessarily produce a transient acceleration stage. It will then eventually lead to a recollapsing universe. We have found the analytical expression for the scale factor $a(t)$ in the regime around the turning point when dustlike matter is negligible compared to the dark sector. On the other hand if the X component is of the phantom type, $w_X < -1$, our Universe will end in a Big Rip as expected and we have found here too an analytical fit for $a(t)$ valid in the asymptotic region when dust-like matter becomes negligible compared to λ while the latter is not yet negligible compared to the X component.

Suggested by high energy physics, the possibility to have a negative cosmological constant is worth investigating as it challenges our intuition about the phenomenology of cosmological models. If this negative cosmological constant is substantial enough to affect the cosmic expansion history like in those models investigated here, a high value for H_o could be a decisive test.

"Las Estrellas dicen que nosotros somos los fugaces."

Macaco

8 Conclusions

It is *rather curious* -to say the least- to note that the Universe seems to have undergone a *De Sitter-like* epoch of *accelerated expansion twice already* in the cosmic history. Yet it seems very challenging to construct a (stable) *De Sitter vacuum* from a more fundamental theory [171]. While the physical mechanism driving these periods of accelerated expansion remains unknown, supernovae [185, 199], CMB [69] and LSS observations [183] suggest the universe is currently accelerating, consistent with a simple (positive) cosmological constant (Λ), and Cold Dark Matter (CDM). The ΛCDM model is in remarkable agreement with a vast array of cosmological probes throughout the cosmic history. The so-called "*tensions*" within the ΛCDM paradigm have shown the robustness of the former, when tested against increasingly precise cosmological measurements. Throughout this thesis, we explored the phenomenology of various beyond ΛCDM scenarios. We focus on those particular observables that could allow us to distinguish between the wide class of dark energy and modified gravity models already existing in the literature. One example is the growth index γ of matter perturbations.

We start this thesis with a thorough review of the homogeneous and isotropic (FLRW) expanding universe in Chapter 1 - focusing on the key *observables* and *assumptions* underlying the concordance model of cosmology (ΛCDM). We briefly mention some of its shortcomings and/or possible discrepancies. The inflationary paradigm is then discussed in Chapter 2, as one possible mechanism for generating the (quantum-mechanical) seeds, that much later on - through gravitational instability - will grow into galaxies and clusters of galaxies we observe in the late Universe. We briefly comment on the potential of future space-based GW observatories to probe new physics, at extremely high-energies. Chapter 3 is devoted to the study of small perturbations around the FLRW universe, we also comment on the various types of Large Scale Structure (LSS) probes and see how these observables allow us to probe the nature of DE - in complementarity with BBN, CMB, SNeIa, BAO and other background probes discussed in Chapter 1. In Chapter 4 we introduce some modified gravity models, beyond Einstein's GR. In such models, the growth of perturbations is modified and one tool to study these modifications is the *growth index* γ. This is indeed the main subject of part II.

In Chapter 5, we shall study the global behaviour of γ in various beyond-ΛCDM scenarios, *i.e.* a varying EoS $w_{\rm DE}(a)$, an $f(R)$-like bump/dip in $G_{\rm eff}(z)$ or more intricate DE models such as the Dvali-Gabadadze-Porrati model. In such models, the behaviour of γ can drastically differ from that of ΛCDM . In particular, we find that all of the above mention scenarios lead to a change in the slope of γ - in *sharp constrast* with the *monotonically decreasing* ΛCDM case. We derive the asymptotic value in the past for $\gamma_{-\infty}$ in such models, and explicitly see the origin of the anomalous $\gamma^{\rm DGP}_{-\infty} = \frac{11}{16}$ value in the DGP model. In Chapter 6, we consider its behaviour in the presence of a (dustlike) unclustered component Ω_x and explore interesting mathematical properties of γ in the asymptotic past.

In Chapter 7, we consider the possibility of having a more intricate Dark Sector. Inspired by high energy physics, we explore the phenomenology of models containing a negative cosmological constant λ on top of an additional X-component, responsible for the late-time accelerated stage. More specifically, we assume the early universe remains unchanged wrt ΛCDM - thereby fixing the value of the sound horizon $r_s$at recombination - and asses the viability of such models when including BAO, SNeIa and CMB data. We also explore the effect of considering a high-H_0 prior in separate runs. We perform a *nested-sampling* of the parameter space associated with our models, and evaluate the Bayesian evidence needed for model selection. Although we find no decisive evidence for a non-vanishing $\Omega_{\lambda,0}$, its presence remains viable as it hides behind an *effective* (positive) Λ with $w_X \sim -1$. Models with higher evidence are found to be those with new

physics appearing at large-z ($w_X \leq -1$). A value of H_0 substantially larger than $H_0 \sim 70\text{km.s}^{-1}\text{.Mpc}^{-1}$ could be a decisive test of their viability. If the "*true*" value of H_0 turns out to be $H_0 \sim 69\text{km.s}^{-1}\text{.Mpc}^{-1}$, it would be interesting to further explore the viability of such models at the level of perturbations. As we have seen in this work, the linear growth of matter perturbations gives stringent constraints on DE models, and the tools presented in this thesis could be useful for that purpose. This could be the subject of future work, especially in light of upcoming (LSS) experiments.

Listing of figures

1.1.1 Left Panel: Distribution of galaxies as a function of distance, taken by 2dFGRS / Sloan Digital Sky Survey (SDSS III)[70]. Each point represents a galaxy, containing about 100 billion stars each. Right Panel: Cosmic Microwave Background Radiation,the heat remnants of the big bang taken by Planck satellite. 9

1.1.2 3-dimensional hypersurfaces Σ_t at different times t, representing the different possible geometries of the universe. Each slice corresponds to a moment in time. Space-time can be thought of as a collection of time-ordered 3-dim hypersurfaces, characterized by the induced metric γ_{ij} defined on such (curved) hypersurfaces (the so-called 3+1 decomposition). 10

1.1.3 Illustration of a comoving coordinate system. The lefthand side shows a grid-like coordinate system at $t = 0$, $a(t)$ is the scale factor accouting for the expansion of spacetime. The righthand side shows the same coordinate system some later moment in time $t = t_1$. Notice the *comoving coordinates* x^i are the same for the two red points, but the physical distance separating them has grown by a factor of $a(t)$. The scale factor $a(t)$ inherits the physical interpretation of distance and becomes the important variable that we need to keep track of. In orange, we represent a photon, whose initial wavelength λ_1 gets *strechted* as the universe expands with time. 11

1.3.1 Schematic view of the relevant processes happening during *Big Bang Nucleosynthesis* (BBN) - The formation of light elements. Essentially all of the elements that are heavier than lithium were cooked and produced much later in the history of our Universe, by *Stellar Nucleosynthesis* in evolving and eventually exploding stars. 22

1.3.2 Schematic picture of recombination. 23

1.3.3 Blackbody spectrum in the range $10 - 10^3$nm for different temperatures (in K) of the black body. From this, we can estimate with great precision the temperature of the *cosmic microwave background*. The sun's temperature is $T_\odot \sim 5777$ K and thus emits visible light. . . 24

1.3.4 Angular (Temperature) Power Spectrum of the Cosmic Microwave Background Radiation, as measured by various experiments. Namely, Planck[69], Atacama Cosmology Telescope (ACT)[64] and South-Pole Telescope (SPT)[87]. Solid line represents the ΛCDM prediction. Credit: D.Baumman 26
1.3.5 Schematic view of the sound horizon. From right to left, the sound horizon r_s propagates through the primordial plasma and grows with time, baryons are carried along this propagating sound wave until recombination happens, when the photons decouple from baryons and can propagate freely. The sound horizon "freezes" and a characteristic wavelength is imprinted in the *surface of last scattering* (CMB). We observers, seat at the origin, and should find a correlation between points separated by the comoving length $r_s(z_{rec})$. This has indeed been measured in various observational probes, such as the correlation function (or matter power spectrum) and in the acoustic peaks of the CMB. 27
1.4.1 Compilation of early vs late-time measurements of H_0. Figure taken from [83]. 28

2.0.1 Schematic representation of the "Horizon problem". *Left Panel:* Points P and P' at the surface of last-scattering never talked to each other, *i.e.* their past light-cones do not overlap in the spacetime diagram. A straightforward calculations leads to $\sim 10^5$ casually disconnected regions in the CMB. Yet, regardless of the direction we observe in the sky, the temperature appears to be homogeneous, with small fluctuations $\mathcal{O}(10^{-5})$ around the mean.*Right Panel:* Solution by the inflationary paradigm. The big bang singularity is pushed to the infinite past $\tau_i \to -\infty$. 31
2.1.1 Solution to the Homogeneity Problem in the standard inflationary picture. From left to right, the evolution of the Hubble Radius (in comoving coordinates) at the beginning and end of Inflation, and nowadays, respectively. The comoving Hubble radius shrinks exponentially during inflation, as can be seen from Eq. (1.28), since $a(t) \propto \exp(Ht)$. Those regions that were causally connected before inflation, exit the horizon during inflation and re-enter progressively after it stops; when the Hubble radius starts to grow again. 33
2.2.1 Schematic picture of the evolution of perturbations generated during inflation, as a function of time. The Hubble crossing corresponds to the time t_k, when the mode $k = aH$ crosses the Hubble radius. The quantity ζ is an extremely important conserved quantity outside the horizon. The power spectrum P_ζ encodes the statistical properties of the fluctuations at horizon crossing. 35

2.3.1 Schematic illustration of an inflationary potential. Cosmic Microwave Background (CMB) and Large Scale Structure (LSS) surveys are consistent with the predictions from slow-roll (single) field inflation. These probe the shape of the inflationary potential around $\sim$ 60 e-folds before the end of inflation. Scales of interest for PBH formation will leave the horizon much later on, only a few e-folds before the end of inflation. The non-observation of PBH in certain mass ranges, could in principle, constrain the shape of the inflationary potential near the reheating epoch. 36
2.4.1 LSS. 38

3.0.1 Schematic view of the differents regimes as function of scale. The study of fluctuations in the superhorizon regime requires treating cosmological perturbations relativistically. For reference, a typical cluster of galaxies with total mass $M \sim 10^{10} M_{\odot}$ has a virial radius $R_{\rm vir} \sim 1$ Mpc below which non-linear gravitational interactions can no longer be neglected. In such cases, one typically relies on numerical N-body simulations. 42
3.1.1 Schematic Illustration of the physics of *Baryonic Acoustic Oscillations* (BAO). A constant battle between gravitational attraction and electromagnetic repulsion. Baryons are constantly shifted out of equilibrium due to a dynamical gravitational potential arena. This in turn translate into areas with higher baryonic density (Hot spots in the temperature of the CMB) and areas with lower density (blue spots). This is just a first approximation, in reality, the non-interacting (cold) Dark Matter sits at the bottom of those wells and enhance the gravitational potential. The fractional abundance of DM compared to baryonic matter determines the shape of the acoustic peaks in the CMB, and allows us to precisely measure the quantities $\omega_{\rm b}$ and $\omega_{\rm CDM}$. 46
3.2.1 Matter Power Spectrum at $z = 0$. Figure taken from [60] 49
3.2.2 Weak gravitational lensing in the Abell 2218 galaxy cluster. The shapes of galaxies appear to be distorted, or elongated in some direction. Advanced Statistical methods can be used to quantify this effect, and estimate the mass distribution along the line of sight[130, 217]. Figure taken by the Hubble Space Telescope. Credit: NASA/ESA https://esahubble.org/images/heic0814a/ 52
3.2.3 Most recent constraints on the (S_8, Ω_m) plane in the ΛCDM model from the 3-year Dark Energy Survey (DES) results. It is seen that both (Kids & DES) weak-lensing surveys prefer a lower value for S_8 than early-universe (CMB) measurements from Planck - although it is not statistically significant yet to call it a "tension". Figure taken from [67] (Fig. 19) . 54

4.3.1 Schematic representation of brane world theories. 60

5.1.1 The growth index with $w = -1$, blue shaded region corresponds to regions satisfying $\frac{d\gamma}{d\Omega_m} > 0$. 67

5.2.1 The (unit time-oriented) vector field tangent to the solutions γ of Eq.(6.1) is displayed for $w_{DE} = -1$. The red curve corresponds to the solution for γ, with boundary condition $\gamma(1) \equiv \gamma_{-\infty} = 6/11$. It is the only solution which is finite on the entire Ω_m interval, physically it corresponds to the presence of the growing mode of (5.6) only. The difference can be important in the far past only. All the other solutions correspond to solutions containing also the decaying mode solution. As explained in the text, these solutions (if physical) tend to the same value of γ, namely $\gamma_\infty = \frac{2}{3}$, for $\Omega_m \to 0$, and they diverge for $\Omega_m \to 1$. 69

5.3.1 The growth index with various constant equations of state $w_{\rm DE}$. As explained before, the monotonically decreasing behaviour of $\gamma(\Omega_m)$ holds in these models. We have used a logarithmic-scale in Ω_m. 72

5.4.1 The evolution of γ is shown for CPL varying w_{DE}. We see that $\gamma(\Omega_m)$ is essentially decreasing except in the remote future and, for $w_a \gtrsim 0.2$, in the far past. Note the value $\gamma_\infty = \frac{1}{2}$ as expected for $w_\infty = -\infty$. 74

5.4.2 (a) *Left-hand panel:* A schematic representation is given when there is a bump in g, chosen here to be slightly in the past (with $\Omega_{m,0} = 0.3$) while the background expansion is fixed ($w_{\rm DE} = -1$). We see that γ decreases first (with the expansion) when g goes up before increasing when g decreases back to one. It is this last behaviour that was found today in many $f(R)$ models. Hence, the sign of the derivative tells us that we (just) passed the maximum of the bump. Note that $\gamma^{\rm Bump}$ and $\gamma^{\Lambda{\rm CDM}}$ shown here have the same asymptotic values both in the past and future because $g \to 1$ in a smooth way and they have identical $w_{\rm DE}$. The behaviour on small redshifts and in the future captures essentially the $f(R)$ phenomenology. (b)*Right-hand panel:* the same as on the left panel but now with a dip in g starting today. At the present time, $\gamma > \gamma^{\Lambda{\rm CDM}}$ and γ are decreasing with the expansion, reflecting that g is increasing and we just have passed the minimum of the dip. 75

5.4.3 Left panel: The growth function $f \equiv \frac{d\ln\delta_m}{d\ln a}$ in the presence of a bump in $g = \frac{G_{\rm eff}}{G}$. Right panel: Evolution of f as a function of redshift. The approximation $f = \Omega_m^\gamma$ is shown for comparison, for different values of γ. It is seen that the growth of perturbations in GR is well approximated by $\gamma \simeq 0.55$. In the past, already at $z \sim 10$ where matter dominates their evolution is nearly identical with $f = 1$, and thus $\delta_m \propto a$ as expected. Small departures from the "*true*" numerical solution (GR) can be seen at low-z, where γ starts to depart from its "nearly constant" regime. 76

5.4.4 The behaviour of γ in DGP models is shown and compared to that in ΛCDM. We see that $\gamma^{DGP} > \Gamma^{DGP}$ and hence $\gamma^{DGP}(\Omega_m)$ is an increasing function, except for the tiny interval $\Omega_m \lesssim 10^{-3}$. While $w^{DGP}_{-\infty} = -\frac{1}{2}$, $\gamma^{DGP}_{-\infty} = \frac{11}{16}$ and not $\frac{9}{16}$ as one would have in GR. This is because the DGP model does not tend to GR in a smooth enough way, namely $\left(\frac{dg^{DGP}}{d\Omega_m}\right)_{-\infty} = \frac{1}{3} \neq 0$. In the future however, while DGP does not tend to GR with $g^{DGP}_{\infty} = \frac{2}{3}$ and $w^{DGP}_{\infty} = -1$, the same asymptotic value $\gamma^{DGP}_{\infty} = \frac{2}{3}$ is obtained as in GR for $w_{\infty} = -1$ because gravity in DGP is weaker than in GR in the far future. Note that all four curves tend to $\frac{2}{3}$ in the future. 77

6.2.1 Streamlines (Phase Portrait) for the dynamical system {(6.8),(6.9)}. Point $A = (\Omega_m = 0, \gamma_{\infty})$ corresponds to an attractor of the system, $S = (\Omega_m = 1, \gamma_{-\infty})$ is a saddle point and $R_{\pm}$ refers to the two critical points at infinity, which are both repellers of the system. The green line denotes the so-called *heteroclinic orbit* (connecting the two critical points S & A.), which corresponds to the solely presence of the growing mode for $\delta(a)$[55]. . . 86

6.3.1 Left panel: The blue curve shows the reconstruction of $\gamma(\Omega^{\rm tot}_m, \varepsilon)$ for $\varepsilon = 0.15$. The red curve is the second order approximation given by Eq. (6.52). We see that they match nicely for $\Omega^{\rm tot}_m \simeq 1$. Right panel shows a zoom for $\Omega^{\rm tot}_m \simeq 1$. 93

7.1.1 3D-Plot showing regions in parameter space (z, w_X) where $\Omega_{DE} < 0$. By construction, $\Omega_{\rm DE,0} = 1 - \Omega_{m,0}$ - we choose $\Omega_{m,0} = 0.3$ here. The color bar on the right, shows the different values for the effective DE density $\Omega_{\rm DE}(z, w_X)$ and for a fixed value of $\Omega_{\lambda,0} = -0.5$ (on the left) and $\Omega_{\lambda,0} = -1.0$ (on the right). The function Ω_{DE} can become negative as we will later see. 104

7.1.2 Evolution of the maximum value of $\ddot{a}/a$ reached from matter era until today, as a function of w_X for two different values of $\Omega_{\lambda,0}$ and $\Omega_{m,0} = 0.3$. 105

7.1.3 Evolution of the universe in the space $(w_X, \Omega_{\lambda,0})$. In white, the universe accelerates today, in light gray, the universe never accelerated until today while in darker gray, we have a transient situation where the universe accelerated in the past but does not accelerate today. In blue, we have represented the SNe Ia data constraints at $(1\sigma, 2\sigma, 3\sigma)$. Finally the red and purple lines represent the $(\Omega_{\lambda,0}, w_X)$ values which satisfy Eq. (7.27) for $h = 0.74$ and $h = 0.72$ respectively. 106

7.2.1 Parameters (h, ω_λ, w_X) which satisfy the relation (7.27) for models with constant w_X. a) In the upper panel, ω_λ is fixed and we see that an increasing $|\omega_\lambda|$ (from left to right) gives the same h with less phantomness. We note the quasilinear relation, which follows from (7.43) for constant ω_λ. b) In the lower panel all parameters are free. For the latter, we show the lines corresponding to a constant h when (7.27) is satisfied: continuous line ($h = 0.68$), long dashed line ($h = 0.7$) and dashed line ($h = 0.74$). They satisfy to good accuracy (7.43). 115

7.2.2 We show iso-h curves for scenarios I (left), II (middle), and III with $\Delta_1 = -0.04$ (right-hand panel) in the $(\Delta_{1,2}, \omega_\lambda)$ parameter plane. The shaded areas correspond to the following H_0 values (in km.s^{-1}.Mpc^{-1} units): 73.30 ± 4 (HST-Mira) [118]), 74.03 ± 1.42 (SHoES) [200] and 69.8 ± 1.9 (TRGB) [102]. 116
7.3.1 Marginalized posteriors for different models using SNIa, BAO, θ_s, and H_0 from HST Mira. The central value is the median, and the shared areas show the 68% credible intervals around it. Left: ΛCDM (blue), III (orange), and λIII (green). Right: ΛCDM (blue), λCPLw_a (orange), λII (green). 118

References

[1] S. Tsujikawa A. De Felice. *f(R)-Theories*. arXiv:1002.4928, (2010). URL https://arxiv.org/pdf/1002.4928.pdf.

[2] G. Aad, T. Abajyan, B. Abbott, J. Abdallah, S. Abdel Khalek, A.A. Abdelalim, O. Abdinov, R. Aben, B. Abi, M. Abolins, and et al. Observation of a new particle in the search for the Standard Model Higgs boson with the ATLAS detector at the LHC. *Physics Letters B*, 716(1):1–29, Sep 2012. ISSN 0370-2693. doi: 10.1016/j.physletb.2012.08.020. URL http://dx.doi.org/10.1016/j.physletb.2012.08.020.

[3] B. P. Abbott, R. Abbott, T. D. Abbott, M. R. Abernathy, F. Acernese, K. Ackley, C. Adams, T. Adams, P. Addesso, R. X. Adhikari, V. B. Adya, C. Affeldt, M. Agathos, K. Agatsuma, N. Aggarwal, O. D. Aguiar, L. Aiello, A. Ain, P. Ajith, B. Allen, A. Allocca, P. A. Altin, S. B. Anderson, W. G. Anderson, K. Arai, M. A. Arain, M. C. Araya, C. C. Arceneaux, J. S. Areeda, N. Arnaud, K. G. Arun, S. Ascenzi, G. Ashton, M. Ast, S. M. Aston, P. Astone, P. Aufmuth, C. Aulbert, S. Babak, P. Bacon, M. K. M. Bader, P. T. Baker, F. Baldaccini, G. Ballardin, S. W. Ballmer, J. C. Barayoga, S. E. Barclay, B. C. Barish, D. Barker, F. Barone, B. Barr, L. Barsotti, M. Barsuglia, D. Barta, J. Bartlett, M. A. Barton, I. Bartos, R. Bassiri, A. Basti, J. C. Batch, C. Baune, V. Bavigadda, M. Bazzan, B. Behnke, M. Bejger, C. Belczynski, A. S. Bell, C. J. Bell, B. K. Berger, J. Bergman, G. Bergmann, C. P. L. Berry, D. Bersanetti, A. Bertolini, J. Betzwieser, S. Bhagwat, R. Bhandare, I. A. Bilenko, G. Billingsley, J. Birch, R. Birney, O. Birnholtz, S. Biscans, A. Bisht, M. Bitossi, C. Biwer, M. A. Bizouard, J. K. Blackburn, C. D. Blair, D. G. Blair, R. M. Blair, S. Bloemen, O. Bock, T. P. Bodiya, M. Boer, G. Bogaert, C. Bogan, A. Bohe, P. Bojtos, C. Bond, F. Bondu, R. Bonnand, B. A. Boom, R. Bork, V. Boschi, S. Bose, Y. Bouffanais, A. Bozzi, C. Bradaschia, P. R. Brady, V. B. Braginsky, M. Branchesi, J. E. Brau, T. Briant, A. Brillet, M. Brinkmann, V. Brisson, P. Brockill, A. F. Brooks, D. A. Brown, D. D. Brown, N. M. Brown, C. C. Buchanan, A. Buikema, T. Bulik, H. J. Bulten, A. Buonanno, D. Buskulic, C. Buy, R. L. Byer, M. Cabero, L. Cadonati, G. Cagnoli, C. Cahillane, J. Calderón Bustillo, T. Callister, E. Calloni, J. B. Camp, K. C. Cannon, J. Cao, C. D. Capano, E. Capocasa, F. Carbognani, S. Caride, J. Casanueva Diaz, C. Casentini, S. Caudill, M. Cavaglià, F. Cavalier, R. Cavalieri, G. Cella, C. B. Cepeda, L. Cerboni Baiardi, G. Cerretani, E. Cesarini, R. Chakraborty, T. Chalermsongsak, S. J. Chamberlin, M. Chan, S. Chao, P. Charlton, E. Chassande-Mottin, H. Y. Chen, Y. Chen, C. Cheng,

A. Chincarini, A. Chiummo, H. S. Cho, M. Cho, J. H. Chow, N. Christensen, Q. Chu, S. Chua, S. Chung, G. Ciani, F. Clara, J. A. Clark, F. Cleva, E. Coccia, P.-F. Cohadon, A. Colla, C. G. Collette, L. Cominsky, M. Constancio, A. Conte, L. Conti, D. Cook, T. R. Corbitt, N. Cornish, A. Corsi, S. Cortese, C. A. Costa, M. W. Coughlin, S. B. Coughlin, J.-P. Coulon, S. T. Countryman, P. Couvares, E. E. Cowan, D. M. Coward, M. J. Cowart, D. C. Coyne, R. Coyne, K. Craig, J. D. E. Creighton, T. D. Creighton, J. Cripe, S. G. Crowder, A. M. Cruise, A. Cumming, L. Cunningham, E. Cuoco, T. Dal Canton, S. L. Danilishin, S. D'Antonio, K. Danzmann, N. S. Darman, C. F. Da Silva Costa, V. Dattilo, I. Dave, H. P. Daveloza, M. Davier, G. S. Davies, E. J. Daw, R. Day, S. De, D. DeBra, G. Debreczeni, J. Degallaix, M. De Laurentis, S. Deléglise, W. Del Pozzo, T. Denker, T. Dent, H. Dereli, V. Dergachev, R. T. DeRosa, R. De Rosa, R. DeSalvo, S. Dhurandhar, M. C. Díaz, L. Di Fiore, M. Di Giovanni, A. Di Lieto, S. Di Pace, I. Di Palma, A. Di Virgilio, G. Dojcinoski, V. Dolique, F. Donovan, K. L. Dooley, S. Doravari, R. Douglas, T. P. Downes, M. Drago, R. W. P. Drever, J. C. Driggers, Z. Du, M. Ducrot, S. E. Dwyer, T. B. Edo, M. C. Edwards, A. Effler, H.-B. Eggenstein, P. Ehrens, J. Eichholz, S. S. Eikenberry, W. Engels, R. C. Essick, T. Etzel, M. Evans, T. M. Evans, R. Everett, M. Factourovich, V. Fafone, H. Fair, S. Fairhurst, X. Fan, Q. Fang, S. Farinon, B. Farr, W. M. Farr, M. Favata, M. Fays, H. Fehrmann, M. M. Fejer, D. Feldbaum, I. Ferrante, E. C. Ferreira, F. Ferrini, F. Fidecaro, L. S. Finn, I. Fiori, D. Fiorucci, R. P. Fisher, R. Flaminio, M. Fletcher, H. Fong, J.-D. Fournier, S. Franco, S. Frasca, F. Frasconi, M. Frede, Z. Frei, A. Freise, R. Frey, V. Frey, T. T. Fricke, P. Fritschel, V. V. Frolov, P. Fulda, M. Fyffe, H. A. G. Gabbard, J. R. Gair, L. Gammaitoni, S. G. Gaonkar, F. Garufi, A. Gatto, G. Gaur, N. Gehrels, G. Gemme, B. Gendre, E. Genin, A. Gennai, J. George, L. Gergely, V. Germain, Abhirup Ghosh, Archisman Ghosh, S. Ghosh, J. A. Giaime, K. D. Giardina, A. Giazotto, K. Gill, A. Glaefke, J. R. Gleason, E. Goetz, R. Goetz, L. Gondan, G. González, J. M. Gonzalez Castro, A. Gopakumar, N. A. Gordon, M. L. Gorodetsky, S. E. Gossan, M. Gosselin, R. Gouaty, C. Graef, P. B. Graff, M. Granata, A. Grant, S. Gras, C. Gray, G. Greco, A. C. Green, R. J. S. Greenhalgh, P. Groot, H. Grote, S. Grunewald, G. M. Guidi, X. Guo, A. Gupta, M. K. Gupta, K. E. Gushwa, E. K. Gustafson, R. Gustafson, J. J. Hacker, B. R. Hall, E. D. Hall, G. Hammond, M. Haney, M. M. Hanke, J. Hanks, C. Hanna, M. D. Hannam, J. Hanson, T. Hardwick, J. Harms, G. M. Harry, I. W. Harry, M. J. Hart, M. T. Hartman, C.-J. Haster, K. Haughian, J. Healy, J. Heefner, A. Heidmann, M. C. Heintze, G. Heinzel, H. Heitmann, P. Hello, G. Hemming, M. Hendry, I. S. Heng, J. Hennig, A. W. Heptonstall, M. Heurs, S. Hild, D. Hoak, K. A. Hodge, D. Hofman, S. E. Hollitt, K. Holt, D. E. Holz, P. Hopkins, D. J. Hosken, J. Hough, E. A. Houston, E. J. Howell, Y. M. Hu, S. Huang, E. A. Huerta, D. Huet, B. Hughey, S. Husa, S. H. Huttner, T. Huynh-Dinh, A. Idrisy, N. Indik, D. R. Ingram, R. Inta, H. N. Isa, J.-M. Isac, M. Isi, G. Islas, T. Isogai, B. R. Iyer, K. Izumi, M. B. Jacobson, T. Jacqmin, H. Jang, K. Jani, P. Jaranowski, S. Jawahar, F. Jiménez-Forteza, W. W. Johnson, N. K. Johnson-McDaniel, D. I. Jones, R. Jones, R. J. G. Jonker, L. Ju, K. Haris, C. V. Kalaghatgi, V. Kalogera, S. Kandhasamy, G. Kang, J. B. Kanner, S. Karki, M. Kasprzack, E. Katsavounidis, W. Katzman, S. Kaufer, T. Kaur, K. Kawabe, F. Kawazoe, F. Kéfélian, M. S. Kehl, D. Keitel, D. B. Kelley, W. Kells, R. Kennedy, D. G. Keppel, J. S. Key, A. Khalaidovski, F. Y. Khalili, I. Khan, S. Khan,

Z. Khan, E. A. Khazanov, N. Kijbunchoo, C. Kim, J. Kim, K. Kim, Nam-Gyu Kim, Namjun Kim, Y.-M. Kim, E. J. King, P. J. King, D. L. Kinzel, J. S. Kissel, L. Kleybolte, S. Klimenko, S. M. Koehlenbeck, K. Kokeyama, S. Koley, V. Kondrashov, A. Kontos, S. Koranda, M. Korobko, W. Z. Korth, I. Kowalska, D. B. Kozak, V. Kringel, B. Krishnan, A. Królak, C. Krueger, G. Kuehn, P. Kumar, R. Kumar, L. Kuo, A. Kutynia, P. Kwee, B. D. Lackey, M. Landry, J. Lange, B. Lantz, P. D. Lasky, A. Lazzarini, C. Lazzaro, P. Leaci, S. Leavey, E. O. Lebigot, C. H. Lee, H. K. Lee, H. M. Lee, K. Lee, A. Lenon, M. Leonardi, J. R. Leong, N. Leroy, N. Letendre, Y. Levin, B. M. Levine, T. G. F. Li, A. Libson, T. B. Littenberg, N. A. Lockerbie, J. Logue, A. L. Lombardi, L. T. London, J. E. Lord, M. Lorenzini, V. Loriette, M. Lormand, G. Losurdo, J. D. Lough, C. O. Lousto, G. Lovelace, H. Lück, A. P. Lundgren, J. Luo, R. Lynch, Y. Ma, T. MacDonald, B. Machenschalk, M. MacInnis, D. M. Macleod, F. Magaña Sandoval, R. M. Magee, M. Mageswaran, E. Majorana, I. Maksimovic, V. Malvezzi, N. Man, I. Mandel, V. Mandic, V. Mangano, G. L. Mansell, M. Manske, M. Mantovani, F. Marchesoni, F. Marion, S. Márka, Z. Márka, A. S. Markosyan, E. Maros, F. Martelli, L. Martellini, I. W. Martin, R. M. Martin, D. V. Martynov, J. N. Marx, K. Mason, A. Masserot, T. J. Massinger, M. Masso-Reid, F. Matichard, L. Matone, N. Mavalvala, N. Mazumder, G. Mazzolo, R. McCarthy, D. E. McClelland, S. McCormick, S. C. McGuire, G. McIntyre, J. McIver, D. J. McManus, S. T. McWilliams, D. Meacher, G. D. Meadors, J. Meidam, A. Melatos, G. Mendell, D. Mendoza-Gandara, R. A. Mercer, E. Merilh, M. Merzougui, S. Meshkov, C. Messenger, C. Messick, P. M. Meyers, F. Mezzani, H. Miao, C. Michel, H. Middleton, E. E. Mikhailov, L. Milano, J. Miller, M. Millhouse, Y. Minenkov, J. Ming, S. Mirshekari, C. Mishra, S. Mitra, V. P. Mitrofanov, G. Mitselmakher, R. Mittleman, A. Moggi, M. Mohan, S. R. P. Mohapatra, M. Montani, B. C. Moore, C. J. Moore, D. Moraru, G. Moreno, S. R. Morriss, K. Mossavi, B. Mours, C. M. Mow-Lowry, C. L. Mueller, G. Mueller, A. W. Muir, Arunava Mukherjee, D. Mukherjee, S. Mukherjee, N. Mukund, A. Mullavey, J. Munch, D. J. Murphy, P. G. Murray, A. Mytidis, I. Nardecchia, L. Naticchioni, R. K. Nayak, V. Necula, K. Nedkova, G. Nelemans, M. Neri, A. Neunzert, G. Newton, T. T. Nguyen, A. B. Nielsen, S. Nissanke, A. Nitz, F. Nocera, D. Nolting, M. E. N. Normandin, L. K. Nuttall, J. Oberling, E. Ochsner, J. O'Dell, E. Oelker, G. H. Ogin, J. J. Oh, S. H. Oh, F. Ohme, M. Oliver, P. Oppermann, Richard J. Oram, B. O'Reilly, R. O'Shaughnessy, C. D. Ott, D. J. Ottaway, R. S. Ottens, H. Overmier, B. J. Owen, A. Pai, S. A. Pai, J. R. Palamos, O. Palashov, C. Palomba, A. Pal-Singh, H. Pan, Y. Pan, C. Pankow, F. Pannarale, B. C. Pant, F. Paoletti, A. Paoli, M. A. Papa, H. R. Paris, W. Parker, D. Pascucci, A. Pasqualetti, R. Passaquieti, D. Passuello, B. Patricelli, Z. Patrick, B. L. Pearlstone, M. Pedraza, R. Pedurand, L. Pekowsky, A. Pele, S. Penn, A. Perreca, H. P. Pfeiffer, M. Phelps, O. Piccinni, M. Pichot, M. Pickenpack, F. Piergiovanni, V. Pierro, G. Pillant, L. Pinard, I. M. Pinto, M. Pitkin, J. H. Poeld, R. Poggiani, P. Popolizio, A. Post, J. Powell, J. Prasad, V. Predoi, S. S. Premachandra, T. Prestegard, L. R. Price, M. Prijatelj, M. Principe, S. Privitera, R. Prix, G. A. Prodi, L. Prokhorov, O. Puncken, M. Punturo, P. Puppo, M. Pürrer, H. Qi, J. Qin, V. Quetschke, E. A. Quintero, R. Quitzow-James, F. J. Raab, D. S. Rabeling, H. Radkins, P. Raffai, S. Raja, M. Rakhmanov, C. R. Ramet, P. Rapagnani, V. Raymond, M. Razzano, V. Re, J. Read, C. M. Reed, T. Regimbau, L. Rei, S. Reid, D. H. Reitze, H. Rew, S. D. Reyes, F. Ricci,

K. Riles, N. A. Robertson, R. Robie, F. Robinet, A. Rocchi, L. Rolland, J. G. Rollins, V. J. Roma, J. D. Romano, R. Romano, G. Romanov, J. H. Romie, D. Rosińska, S. Rowan, A. Rüdiger, P. Ruggi, K. Ryan, S. Sachdev, T. Sadecki, L. Sadeghian, L. Salconi, M. Saleem, F. Salemi, A. Samajdar, L. Sammut, L. M. Sampson, E. J. Sanchez, V. Sandberg, B. Sandeen, G. H. Sanders, J. R. Sanders, B. Sassolas, B. S. Sathyaprakash, P. R. Saulson, O. Sauter, R. L. Savage, A. Sawadsky, P. Schale, R. Schilling, J. Schmidt, P. Schmidt, R. Schnabel, R. M. S. Schofield, A. Schönbeck, E. Schreiber, D. Schuette, B. F. Schutz, J. Scott, S. M. Scott, D. Sellers, A. S. Sengupta, D. Sentenac, V. Sequino, A. Sergeev, G. Serna, Y. Setyawati, A. Sevigny, D. A. Shaddock, T. Shaffer, S. Shah, M. S. Shahriar, M. Shaltev, Z. Shao, B. Shapiro, P. Shawhan, A. Sheperd, D. H. Shoemaker, D. M. Shoemaker, K. Siellez, X. Siemens, D. Sigg, A. D. Silva, D. Simakov, A. Singer, L. P. Singer, A. Singh, R. Singh, A. Singhal, A. M. Sintes, B. J. J. Slagmolen, J. R. Smith, M. R. Smith, N. D. Smith, R. J. E. Smith, E. J. Son, B. Sorazu, F. Sorrentino, T. Souradeep, A. K. Srivastava, A. Staley, M. Steinke, J. Steinlechner, S. Steinlechner, D. Steinmeyer, B. C. Stephens, S. P. Stevenson, R. Stone, K. A. Strain, N. Straniero, G. Stratta, N. A. Strauss, S. Strigin, R. Sturani, A. L. Stuver, T. Z. Summerscales, L. Sun, P. J. Sutton, B. L. Swinkels, M. J. Szczepańczyk, M. Tacca, D. Talukder, D. B. Tanner, M. Tápai, S. P. Tarabrin, A. Taracchini, R. Taylor, T. Theeg, M. P. Thirugnanasambandam, E. G. Thomas, M. Thomas, P. Thomas, K. A. Thorne, K. S. Thorne, E. Thrane, S. Tiwari, V. Tiwari, K. V. Tokmakov, C. Tomlinson, M. Tonelli, C. V. Torres, C. I. Torrie, D. Töyrä, F. Travasso, G. Traylor, D. Trifirò, M. C. Tringali, L. Trozzo, M. Tse, M. Turconi, D. Tuyenbayev, D. Ugolini, C. S. Unnikrishnan, A. L. Urban, S. A. Usman, H. Vahlbruch, G. Vajente, G. Valdes, M. Vallisneri, N. van Bakel, M. van Beuzekom, J. F. J. van den Brand, C. Van Den Broeck, D. C. Vander-Hyde, L. van der Schaaf, J. V. van Heijningen, A. A. van Veggel, M. Vardaro, S. Vass, M. Vasúth, R. Vaulin, A. Vecchio, G. Vedovato, J. Veitch, P. J. Veitch, K. Venkateswara, D. Verkindt, F. Vetrano, A. Viceré, S. Vinciguerra, D. J. Vine, J.-Y. Vinet, S. Vitale, T. Vo, H. Vocca, C. Vorvick, D. Voss, W. D. Vousden, S. P. Vyatchanin, A. R. Wade, L. E. Wade, M. Wade, S. J. Waldman, M. Walker, L. Wallace, S. Walsh, G. Wang, H. Wang, M. Wang, X. Wang, Y. Wang, H. Ward, R. L. Ward, J. Warner, M. Was, B. Weaver, L.-W. Wei, M. Weinert, A. J. Weinstein, R. Weiss, T. Welborn, L. Wen, P. Weßels, T. Westphal, K. Wette, J. T. Whelan, S. E. Whitcomb, D. J. White, B. F. Whiting, K. Wiesner, C. Wilkinson, P. A. Willems, L. Williams, R. D. Williams, A. R. Williamson, J. L. Willis, B. Willke, M. H. Wimmer, L. Winkelmann, W. Winkler, C. C. Wipf, A. G. Wiseman, H. Wittel, G. Woan, J. Worden, J. L. Wright, G. Wu, J. Yablon, I. Yakushin, W. Yam, H. Yamamoto, C. C. Yancey, M. J. Yap, H. Yu, M. Yvert, A. Zadrożny, L. Zangrando, M. Zanolin, J.-P. Zendri, M. Zevin, F. Zhang, L. Zhang, M. Zhang, Y. Zhang, C. Zhao, M. Zhou, Z. Zhou, X. J. Zhu, M. E. Zucker, S. E. Zuraw, and J. Zweizig. Observation of gravitational waves from a binary black hole merger. *Phys. Rev. Lett.*, 116:061102, Feb 2016. doi: 10.1103/PhysRevLett.116.061102. URL https://link.aps.org/doi/10.1103/PhysRevLett.116.061102.

[4] B. P. Abbott, R. Abbott, T. D. Abbott, F. Acernese, K. Ackley, C. Adams, T. Adams, P. Addesso, R. X. Adhikari, V. B. Adya, C. Affeldt, M. Afrough, B. Agarwal, M. Agathos, K. Agatsuma, N. Aggar-

wal, O. D. Aguiar, L. Aiello, A. Ain, P. Ajith, B. Allen, G. Allen, A. Allocca, P. A. Altin, A. Amato, A. Ananyeva, S. B. Anderson, W. G. Anderson, S. V. Angelova, S. Antier, S. Appert, K. Arai, M. C. Araya, J. S. Areeda, N. Arnaud, K. G. Arun, S. Ascenzi, G. Ashton, M. Ast, S. M. Aston, P. Astone, D. V. Atallah, P. Aufmuth, C. Aulbert, K. AultONeal, C. Austin, A. Avila-Alvarez, S. Babak, P. Bacon, M. K. M. Bader, S. Bae, M. Bailes, P. T. Baker, F. Baldaccini, G. Ballardin, S. W. Ballmer, S. Banagiri, J. C. Barayoga, S. E. Barclay, B. C. Barish, D. Barker, K. Barkett, F. Barone, B. Barr, L. Barsotti, M. Barsuglia, D. Barta, S. D. Barthelmy, J. Bartlett, I. Bartos, R. Bassiri, A. Basti, J. C. Batch, M. Bawaj, J. C. Bayley, M. Bazzan, B. Bécsy, C. Beer, M. Bejger, I. Belahcene, A. S. Bell, B. K. Berger, G. Bergmann, S. Bernuzzi, J. J. Bero, C. P. L. Berry, D. Bersanetti, A. Bertolini, J. Betzwieser, S. Bhagwat, R. Bhandare, I. A. Bilenko, G. Billingsley, C. R. Billman, J. Birch, R. Birney, O. Birnholtz, S. Biscans, S. Biscoveanu, A. Bisht, M. Bitossi, C. Biwer, M. A. Bizouard, J. K. Blackburn, J. Blackman, C. D. Blair, D. G. Blair, R. M. Blair, S. Bloemen, O. Bock, N. Bode, M. Boer, G. Bogaert, A. Bohe, F. Bondu, E. Bonilla, R. Bonnand, B. A. Boom, R. Bork, V. Boschi, S. Bose, K. Bossie, Y. Bouffanais, A. Bozzi, C. Bradaschia, P. R. Brady, M. Branchesi, J. E. Brau, T. Briant, A. Brillet, M. Brinkmann, V. Brisson, P. Brockill, J. E. Broida, A. F. Brooks, D. A. Brown, D. D. Brown, S. Brunett, C. C. Buchanan, A. Buikema, T. Bulik, H. J. Bulten, A. Buonanno, D. Buskulic, C. Buy, R. L. Byer, M. Cabero, L. Cadonati, G. Cagnoli, C. Cahillane, J. Calderón Bustillo, T. A. Callister, E. Calloni, J. B. Camp, M. Canepa, P. Canizares, K. C. Cannon, H. Cao, J. Cao, C. D. Capano, E. Capocasa, F. Carbognani, S. Caride, M. F. Carney, G. Carullo, J. Casanueva Diaz, C. Casentini, S. Caudill, M. Cavaglià, F. Cavalier, R. Cavalieri, G. Cella, C. B. Cepeda, P. Cerdá-Durán, G. Cerretani, E. Cesarini, S. J. Chamberlin, M. Chan, S. Chao, P. Charlton, E. Chase, E. Chassande-Mottin, D. Chatterjee, K. Chatziioannou, B. D. Cheeseboro, H. Y. Chen, X. Chen, Y. Chen, H.-P. Cheng, H. Chia, A. Chincarini, A. Chiummo, T. Chmiel, H. S. Cho, M. Cho, J. H. Chow, N. Christensen, Q. Chu, A. J. K. Chua, S. Chua, A. K. W. Chung, S. Chung, G. Ciani, R. Ciolfi, C. E. Cirelli, A. Cirone, F. Clara, J. A. Clark, P. Clearwater, F. Cleva, C. Cocchieri, E. Coccia, P.-F. Cohadon, D. Cohen, A. Colla, C. G. Collette, L. R. Cominsky, M. Constancio, L. Conti, S. J. Cooper, P. Corban, T. R. Corbitt, I. Cordero-Carrión, K. R. Corley, N. Cornish, A. Corsi, S. Cortese, C. A. Costa, M. W. Coughlin, S. B. Coughlin, J.-P. Coulon, S. T. Countryman, P. Couvares, P. B. Covas, E. E. Cowan, D. M. Coward, M. J. Cowart, D. C. Coyne, R. Coyne, J. D. E. Creighton, T. D. Creighton, J. Cripe, S. G. Crowder, T. J. Cullen, A. Cumming, L. Cunningham, E. Cuoco, T. Dal Canton, G. Dálya, S. L. Danilishin, S. D'Antonio, K. Danzmann, A. Dasgupta, C. F. Da Silva Costa, V. Dattilo, I. Dave, M. Davier, D. Davis, E. J. Daw, B. Day, S. De, D. DeBra, J. Degallaix, M. De Laurentis, S. Deléglise, W. Del Pozzo, N. Demos, T. Denker, T. Dent, R. De Pietri, V. Dergachev, R. De Rosa, R. T. DeRosa, C. De Rossi, R. DeSalvo, O. de Varona, J. Devenson, S. Dhurandhar, M. C. Díaz, T. Dietrich, L. Di Fiore, M. Di Giovanni, T. Di Girolamo, A. Di Lieto, S. Di Pace, I. Di Palma, F. Di Renzo, Z. Doctor, V. Dolique, F. Donovan, K. L. Dooley, S. Doravari, I. Dorrington, R. Douglas, M. Dovale Álvarez, T. P. Downes, M. Drago, C. Dreissigacker, J. C. Driggers, Z. Du, M. Ducrot, R. Dudi, P. Dupej, S. E. Dwyer, T. B. Edo, M. C. Edwards, A. Effler, H.-B. Eggenstein, P. Ehrens, J. Eichholz, S. S. Eikenberry, R. A. Eisenstein, R. C. Essick,

D. Estevez, Z. B. Etienne, T. Etzel, M. Evans, T. M. Evans, M. Factourovich, V. Fafone, H. Fair, S. Fairhurst, X. Fan, S. Farinon, B. Farr, W. M. Farr, E. J. Fauchon-Jones, M. Favata, M. Fays, C. Fee, H. Fehrmann, J. Feicht, M. M. Fejer, A. Fernandez-Galiana, I. Ferrante, E. C. Ferreira, F. Ferrini, F. Fidecaro, D. Finstad, I. Fiori, D. Fiorucci, M. Fishbach, R. P. Fisher, M. Fitz-Axen, R. Flaminio, M. Fletcher, H. Fong, J. A. Font, P. W. F. Forsyth, S. S. Forsyth, J.-D. Fournier, S. Frasca, F. Frasconi, Z. Frei, A. Freise, R. Frey, V. Frey, E. M. Fries, P. Fritschel, V. V. Frolov, P. Fulda, M. Fyffe, H. Gabbard, B. U. Gadre, S. M. Gaebel, J. R. Gair, L. Gammaitoni, M. R. Ganija, S. G. Gaonkar, C. Garcia-Quiros, F. Garufi, B. Gateley, S. Gaudio, G. Gaur, V. Gayathri, N. Gehrels, G. Gemme, E. Genin, A. Gennai, D. George, J. George, L. Gergely, V. Germain, S. Ghonge, Abhirup Ghosh, Archisman Ghosh, S. Ghosh, J. A. Giaime, K. D. Giardina, A. Giazotto, K. Gill, L. Glover, E. Goetz, R. Goetz, S. Gomes, B. Goncharov, G. González, J. M. Gonzalez Castro, A. Gopakumar, M. L. Gorodetsky, S. E. Gossan, M. Gosselin, R. Gouaty, A. Grado, C. Graef, M. Granata, A. Grant, S. Gras, C. Gray, G. Greco, A. C. Green, E. M. Gretarsson, P. Groot, H. Grote, S. Grunewald, P. Gruning, G. M. Guidi, X. Guo, A. Gupta, M. K. Gupta, K. E. Gushwa, E. K. Gustafson, R. Gustafson, O. Halim, B. R. Hall, E. D. Hall, E. Z. Hamilton, G. Hammond, M. Haney, M. M. Hanke, J. Hanks, C. Hanna, M. D. Hannam, O. A. Hannuksela, J. Hanson, T. Hardwick, J. Harms, G. M. Harry, I. W. Harry, M. J. Hart, C.-J. Haster, K. Haughian, J. Healy, A. Heidmann, M. C. Heintze, H. Heitmann, P. Hello, G. Hemming, M. Hendry, I. S. Heng, J. Hennig, A. W. Heptonstall, M. Heurs, S. Hild, T. Hinderer, W. C. G. Ho, D. Hoak, D. Hofman, K. Holt, D. E. Holz, P. Hopkins, C. Horst, J. Hough, E. A. Houston, E. J. Howell, A. Hreibi, Y. M. Hu, E. A. Huerta, D. Huet, B. Hughey, S. Husa, S. H. Huttner, T. Huynh-Dinh, N. Indik, R. Inta, G. Intini, H. N. Isa, J.-M. Isac, M. Isi, B. R. Iyer, K. Izumi, T. Jacqmin, K. Jani, P. Jaranowski, S. Jawahar, F. Jiménez-Forteza, W. W. Johnson, N. K. Johnson-McDaniel, D. I. Jones, R. Jones, R. J. G. Jonker, L. Ju, J. Junker, C. V. Kalaghatgi, V. Kalogera, B. Kamai, S. Kandhasamy, G. Kang, J. B. Kanner, S. J. Kapadia, S. Karki, K. S. Karvinen, M. Kasprzack, W. Kastaun, M. Katolik, E. Katsavounidis, W. Katzman, S. Kaufer, K. Kawabe, F. Kéfélian, D. Keitel, A. J. Kemball, R. Kennedy, C. Kent, J. S. Key, F. Y. Khalili, I. Khan, S. Khan, Z. Khan, E. A. Khazanov, N. Kijbunchoo, Chunglee Kim, J. C. Kim, K. Kim, W. Kim, W. S. Kim, Y.-M. Kim, S. J. Kimbrell, E. J. King, P. J. King, M. Kinley-Hanlon, R. Kirchhoff, J. S. Kissel, L. Kleybolte, S. Klimenko, T. D. Knowles, P. Koch, S. M. Koehlenbeck, S. Koley, V. Kondrashov, A. Kontos, M. Korobko, W. Z. Korth, I. Kowalska, D. B. Kozak, C. Krämer, V. Kringel, B. Krishnan, A. Królak, G. Kuehn, P. Kumar, R. Kumar, S. Kumar, L. Kuo, A. Kutynia, S. Kwang, B. D. Lackey, K. H. Lai, M. Landry, R. N. Lang, J. Lange, B. Lantz, R. K. Lanza, S. L. Larson, A. Lartaux-Vollard, P. D. Lasky, M. Laxen, A. Lazzarini, C. Lazzaro, P. Leaci, S. Leavey, C. H. Lee, H. K. Lee, H. M. Lee, H. W. Lee, K. Lee, J. Lehmann, A. Lenon, E. Leon, M. Leonardi, N. Leroy, N. Letendre, Y. Levin, T. G. F. Li, S. D. Linker, T. B. Littenberg, J. Liu, X. Liu, R. K. L. Lo, N. A. Lockerbie, L. T. London, J. E. Lord, M. Lorenzini, V. Loriette, M. Lormand, G. Losurdo, J. D. Lough, C. O. Lousto, G. Lovelace, H. Lück, D. Lumaca, A. P. Lundgren, R. Lynch, Y. Ma, R. Macas, S. Macfoy, B. Machenschalk, M. MacInnis, D. M. Macleod, I. Magaña Hernandez, F. Magaña Sandoval, L. Magaña Zertuche, R. M. Magee, E. Ma-

jorana, I. Maksimovic, N. Man, V. Mandic, V. Mangano, G. L. Mansell, M. Manske, M. Mantovani, F. Marchesoni, F. Marion, S. Márka, Z. Márka, C. Markakis, A. S. Markosyan, A. Markowitz, E. Maros, A. Marquina, P. Marsh, F. Martelli, L. Martellini, I. W. Martin, R. M. Martin, D. V. Martynov, J. N. Marx, K. Mason, E. Massera, A. Masserot, T. J. Massinger, M. Masso-Reid, S. Mastrogiovanni, A. Matas, F. Matichard, L. Matone, N. Mavalvala, N. Mazumder, R. McCarthy, D. E. McClelland, S. McCormick, L. McCuller, S. C. McGuire, G. McIntyre, J. McIver, D. J. McManus, L. McNeill, T. McRae, S. T. McWilliams, D. Meacher, G. D. Meadors, M. Mehmet, J. Meidam, E. Mejuto-Villa, A. Melatos, G. Mendell, R. A. Mercer, E. L. Merilh, M. Merzougui, S. Meshkov, C. Messenger, C. Messick, R. Metzdorff, P. M. Meyers, H. Miao, C. Michel, H. Middleton, E. E. Mikhailov, L. Milano, A. L. Miller, B. B. Miller, J. Miller, M. Millhouse, M. C. Milovich-Goff, O. Minazzoli, Y. Minenkov, J. Ming, C. Mishra, S. Mitra, V. P. Mitrofanov, G. Mitselmakher, R. Mittleman, D. Moffa, A. Moggi, K. Mogushi, M. Mohan, S. R. P. Mohapatra, I. Molina, M. Montani, C. J. Moore, D. Moraru, G. Moreno, S. Morisaki, S. R. Morriss, B. Mours, C. M. Mow-Lowry, G. Mueller, A. W. Muir, Arunava Mukherjee, D. Mukherjee, S. Mukherjee, N. Mukund, A. Mullavey, J. Munch, E. A. Muñiz, M. Muratore, P. G. Murray, A. Nagar, K. Napier, I. Nardecchia, L. Naticchioni, R. K. Nayak, J. Neilson, G. Nelemans, T. J. N. Nelson, M. Nery, A. Neunzert, L. Nevin, J. M. Newport, G. Newton, K. K. Y. Ng, P. Nguyen, T. T. Nguyen, D. Nichols, A. B. Nielsen, S. Nissanke, A. Nitz, A. Noack, F. Nocera, D. Nolting, C. North, L. K. Nuttall, J. Oberling, G. D. O'Dea, G. H. Ogin, J. J. Oh, S. H. Oh, F. Ohme, M. A. Okada, M. Oliver, P. Oppermann, Richard J. Oram, B. O'Reilly, R. Ormiston, L. F. Ortega, R. O'Shaughnessy, S. Ossokine, D. J. Ottaway, H. Overmier, B. J. Owen, A. E. Pace, J. Page, M. A. Page, A. Pai, S. A. Pai, J. R. Palamos, O. Palashov, C. Palomba, A. Pal-Singh, Howard Pan, Huang-Wei Pan, B. Pang, P. T. H. Pang, C. Pankow, F. Pannarale, B. C. Pant, F. Paoletti, A. Paoli, M. A. Papa, A. Parida, W. Parker, D. Pascucci, A. Pasqualetti, R. Passaquieti, D. Passuello, M. Patil, B. Patricelli, B. L. Pearlstone, M. Pedraza, R. Pedurand, L. Pekowsky, A. Pele, S. Penn, C. J. Perez, A. Perreca, L. M. Perri, H. P. Pfeiffer, M. Phelps, O. J. Piccinni, M. Pichot, F. Piergiovanni, V. Pierro, G. Pillant, L. Pinard, I. M. Pinto, M. Pirello, M. Pitkin, M. Poe, R. Poggiani, P. Popolizio, E. K. Porter, A. Post, J. Powell, J. Prasad, J. W. W. Pratt, G. Pratten, V. Predoi, T. Prestegard, M. Prijatelj, M. Principe, S. Privitera, R. Prix, G. A. Prodi, L. G. Prokhorov, O. Puncken, M. Punturo, P. Puppo, M. Pürrer, H. Qi, V. Quetschke, E. A. Quintero, R. Quitzow-James, F. J. Raab, D. S. Rabeling, H. Radkins, P. Raffai, S. Raja, C. Rajan, B. Rajbhandari, M. Rakhmanov, K. E. Ramirez, A. Ramos-Buades, P. Rapagnani, V. Raymond, M. Razzano, J. Read, T. Regimbau, L. Rei, S. Reid, D. H. Reitze, W. Ren, S. D. Reyes, F. Ricci, P. M. Ricker, S. Rieger, K. Riles, M. Rizzo, N. A. Robertson, R. Robie, F. Robinet, A. Rocchi, L. Rolland, J. G. Rollins, V. J. Roma, J. D. Romano, R. Romano, C. L. Romel, J. H. Romie, D. Rosińska, M. P. Ross, S. Rowan, A. Rüdiger, P. Ruggi, G. Rutins, K. Ryan, S. Sachdev, T. Sadecki, L. Sadeghian, M. Sakellariadou, L. Salconi, M. Saleem, F. Salemi, A. Samajdar, L. Sammut, L. M. Sampson, E. J. Sanchez, L. E. Sanchez, N. Sanchis-Gual, V. Sandberg, J. R. Sanders, B. Sassolas, B. S. Sathyaprakash, P. R. Saulson, O. Sauter, R. L. Savage, A. Sawadsky, P. Schale, M. Scheel, J. Scheuer, J. Schmidt, P. Schmidt, R. Schnabel, R. M. S. Schofield, A. Schön-

beck, E. Schreiber, D. Schuette, B. W. Schulte, B. F. Schutz, S. G. Schwalbe, J. Scott, S. M. Scott, E. Seidel, D. Sellers, A. S. Sengupta, D. Sentenac, V. Sequino, A. Sergeev, D. A. Shaddock, T. J. Shaffer, A. A. Shah, M. S. Shahriar, M. B. Shaner, L. Shao, B. Shapiro, P. Shawhan, A. Sheperd, D. H. Shoemaker, D. M. Shoemaker, K. Siellez, X. Siemens, M. Sieniawska, D. Sigg, A. D. Silva, L. P. Singer, A. Singh, A. Singhal, A. M. Sintes, B. J. J. Slagmolen, B. Smith, J. R. Smith, R. J. E. Smith, S. Somala, E. J. Son, J. A. Sonnenberg, B. Sorazu, F. Sorrentino, T. Souradeep, A. P. Spencer, A. K. Srivastava, K. Staats, A. Staley, M. Steinke, J. Steinlechner, S. Steinlechner, D. Steinmeyer, S. P. Stevenson, R. Stone, D. J. Stops, K. A. Strain, G. Stratta, S. E. Strigin, A. Strunk, R. Sturani, A. L. Stuver, T. Z. Summerscales, L. Sun, S. Sunil, J. Suresh, P. J. Sutton, B. L. Swinkels, M. J. Szczepańczyk, M. Tacca, S. C. Tait, C. Talbot, D. Talukder, D. B. Tanner, M. Tápai, A. Taracchini, J. D. Tasson, J. A. Taylor, R. Taylor, S. V. Tewari, T. Theeg, F. Thies, E. G. Thomas, M. Thomas, P. Thomas, K. A. Thorne, K. S. Thorne, E. Thrane, S. Tiwari, V. Tiwari, K. V. Tokmakov, K. Toland, M. Tonelli, Z. Tornasi, A. Torres-Forné, C. I. Torrie, D. Töyrä, F. Travasso, G. Traylor, J. Trinastic, M. C. Tringali, L. Trozzo, K. W. Tsang, M. Tse, R. Tso, L. Tsukada, D. Tsuna, D. Tuyenbayev, K. Ueno, D. Ugolini, C. S. Unnikrishnan, A. L. Urban, S. A. Usman, H. Vahlbruch, G. Vajente, G. Valdes, M. Vallisneri, N. van Bakel, M. van Beuzekom, J. F. J. van den Brand, C. Van Den Broeck, D. C. Vander-Hyde, L. van der Schaaf, J. V. van Heijningen, A. A. van Veggel, M. Vardaro, V. Varma, S. Vass, M. Vasúth, A. Vecchio, G. Vedovato, J. Veitch, P. J. Veitch, K. Venkateswara, G. Venugopalan, D. Verkindt, F. Vetrano, A. Viceré, A. D. Viets, S. Vinciguerra, D. J. Vine, J.-Y. Vinet, S. Vitale, T. Vo, H. Vocca, C. Vorvick, S. P. Vyatchanin, A. R. Wade, L. E. Wade, M. Wade, R. Walet, M. Walker, L. Wallace, S. Walsh, G. Wang, H. Wang, J. Z. Wang, W. H. Wang, Y. F. Wang, R. L. Ward, J. Warner, M. Was, J. Watchi, B. Weaver, L.-W. Wei, M. Weinert, A. J. Weinstein, R. Weiss, L. Wen, E. K. Wessel, P. Weßels, J. Westerweck, T. Westphal, K. Wette, J. T. Whelan, S. E. Whitcomb, B. F. Whiting, C. Whittle, D. Wilken, D. Williams, R. D. Williams, A. R. Williamson, J. L. Willis, B. Willke, M. H. Wimmer, W. Winkler, C. C. Wipf, H. Wittel, G. Woan, J. Woehler, J. Wofford, K. W. K. Wong, J. Worden, J. L. Wright, D. S. Wu, D. M. Wysocki, S. Xiao, H. Yamamoto, C. C. Yancey, L. Yang, M. J. Yap, M. Yazback, Hang Yu, Haocun Yu, M. Yvert, A. Zadrożny, M. Zanolin, T. Zelenova, J.-P. Zendri, M. Zevin, L. Zhang, M. Zhang, T. Zhang, Y.-H. Zhang, C. Zhao, M. Zhou, Z. Zhou, S. J. Zhu, X. J. Zhu, A. B. Zimmerman, M. E. Zucker, and J. Zweizig. Gw170817: Observation of gravitational waves from a binary neutron star inspiral. *Phys. Rev. Lett.*, 119:161101, Oct 2017. doi: 10.1103/PhysRevLett.119.161101. URL https://link.aps.org/doi/10.1103/PhysRevLett.119.161101.

[5] B. P. Abbott, R. Abbott, T. D. Abbott, F. Acernese, K. Ackley, C. Adams, T. Adams, P. Addesso, R. X. Adhikari, V. B. Adya, and et al. Gravitational waves and gamma-rays from a binary neutron star merger: Gw170817 and grb 170817a. *The Astrophysical Journal*, 848(2):L13, Oct 2017. ISSN 2041-8213. doi: 10.3847/2041-8213/aa920c. URL http://dx.doi.org/10.3847/2041-8213/aa920c.

[6] B. Abi, T. Albahri, S. Al-Kilani, D. Allspach, L. P. Alonzi, A. Anastasi, A. Anisenkov, F. Azfar, K. Badgley, S. Baeßler, I. Bailey, V. A. Baranov, E. Barlas-Yucel, T. Barrett, E. Barzi, A. Basti, F. Bedeschi,

A. Behnke, M. Berz, M. Bhattacharya, H. P. Binney, R. Bjorkquist, P. Bloom, J. Bono, E. Bottalico, T. Bowcock, D. Boyden, G. Cantatore, R. M. Carey, J. Carroll, B. C. K. Casey, D. Cauz, S. Ceravolo, R. Chakraborty, S. P. Chang, A. Chapelain, S. Chappa, S. Charity, R. Chislett, J. Choi, Z. Chu, T. E. Chupp, M. E. Convery, A. Conway, G. Corradi, S. Corrodi, L. Cotrozzi, J. D. Crnkovic, S. Dabagov, P. M. De Lurgio, P. T. Debevec, S. Di Falco, P. Di Meo, G. Di Sciascio, R. Di Stefano, B. Drendel, A. Driutti, V. N. Duginov, M. Eads, N. Eggert, A. Epps, J. Esquivel, M. Farooq, R. Fatemi, C. Ferrari, M. Fertl, A. Fiedler, A. T. Fienberg, A. Fioretti, D. Flay, S. B. Foster, H. Friedsam, E. Frlež, N. S. Froemming, J. Fry, C. Fu, C. Gabbanini, M. D. Galati, S. Ganguly, A. Garcia, D. E. Gastler, J. George, L. K. Gibbons, A. Gioiosa, K. L. Giovanetti, P. Girotti, W. Gohn, T. Gorringe, J. Grange, S. Grant, F. Gray, S. Haciomeroglu, D. Hahn, T. Halewood-Leagas, D. Hampai, F. Han, E. Hazen, J. Hempstead, S. Henry, A. T. Herrod, D. W. Hertzog, G. Hesketh, A. Hibbert, Z. Hodge, J. L. Holzbauer, K. W. Hong, R. Hong, M. Iacovacci, M. Incagli, C. Johnstone, J. A. Johnstone, P. Kammel, M. Kargiantoulakis, M. Karuza, J. Kaspar, D. Kawall, L. Kelton, A. Keshavarzi, D. Kessler, K. S. Khaw, Z. Khechadoorian, N. V. Khomutov, B. Kiburg, M. Kiburg, O. Kim, S. C. Kim, Y. I. Kim, B. King, N. Kinnaird, M. Korostelev, I. Kourbanis, E. Kraegeloh, V. A. Krylov, A. Kuchibhotla, N. A. Kuchinskiy, K. R. Labe, J. LaBounty, M. Lancaster, M. J. Lee, S. Lee, S. Leo, B. Li, D. Li, L. Li, I. Logashenko, A. Lorente Campos, A. Lucà, G. Lukicov, G. Luo, A. Lusiani, A. L. Lyon, B. MacCoy, R. Madrak, K. Makino, F. Marignetti, S. Mastroianni, S. Maxfield, M. McEvoy, W. Merritt, A. A. Mikhailichenko, J. P. Miller, S. Miozzi, J. P. Morgan, W. M. Morse, J. Mott, E. Motuk, A. Nath, D. Newton, H. Nguyen, M. Oberling, R. Osofsky, J.-F. Ostiguy, S. Park, G. Pauletta, G. M. Piacentino, R. N. Pilato, K. T. Pitts, B. Plaster, D. Počanić, N. Pohlman, C. C. Polly, M. Popovic, J. Price, B. Quinn, N. Raha, S. Ramachandran, E. Ramberg, N. T. Rider, J. L. Ritchie, B. L. Roberts, D. L. Rubin, L. Santi, D. Sathyan, H. Schellman, C. Schlesier, A. Schreckenberger, Y. K. Semertzidis, Y. M. Shatunov, D. Shemyakin, M. Shenk, D. Sim, M. W. Smith, A. Smith, A. K. Soha, M. Sorbara, D. Stöckinger, J. Stapleton, D. Still, C. Stoughton, D. Stratakis, C. Strohman, T. Stuttard, H. E. Swanson, G. Sweetmore, D. A. Sweigart, M. J. Syphers, D. A. Tarazona, T. Teubner, A. E. Tewsley-Booth, K. Thomson, V. Tishchenko, N. H. Tran, W. Turner, E. Valetov, D. Vasilkova, G. Venanzoni, V. P. Volnykh, T. Walton, M. Warren, A. Weisskopf, L. Welty-Rieger, M. Whitley, P. Winter, A. Wolski, M. Wormald, W. Wu, and C. Yoshikawa. Measurement of the positive muon anomalous magnetic moment to 0.46 ppm. *Phys. Rev. Lett.*, 126:141801, Apr 2021. doi: 10.1103/PhysRevLett.126.141801. URL https://link.aps.org/doi/10.1103/PhysRevLett.126.141801.

[7] Viviana Acquaviva, Amir Hajian, David N. Spergel, and Sudeep Das. Next Generation Redshift Surveys and the Origin of Cosmic Acceleration. *Phys. Rev. D*, 78:043514, 2008. doi: 10.1103/PhysRevD.78.043514.

[8] Prateek Agrawal, Georges Obied, and Cumrun Vafa. H_0 Tension, Swampland Conjectures and the Epoch of Fading Dark Matter. *arXiv e-prints*, art. arXiv:1906.08261, June 2019.

[9] Özgür Akarsu, John D. Barrow, Luis A. Escamilla, and J. Alberto Vazquez. Graduated dark energy: Observational hints of a spontaneous sign switch in the cosmological constant. *Phys. Rev.*, D101 (6):063528, 2020. doi: 10.1103/PhysRevD.101.063528.

[10] Shadab Alam, Metin Ata, Stephen Bailey, Florian Beutler, Dmitry Bizyaev, Jonathan A. Blazek, Adam S. Bolton, Joel R. Brownstein, Angela Burden, Chia-Hsun Chuang, et al. The clustering of galaxies in the completed SDSS-III Baryon Oscillation Spectroscopic Survey: cosmological analysis of the DR12 galaxy sample. *Monthly Notices of the Royal Astronomical Society*, 470(3):2617–2652, September 2017. doi: 10.1093/mnras/stx721.

[11] Shadab Alam et al. Completed SDSS-IV extended Baryon Oscillation Spectroscopic Survey: Cosmological implications from two decades of spectroscopic surveys at the Apache Point Observatory. *Phys. Rev. D*, 103(8):083533, 2021. doi: 10.1103/PhysRevD.103.083533.

[12] Andreas Albrecht and Paul J. Steinhardt. Cosmology for grand unified theories with radiatively induced symmetry breaking. *Phys. Rev. Lett.*, 48:1220–1223, Apr 1982. doi: 10.1103/PhysRevLett.48.1220. URL https://link.aps.org/doi/10.1103/PhysRevLett.48.1220.

[13] G. Alestas, L. Kazantzidis, and L. Perivolaropoulos. H_0 tension, phantom dark energy, and cosmological parameter degeneracies. *Phys. Rev. D*, 101(12):123516, 2020. doi: 10.1103/PhysRevD.101.123516.

[14] Yacine Ali-Haïmoud, Jens Chluba, and Marc Kamionkowski. Constraints on Dark Matter Interactions with Standard Model Particles from Cosmic Microwave Background Spectral Distortions. *Phys. Rev. Lett.*, 115(7):071304, 2015. doi: 10.1103/PhysRevLett.115.071304.

[15] Yacine Ali-Haïmoud. Testing dark matter interactions with cmb spectral distortions. *Physical Review D*, 103(4), Feb 2021. ISSN 2470-0029. doi: 10.1103/physrevd.103.043541. URL http://dx.doi.org/10.1103/PhysRevD.103.043541.

[16] Yacine Ali-Haïmoud and Christopher M. Hirata. Hyrec: A fast and highly accurate primordial hydrogen and helium recombination code. *Physical Review D*, 83(4), Feb 2011. ISSN 1550-2368. doi: 10.1103/physrevd.83.043513. URL http://dx.doi.org/10.1103/PhysRevD.83.043513.

[17] James Alvey, Nashwan Sabti, Miguel Escudero, and Malcolm Fairbairn. Improved bbn constraints on the variation of the gravitational constant. *The European Physical Journal C*, 80(2), Feb 2020. ISSN 1434-6052. doi: 10.1140/epjc/s10052-020-7727-y. URL http://dx.doi.org/10.1140/epjc/s10052-020-7727-y.

[18] Luca Amendola, Radouane Gannouji, David Polarski, and Shinji Tsujikawa. Conditions for the cosmological viability of $f(R)$ Dark Energy models. *Physical Review D*, 75(8), Apr 2007. ISSN

1550-2368. doi: 10.1103/physrevd.75.083504. URL http://dx.doi.org/10.1103/PhysRevD.75.083504.

[19] Luca Amendola, Stephen Appleby, David Bacon, Tessa Baker, Marco Baldi, Nicola Bartolo, Alain Blanchard, Camille Bonvin, Stefano Borgani, and et al. Cosmology and fundamental physics with the euclid satellite. *Living Reviews in Relativity*, 16(1), Sep 2013. ISSN 1433-8351. doi: 10.12942/lrr-2013-6. URL http://dx.doi.org/10.12942/lrr-2013-6.

[20] Luca Amendola et al. Cosmology and fundamental physics with the Euclid satellite. *Living Rev. Rel.*, 16:6, 2013. doi: 10.12942/lrr-2013-6.

[21] Luis A. Anchordoqui, Ignatios Antoniadis, Dieter Lüst, Jorge F. Soriano, and Tomasz R. Taylor. H_0 tension and the String Swampland. *Phys. Rev. D*, 101:083532, 2020. doi: 10.1103/PhysRevD.101.083532.

[22] Nima Arkani-Hamed, Savas Dimopoulos, and G. R. Dvali. The Hierarchy problem and new dimensions at a millimeter. *Phys. Lett. B*, 429:263–272, 1998. doi: 10.1016/S0370-2693(98)00466-3.

[23] Éric Aubourg, Stephen Bailey, Julian E. Bautista, Florian Beutler, Vaishali Bhardwaj, Dmitry Bizyaev, Michael Blanton, Michael Blomqvist, Adam S. Bolton, Jo Bovy, and et al. Cosmological implications of Baryon Acoustic Oscillation measurements. *Physical Review D*, 92(12), Dec 2015. ISSN 1550-2368. doi: 10.1103/physrevd.92.123516. URL http://dx.doi.org/10.1103/PhysRevD.92.123516.

[24] Kevin Aylor, Mackenzie Joy, Lloyd Knox, Marius Millea, Srinivasan Raghunathan, and W. L. Kimmy Wu. Sounds discordant: Classical distance ladder and ΛCDM-based determinations of the cosmological sound horizon. *The Astrophysical Journal*, 874(1):4, Mar 2019. ISSN 1538-4357. doi: 10.3847/1538-4357/ab0898. URL http://dx.doi.org/10.3847/1538-4357/ab0898.

[25] Alberto Bailoni, Alessio Spurio Mancini, and Luca Amendola. Improving Fisher matrix forecasts for galaxy surveys: window function, bin cross-correlation, and bin redshift uncertainty. *Mon. Not. Roy. Astron. Soc.*, 470(1):688–705, 2017. doi: 10.1093/mnras/stx1209.

[26] T. Baker, E. Bellini, P. G. Ferreira, M. Lagos, J. Noller, and I. Sawicki. Strong constraints on cosmological gravity from gw170817 and grb 170817a. *Physical Review Letters*, 119(25), Dec 2017. ISSN 1079-7114. doi: 10.1103/physrevlett.119.251301. URL http://dx.doi.org/10.1103/PhysRevLett.119.251301.

[27] Mario Ballardini, Matteo Braglia, Fabio Finelli, Daniela Paoletti, Alexei A. Starobinsky, and Caterina Umiltà. Scalar-tensor theories of gravity, neutrino physics, and the H_0 tension. *Journal of Cosmology and Astroparticle Physics*, 2020(10):044–044, Oct 2020. ISSN 1475-7516. doi: 10.1088/1475-7516/2020/10/044. URL http://dx.doi.org/10.1088/1475-7516/2020/10/044.

[28] Guillermo Ballesteros, Alessio Notari, and Fabrizio Rompineve. The H_0 tension: ΔG_N vs. $\Delta N_{\rm eff}$. *Journal of Cosmology and Astroparticle Physics*, 2020(11):024–024, Nov 2020. ISSN 1475-7516. doi: 10.1088/1475-7516/2020/11/024. URL http://dx.doi.org/10.1088/1475-7516/2020/11/024.

[29] Kazuharu Bamba, Antonio Lopez-Revelles, R. Myrzakulov, S. D. Odintsov, and L. Sebastiani. Cosmic history of viable exponential gravity: Equation of state oscillations and growth index from inflation to dark energy era. *Class. Quant. Grav.*, 30:015008, 2013. doi: 10.1088/0264-9381/30/1/015008.

[30] Aritra Banerjee, Haiying Cai, Lavinia Heisenberg, Eoin Ó Colgáin, M. M. Sheikh-Jabbari, and Tao Yang. Hubble Sinks In The Low-Redshift Swampland. *arXiv e-prints*, art. arXiv:2006.00244, May 2020.

[31] J. M. Bardeen, J. R. Bond, N. Kaiser, and A. S. Szalay. The Statistics of Peaks of Gaussian Random Fields. *Astrophys. Journ.*, 304:15, May 1986. doi: 10.1086/164143.

[32] W. E. V. Barker, A. N. Lasenby, M. P. Hobson, and W. J. Handley. Systematic study of background cosmology in unitary Poincaré gauge theories with application to emergent dark radiation and H_0 tension. *Phys. Rev.*, D102(2):024048, 2020. doi: 10.1103/PhysRevD.102.024048.

[33] Spyros Basilakos and Joan Solà. Growth index of matter perturbations in running vacuum models. *Phys. Rev. D*, 92(12):123501, 2015. doi: 10.1103/PhysRevD.92.123501.

[34] Richard A. Battye, Boris Bolliet, and Francesco Pace. Do cosmological data rule out f(r) with w≠−1 ? *Physical Review D*, 97(10), May 2018. ISSN 2470-0029. doi: 10.1103/physrevd.97.104070. URL http://dx.doi.org/10.1103/PhysRevD.97.104070.

[35] Daniel Baumann. TASI lectures on primordial cosmology, 2018.

[36] Rachel Bean and Matipon Tangmatitham. Current constraints on the cosmic growth history. *Phys. Rev. D*, 81:083534, 2010. doi: 10.1103/PhysRevD.81.083534.

[37] Emilio Bellini and Ignacy Sawicki. Maximal freedom at minimum cost: linear large-scale structure in general modifications of gravity. *Journal of Cosmology and Astroparticle Physics*, 2014(07):050–050, Jul 2014. ISSN 1475-7516. doi: 10.1088/1475-7516/2014/07/050. URL http://dx.doi.org/10.1088/1475-7516/2014/07/050.

[38] H.B. Benaoum, Weiqiang Yang, Supriya Pan, and Eleonora Di Valentino. Modified Emergent Dark Energy and its Astronomical Constraints. *arXiv e-prints*, 8 2020.

[39] Giampaolo Benevento, Wayne Hu, and Marco Raveri. Can late dark energy transitions raise the Hubble constant? *Physical Review D*, 101(10):103517, May 2020. doi: 10.1103/PhysRevD.101.103517.

[40] Jose Luis Bernal, Licia Verde, and Adam G. Riess. The trouble with H_0. *JCAP*, 10:019, 2016. doi: 10.1088/1475-7516/2016/10/019.

[41] F. Bernardeau, S. Colombi, E. Gaztañaga, and R. Scoccimarro. Large-scale structure of the universe and cosmological perturbation theory. *Physics Reports*, 367(1-3):1–248, Sep 2002. ISSN 0370-1573. doi: 10.1016/s0370-1573(02)00135-7. URL http://dx.doi.org/10.1016/S0370-1573(02)00135-7.

[42] Edmund Bertschinger. Cosmological dynamics, 1995.

[43] Diego Blas, Julien Lesgourgues, and Thomas Tram. The cosmic linear anisotropy solving system (class). part ii: Approximation schemes. *Journal of Cosmology and Astroparticle Physics*, 2011(07): 034–034, Jul 2011. ISSN 1475-7516. doi: 10.1088/1475-7516/2011/07/034. URL http://dx.doi.org/10.1088/1475-7516/2011/07/034.

[44] B. Boisseau, G. Esposito-Farèse, D. Polarski, and A. A. Starobinsky. Reconstruction of a scalar-tensor theory of gravity in an accelerating universe. *Physical Review Letters*, 85(11):2236–2239, Sep 2000. ISSN 1079-7114. doi: 10.1103/physrevlett.85.2236. URL http://dx.doi.org/10.1103/PhysRevLett.85.2236.

[45] B. Boisseau, H. Giacomini, D. Polarski, and A.A. Starobinsky. Bouncing Universes in Scalar-Tensor Gravity Models admitting Negative Potentials. *JCAP*, 07:002, 2015. doi: 10.1088/1475-7516/2015/07/002.

[46] B. Boisseau, H. Giacomini, D. Polarski, and A.A. Starobinsky. Bouncing universes in scalar-tensor gravity models admitting negative potentials. *Journal of Cosmology and Astroparticle Physics*, 2015 (07):002–002, Jul 2015. ISSN 1475-7516. doi: 10.1088/1475-7516/2015/07/002. URL http://dx.doi.org/10.1088/1475-7516/2015/07/002.

[47] Robert Brandenberger and Patrick Peter. Bouncing cosmologies: Progress and problems. *Foundations of Physics*, 47(6):797–850, Feb 2017. ISSN 1572-9516. doi: 10.1007/s10701-016-0057-0. URL http://dx.doi.org/10.1007/s10701-016-0057-0.

[48] Philippe Brax. Screening mechanisms in modified gravity. *Classical and Quantum Gravity*, 30(21): 214005, oct 2013. doi: 10.1088/0264-9381/30/21/214005. URL https://doi.org/10.1088/0264-9381/30/21/214005.

[49] Philippe Brax, Carsten van de Bruck, Anne-Christine Davis, and Douglas J. Shaw. $f(r)$ gravity and chameleon theories. *Phys. Rev. D*, 78:104021, Nov 2008. doi: 10.1103/PhysRevD.78.104021. URL https://link.aps.org/doi/10.1103/PhysRevD.78.104021.

[50] Vedran Brdar, Alexander J. Helmboldt, and Jisuke Kubo. Gravitational waves from first-order phase transitions: Ligo as a window to unexplored seesaw scales. *Journal of Cosmology and Astroparticle Physics*, 2019(02):021–021, Feb 2019. ISSN 1475-7516. doi: 10.1088/1475-7516/2019/02/021. URL http://dx.doi.org/10.1088/1475-7516/2019/02/021.

[51] J. Buchner, A. Georgakakis, K. Nandra, L. Hsu, C. Rangel, M. Brightman, A. Merloni, M. Salvato, J. Donley, and D. Kocevski. X-ray spectral modelling of the AGN obscuring region in the CDFS: Bayesian model selection and catalogue. *AAP*, 564:A125, April 2014. doi: 10.1051/0004-6361/201322971.

[52] Alicia Bueno belloso, Juan Garcia-Bellido, and Domenico Sapone. A parametrization of the growth index of matter perturbations in various Dark Energy models and observational prospects using a Euclid-like survey. *JCAP*, 10:010, 2011. doi: 10.1088/1475-7516/2011/10/010.

[53] Philip Bull, Yashar Akrami, Julian Adamek, Tessa Baker, Emilio Bellini, Jose Beltrán Jiménez, Eloisa Bentivegna, Stefano Camera, Sébastien Clesse, Jonathan H. Davis, and et al. Beyond ΛCDM: Problems, solutions, and the road ahead. *Physics of the Dark Universe*, 12:56–99, Jun 2016. ISSN 2212-6864. doi: 10.1016/j.dark.2016.02.001. URL http://dx.doi.org/10.1016/j.dark.2016.02.001.

[54] James S. Bullock and Michael Boylan-Kolchin. Small-Scale Challenges to the ΛCDM Paradigm. *Ann. Rev. Astron. Astrophys.*, 55:343–387, 2017. doi: 10.1146/annurev-astro-091916-055313.

[55] R. Calderon, D. Felbacq, R. Gannouji, D. Polarski, and A. A. Starobinsky. Global properties of the growth index of matter inhomogeneities in the universe. *Physical Review D*, 100(8), Oct 2019. ISSN 2470-0029. doi: 10.1103/physrevd.100.083503. URL http://dx.doi.org/10.1103/PhysRevD.100.083503.

[56] R. Calderon, D. Felbacq, R. Gannouji, D. Polarski, and A. A. Starobinsky. Global properties of the growth index: Mathematical aspects and physical relevance. *Phys. Rev. D*, 101:103501, May 2020. doi: 10.1103/PhysRevD.101.103501. URL https://link.aps.org/doi/10.1103/PhysRevD.101.103501.

[57] Rodrigo Calderón, Radouane Gannouji, Benjamin L'Huillier, and David Polarski. A negative cosmological constant in the dark sector? *Physical Review D*, 8 2020.

[58] Robert R. Caldwell, Tristan L. Smith, and Devin G.E. Walker. Using a Primordial Gravitational Wave Background to Illuminate New Physics. *Phys. Rev. D*, 100(4):043513, 2019. doi: 10.1103/PhysRevD.100.043513.

[59] Rolando Cardenas, Tame Gonzalez, Yoelsy Leiva, Osmel Martin, and Israel Quiros. A model of the universe including dark energy accounted for by both a quintessence field and a (negative) cosmological constant. *Phys. Rev.*, D67:083501, 2003. doi: 10.1103/PhysRevD.67.083501.

[60] Solène Chabanier, Marius Millea, and Nathalie Palanque-Delabrouille. Matter power spectrum: from ly α forest to cmb scales. *Monthly Notices of the Royal Astronomical Society*, 489(2):2247–2253, Aug 2019. ISSN 1365-2966. doi: 10.1093/mnras/stz2310. URL http://dx.doi.org/10.1093/mnras/stz2310.

[61] Serguei Chatrchyan et al. Observation of a New Boson at a Mass of 125 GeV with the CMS Experiment at the LHC. *Phys. Lett.*, B716:30–61, 2012. doi: 10.1016/j.physletb.2012.08.021.

[62] MICHEL CHEVALLIER and DAVID POLARSKI. Accelerating universes with scaling dark matter. *International Journal of Modern Physics D*, 10(02):213–223, Apr 2001. ISSN 1793-6594. doi: 10.1142/s0218271801000822. URL http://dx.doi.org/10.1142/S0218271801000822.

[63] Michel Chevallier and David Polarski. Accelerating universes with scaling dark matter. *Int. J. Mod. Phys. D*, 10:213–224, 2001. doi: 10.1142/S0218271801000822.

[64] Steve K. Choi, Matthew Hasselfield, Shuay-Pwu Patty Ho, Brian Koopman, Marius Lungu, Maximilian H. Abitbol, Graeme E. Addison, Peter A. R. Ade, Simone Aiola, David Alonso, and et al. The atacama cosmology telescope: a measurement of the cosmic microwave background power spectra at 98 and 150 ghz. *Journal of Cosmology and Astroparticle Physics*, 2020(12):045–045, Dec 2020. ISSN 1475-7516. doi: 10.1088/1475-7516/2020/12/045. URL http://dx.doi.org/10.1088/1475-7516/2020/12/045.

[65] Debika Chowdhury, Jerome Martin, Christophe Ringeval, and Vincent Vennin. Inflation after Planck: Judgment Day. *Phys. Rev.*, D100(8):083537, 2019. doi: 10.1103/PhysRevD.100.083537.

[66] Timothy Clifton, Pedro G. Ferreira, Antonio Padilla, and Constantinos Skordis. Modified gravity and cosmology. *Physics Reports*, 513(1-3):1–189, Mar 2012. ISSN 0370-1573. doi: 10.1016/j.physrep.2012.01.001. URL http://dx.doi.org/10.1016/j.physrep.2012.01.001.

[67] DES Collaboration, T. M. C. Abbott, M. Aguena, A. Alarcon, S. Allam, O. Alves, A. Amon, F. Andrade-Oliveira, J. Annis, S. Avila, D. Bacon, E. Baxter, K. Bechtol, M. R. Becker, G. M. Bernstein, S. Bhargava, S. Birrer, J. Blazek, A. Brandao-Souza, S. L. Bridle, D. Brooks, E. Buckley-Geer, D. L. Burke, H. Camacho, A. Campos, A. Carnero Rosell, M. Carrasco Kind, J. Carretero, F. J. Castander, R. Cawthon, C. Chang, A. Chen, R. Chen, A. Choi, C. Conselice, J. Cordero, M. Costanzi, M. Crocce, L. N. da Costa, M. E. da Silva Pereira, C. Davis, T. M. Davis, J. De Vicente, J. DeRose, S. Desai, E. Di Valentino, H. T. Diehl, J. P. Dietrich, S. Dodelson, P. Doel, C. Doux, A. Drlica-Wagner, K. Eckert, T. F. Eifler, F. Elsner, J. Elvin-Poole, S. Everett, A. E. Evrard, X. Fang, A. Farahi,

E. Fernandez, I. Ferrero, A. Ferté, P. Fosalba, O. Friedrich, J. Frieman, J. García-Bellido, M. Gatti, E. Gaztanaga, D. W. Gerdes, T. Giannantonio, G. Giannini, D. Gruen, R. A. Gruendl, J. Gschwend, G. Gutierrez, I. Harrison, W. G. Hartley, K. Herner, S. R. Hinton, D. L. Hollowood, K. Honscheid, B. Hoyle, E. M. Huff, D. Huterer, B. Jain, D. J. James, M. Jarvis, N. Jeffrey, T. Jeltema, A. Kovacs, E. Krause, R. Kron, K. Kuehn, N. Kuropatkin, O. Lahav, P. F. Leget, P. Lemos, A. R. Liddle, C. Lidman, M. Lima, H. Lin, N. MacCrann, M. A. G. Maia, J. L. Marshall, P. Martini, J. McCullough, P. Melchior, J. Mena-Fernández, F. Menanteau, R. Miquel, J. J. Mohr, R. Morgan, J. Muir, J. Myles, S. Nadathur, A. Navarro-Alsina, R. C. Nichol, R. L. C. Ogando, Y. Omori, A. Palmese, S. Pandey, Y. Park, F. Paz-Chinchón, D. Petravick, A. Pieres, A. A. Plazas Malagón, A. Porredon, J. Prat, M. Raveri, M. Rodriguez-Monroy, R. P. Rollins, A. K. Romer, A. Roodman, R. Rosenfeld, A. J. Ross, E. S. Rykoff, S. Samuroff, C. Sánchez, E. Sanchez, J. Sanchez, D. Sanchez Cid, V. Scarpine, M. Schubnell, D. Scolnic, L. F. Secco, S. Serrano, I. Sevilla-Noarbe, E. Sheldon, T. Shin, M. Smith, M. Soares-Santos, E. Suchyta, M. E. C. Swanson, M. Tabbutt, G. Tarle, D. Thomas, C. To, A. Troja, M. A. Troxel, D. L. Tucker, I. Tutusaus, T. N. Varga, A. R. Walker, N. Weaverdyck, J. Weller, B. Yanny, B. Yin, Y. Zhang, and J. Zuntz. Dark energy survey year 3 results: Cosmological constraints from galaxy clustering and weak lensing, 2021.

[68] LHCb collaboration, R. Aaij, C. Abellán Beteta, T. Ackernley, B. Adeva, M. Adinolfi, H. Afsharnia, C. A. Aidala, S. Aiola, Z. Ajaltouni, S. Akar, J. Albrecht, F. Alessio, M. Alexander, A. Alfonso Albero, Z. Aliouche, G. Alkhazov, P. Alvarez Cartelle, S. Amato, Y. Amhis, L. An, L. Anderlini, A. Andreianov, M. Andreotti, F. Archilli, A. Artamonov, M. Artuso, K. Arzymatov, E. Aslanides, M. Atzeni, B. Audurier, S. Bachmann, M. Bachmayer, J. J. Back, P. Baladron Rodriguez, V. Balagura, W. Baldini, J. Baptista Leite, R. J. Barlow, S. Barsuk, W. Barter, M. Bartolini, F. Baryshnikov, J. M. Basels, G. Bassi, B. Batsukh, A. Battig, A. Bay, M. Becker, F. Bedeschi, I. Bediaga, A. Beiter, V. Belavin, S. Belin, V. Bellee, K. Belous, I. Belov, I. Belyaev, G. Bencivenni, E. Ben-Haim, A. Berezhnoy, R. Bernet, D. Berninghoff, H. C. Bernstein, C. Bertella, A. Bertolin, C. Betancourt, F. Betti, Ia. Bezshyiko, S. Bhasin, J. Bhom, L. Bian, M. S. Bieker, S. Bifani, P. Billoir, M. Birch, F. C. R. Bishop, A. Bitadze, A. Bizzeti, M. Bjørn, M. P. Blago, T. Blake, F. Blanc, S. Blusk, D. Bobulska, J. A. Boelhauve, O. Boente Garcia, T. Boettcher, A. Boldyrev, A. Bondar, N. Bondar, S. Borghi, M. Borisyak, M. Borsato, J. T. Borsuk, S. A. Bouchiba, T. J. V. Bowcock, A. Boyer, C. Bozzi, M. J. Bradley, S. Braun, A. Brea Rodriguez, M. Brodski, J. Brodzicka, A. Brossa Gonzalo, D. Brundu, A. Buonaura, C. Burr, A. Bursche, A. Butkevich, J. S. Butter, J. Buytaert, W. Byczynski, S. Cadeddu, H. Cai, R. Calabrese, L. Calefice, L. Calero Diaz, S. Cali, R. Calladine, M. Calvi, M. Calvo Gomez, P. Camargo Magalhaes, A. Camboni, P. Campana, A. F. Campoverde Quezada, S. Capelli, L. Capriotti, A. Carbone, G. Carboni, R. Cardinale, A. Cardini, I. Carli, P. Carniti, L. Carus, K. Carvalho Akiba, A. Casais Vidal, G. Casse, M. Cattaneo, G. Cavallero, S. Celani, J. Cerasoli, A. J. Chadwick, M. G. Chapman, M. Charles, Ph. Charpentier, G. Chatzikonstantinidis, C. A. Chavez Barajas, M. Chefdeville, C. Chen, S. Chen, A. Chernov, V. Chobanova, S. Cholak, M. Chrzaszcz, A. Chubykin, V. Chu-

likov, P. Ciambrone, M. F. Cicala, X. Cid Vidal, G. Ciezarek, P. E. L. Clarke, M. Clemencic, H. V. Cliff, J. Closier, J. L. Cobbledick, V. Coco, J. A. B. Coelho, J. Cogan, E. Cogneras, L. Cojocariu, P. Collins, T. Colombo, L. Congedo, A. Contu, N. Cooke, G. Coombs, G. Corti, C. M. Costa Sobral, B. Couturier, D. C. Craik, J. Crkovská, M. Cruz Torres, R. Currie, C. L. Da Silva, E. Dall'Occo, J. Dalseno, C. D'Ambrosio, A. Danilina, P. d'Argent, A. Davis, O. De Aguiar Francisco, K. De Bruyn, S. De Capua, M. De Cian, J. M. De Miranda, L. De Paula, M. De Serio, D. De Simone, P. De Simone, J. A. de Vries, C. T. Dean, D. Decamp, L. Del Buono, B. Delaney, H. P. Dembinski, A. Dendek, V. Denysenko, D. Derkach, O. Deschamps, F. Desse, F. Dettori, B. Dey, P. Di Nezza, S. Didenko, L. Dieste Maronas, H. Dijkstra, V. Dobishuk, A. M. Donohoe, F. Dordei, A. C. dos Reis, L. Douglas, A. Dovbnya, A. G. Downes, K. Dreimanis, M. W. Dudek, L. Dufour, V. Duk, P. Durante, J. M. Durham, D. Dutta, A. Dziurda, A. Dzyuba, S. Easo, U. Egede, V. Egorychev, S. Eidelman, S. Eisenhardt, S. Ek-In, L. Eklund, S. Ely, A. Ene, E. Epple, S. Escher, J. Eschle, S. Esen, T. Evans, A. Falabella, J. Fan, Y. Fan, B. Fang, S. Farry, D. Fazzini, M. Féo, A. Fernandez Prieto, J. M. Fernandez tenllado Arribas, A. D. Fernez, F. Ferrari, L. Ferreira Lopes, F. Ferreira Rodrigues, S. Ferreres Sole, M. Ferrillo, M. Ferro-Luzzi, S. Filippov, R. A. Fini, M. Fiorini, M. Firlej, K. M. Fischer, D. Fitzgerald, C. Fitzpatrick, T. Fiutowski, F. Fleuret, M. Fontana, F. Fontanelli, R. Forty, V. Franco Lima, M. Franco Sevilla, M. Frank, E. Franzoso, G. Frau, C. Frei, D. A. Friday, J. Fu, Q. Fuehring, W. Funk, E. Gabriel, T. Gaintseva, A. Gallas Torreira, D. Galli, S. Gambetta, Y. Gan, M. Gandelman, P. Gandini, Y. Gao, M. Garau, L. M. Garcia Martin, P. Garcia Moreno, J. García Pardiñas, B. Garcia Plana, F. A. Garcia Rosales, L. Garrido, C. Gaspar, R. E. Geertsema, D. Gerick, L. L. Gerken, E. Gersabeck, M. Gersabeck, T. Gershon, D. Gerstel, Ph. Ghez, V. Gibson, H. K. Giemza, M. Giovannetti, A. Gioventù, P. Gironella Gironell, L. Giubega, C. Giugliano, K. Gizdov, E. L. Gkougkousis, V. V. Gligorov, C. Göbel, E. Golobardes, D. Golubkov, A. Golutvin, A. Gomes, S. Gomez Fernandez, F. Goncalves Abrantes, M. Goncerz, G. Gong, P. Gorbounov, I. V. Gorelov, C. Gotti, E. Govorkova, J. P. Grabowski, T. Grammatico, L. A. Granado Cardoso, E. Graugés, E. Graverini, G. Graziani, A. Grecu, L. M. Greeven, P. Griffith, L. Grillo, S. Gromov, B. R. Gruberg Cazon, C. Gu, M. Guarise, P. A. Günther, E. Gushchin, A. Guth, Y. Guz, T. Gys, T. Hadavizadeh, G. Haefeli, C. Haen, J. Haimberger, T. Halewood-leagas, P. M. Hamilton, J. P. Hammerich, Q. Han, X. Han, T. H. Hancock, S. Hansmann-Menzemer, N. Harnew, T. Harrison, C. Hasse, M. Hatch, J. He, M. Hecker, K. Heijhoff, K. Heinicke, A. M. Hennequin, K. Hennessy, L. Henry, J. Heuel, A. Hicheur, D. Hill, M. Hilton, S. E. Hollitt, J. Hu, J. Hu, W. Hu, W. Huang, X. Huang, W. Hulsbergen, R. J. Hunter, M. Hushchyn, D. Hutchcroft, D. Hynds, P. Ibis, M. Idzik, D. Ilin, P. Ilten, A. Inglessi, A. Ishteev, K. Ivshin, R. Jacobsson, S. Jakobsen, E. Jans, B. K. Jashal, A. Jawahery, V. Jevtic, M. Jezabek, F. Jiang, M. John, D. Johnson, C. R. Jones, T. P. Jones, B. Jost, N. Jurik, S. Kandybei, Y. Kang, M. Karacson, M. Karpov, F. Keizer, M. Kenzie, T. Ketel, B. Khanji, A. Kharisova, S. Kholodenko, T. Kirn, V. S. Kirsebom, O. Kitouni, S. Klaver, K. Klimaszewski, S. Koliiev, A. Kondybayeva, A. Konoplyannikov, P. Kopciewicz, R. Kopecna, P. Koppenburg, M. Korolev, I. Kostiuk, O. Kot, S. Kotriakhova, P. Kravchenko, L. Kravchuk, R. D. Krawczyk, M. Kreps, F. Kress, S. Kretzschmar,

P. Krokovny, W. Krupa, W. Krzemien, W. Kucewicz, M. Kucharczyk, V. Kudryavtsev, H. S. Kuindersma, G. J. Kunde, T. Kvaratskheliya, D. Lacarrere, G. Lafferty, A. Lai, A. Lampis, D. Lancierini, J. J. Lane, R. Lane, G. Lanfranchi, C. Langenbruch, J. Langer, O. Lantwin, T. Latham, F. Lazzari, R. Le Gac, S. H. Lee, R. Lefèvre, A. Leflat, S. Legotin, O. Leroy, T. Lesiak, B. Leverington, H. Li, L. Li, P. Li, S. Li, Y. Li, Y. Li, Z. Li, X. Liang, T. Lin, R. Lindner, V. Lisovskyi, R. Litvinov, G. Liu, H. Liu, S. Liu, X. Liu, A. Loi, J. Lomba Castro, I. Longstaff, J. H. Lopes, G. H. Lovell, Y. Lu, D. Lucchesi, S. Luchuk, M. Lucio Martinez, V. Lukashenko, Y. Luo, A. Lupato, E. Luppi, O. Lupton, A. Lusiani, X. Lyu, L. Ma, R. Ma, S. Maccolini, F. Machefert, F. Maciuc, V. Macko, P. Mackowiak, S. Maddrell-Mander, O. Madejczyk, L. R. Madhan Mohan, O. Maev, A. Maevskiy, D. Maisuzenko, M. W. Majewski, J. J. Malczewski, S. Malde, B. Malecki, A. Malinin, T. Maltsev, H. Malygina, G. Manca, G. Mancinelli, D. Manuzzi, D. Marangotto, J. Maratas, J. F. Marchand, U. Marconi, S. Mariani, C. Marin Benito, M. Marinangeli, J. Marks, A. M. Marshall, P. J. Marshall, G. Martellotti, L. Martinazzoli, M. Martinelli, D. Martinez Santos, F. Martinez Vidal, A. Massafferri, M. Materok, R. Matev, A. Mathad, Z. Mathe, V. Matiunin, C. Matteuzzi, K. R. Mattioli, A. Mauri, E. Maurice, J. Mauricio, M. Mazurek, M. McCann, L. Mcconnell, T. H. Mcgrath, A. McNab, R. McNulty, J. V. Mead, B. Meadows, C. Meaux, G. Meier, N. Meinert, D. Melnychuk, S. Meloni, M. Merk, A. Merli, L. Meyer Garcia, M. Mikhasenko, D. A. Milanes, E. Millard, M. Milovanovic, M. N. Minard, A. Minotti, L. Minzoni, S. E. Mitchell, B. Mitreska, D. S. Mitzel, A. Mödden, R. A. Mohammed, R. D. Moise, T. Mombächer, I. A. Monroy, S. Monteil, M. Morandin, G. Morello, M. J. Morello, J. Moron, A. B. Morris, A. G. Morris, R. Mountain, H. Mu, F. Muheim, M. Mulder, D. Müller, K. Müller, C. H. Murphy, D. Murray, P. Muzzetto, P. Naik, T. Nakada, R. Nandakumar, T. Nanut, I. Nasteva, M. Needham, I. Neri, N. Neri, S. Neubert, N. Neufeld, R. Newcombe, T. D. Nguyen, C. Nguyen-Mau, E. M. Niel, S. Nieswand, N. Nikitin, N. S. Nolte, C. Nunez, A. Oblakowska-Mucha, V. Obraztsov, D. P. O'Hanlon, R. Oldeman, M. E. Olivares, C. J. G. Onderwater, A. Ossowska, J. M. Otalora Goicochea, T. Ovsiannikova, P. Owen, A. Oyanguren, B. Pagare, P. R. Pais, T. Pajero, A. Palano, M. Palutan, Y. Pan, G. Panshin, A. Papanestis, M. Pappagallo, L. L. Pappalardo, C. Pappenheimer, W. Parker, C. Parkes, C. J. Parkinson, B. Passalacqua, G. Passaleva, A. Pastore, M. Patel, C. Patrignani, C. J. Pawley, A. Pearce, A. Pellegrino, M. Pepe Altarelli, S. Perazzini, D. Pereima, P. Perret, M. Petric, K. Petridis, A. Petrolini, A. Petrov, S. Petrucci, M. Petruzzo, T. T. H. Pham, A. Philippov, L. Pica, M. Piccini, B. Pietrzyk, G. Pietrzyk, M. Pili, D. Pinci, F. Pisani, Resmi P. K, V. Placinta, J. Plews, M. Plo Casasus, F. Polci, M. Poli Lener, M. Poliakova, A. Poluektov, N. Polukhina, I. Polyakov, E. Polycarpo, G. J. Pomery, S. Ponce, D. Popov, S. Popov, S. Poslavskii, K. Prasanth, L. Promberger, C. Prouve, V. Pugatch, H. Pullen, G. Punzi, W. Qian, J. Qin, R. Quagliani, B. Quintana, N. V. Raab, R. I. Rabadan Trejo, B. Rachwal, J. H. Rademacker, M. Rama, M. Ramos Pernas, M. S. Rangel, F. Ratnikov, G. Raven, M. Reboud, F. Redi, F. Reiss, C. Remon Alepuz, Z. Ren, V. Renaudin, R. Ribatti, S. Ricciardi, K. Rinnert, P. Robbe, G. Robertson, A. B. Rodrigues, E. Rodrigues, J. A. Rodriguez Lopez, A. Rollings, P. Roloff, V. Romanovskiy, M. Romero Lamas, A. Romero Vidal, J. D. Roth, M. Rotondo, M. S. Rudolph, T. Ruf, J. Ruiz Vidal, A. Ryzhikov, J. Ryzka, J. J. Sa-

borido Silva, N. Sagidova, N. Sahoo, B. Saitta, M. Salomoni, D. Sanchez Gonzalo, C. Sanchez Gras, R. Santacesaria, C. Santamarina Rios, M. Santimaria, E. Santovetti, D. Saranin, G. Sarpis, M. Sarpis, A. Sarti, C. Satriano, A. Satta, M. Saur, D. Savrina, H. Sazak, L. G. Scantlebury Smead, S. Schael, M. Schellenberg, M. Schiller, H. Schindler, M. Schmelling, B. Schmidt, O. Schneider, A. Schopper, M. Schubiger, S. Schulte, M. H. Schune, R. Schwemmer, B. Sciascia, S. Sellam, A. Semennikov, M. Senghi Soares, A. Sergi, N. Serra, L. Sestini, A. Seuthe, P. Seyfert, Y. Shang, D. M. Shangase, M. Shapkin, I. Shchemerov, L. Shchutska, T. Shears, L. Shekhtman, Z. Shen, V. Shevchenko, E. B. Shields, E. Shmanin, J. D. Shupperd, B. G. Siddi, R. Silva Coutinho, G. Simi, S. Simone, N. Skidmore, T. Skwarnicki, M. W. Slater, I. Slazyk, J. C. Smallwood, J. G. Smeaton, A. Smetkina, E. Smith, M. Smith, A. Snoch, M. Soares, L. Soares Lavra, M. D. Sokoloff, F. J. P. Soler, A. Solovev, I. Solovyev, F. L. Souza De Almeida, B. Souza De Paula, B. Spaan, E. Spadaro Norella, P. Spradlin, F. Stagni, M. Stahl, S. Stahl, P. Stefko, O. Steinkamp, O. Stenyakin, H. Stevens, S. Stone, M. E. Stramaglia, M. Straticiuc, D. Strekalina, F. Suljik, J. Sun, L. Sun, Y. Sun, P. Svihra, P. N. Swallow, K. Swientek, A. Szabelski, T. Szumlak, M. Szymanski, S. Taneja, F. Teubert, E. Thomas, K. A. Thomson, V. Tisserand, S. T'Jampens, M. Tobin, L. Tomassetti, D. Torres Machado, D. Y. Tou, M. T. Tran, E. Trifonova, C. Trippl, G. Tuci, A. Tully, N. Tuning, A. Ukleja, D. J. Unverzagt, E. Ursov, A. Usachov, A. Ustyuzhanin, U. Uwer, A. Vagner, V. Vagnoni, A. Valassi, G. Valenti, N. Valls Canudas, M. van Beuzekom, M. Van Dijk, E. van Herwijnen, C. B. Van Hulse, M. van Veghel, R. Vazquez Gomez, P. Vazquez Regueiro, C. Vázquez Sierra, S. Vecchi, J. J. Velthuis, M. Veltri, A. Venkateswaran, M. Veronesi, M. Vesterinen, D. Vieira, M. Vieites Diaz, H. Viemann, X. Vilasis-Cardona, E. Vilella Figueras, P. Vincent, D. Vom Bruch, A. Vorobyev, V. Vorobyev, N. Voropaev, R. Waldi, J. Walsh, C. Wang, J. Wang, J. Wang, J. Wang, J. Wang, M. Wang, R. Wang, Y. Wang, Z. Wang, Z. Wang, H. M. Wark, N. K. Watson, S. G. Weber, D. Websdale, C. Weisser, B. D. C. Westhenry, D. J. White, M. Whitehead, D. Wiedner, G. Wilkinson, M. Wilkinson, I. Williams, M. Williams, M. R. J. Williams, F. F. Wilson, W. Wislicki, M. Witek, L. Witola, G. Wormser, S. A. Wotton, H. Wu, K. Wyllie, Z. Xiang, D. Xiao, Y. Xie, A. Xu, J. Xu, L. Xu, M. Xu, Q. Xu, Z. Xu, Z. Xu, D. Yang, S. Yang, Y. Yang, Z. Yang, Z. Yang, Y. Yao, L. E. Yeomans, H. Yin, J. Yu, X. Yuan, O. Yushchenko, E. Zaffaroni, M. Zavertyaev, M. Zdybal, O. Zenaiev, M. Zeng, D. Zhang, L. Zhang, S. Zhang, Y. Zhang, Y. Zhang, A. Zhelezov, Y. Zheng, X. Zhou, Y. Zhou, X. Zhu, Z. Zhu, V. Zhukov, J. B. Zonneveld, Q. Zou, S. Zucchelli, D. Zuliani, and G. Zunica. Test of lepton universality in beauty-quark decays, 2021.

[69] Planck Collaboration, N. Aghanim, Y. Akrami, M. Ashdown, J. Aumont, C. Baccigalupi, M. Ballardini, A. J. Banday, R. B. Barreiro, N. Bartolo, S. Basak, R. Battye, K. Benabed, J. P. Bernard, M. Bersanelli, P. Bielewicz, J. J. Bock, J. R. Bond, J. Borrill, F. R. Bouchet, F. Boulanger, M. Bucher, C. Burigana, R. C. Butler, E. Calabrese, J. F. Cardoso, J. Carron, A. Challinor, H. C. Chiang, J. Chluba, L. P. L. Colombo, C. Combet, D. Contreras, B. P. Crill, F. Cuttaia, P. de Bernardis, G. de Zotti, J. Delabrouille, J. M. Delouis, E. Di Valentino, J. M. Diego, O. Doré, M. Douspis, A. Ducout, X. Dupac, S. Dusini, G. Efstathiou, F. Elsner, T. A. Enßlin, H. K. Eriksen, Y. Fantaye,

M. Farhang, J. Fergusson, R. Fernandez-Cobos, F. Finelli, F. Forastieri, M. Frailis, A. A. Fraisse, E. Franceschi, A. Frolov, S. Galeotta, S. Galli, K. Ganga, R. T. Génova-Santos, M. Gerbino, T. Ghosh, J. González-Nuevo, K. M. Górski, S. Gratton, A. Gruppuso, J. E. Gudmundsson, J. Hamann, W. Handley, F. K. Hansen, D. Herranz, S. R. Hildebrandt, E. Hivon, Z. Huang, A. H. Jaffe, W. C. Jones, A. Karakci, E. Keihänen, R. Keskitalo, K. Kiiveri, J. Kim, T. S. Kisner, L. Knox, N. Krachmalnicoff, M. Kunz, H. Kurki-Suonio, G. Lagache, J. M. Lamarre, A. Lasenby, M. Lattanzi, C. R. Lawrence, M. Le Jeune, P. Lemos, J. Lesgourgues, F. Levrier, A. Lewis, M. Liguori, P. B. Lilje, M. Lilley, V. Lindholm, M. López-Caniego, P. M. Lubin, Y. Z. Ma, J. F. Macías-Pérez, G. Maggio, D. Maino, N. Mandolesi, A. Mangilli, A. Marcos-Caballero, M. Maris, P. G. Martin, M. Martinelli, E. Martínez-González, S. Matarrese, N. Mauri, J. D. McEwen, P. R. Meinhold, A. Melchiorri, A. Mennella, M. Migliaccio, M. Millea, S. Mitra, M. A. Miville-Deschênes, D. Molinari, L. Montier, G. Morgante, A. Moss, P. Natoli, H. U. Nørgaard-Nielsen, L. Pagano, D. Paoletti, B. Partridge, G. Patanchon, H. V. Peiris, F. Perrotta, V. Pettorino, F. Piacentini, L. Polastri, G. Polenta, J. L. Puget, J. P. Rachen, M. Reinecke, M. Remazeilles, A. Renzi, G. Rocha, C. Rosset, G. Roudier, J. A. Rubiño-Martín, B. Ruiz-Granados, L. Salvati, M. Sandri, M. Savelainen, D. Scott, E. P. S. Shellard, C. Sirignano, G. Sirri, L. D. Spencer, R. Sunyaev, A. S. Suur-Uski, J. A. Tauber, D. Tavagnacco, M. Tenti, L. Toffolatti, M. Tomasi, T. Trombetti, L. Valenziano, J. Valiviita, B. Van Tent, L. Vibert, P. Vielva, F. Villa, N. Vittorio, B. D. Wandelt, I. K. Wehus, M. White, S. D. M. White, A. Zacchei, and A. Zonca. Planck 2018 results. VI. Cosmological parameters, 2018.

[70] Matthew Colless et al. The 2dF Galaxy Redshift Survey: Final data release. 6 2003.

[71] Edmund J. Copeland, M. Sami, and Shinji Tsujikawa. Dynamics of dark energy. *Int. J. Mod. Phys.*, D15:1753–1936, 2006. doi: 10.1142/S0218271806009942X.

[72] Edmund J. Copeland, Michael Kopp, Antonio Padilla, Paul M. Saffin, and Constantinos Skordis. Dark energy after gw170817 revisited. *Physical Review Letters*, 122(6), Feb 2019. ISSN 1079-7114. doi: 10.1103/physrevlett.122.061301. URL http://dx.doi.org/10.1103/PhysRevLett.122.061301.

[73] Craig J. Copi, Adam N. Davis, and Lawrence M. Krauss. New nucleosynthesis constraint on the variation ofg. *Physical Review Letters*, 92(17), Apr 2004. ISSN 1079-7114. doi: 10.1103/physrevlett.92.171301. URL http://dx.doi.org/10.1103/PhysRevLett.92.171301.

[74] J. Coupon, M. Kilbinger, H. J. McCracken, O. Ilbert, S. Arnouts, Y. Mellier, U. Abbas, S. de la Torre, Y. Goranova, P. Hudelot, and et al. Galaxy clustering in the cfhtls-wide: the changing relationship between galaxies and haloes since $z \sim 1.2$. *Astronomy & Astrophysics*, 542:A5, May 2012. ISSN 1432-0746. doi: 10.1051/0004-6361/201117625. URL http://dx.doi.org/10.1051/0004-6361/201117625.

[75] Paolo Creminelli and Filippo Vernizzi. Dark energy after gw170817 and grb170817a. *Physical Review Letters*, 119(25), Dec 2017. ISSN 1079-7114. doi: 10.1103/physrevlett.119.251302. URL http://dx.doi.org/10.1103/PhysRevLett.119.251302.

[76] Richard H. Cyburt, Brian D. Fields, Keith A. Olive, and Tsung-Han Yeh. Big Bang Nucleosynthesis: 2015. *Rev. Mod. Phys.*, 88:015004, 2016. doi: 10.1103/RevModPhys.88.015004.

[77] Antonio De Felice and Shinji Tsujikawa. $f(R)$ theories. *Living Reviews in Relativity*, 13(1), Jun 2010. ISSN 1433-8351. doi: 10.12942/lrr-2010-3. URL http://dx.doi.org/10.12942/lrr-2010-3.

[78] Ivan de Martino, Mariafelicia De Laurentis, and Salvatore Capozziello. Constraining $f(R)$ Gravity by the Large-Scale Structure. *Universe*, 1(2):123–157, 2015. doi: 10.3390/universe1020123.

[79] Timothée Delubac, Julian E. Bautista, Nicolás G. Busca, James Rich, David Kirkby, Stephen Bailey, Andreu Font-Ribera, Anže Slosar, Khee-Gan Lee, Matthew M. Pieri, and et al. Baryon acoustic oscillations in the Ly-α forest of BOSS DR11 quasars. *Astronomy & Astrophysics*, 574:A59, Jan 2015. ISSN 1432-0746. doi: 10.1051/0004-6361/201423969. URL http://dx.doi.org/10.1051/0004-6361/201423969.

[80] M. Demianski, E. Piedipalumbo, D. Sawant, and L. Amati. High redshift constraints on dark energy models and tension with the flat LambdaCDM model. *arXiv e-prints*, art. arXiv:1911.08228, November 2019.

[81] Vincent Desjacques, Donghui Jeong, and Fabian Schmidt. Large-scale galaxy bias. *Physics Reports*, 733:1–193, Feb 2018. ISSN 0370-1573. doi: 10.1016/j.physrep.2017.12.002. URL http://dx.doi.org/10.1016/j.physrep.2017.12.002.

[82] Eleonora Di Valentino, Alessandro Melchiorri, Olga Mena, and Sunny Vagnozzi. Interacting dark energy in the early 2020s: A promising solution to the H_o and cosmic shear tensions. *Physics of the Dark Universe*, 30:100666, December 2020. doi: 10.1016/j.dark.2020.100666.

[83] eleonora di valentino, olga mena, Supriya Pan, Luca Visinelli, Weiqiang Yang, Alessandro Melchiorri, David Fonseca Mota, Adam G Riess, and Joseph Silk. In the realm of the hubble tension - a review of solutions. *Classical and Quantum Gravity*, Jun 2021. ISSN 1361-6382. doi: 10.1088/1361-6382/ac086d. URL http://dx.doi.org/10.1088/1361-6382/ac086d.

[84] Eleonora Di Valentino et al. Cosmology Intertwined III: $f\sigma_8$ and S_8. 9 2020.

[85] Scott Dodelson. *Modern Cosmology*. Academic Press, (2002).

[86] Jason N. Dossett, Mustapha Ishak, David Parkinson, and Tamara Davis. Constraints and tensions in testing general relativity from Planck and CFHTLenS data including intrinsic alignment systematics. *Phys. Rev. D*, 92(2):023003, 2015. doi: 10.1103/PhysRevD.92.023003.

[87] D. Dutcher, L. Balkenhol, P. A. R. Ade, Z. Ahmed, E. Anderes, A. J. Anderson, M. Archipley, J. S. Avva, K. Aylor, P. S. Barry, R. Basu Thakur, K. Benabed, A. N. Bender, B. A. Benson, F. Bianchini, L. E. Bleem, F. R. Bouchet, L. Bryant, K. Byrum, J. E. Carlstrom, F. W. Carter, T. W. Cecil, C. L. Chang, P. Chaubal, G. Chen, H. M. Cho, T. L. Chou, J. F. Cliche, T. M. Crawford, A. Cukierman, C. Daley, T. de Haan, E. V. Denison, K. Dibert, J. Ding, M. A. Dobbs, W. Everett, C. Feng, K. R. Ferguson, A. Foster, J. Fu, S. Galli, A. E. Gambrel, R. W. Gardner, N. Goeckner-Wald, R. Gualtieri, S. Guns, N. Gupta, R. Guyser, N. W. Halverson, A. H. Harke-Hosemann, N. L. Harrington, J. W. Henning, G. C. Hilton, E. Hivon, G. P. Holder, W. L. Holzapfel, J. C. Hood, D. Howe, N. Huang, K. D. Irwin, O. B. Jeong, M. Jonas, A. Jones, T. S. Khaire, L. Knox, A. M. Kofman, M. Korman, D. L. Kubik, S. Kuhlmann, C. L. Kuo, A. T. Lee, E. M. Leitch, A. E. Lowitz, C. Lu, S. S. Meyer, D. Michalik, M. Millea, J. Montgomery, A. Nadolski, T. Natoli, H. Nguyen, G. I. Noble, V. Novosad, Y. Omori, S. Padin, Z. Pan, P. Paschos, J. Pearson, C. M. Posada, K. Prabhu, W. Quan, S. Raghunathan, A. Rahlin, C. L. Reichardt, D. Riebel, B. Riedel, M. Rouble, J. E. Ruhl, J. T. Sayre, E. Schiappucci, E. Shirokoff, G. Smecher, J. A. Sobrin, A. A. Stark, J. Stephen, K. T. Story, A. Suzuki, K. L. Thompson, B. Thorne, C. Tucker, C. Umilta, L. R. Vale, K. Vanderlinde, J. D. Vieira, G. Wang, N. Whitehorn, W. L. K. Wu, V. Yefremenko, K. W. Yoon, and M. R. Young. Measurements of the e-mode polarization and temperature-e-mode correlation of the cmb from spt-3g 2018 data, 2021.

[88] Koushik Dutta, Ruchika, Anirban Roy, Anjan A. Sen, and M. M. Sheikh-Jabbari. Beyond ΛCDM with low and high redshift data: implications for dark energy. *Gen. Rel. Grav.*, 52(2):15, 2020. doi: 10.1007/s10714-020-2665-4.

[89] Gia Dvali, Gregory Gabadadze, and Massimo Porrati. 4D gravity on a brane in 5D Minkowski space. *Physics Letters B*, 485(1-3):208–214, Jul 2000. ISSN 0370-2693. doi: 10.1016/s0370-2693(00)00669-9. URL http://dx.doi.org/10.1016/S0370-2693(00)00669-9.

[90] G. Efstathiou, W. J. Sutherland, and S. J. Maddox. The cosmological constant and cold dark matter. *Nature*, 348:705–707, 1990. doi: 10.1038/348705a0.

[91] Daniel Eisenstein and Martin White. Theoretical uncertainty in baryon oscillations. *Physical Review D*, 70(10), Nov 2004. ISSN 1550-2368. doi: 10.1103/physrevd.70.103523. URL http://dx.doi.org/10.1103/PhysRevD.70.103523.

[92] Daniel J. Eisenstein and Wayne Hu. Baryonic features in the matter transfer function. *The Astrophysical Journal*, 496(2):605–614, Apr 1998. ISSN 1538-4357. doi: 10.1086/305424. URL http://dx.doi.org/10.1086/305424.

[93] Daniel J. Eisenstein, Idit Zehavi, David W. Hogg, Roman Scoccimarro, Michael R. Blanton, Robert C. Nichol, Ryan Scranton, Hee-Jong Seo, Max Tegmark, Zheng Zheng, and et al. Detection of the baryon acoustic peak in the large-scale correlation function of sdss luminous red galaxies.

The Astrophysical Journal, 633(2):560–574, Nov 2005. ISSN 1538-4357. doi: 10.1086/466512. URL http://dx.doi.org/10.1086/466512.

[94] F. Englert and R. Brout. Broken Symmetry and the Mass of Gauge Vector Mesons. *Phys. Rev. Lett.*, 13:321–323, 1964. doi: 10.1103/PhysRevLett.13.321.

[95] Jose María Ezquiaga and Miguel Zumalacárregui. Dark Energy After GW170817: Dead Ends and the Road Ahead. *Phys. Rev. Lett.*, 119(25):251304, 2017. doi: 10.1103/PhysRevLett.119.251304.

[96] Jose María Ezquiaga and Miguel Zumalacárregui. Dark Energy in light of Multi-Messenger Gravitational-Wave astronomy. *Front. Astron. Space Sci.*, 5:44, 2018. doi: 10.3389/fspas.2018.00044.

[97] Jose María Ezquiaga, Juan García-Bellido, and Vincent Vennin. The exponential tail of inflationary fluctuations: consequences for primordial black holes. *Journal of Cosmology and Astroparticle Physics*, 2020(03):029–029, Mar 2020. ISSN 1475-7516. doi: 10.1088/1475-7516/2020/03/029. URL http://dx.doi.org/10.1088/1475-7516/2020/03/029.

[98] Thomas Faulkner, Max Tegmark, Emory F. Bunn, and Yi Mao. Constraining $f(r)$ gravity as a scalar-tensor theory. *Phys. Rev. D*, 76:063505, Sep 2007. doi: 10.1103/PhysRevD.76.063505. URL https://link.aps.org/doi/10.1103/PhysRevD.76.063505.

[99] F. Feroz, M. P. Hobson, and M. Bridges. MULTINEST: an efficient and robust Bayesian inference tool for cosmology and particle physics. *Monthly Notices of the Royal Astronomical Society*, 398(4):1601–1614, October 2009. doi: 10.1111/j.1365-2966.2009.14548.x.

[100] D. J. Fixsen. The temperature of the cosmic microwave background, (2009).

[101] Gabriele Franciolini, Vishal Baibhav, Valerio De Luca, Ken K. Y. Ng, Kaze W. K. Wong, Emanuele Berti, Paolo Pani, Antonio Riotto, and Salvatore Vitale. Evidence for primordial black holes in ligo/virgo gravitational-wave data, 2021.

[102] Wendy L. Freedman, Barry F. Madore, Dylan Hatt, Taylor J. Hoyt, In Sung Jang, Rachael L. Beaton, Christopher R. Burns, Myung Gyoon Lee, Andrew J. Monson, Jillian R. Neeley, M. M. Phillips, Jeffrey A. Rich, and Mark Seibert. The Carnegie-Chicago Hubble Program. VIII. An Independent Determination of the Hubble Constant Based on the Tip of the Red Giant Branch. *APJ*, 882(1):34, September 2019. doi: 10.3847/1538-4357/ab2f73.

[103] Noemi Frusciante and Louis Perenon. Effective field theory of dark energy: A review. *Physics Reports*, 857:1–63, May 2020. ISSN 0370-1573. doi: 10.1016/j.physrep.2020.02.004. URL http://dx.doi.org/10.1016/j.physrep.2020.02.004.

[104] R Gannouji, B Moraes, and D Polarski. The growth of matter perturbations in $f(R)$ models. *Journal of Cosmology and Astroparticle Physics*, 2009(02):034–034, Feb 2009. ISSN 1475-7516. doi: 10.1088/1475-7516/2009/02/034. URL http://dx.doi.org/10.1088/1475-7516/2009/02/034.

[105] Radouane Gannouji, Lavrentios Kazantzidis, Leandros Perivolaropoulos, and David Polarski. Consistency of modified gravity with a decreasing $G_{\rm eff}(z)$ in a ΛCDM background. *Phys. Rev.*, D98(10): 104044, 2018. doi: 10.1103/PhysRevD.98.104044.

[106] Jérôme Gleyzes, David Langlois, Federico Piazza, and Filippo Vernizzi. New class of consistent scalar-tensor theories. *Physical Review Letters*, 114(21), May 2015. ISSN 1079-7114. doi: 10.1103/physrevlett.114.211101. URL http://dx.doi.org/10.1103/PhysRevLett.114.211101.

[107] Yungui Gong. Growth factor parametrization and modified gravity. *Physical Review D*, 78(12), Dec 2008. ISSN 1550-2368. doi: 10.1103/physrevd.78.123010. URL http://dx.doi.org/10.1103/PhysRevD.78.123010.

[108] Javier Grande, Joan Solà, and Hrvoje Štefančić. Λxcdm: a common model solution to the cosmological coincidence problem? *Journal of Cosmology and Astroparticle Physics*, 2006(08):011–011, Aug 2006. ISSN 1475-7516. doi: 10.1088/1475-7516/2006/08/011. URL http://dx.doi.org/10.1088/1475-7516/2006/08/011.

[109] Stephen Hawking. Gravitationally collapsed objects of very low mass. *Mon. Not. R. Astron. Soc.*, 152:75, January 1971. doi: 10.1093/mnras/152.1.75.

[110] A. Hernández-Almada, Genly Leon, Juan Magaña, Miguel A. García-Aspeitia, and V. Motta. Generalized emergent dark energy: observational Hubble data constraints and stability analysis. *Monthly Notices of the Royal Astronomical Society*, 497(2):1590–1602, July 2020. doi: 10.1093/mnras/staa2052.

[111] Catherine Heymans, Tilman Tröster, Marika Asgari, Chris Blake, Hendrik Hildebrandt, Benjamin Joachimi, Konrad Kuijken, Chieh-An Lin, Ariel G. Sánchez, Jan Luca van den Busch, and et al. Kids-1000 cosmology: Multi-probe weak gravitational lensing and spectroscopic galaxy clustering constraints. *Astronomy & Astrophysics*, 646:A140, Feb 2021. ISSN 1432-0746. doi: 10.1051/0004-6361/202039063. URL http://dx.doi.org/10.1051/0004-6361/202039063.

[112] Peter W. Higgs. Broken symmetries and the masses of gauge bosons. *Phys. Rev. Lett.*, 13:508–509, Oct 1964. doi: 10.1103/PhysRevLett.13.508. URL https://link.aps.org/doi/10.1103/PhysRevLett.13.508.

[113] David W. Hogg. Distance measures in cosmology, 1999.

[114] Gregory Walter Horndeski. Second-order scalar-tensor field equations in a four-dimensional space. *Int. J. Theor. Phys.*, 10:363–384, 1974. doi: 10.1007/BF01807638.

[115] Wayne Hu. Wandering in the background: A CMB explorer, 1995.

[116] Wayne Hu and Scott Dodelson. Cosmic microwave background anisotropies. *Annual Review of Astronomy and Astrophysics*, 40(1):171–216, Sep 2002. ISSN 1545-4282. doi: 10.1146/annurev.astro.40.060401.093926. URL http://dx.doi.org/10.1146/annurev.astro.40.060401.093926.

[117] Wayne Hu and Ignacy Sawicki. Models off(r)cosmic acceleration that evade solar system tests. *Physical Review D*, 76(6), Sep 2007. ISSN 1550-2368. doi: 10.1103/physrevd.76.064004. URL http://dx.doi.org/10.1103/PhysRevD.76.064004.

[118] Caroline D. Huang, Adam G. Riess, Wenlong Yuan, Lucas M. Macri, Nadia L. Zakamska, Stefano Casertano, Patricia A. Whitelock, Samantha L. Hoffmann, Alexei V. Filippenko, and Daniel Scolnic. Hubble Space Telescope Observations of Mira Variables in the SN Ia Host NGC 1559: An Alternative Candle to Measure the Hubble Constant. *APJ*, 889(1):5, January 2020. doi: 10.3847/1538-4357/ab5dbd.

[119] Qing-Guo Huang. An analytic calculation of the growth index for $f(R)$ Dark Energy model. *The European Physical Journal C*, 74(7), Jul 2014. ISSN 1434-6052. doi: 10.1140/epjc/s10052-014-2964-6. URL http://dx.doi.org/10.1140/epjc/s10052-014-2964-6.

[120] Edwin Hubble. A relation between distance and radial velocity among extra-galactic nebulae. *Proc. Nat. Acad. Sci.*, 15:168–173, 1929. doi: 10.1073/pnas.15.3.168.

[121] Mikhail M. Ivanov, Yacine Ali-Haïmoud, and Julien Lesgourgues. Ho tension or to tension? *Physical Review D*, 102(6), Sep 2020. ISSN 2470-0029. doi: 10.1103/physrevd.102.063515. URL http://dx.doi.org/10.1103/PhysRevD.102.063515.

[122] Karsten Jedamzik and Levon Pogosian. Relieving the Hubble tension with primordial magnetic fields. *arXiv e-prints*, art. arXiv:2004.09487, April 2020.

[123] Karsten Jedamzik, Levon Pogosian, and Gong-Bo Zhao. Why reducing the cosmic sound horizon alone can not fully resolve the hubble tension. *Communications Physics*, 4(1), Jun 2021. ISSN 2399-3650. doi: 10.1038/s42005-021-00628-x. URL http://dx.doi.org/10.1038/s42005-021-00628-x.

[124] Nick Kaiser. Clustering in real space and in redshift space. *Month. Not. Roy. Astron. Soc*, 227:1–21, July 1987. doi: 10.1093/mnras/227.1.1.

[125] Ryotaro Kase and Shinji Tsujikawa. Dark energy in horndeski theories after gw170817: A review. *International Journal of Modern Physics D*, 28(05):1942005, Apr 2019. ISSN 1793-6594. doi: 10.1142/s0218271819420057. URL http://dx.doi.org/10.1142/S0218271819420057.

[126] Rishi Khatri and Rashid A Sunyaev. Beyond y and μ: the shape of the cmb spectral distortions in the intermediate epoch, $1.5 10^4 \lesssim z \lesssim 2 10^5$. *Journal of Cosmology and Astroparticle Physics*, 2012 (09):016–016, Sep 2012. ISSN 1475-7516. doi: 10.1088/1475-7516/2012/09/016. URL http://dx.doi.org/10.1088/1475-7516/2012/09/016.

[127] Claus Kiefer and David Polarski. Why do cosmological perturbations look classical to us?, 2009.

[128] Martin Kilbinger. Cosmology with cosmic shear observations: a review. *Reports on Progress in Physics*, 78(8):086901, Jul 2015. ISSN 1361-6633. doi: 10.1088/0034-4885/78/8/086901. URL http://dx.doi.org/10.1088/0034-4885/78/8/086901.

[129] Oskar Klein. Quantentheorie und fünfdimensionale Relativitätstheorie. *Zeitschrift fur Physik*, 37 (12):895–906, December 1926. doi: 10.1007/BF01397481.

[130] J.-P. Kneib, R. S. Ellis, I. Smail, W. J. Couch, and R. M. Sharples. Hubble space TelescopeObservations of the lensing cluster abell 2218. *The Astrophysical Journal*, 471(2):643–656, nov 1996. doi: 10.1086/177995. URL https://doi.org/10.1086/177995.

[131] Christian Knobel. An introduction into the theory of cosmological structure formation, 2012.

[132] Lloyd Knox and Marius Millea. Hubble constant hunter's guide. *Phys. Rev. D*, 101(4):043533, 2020. doi: 10.1103/PhysRevD.101.043533.

[133] E. Komatsu, K. M. Smith, J. Dunkley, C. L. Bennett, B. Gold, G. Hinshaw, N. Jarosik, D. Larson, M. R. Nolta, L. Page, et al. Seven-year Wilkinson Microwave Anisotropy Probe (WMAP) Observations: Cosmological Interpretation. *APJS*, 192(2):18, February 2011. doi: 10.1088/0067-0049/192/2/18.

[134] E. Komatsu et al. Seven-Year Wilkinson Microwave Anisotropy Probe (WMAP) Observations: Cosmological Interpretation. *Astrophys. J. Suppl.*, 192:18, 2011. doi: 10.1088/0067-0049/192/2/18.

[135] Kazuya Koyama. Ghosts in the self-accelerating universe. *Classical and Quantum Gravity*, 24(24): R231–R253, Nov 2007. ISSN 1361-6382. doi: 10.1088/0264-9381/24/24/r01. URL http://dx.doi.org/10.1088/0264-9381/24/24/R01.

[136] Ofer Lahav, Per B. Lilje, Joel R. Primack, and Martin J. Rees. Dynamical effects of the cosmological constant. *Mon. Not. R. Astron. Soc.*, 251:128–136, July 1991. doi: 10.1093/mnras/251.1.128.

[137] David Langlois. Degenerate higher-order scalar-tensor (dhost) theories, 2018.

[138] David Langlois and Karim Noui. Degenerate higher derivative theories beyond horndeski: evading the ostrogradski instability. *Journal of Cosmology and Astroparticle Physics*, 2016(02):034–034, Feb 2016. ISSN 1475-7516. doi: 10.1088/1475-7516/2016/02/034. URL http://dx.doi.org/10.1088/1475-7516/2016/02/034.

[139] Nanoom Lee and Yacine Ali-Haïmoud. hyrec-2: A highly accurate sub-millisecond recombination code. *Physical Review D*, 102(8), Oct 2020. ISSN 2470-0029. doi: 10.1103/physrevd.102.083517. URL http://dx.doi.org/10.1103/PhysRevD.102.083517.

[140] Seokcheon Lee and Kin-Wang Ng. Growth index with the exact analytic solution of sub-horizon scale linear perturbation for dark energy models with constant equation of state. *Phys. Lett. B*, 688: 1–3, 2010. doi: 10.1016/j.physletb.2010.03.082.

[141] J. Lesgourgues, David Polarski, and A.A. Starobinsky. Quantum-to-classical transition of cosmological perturbations for non-vacuum initial states. *Nuclear Physics B*, 497(1-2):479–508, Jul 1997. ISSN 0550-3213. doi: 10.1016/s0550-3213(97)00224-1. URL http://dx.doi.org/10.1016/S0550-3213(97)00224-1.

[142] Julien Lesgourgues. The cosmic linear anisotropy solving system (class) i: Overview, 2011.

[143] Antony Lewis, Anthony Challinor, and Anthony Lasenby. Efficient computation of CMB anisotropies in closed FRW models. *Astrophys. J.*, 538:473–476, 2000. doi: 10.1086/309179.

[144] Benjamin L'Huillier and Arman Shafieloo. Model-independent test of the flrw metric, the flatness of the universe, and non-local estimation of h_o r_d.

[145] Miao Li, Xiao-Dong Li, Shuang Wang, and Yi Wang. Dark energy. *Communications in Theoretical Physics*, 56(3):525–604, Sep 2011. ISSN 0253-6102. doi: 10.1088/0253-6102/56/3/24. URL http://dx.doi.org/10.1088/0253-6102/56/3/24.

[146] Peikai Li, Rupert A. C. Croft, and Scott Dodelson. New probes of large scale structure, 2021.

[147] Xiaolei Li and Arman Shafieloo. A Simple Phenomenological Emergent Dark Energy Model can Resolve the Hubble Tension. *APJl*, 883(1):L3, September 2019. doi: 10.3847/2041-8213/ab3e09.

[148] Andrew R. Liddle, Paul Parsons, and John D. Barrow. Formalizing the slow-roll approximation in Inflation. *Physical Review D*, 50(12):7222–7232, Dec 1994. ISSN 0556-2821. doi: 10.1103/physrevd.50.7222. URL http://dx.doi.org/10.1103/PhysRevD.50.7222.

[149] Paul J. Steinhardt Limin Wang. Cluster abundance constraints on quintessence models, (1998).

[150] Eric V. Linder. Exploring the expansion history of the universe. *Phys. Rev. Lett.*, 90:091301, 2003. doi: 10.1103/PhysRevLett.90.091301.

[151] Eric V. Linder. Cosmic growth history and expansion history. *Physical Review D*, 72(4), Aug 2005. ISSN 1550-2368. doi: 10.1103/physrevd.72.043529. URL http://dx.doi.org/10.1103/PhysRevD.72.043529.

[152] Eric V. Linder. No Slip Gravity. *JCAP*, 03:005, 2018. doi: 10.1088/1475-7516/2018/03/005.

[153] Eric V. Linder and Robert N. Cahn. Parameterized beyond-einstein growth. *Astroparticle Physics*, 28(4-5):481–488, Dec 2007. ISSN 0927-6505. doi: 10.1016/j.astropartphys.2007.09.003. URL http://dx.doi.org/10.1016/j.astropartphys.2007.09.003.

[154] Eric V. Linder and David Polarski. End of cosmic growth. *Physical Review D*, 99(2), Jan 2019. ISSN 2470-0029. doi: 10.1103/physrevd.99.023503. URL http://dx.doi.org/10.1103/PhysRevD.99.023503.

[155] David Lovelock. The Einstein Tensor and Its Generalizations. *Journal of Mathematical Physics*, 12 (3):498–501, March 1971. doi: 10.1063/1.1665613.

[156] Arthur Lue, Román Scoccimarro, and Glenn D. Starkman. Probing newton's constant on vast scales: Dvali-gabadadze-porrati gravity, cosmic acceleration, and large scale structure. *Physical Review D*, 69(12), Jun 2004. ISSN 1550-2368. doi: 10.1103/physrevd.69.124015. URL http://dx.doi.org/10.1103/PhysRevD.69.124015.

[157] D. H. Lyth. Large-scale energy-density perturbations and inflation. *Phys. Rev. D*, 31:1792–1798, Apr 1985. doi: 10.1103/PhysRevD.31.1792. URL https://link.aps.org/doi/10.1103/PhysRevD.31.1792.

[158] Benjamin L'Huillier, Arman Shafieloo, David Polarski, and Alexei A Starobinsky. Defying the laws of gravity i: model-independent reconstruction of the universe expansion from growth data. *Monthly Notices of the Royal Astronomical Society*, 494(1):819–826, Mar 2020. ISSN 1365-2966. doi: 10.1093/mnras/staa633. URL http://dx.doi.org/10.1093/mnras/staa633.

[159] M. Malekjani, S. Basilakos, Z. Davari, A. Mehrabi, and M. Rezaei. Agegraphic dark energy: growth index and cosmological implications. *Mon. Not. Roy. Astron. Soc.*, 464(1):1192–1201, 2017. doi: 10.1093/mnras/stw2426.

[160] Adam B. Mantz et al. Weighing the giants – IV. Cosmology and neutrino mass. *Mon. Not. Roy. Astron. Soc.*, 446:2205–2225, 2015. doi: 10.1093/mnras/stu2096.

[161] David J.E. Marsh. Axion cosmology. *Physics Reports*, 643:1–79, Jul 2016. ISSN 0370-1573. doi: 10.1016/j.physrep.2016.06.005. URL http://dx.doi.org/10.1016/j.physrep.2016.06.005.

[162] Jerome Martin, Christophe Ringeval, and Vincent Vennin. Encyclopaedia Inflationaris, 2013.

[163] Grant J. Mathews, Motohiko Kusakabe, and Toshitaka Kajino. Introduction to big bang nucleosynthesis and modern cosmology. *International Journal of Modern Physics E*, 26(08):1741001, Aug 2017. ISSN 1793-6608. doi: 10.1142/s0218301317410014. URL http://dx.doi.org/10.1142/S0218301317410014.

[164] Ayan Mitra, Jurgen Mifsud, David F. Mota, and David Parkinson. Cosmology with the Einstein Telescope: No slip gravity model and redshift specifications, 2020.

[165] H. Motohashi, A. A. Starobinsky, and J. Yokoyama. Phantom boundary crossing and anomalous growth index of fluctuations in viable $f(R)$ models of cosmic acceleration. *Progress of Theoretical Physics*, 123(5):887–902, May 2010. ISSN 1347-4081. doi: 10.1143/ptp.123.887. URL http://dx.doi.org/10.1143/PTP.123.887.

[166] Riccardo Murgia, Guillermo F. Abellán, and Vivian Poulin. Early dark energy resolution to the hubble tension in light of weak lensing surveys and lensing anomalies. *Physical Review D*, 103(6), Mar 2021. ISSN 2470-0029. doi: 10.1103/physrevd.103.063502. URL http://dx.doi.org/10.1103/PhysRevD.103.063502.

[167] N. Nazari-Pooya, M. Malekjani, F. Pace, and D. Mohammad-Zadeh Jassur. Growth of spherical overdensities in scalar-tensor cosmologies. *Mon. Not. Roy. Astron. Soc.*, 458(4):3795–3807, 2016. doi: 10.1093/mnras/stw582.

[168] S. Nesseris and Leandros Perivolaropoulos. Testing Lambda CDM with the Growth Function delta(a): Current Constraints. *Phys. Rev. D*, 77:023504, 2008. doi: 10.1103/PhysRevD.77.023504.

[169] S. Nesseris, S. Basilakos, E. N. Saridakis, and L. Perivolaropoulos. Viable $f(T)$ models are practically indistinguishable from ΛCDM. *Phys. Rev. D*, 88:103010, 2013. doi: 10.1103/PhysRevD.88.103010.

[170] Savvas Nesseris and Anupam Mazumdar. Newton's constant inf(r,rμνrμν,□r)theories of gravity and constraints from bbn. *Physical Review D*, 79(10), May 2009. ISSN 1550-2368. doi: 10.1103/physrevd.79.104006. URL http://dx.doi.org/10.1103/PhysRevD.79.104006.

[171] Georges Obied, Hirosi Ooguri, Lev Spodyneiko, and Cumrun Vafa. De sitter space and the swampland, 2018.

[172] Nobuyoshi Ohta. Quantum equivalence of $f(R)$ gravity and scalar–tensor theories in the jordan and einstein frames. *Progress of Theoretical and Experimental Physics*, 2018(3), Mar 2018. ISSN 2050-3911. doi: 10.1093/ptep/pty008. URL http://dx.doi.org/10.1093/ptep/pty008.

[173] T. Padmanabhan. Cosmological constant: The Weight of the vacuum. *Phys. Rept.*, 380:235–320, 2003. doi: 10.1016/S0370-1573(03)00120-0.

[174] R. D. Peccei and Helen R. Quinn. CP conservation in the presence of pseudoparticles. *Phys. Rev. Lett.*, 38:1440–1443, Jun 1977. doi: 10.1103/PhysRevLett.38.1440. URL https://link.aps.org/doi/10.1103/PhysRevLett.38.1440.

[175] Roberto D. Peccei. The Strong CP Problem and Axions. *Axions*, page 3–17, 2008. ISSN 0075-8450. doi: 10.1007/978-3-540-73518-2_1. URL http://dx.doi.org/10.1007/978-3-540-73518-2_1.

[176] P. J. E. Peebles. Recombination of the Primeval Plasma. *Astrophys. J.*, 153:1, July 1968. doi: 10.1086/149628.

[177] P. J. E. Peebles. Tests of cosmological models constrained by inflation. *Astrophys. J.*, 284:439–444, September 1984. doi: 10.1086/162425.

[178] P. J. E. Peebles and Bharat Ratra. Cosmology with a Time Variable Cosmological Constant. *Astrophys. J. Lett.*, 325:L17, 1988. doi: 10.1086/185100.

[179] P. J. E. Peebles and Bharat Ratra. The Cosmological Constant and Dark Energy. *Rev. Mod. Phys.*, 75: 559–606, 2003. doi: 10.1103/RevModPhys.75.559.

[180] Roger Penrose. Gravitational collapse and space-time singularities. *Phys. Rev. Lett.*, 14:57–59, Jan 1965. doi: 10.1103/PhysRevLett.14.57. URL https://link.aps.org/doi/10.1103/PhysRevLett.14.57.

[181] A. A. Penzias and R. W. Wilson. A Measurement of Excess Antenna Temperature at 4080 Mc/s. *Astrophys. J.*, 142:419–421, July 1965. doi: 10.1086/148307.

[182] Will J. Percival and Martin White. Testing cosmological structure formation using redshift-space distortions. *Mon. Not. R. Astron. Soc.*, 393(1):297–308, February 2009. doi: 10.1111/j.1365-2966.2008.14211.x.

[183] Will J. Percival, Beth A. Reid, Daniel J. Eisenstein, Neta A. Bahcall, Tamas Budavari, Joshua A. Frieman, Masataka Fukugita, James E. Gunn, Željko Ivezić, Gillian R. Knapp, and et al. Baryon acoustic oscillations in the sloan digital sky survey data release 7 galaxy sample. *Monthly Notices of the Royal Astronomical Society*, 401(4):2148–2168, Feb 2010. ISSN 1365-2966. doi: 10.1111/j.1365-2966.2009.15812.x. URL http://dx.doi.org/10.1111/j.1365-2966.2009.15812.x.

[184] Leandros Perivolaropoulos and Foteini Skara. Challenges for ΛCDM: An update, 2021.

[185] S. Perlmutter et al. Measurements of Ω and Λ from 42 high redshift supernovae. *Astrophys. J.*, 517: 565–586, 1999. doi: 10.1086/307221.

[186] Cyril Pitrou, Alain Coc, Jean-Philippe Uzan, and Elisabeth Vangioni. Precision big bang nucleosynthesis with improved helium-4 predictions. *Physics Reports*, 754:1–66, Sep 2018. ISSN 0370-1573. doi: 10.1016/j.physrep.2018.04.005. URL http://dx.doi.org/10.1016/j.physrep.2018.04.005.

[187] Planck Collaboration, P. A. R. Ade, N. Aghanim, M. Arnaud, M. Ashdown, J. Aumont, C. Baccigalupi, A. J. Banday, R. B. Barreiro, J. G. Bartlett, et al. Planck 2015 results. XIII. Cosmological parameters. *AAP*, 594:A13, September 2016. doi: 10.1051/0004-6361/201525830.

[188] Planck Collaboration, N. Aghanim, Y. Akrami, M. Ashdown, J. Aumont, C. Baccigalupi, M. Ballardini, A. J. Banday, R. B. Barreiro, N. Bartolo, et al. Planck 2018 results. VI. Cosmological parameters. *arXiv e-prints*, art. arXiv:1807.06209, July 2018.

[189] David Polarski and Radouane Gannouji. On the growth of linear perturbations. *Physics Letters B*, 660(5):439–443, Mar 2008. ISSN 0370-2693. doi: 10.1016/j.physletb.2008.01.032. URL http://dx.doi.org/10.1016/j.physletb.2008.01.032.

[190] David Polarski and Alexei A Starobinsky. Semiclassicality and decoherence of cosmological perturbations. *Classical and Quantum Gravity*, 13(3):377–391, Mar 1996. ISSN 1361-6382. doi: 10.1088/0264-9381/13/3/006. URL http://dx.doi.org/10.1088/0264-9381/13/3/006.

[191] David Polarski, Alexei A. Starobinsky, and Hector Giacomini. When is the growth index constant? *Journal of Cosmology and Astroparticle Physics*, 2016(12):037–037, Dec 2016. ISSN 1475-7516. doi: 10.1088/1475-7516/2016/12/037. URL http://dx.doi.org/10.1088/1475-7516/2016/12/037.

[192] Vivian Poulin, Kimberly K. Boddy, Simeon Bird, and Marc Kamionkowski. Implications of an extended dark energy cosmology with massive neutrinos for cosmological tensions. *Physical Review D*, 97(12), Jun 2018. ISSN 2470-0029. doi: 10.1103/physrevd.97.123504. URL http://dx.doi.org/10.1103/PhysRevD.97.123504.

[193] Vivian Poulin, Tristan L. Smith, Daniel Grin, Tanvi Karwal, and Marc Kamionkowski. Cosmological implications of ultralight axionlike fields. *Physical Review D*, 98(8), Oct 2018. ISSN 2470-0029. doi: 10.1103/physrevd.98.083525. URL http://dx.doi.org/10.1103/PhysRevD.98.083525.

[194] Vivian Poulin, Tristan L. Smith, Tanvi Karwal, and Marc Kamionkowski. Early Dark Energy Can Resolve The Hubble Tension. *Phys. Rev. Lett.*, 122(22):221301, 2019. doi: 10.1103/PhysRevLett.122.221301.

[195] Harry Poulter, Yacine Ali-Haïmoud, Jan Hamann, Martin White, and Anthony G. Williams. CMB constraints on ultra-light primordial black holes with extended mass distributions. 7 2019.

[196] Lisa Randall and Raman Sundrum. A Large mass hierarchy from a small extra dimension. *Phys. Rev. Lett.*, 83:3370–3373, 1999. doi: 10.1103/PhysRevLett.83.3370.

[197] Marco Raveri and Wayne Hu. Concordance and discordance in cosmology. *Physical Review D*, 99 (4):043506, February 2019. doi: 10.1103/PhysRevD.99.043506.

[198] Marco Raveri, Bin Hu, Noemi Frusciante, and Alessandra Silvestri. Effective field theory of cosmic acceleration: Constraining dark energy with cmb data. *Phys. Rev. D*, 90:043513, Aug 2014. doi: 10.1103/PhysRevD.90.043513. URL https://link.aps.org/doi/10.1103/PhysRevD.90.043513.

[199] Adam G. Riess, Alexei V. Filippenko, Peter Challis, Alejandro Clocchiatti, Alan Diercks, Peter M. Garnavich, Ron L. Gilliland, Craig J. Hogan, Saurabh Jha, Robert P. Kirshner, and et al. Observational evidence from supernovae for an accelerating universe and a cosmological constant. *The Astronomical Journal*, 116(3):1009–1038, Sep 1998. ISSN 0004-6256. doi: 10.1086/300499. URL http://dx.doi.org/10.1086/300499.

[200] Adam G. Riess, Stefano Casertano, Wenlong Yuan, Lucas M. Macri, and Dan Scolnic. Large Magellanic Cloud Cepheid Standards Provide a 1% Foundation for the Determination of the Hubble Constant and Stronger Evidence for Physics beyond ΛCDM. *Astrophys. J.*, 876(1):85, 2019. doi: 10.3847/1538-4357/ab1422.

[201] V. Sahni, A. Shafieloo, and A. A. Starobinsky. Model-independent evidence for dark energy evolution from baryon acoustic oscillations. *The Astrophysical Journal*, 793(2):L40, Sep 2014. ISSN 2041-8213. doi: 10.1088/2041-8205/793/2/l40. URL http://dx.doi.org/10.1088/2041-8205/793/2/L40.

[202] Varun Sahni and Alexei Starobinsky. The Case for a Positive Cosmological Λ-Term. *Int. J. Mod. Phys. D*, 09(4):373–443, January 2000. doi: 10.1142/S0218271800000542.

[203] VARUN SAHNI and ALEXEI STAROBINSKY. Reconstructing dark energy. *International Journal of Modern Physics D*, 15(12):2105–2132, Dec 2006. ISSN 1793-6594. doi: 10.1142/s0218271806009704. URL http://dx.doi.org/10.1142/S0218271806009704.

[204] Varun Sahni and Alexei A. Starobinsky. The Case for a positive cosmological Lambda term. *Int. J. Mod. Phys.*, D9:373–444, 2000. doi: 10.1142/S0218271800000542.

[205] Abdus Salam. Weak and Electromagnetic Interactions. *Conf. Proc. C*, 680519:367–377, 1968. doi: 10.1142/9789812795915_0034.

[206] W. L. W. Sargent and E. L. Turner. A statistical method for determining the cosmological density parameter from the redshifts of a complete sample of galaxies. *Astrophys. J.*, 212:L3–L7, February 1977. doi: 10.1086/182362.

[207] Fulvio Sbisà. Classical and quantum ghosts. *European Journal of Physics*, 36(1):015009, Nov 2014. ISSN 1361-6404. doi: 10.1088/0143-0807/36/1/015009. URL http://dx.doi.org/10.1088/0143-0807/36/1/015009.

[208] D. M. Scolnic, D. O. Jones, A. Rest, Y. C. Pan, R. Chornock, R. J. Foley, M. E. Huber, R. Kessler, G. Narayan, A. G. Riess, et al. The Complete Light-curve Sample of Spectroscopically Confirmed SNe Ia from Pan-STARRS1 and Cosmological Constraints from the Combined Pantheon Sample. *APJ*, 859(2):101, June 2018. doi: 10.3847/1538-4357/aab9bb.

[209] Toyokazu Sekiguchi and Tomo Takahashi. Early recombination as a solution to the H_0 tension. *arXiv e-prints*, art. arXiv:2007.03381, July 2020.

[210] Pasquale D. Serpico, Vivian Poulin, Derek Inman, and Kazunori Kohri. Cosmic microwave background bounds on primordial black holes including dark matter halo accretion. *Physical Review Research*, 2(2), May 2020. ISSN 2643-1564. doi: 10.1103/physrevresearch.2.023204. URL http://dx.doi.org/10.1103/PhysRevResearch.2.023204.

[211] Arman Shafieloo, Benjamin L'Huillier, and Alexei A. Starobinsky. Falsifying ΛCDM: Model-independent tests of the concordance model with eBOSS DR14Q and Pantheon. *Physical Review D*, 98(8):083526, oct 2018. doi: 10.1103/PhysRevD.98.083526.

[212] J. R. Shaw and J. Chluba. Precise cosmological parameter estimation using cosmorec. *Monthly Notices of the Royal Astronomical Society*, 415(2):1343–1354, Jun 2011. ISSN 0035-8711. doi: 10.1111/j.1365-2966.2011.18782.x. URL http://dx.doi.org/10.1111/j.1365-2966.2011.18782.x.

[213] John Skilling. Nested Sampling. In Rainer Fischer, Roland Preuss, and Udo Von Toussaint, editors, *American Institute of Physics Conference Series*, volume 735 of *American Institute of Physics Conference Series*, pages 395–405, November 2004. doi: 10.1063/1.1835238.

[214] Tristan L. Smith, Vivian Poulin, José Luis Bernal, Kimberly K. Boddy, Marc Kamionkowski, and Riccardo Murgia. Early dark energy is not excluded by current large-scale structure data, 2020.

[215] Joan Sola, Adria Gomez-Valent, Javier de Cruz Perez, and Cristian Moreno-Pulido. Brans-Dicke cosmology with a Λ- term: a possible solution to ΛCDM tensions. *arXiv e-prints*, 6 2020.

[216] Volker Springel, Carlos S. Frenk, and Simon D. M. White. The large-scale structure of the universe, Apr 2006. ISSN 1476-4687. URL http://dx.doi.org/10.1038/nature04805.

[217] G. Squires, N. Kaiser, A. Babul, G. Fahlman, D. Woods, D. M. Neumann, and H. Boehringer. The Dark Matter, Gas, and Galaxy Distributions in Abell 2218: A Weak Gravitational Lensing and X-Ray Analysis. *Astrophys. J.*, 461:572, April 1996. doi: 10.1086/177085.

[218] A. A. Starobinsky. How to determine an effective potential for a variable cosmological term. *Journal of Experimental and Theoretical Physics Letters*, 68(10):757–763, Nov 1998. ISSN 1090-6487. doi: 10.1134/1.567941. URL http://dx.doi.org/10.1134/1.567941.

[219] A. A. Starobinsky. Disappearing cosmological constant in $f(R)$ gravity. *JETP Letters*, 86(3):157–163, Oct 2007. ISSN 1090-6487. doi: 10.1134/s0021364007150027. URL http://dx.doi.org/10.1134/S0021364007150027.

[220] Alexei A. Starobinsky. A New Type of Isotropic Cosmological Models Without Singularity. *Phys. Lett.*, 91B:99–102, 1980. doi: 10.1016/0370-2693(80)90670-X. [,771(1980)].

[221] Alexei A. Starobinsky. STOCHASTIC DE SITTER (INFLATIONARY) STAGE IN THE EARLY UNIVERSE. *Lect. Notes Phys.*, 246:107–126, 1986. doi: 10.1007/3-540-16452-9_6.

[222] Alexei A. Starobinsky and Jun'ichi Yokoyama. Equilibrium state of a self-interacting scalar field in the de sitter background. *Physical Review D*, 50(10):6357–6368, Nov 1994. ISSN 0556-2821. doi: 10.1103/physrevd.50.6357. URL http://dx.doi.org/10.1103/PhysRevD.50.6357.

[223] Ariel G. Sánchez. Arguments against using h^{-1}.Mpc units in observational cosmology. *Physical Review D*, 102(12), Dec 2020. ISSN 2470-0029. doi: 10.1103/physrevd.102.123511. URL http://dx.doi.org/10.1103/PhysRevD.102.123511.

[224] M. Tanabashi, K. Hagiwara, K. Hikasa, K. Nakamura, Y. Sumino, F. Takahashi, J. Tanaka, K. Agashe, G. Aielli, C. Amsler, M. Antonelli, D. M. Asner, H. Baer, Sw. Banerjee, R. M. Barnett, T. Basaglia, C. W. Bauer, J. J. Beatty, V. I. Belousov, J. Beringer, S. Bethke, A. Bettini, H. Bichsel, O. Biebel, K. M. Black, E. Blucher, O. Buchmuller, V. Burkert, M. A. Bychkov, R. N. Cahn, M. Carena, A. Ceccucci, A. Cerri, D. Chakraborty, M.-C. Chen, R. S. Chivukula, G. Cowan, O. Dahl, G. D'Ambrosio, T. Damour, D. de Florian, A. de Gouvêa, T. DeGrand, P. de Jong, G. Dissertori, B. A. Dobrescu, M. D'Onofrio, M. Doser, M. Drees, H. K. Dreiner, D. A. Dwyer, P. Eerola, S. Eidelman, J. Ellis, J. Erler, V. V. Ezhela, W. Fetscher, B. D. Fields, R. Firestone, B. Foster, A. Freitas, H. Gallagher, L. Garren, H.-J. Gerber, G. Gerbier, T. Gershon, Y. Gershtein, T. Gherghetta, A. A. Godizov, M. Goodman, C. Grab, A. V. Gritsan, C. Grojean, D. E. Groom, M. Grünewald, A. Gurtu, T. Gutsche, H. E. Haber, C. Hanhart, S. Hashimoto, Y. Hayato, K. G. Hayes, A. Hebecker, S. Heinemeyer, B. Heltsley, J. J. Hernández-Rey, J. Hisano, A. Höcker, J. Holder, A. Holtkamp, T. Hyodo, K. D. Irwin, K. F. Johnson, M. Kado, M. Karliner, U. F. Katz, S. R. Klein, E. Klempt, R. V. Kowalewski, F. Krauss, M. Kreps, B. Krusche, Yu. V. Kuyanov, Y. Kwon, O. Lahav, J. Laiho, J. Lesgourgues, A. Liddle, Z. Ligeti, C.-J. Lin, C. Lippmann, T. M. Liss, L. Littenberg, K. S. Lugovsky, S. B. Lugovsky, A. Lusiani, Y. Makida,

F. Maltoni, T. Mannel, A. V. Manohar, W. J. Marciano, A. D. Martin, A. Masoni, J. Matthews, U.-G. Meißner, D. Milstead, R. E. Mitchell, K. Mönig, P. Molaro, F. Moortgat, M. Moskovic, H. Murayama, M. Narain, P. Nason, S. Navas, M. Neubert, P. Nevski, Y. Nir, K. A. Olive, S. Pagan Griso, J. Parsons, C. Patrignani, J. A. Peacock, M. Pennington, S. T. Petcov, V. A. Petrov, E. Pianori, A. Piepke, A. Pomarol, A. Quadt, J. Rademacker, G. Raffelt, B. N. Ratcliff, P. Richardson, A. Ringwald, S. Roesler, S. Rolli, A. Romaniouk, L. J. Rosenberg, J. L. Rosner, G. Rybka, R. A. Ryutin, C. T. Sachrajda, Y. Sakai, G. P. Salam, S. Sarkar, F. Sauli, O. Schneider, K. Scholberg, A. J. Schwartz, D. Scott, V. Sharma, S. R. Sharpe, T. Shutt, M. Silari, T. Sjöstrand, P. Skands, T. Skwarnicki, J. G. Smith, G. F. Smoot, S. Spanier, H. Spieler, C. Spiering, A. Stahl, S. L. Stone, T. Sumiyoshi, M. J. Syphers, K. Terashi, J. Terning, U. Thoma, R. S. Thorne, L. Tiator, M. Titov, N. P. Tkachenko, N. A. Törnqvist, D. R. Tovey, G. Valencia, R. Van de Water, N. Varelas, G. Venanzoni, L. Verde, M. G. Vincter, P. Vogel, A. Vogt, S. P. Wakely, W. Walkowiak, C. W. Walter, D. Wands, D. R. Ward, M. O. Wascko, G. Weiglein, D. H. Weinberg, E. J. Weinberg, M. White, L. R. Wiencke, S. Willocq, C. G. Wohl, J. Womersley, C. L. Woody, R. L. Workman, W.-M. Yao, G. P. Zeller, O. V. Zenin, R.-Y. Zhu, S.-L. Zhu, F. Zimmermann, P. A. Zyla, J. Anderson, L. Fuller, V. S. Lugovsky, and P. Schaffner. Review of particle physics. *Phys. Rev. D*, 98:030001, Aug 2018. doi: 10.1103/PhysRevD.98.030001. URL https://link.aps.org/doi/10.1103/PhysRevD.98.030001.

[225] Max Tegmark. Cosmological neutrino bounds for non-cosmologists. *Physica Scripta*, T121:153–155, Jan 2005. ISSN 1402-4896. doi: 10.1088/0031-8949/2005/t121/023. URL http://dx.doi.org/10.1088/0031-8949/2005/T121/023.

[226] Davide Trezzi. Study of the 2H(p,γ)3He reaction in the BBN energy range at LUNA. *J. Phys. Conf. Ser.*, 940(1):012059, 2018. doi: 10.1088/1742-6596/940/1/012059.

[227] Shinji Tsujikawa. Matter density perturbations and effective gravitational constant in modified gravity models of Dark Energy. *Physical Review D*, 76(2), Jul 2007. ISSN 1550-2368. doi: 10.1103/physrevd.76.023514. URL http://dx.doi.org/10.1103/PhysRevD.76.023514.

[228] Sunny Vagnozzi. New physics in light of the H_0 tension: An alternative view. *Phys. Rev.*, D102(2): 023518, 2020. doi: 10.1103/PhysRevD.102.023518.

[229] Sunny Vagnozzi, Eleonora Di Valentino, Stefano Gariazzo, Alessandro Melchiorri, Olga Mena, and Joseph Silk. Listening to the BOSS: the galaxy power spectrum take on spatial curvature and cosmic concordance, 2020.

[230] Sunny Vagnozzi, Luca Visinelli, Philippe Brax, Anne-Christine Davis, and Jeremy Sakstein. Direct detection of dark energy: the xenon1t excess and future prospects, 2021.

[231] Kyriakos Vattis, Savvas M. Koushiappas, and Abraham Loeb. Dark matter decaying in the late Universe can relieve the Ho tension. *Phys. Rev. D*, 99(12):121302, 2019. doi: 10.1103/PhysRevD.99.121302.

[232] J. Alberto Vazquez, S. Hee, M. P. Hobson, A. N. Lasenby, M. Ibison, and M. Bridges. Observational constraints on conformal time symmetry, missing matter and double dark energy. *JCAP*, 1807:062, 2018. doi: 10.1088/1475-7516/2018/07/062.

[233] Vincent Vennin. Stochastic inflation and primordial black holes, 2020.

[234] Licia Verde, Jose Luis Bernal, Alan F. Heavens, and Raul Jimenez. The length of the low-redshift standard ruler. *Mon. Not. Roy. Astron. Soc.*, 467(1):731–736, 2017. doi: 10.1093/mnras/stx116.

[235] Licia Verde, Tommaso Treu, and Adam G. Riess. Tensions between the early and late Universe. *Nat. Astron.*, 3:891–895, September 2019. doi: 10.1038/s41550-019-0902-0.

[236] Luca Visinelli, Sunny Vagnozzi, and Ulf Danielsson. Revisiting a negative cosmological constant from low-redshift data. *Symmetry*, 11(8):1035, 2019. doi: 10.3390/sym11081035.

[237] B. Wang, E. Abdalla, F. Atrio-Barandela, and D. Pavon. Dark Matter and Dark Energy Interactions: Theoretical Challenges, Cosmological Implications and Observational Signatures. *Rept. Prog. Phys.*, 79(9):096901, 2016. doi: 10.1088/0034-4885/79/9/096901.

[238] Hao Wei. Growth index of DGP model and current growth rate data. *Physics Letters B*, 664(1-2): 1–6, Jun 2008. ISSN 0370-2693. doi: 10.1016/j.physletb.2008.04.060. URL http://dx.doi.org/10.1016/j.physletb.2008.04.060.

[239] David H. Weinberg, Michael J. Mortonson, Daniel J. Eisenstein, Christopher Hirata, Adam G. Riess, and Eduardo Rozo. Observational probes of cosmic acceleration. *Physics Reports*, 530(2):87–255, Sep 2013. ISSN 0370-1573. doi: 10.1016/j.physrep.2013.05.001. URL http://dx.doi.org/10.1016/j.physrep.2013.05.001.

[240] Puxun Wu, Hong Wei Yu, and Xiangyun Fu. A Parametrization for the growth index of linear matter perturbations. *JCAP*, 06:019, 2009. doi: 10.1088/1475-7516/2009/06/019.

[241] Gen Ye and Yun-Song Piao. Is the Hubble tension a hint of AdS phase around recombination? *Phys. Rev.*, D101(8):083507, 2020. doi: 10.1103/PhysRevD.101.083507.

[242] Tsung-Han Yeh, Keith A. Olive, and Brian D. Fields. The impact of new d(p,γ)3 rates on big bang nucleosynthesis. *Journal of Cosmology and Astroparticle Physics*, 2021(03):046, Mar 2021. ISSN 1475-7516. doi: 10.1088/1475-7516/2021/03/046. URL http://dx.doi.org/10.1088/1475-7516/2021/03/046.

[243] Gong-Bo Zhao, Yuting Wang, Shun Saito, Dandan Wang, Ashley J. Ross, Florian Beutler, Jan Niklas Grieb, Chia-Hsun Chuang, Francisco-Shu Kitaura, Sergio Rodriguez-Torres, et al. The clustering of galaxies in the completed SDSS-III Baryon Oscillation Spectroscopic Survey: tomographic BAO analysis of DR12 combined sample in Fourier space. *Monthly Notices of the Royal Astronomical Society*, 466(1):762–779, April 2017. doi: 10.1093/mnras/stw3199.

[244] Ruiyu Zhou, Jing Yang, and Ligong Bian. Gravitational waves from first-order phase transition and domain wall. *Journal of High Energy Physics*, 2020(4), Apr 2020. ISSN 1029-8479. doi: 10.1007/jhep04(2020)071. URL http://dx.doi.org/10.1007/JHEP04(2020)071.

[245] Miguel Zumalacárregui. Gravity in the era of equality: Towards solutions to the hubble problem without fine-tuned initial conditions. *Physical Review D*, 102(2), Jul 2020. ISSN 2470-0029. doi: 10.1103/physrevd.102.023523. URL http://dx.doi.org/10.1103/PhysRevD.102.023523.

[246] Eoin Ó Colgáin, Maurice H.P.M. van Putten, and Hossein Yavartanoo. de Sitter Swampland, H_0 tension & observation. *Phys. Lett. B*, 793:126–129, 2019. doi: 10.1016/j.physletb.2019.04.032.

Colophon

This thesis was typeset using LaTeX, originally developed by Leslie Lamport and based on Donald Knuth's TeX. The body text is set in 11 point Arno Pro, designed by Robert Slimbach in the style of book types from the Aldine Press in Venice, and issued by Adobe in 2007. A template, which can be used to format a PhD thesis with this look and feel, has been released under the permissive MIT (X11) license, and can be found online at github.com/suchow/ or from the author at suchow@post.harvard.edu.